



University
of Glasgow

Boyi Bukata, Bala (2013) *Evolutionary optimisation for Volt-VAR power quality control*. PhD thesis.

<http://theses.gla.ac.uk/3882/>

Copyright and moral rights for this thesis are retained by the author

A copy can be downloaded for personal non-commercial research or study, without prior permission or charge

This thesis cannot be reproduced or quoted extensively from without first obtaining permission in writing from the Author

The content must not be changed in any way or sold commercially in any format or medium without the formal permission of the Author

When referring to this work, full bibliographic details including the author, title, awarding institution and date of the thesis must be given



Evolutionary Optimisation for Volt-VAR Power Quality Control

by

Bala Boyi Bukata

Thesis Submitted to the
School of Engineering
University of Glasgow
for the degree of
DOCTOR OF PHILOSOPHY

October 01, 2012

© Copyright 2012 by Bala Boyi Bukata
All Rights Reserved

Dedications

To My Family:

For their perseverance, continued support and prayers throughout the duration of this Ph.D course in the UK.

Acknowledgements

All praise is due to Allah (God or Yahweh), the Living and the Self-subsisting, who has again shown me to another successful turning-point in my life. My sincere gratitude and appreciation go to my value adding supervisor, Professor Yun Li who has made my PhD contribution a reality through his skillful guidance. The level of knowledge and experience he has demonstrated during the course of his supervision must be reckoned with.

I would also like to acknowledge the appreciation of my second supervisor, Professor Enrique Acha who has provided the intial drive on DSTATCOM technology before his retirement in 2011. Mr. Calum Cossar, who acted as my pastoral supervisor has been very helpful too, I appreciated. Then to Mr. Tom O’Hara, someone not likely to be forgotten either, for his continued technical support and lively humour when ever he appeared in the control lab e.g., story of the camel’s dung coffee gift.

I then would like to thank my family (wife and children) without whose love, patience, prayers and support, this work may never have been accomplished. Special thanks to my brother El-hajj Ibrahim Boyi, and to the entire members of my family too numerous to mention here.

I am also grateful to the petroleum technological development fund (PTDF) for funding this entire project. The moral support obtained from the Bayero University Kano (BUK), in particular the electrical engineering department is also appreciated. I will never forget my mentor, the VC of Yobe State University, Professor Musa Alabe for all his earnest care and help.

Last but not the least, to all my friends and colleagues in the intelligent control systems group (R507, Rankine Building) for the mutual support, understanding and friendliness we shared at both happy and distressing moments, while we were together. Particularly, Dr. Fang Sun, Dr. Hammad Sherazi Iqbal, Lutz-Chris Schoening, Emrah Kaplan, Niel Geoghegan and Ben Tiller the chess master. A special one to Chris and Emrah for the “espri-de-coups” that transpired during those hard moments.

I say a BIG thank you to you all!

Abstract

With the more environmentally friendly smart grid initiatives during the past few years, intelligent operation and optimisation of the electricity distribution system have received an increasing attention in power system research worldwide. Power flow from the distribution substation to the customer can be optimised at Volt-Ampere-Reactive (VAR) level by reducing the reactive power. Distributed Generation (DG) and Renewable Energy Sources (RES) represent both the broadest potentials and the broadest challenges for intelligent distribution systems and smart grid control. In general, the flexibility envisaged by integrating RES during smart grid transformation is often surrounded by nonlinearities such as wave-form deformations caused by harmonic currents or voltages, which impliedly increase control system complexity. Therefore, conventional controllers presently implemented need to be re-engineered in order to solve power quality (PQ) problems therein.

This work aims to improve the controllability of Distribution Static Compensators (DSTATCOMs) through the development of improved control systems using evolutionary computation enabled design automation and optimisation. The resultant Volt-VAR Control (VVC) optimises PQ in the presence of nonlinearities and uncertainties. It also aims at increasing overall system's sensitivity to unconsidered parameters in the design stage like measurement noise, unmodelled dynamics and disturbances. This is otherwise known as the robustness of the system offering it with valuable potential for future smart grids control, which are anticipated to present more nonlinearities due to virtual power plant (VPP) configuration. According to European Project FENIX, a Virtual Power Plant (VPP) aggregates the capacity of many diverse Distributed Energy Resources (DER), it creates a single operating profile from a composite of the parameters characterizing each DER and can incorporate the impact of the network on aggregate DER output.

To particularly solve PQ problems, two objectives are realised in this thesis. First, a non-deterministic evolutionary algorithm (EA) is adopted to generate optimum fuzzy logic controllers for DSTATCOMs. This design methodology extends the traditional

computer-aided-design (CAD) to computer-automated-design (CAutoD), which provides a unified solution to diverse PQ problems automatically and efficiently. While realizing this objective, the prediction ability of the derivative term in a proportional and derivative (PD) controller is improved by placing a re-routed derivative filter in the feedback path to tame ensuing oscillations. This method is then replicated in a fuzzy PD scheme and is automated through the capability of a “generational” tuning using evolutionary algorithm.

Fuzzy logic controllers (FLCs) are rule-based systems which are designed around a fuzzy rule base (RB) related through an inference engine by means of fuzzy implication and compositional procedures. RBs are normally formulated in linguistic terms, in the form of *if... then* rules which can be driven through various techniques. Fundamentally, the correct choice of the membership functions of the linguistic set defines the performance of an FLC. In this context, a three rule-base fuzzy mapping using Macvicar-Whelan matrix has been incorporated in this scheme to reduce the computational cost, and to avoid firing of redundant rules. The EA-Fuzzy strategy is proven to overcome the limitation of conventional optimisation which may be trapped in local minima, as the optimisation problem is often multi-modal.

The second objective of the thesis is the development of a novel advanced model-free predictive control (MFPC) system for DSTATCOMs through a deterministic non-gradient algorithm. The new method uses its “look-ahead” feature to predict and propose solutions to anticipated power quality problems before they occur. A describing function augmented DSTATCOM regime is so arranged in a closed-loop fashion to locate limit cycles for settling the systems nonlinearities in a model-free zone. Predictive control is performed upon the online generated input-output data-set through the power of a non-gradient simplex algorithm. The strategy is to boycott the usage of a system model which is often based on gradient information and may thus be trapped in a local optimum or hindered by noisy data.

As a model-free technique, the resultant system offers the advantage of reduction in system modelling or identification, which is often inaccurate, and also in computational load, since it operates directly on raw data from a direct online procession while at the same time dealing with a partially known system normally encountered in a practical industrial problem. Steady-state and dynamic simulations of both control and simulation models in Matlab/Simulink environment demonstrate the superiority of the new model-free approach over the traditional trial-and-error based methods. The method has been varified to offer faster response speed and shorter settling time at zero overshoot when compared to existing methods.

A SimPowerSystems software simulation model is also developed to check experimental validity of the designs. Where specific PQ problems such as harmonics distortion,

voltage swells, voltage sags and flicker are solved. A noticeable record level of THD reduction to 0.04% and 0.05% has respectively been achieved. It is therefore safe to recommend to the industry the implementation of this model-free predictive control scheme at the distribution level. As the distribution system metamorphoses into decentralised smart grid featuring connectivity of virtual power plants mostly through power electronic converters, e.g., DSTATCOM, it stands to benefit from the full Volt-VAR automated controllability of the MFPCs low control rate.

Based on CAutoD, the practical implementation of this technique is made possible through digital prototyping within the real-time workshop to automatically generate C or C++ codes from Simulink, which executes continuous and discrete time models directly on a vast range of computer applications. Its overall wired closed-loop structure with the DSTATCOM would offer reliable and competitive advantages over its PID and SVC (CAD-based) counterparts currently being implemented through physical prototyping, in terms of; quick product-to-market pace, reduced hardwire size, small footprint, maintenance free as it is model-free (and automated), where pickling the controller timers and model contingencies are unnecessary as would be with the conventional controllers. More importantly, the scheme performs the aforementioned control functions robustly at a high speed in the range of $0.005 \rightarrow 0.01$ seconds. High enough to capture and deal with any ensuing PQ problem emanating from changes in customer's load and system disturbances in an environmentally friendly, but less grid-friendly renewable generators.

List of Publications

- [1] B B Bukata and Y li, “A new Smart DSTATCOM for Enhancing Reactive Power Exchange and Voltage Support at the Distribution Level”, in Proc 15th Int. Conf. on Automation and Computing (ICAC’09), pp 52 – 57, ISBN: 978 – 0 – 9555293 – 4 – 4, Luton, U.K, 19 September, 2009.
- [2] B B Bukata and Y li, “Fuzzy Smart DSTATCOM for Solving Power Quality Problems”, in Proc 16th Int. Conf. on Automation and Computing (ICAC’10), pp 220 – 225, ISBN: 978 – 0 – 9555293 – 6 – 8, Birmingham, U.K, 11 September, 2010.
- [3] B B Bukata and Y li, “Reviewing DSTATCOM for Smart Distribution Grid Applications in Solving Power Quality Problems”, in 17th Int. Conf. on Automation and Computing (ICAC’11), pp 294 – 299, IEEE Control Systems Society, ISBN: 978 – 1 – 4673 – 0000 – 1, Huddersfield, U.K, 11 September, 2011.
- [4] B B Bukata and Y li, “A Novel Model-Free Prediction of Power Quality Problems Via DSTATCOM”, in 18th Int. Conf. on Automation and Computing (ICAC’12), pp 37 – 42, IEEE Control Systems Society, ISBN: 978 – 1 – 908549 – 00 – 6, Loughborough, U.K, 08 September, 2012.
- [5] B B Bukata and Y Li, “Evolving Optimal Fuzzy Logic Controllers for Power Distribution Systems”, IEEE Transactions on Power Systems. Submitted.
- [6] B B Bukata and Y Li, “A New Self-Healing DSTATCOM for Volt-VAR and Power Quality Control”, IEEE Transactions on Smart Grid. Submitted.

Abbreviations

AMIGO	Approximate M-Constraint Integral Gain Optimisation
ANFIS	Adaptive Neuro-Fuzzy Inference System
ANSI	American National Standards Institute
CAD	Computer-Aided-Design
CAutoD	Computer-Automated-Design
CHR	Chien Hrones Reswick
CPD	Custom Power Devices
GDP	Gross Domestic Product
DER	Distributed Energy Resources
DF	Describing Function
DG	Distributed Generation
DMC	Dynamic Matrix Control
DOL	Direct-On-Line
DSA	Distribution System Automation
DSTATCOM	Distribution Static Compensator
DVR	Dynamic Voltage Restorer
EA	Evolutionary Algorithm
EPRI	Electrical Power Research Institute
EV	Electric Vehicle
FACTS	Flexible AC Transmission Systems
FIR	Finite Impulse Response
FLC	Fuzzy Logic Control
FOPDT	First-Order-Plus-Delay-Time
FPD	Fuzzy Proportional-plus-Derivative
GA	Genetic Algorithm
IAE	Integral Absolute Error
IAED	Integral Absolute Error Derivative
IEC	International Electrotechnical Commission
IEEE	Institute of Electrical and Electronic Engineering
IFT	Iterative Feedback Tuning
IGBT	Insulated Gate Bipolar Transistor
ISE	Integral Squared Error
ISED	Integral Squared Error Derivative
ISTSE	Integral Squared Time Squared Error
ISTSED	Integral Squared Time Squared Error Derivative
ITAE	Integral Time Absolute Error
ITAED	Integral Time Absolute Error Derivative
ITSE	Integral Time Squared Error
ITSED	Integral Time Squared Error Derivative
IVVC	Integrated Volt-VAR Control
LQP	Linear Quadratic Programming
LQR	Linear Quadratic Regulator
LTI	Linear Time Invariant
MFPC	Model-Free Predictive Control
MPC	Model Predictive Control

NMPC	Nonlinear Model Predictive Control
NN	Neural Network
PCC	Point of Common Coupling
PD	Proportional-plus-Derivative
PF	Power Factor
PI	Proportional-plus-Integral
P/I	Performance Index
PID	Proportional-plus-Integral-plus-Derivative
PQ	Power Quality
PSS	Power System Stability
PWM	Pulse Width Modulator
RB	Rule Base
RES	Renewable Energy Sources
RMS	Root Mean Square
SCADA	Supervisory Control And Data Acquisition
SGA	Simple Genetic Algorithm
SIDF	Sinusoidal Input Describing Function
SPS	SimPowerSystems
SVC	Static VAR Compensator
TDD	Total Dynamic Demand
THD	Total Harmonic Distortion
TSK	Tagaki Sugeno Kang
UPFC	Unified Power Factor Controller
UPS	Universal Power Supply
VAR	Volt-Ampere-Reactive
ZN	Ziegler Nichols

Contents

1	Introduction	1
1.1	Power Quality Control Problems in Distribution Networks	1
1.2	The Challenges Facing DSTATCOM	5
1.2.1	Rating the DSTATCOM	5
1.2.2	Intrinsic Harmonic Generation	6
1.2.3	Extrinsic Harmonic Generation	6
1.2.4	Control of the Switching Angle	6
1.2.5	Heuristic Rule-Based and Other Solutions	7
1.3	Proposed Solutions to PQ Problems	8
1.3.1	Automation of Rule-Based Designs	8
1.3.2	Model Predictive Control	8
1.4	Contributions of the Thesis	9
1.5	Thesis Outline	9
2	Review of DSTATCOM Control for PQ Problems	12
2.1	Introduction	12
2.2	System Configuration	12
2.3	PQ Challenges and Trends	13
2.4	Existing PQ Control Schemes	15
2.4.1	PID Control	15
2.4.2	Fuzzy Logic Control	16
2.4.3	Artificial Neural Networks	17
2.4.4	Model Predictive Control	17
2.5	Summary	18
3	DSTATCOM System Analysis	20
3.1	Introduction	20
3.2	Open-Loop Analysis	21
3.2.1	Power Exchange at the PCC	22
3.2.2	Steady-State Analysis	24
3.3	Open-Loop Simulations	29
3.3.1	Model Comparison	29
3.3.2	Locating Operating Points	30

3.4	Analysis for DSTATCOM PID Control	31
3.4.1	Effect of the Proportional Term	34
3.4.2	Effect of the Linear PI Terms	35
3.4.3	Effect of the Linear PD Terms	35
3.5	Summary	36
4	CAutoD of Fuzzy Controllers for Improved PQ	37
4.1	FLC for PQ Applications	37
4.2	Generic PID Control Paradigm	38
4.2.1	PID Tuning Methods	39
4.2.2	Design Specifications	40
4.2.3	Linear Model Identification	40
4.3	PID Design Case Study - a Linear DSTATCOM Plant	42
4.4	A-Priori Tuning of FPD Controllers	43
4.4.1	Input-Output Scaling Factor Tuning	43
4.4.2	Deficiency of the A-Priori Tuning	46
4.5	Prelims to CAutoD Tuning	46
4.5.1	Effect of Scaling Factors	47
4.5.2	Robustness to Model Changes	49
4.5.3	Scenario No. 1: Changes in Circuit Inductance	52
4.5.4	Scenario No. 2: Changes in circuit Resistance	52
4.5.5	Scenario No. 3: Changes in Circuit Capacitance	53
4.5.6	Setpoint Following	55
4.5.7	Test for Step Changes	57
4.5.8	Benefits of the CAutoD Scheme	59
4.6	From Manual to Automatic Design	60
4.6.1	Evolutionary Stage	61
4.6.2	Genetic-Fuzzy PD Encoding	63
4.6.3	Problem Formulation	63
4.6.4	Choice of the Performance Index	65
4.7	Conventional Optimisation Tools	66
4.8	Methods for PQ Control System Design	69
4.8.1	Automated Fuzzy Control System Design	70
4.8.2	CAutoD Tuning of FPD Control Systems	70
4.8.3	CAutoD for Fuzzy PD Systems	71
4.9	Summary	76
5	Evolutionary Design of Model-Free Predictive Control Systems	77
5.1	Methodologies	77
5.2	Revisiting the MPC Structure	79
5.2.1	Description of the Basic Principle	80
5.2.2	Model-Based Formulation	80

5.2.3	Step Response as a Model	83
5.3	Preliminary MPC Simulations	85
5.3.1	Tuning Effects on MPCs	85
5.3.2	Effects of Tuning Horizons	86
5.3.3	Effects of Tuning Filter Coefficients	86
5.3.4	Effects of Weight Tuning	100
5.3.5	Problem of the Model-Based Prediction	101
5.4	Switching to Model-Free Prediction Control	101
5.4.1	The Describing Functions	102
5.4.2	Augmented DSTATCOM	103
5.5	MFPC Direct Online Design	106
5.5.1	Model-Free Predictive Control Paradigm	108
5.6	Test for Step-Change	114
5.7	Experimental DSTATCOM Model	117
5.8	Power Quality Simulations	118
5.8.1	Dynamic Performance Test	120
5.8.2	Flicker Control	121
5.8.3	Sag and Swell Control	124
5.8.4	Harmonics Control	128
5.9	Considerations for Practical Implementations	128
5.10	Summary	129
6	Comparison and Discussions	130
6.1	Methods and Schemes Studied	130
6.2	Analysis of Results	131
6.2.1	Automatic FPD Vs. Manual FPD	131
6.2.2	MFPC Vs. Other Controllers	131
6.2.3	Self-Healing Property of MFPC Vs. MPC	136
6.2.4	Gradient Vs. Non-Gradient Optimisers	139
6.2.5	Performance Decision Criteria	143
6.2.6	Harmonics Reduction	146
6.3	Summary	149
7	Conclusion and Future Work	150
7.1	Reconstruction of Enhanced DSTATCOM Controllers	150
7.2	Manual Computer-Aided Design for FPD Systems	151
7.3	CAutoD for PQ Control System Design	151
7.4	Evolving MFPC for PQ Control System Design	151
7.5	Future Perspectives	153
7.5.1	Single-Layered Neuro-Model-Free Predictive Control	153
7.5.2	Fault Tolerant Fuzzy-Prediction in DSTATCOM	153

A	1.1 Model of DSTATCOM	I
B	4.1 System Design	VII
C	5.1 I/O Mappings and Robustness Tables	XI
D	6.1 Control Strategy	XIX

List of Figures

2.1	Shunt DSTATCOM with a PI controller	13
3.1	Active and reactive power in steady state	24
3.2	i_q , i_d , and V_{dc} in steady state	25
3.3	Linear alpha-voltage relation	25
3.4	Step cahnges in alpha [rads]	26
3.5	Receiving end voltage transfer Limit	28
3.6	Model comparison	29
3.7	System operating points	30
3.8	Closed-loop circuit	31
3.9	Unstable DSTATCOM	32
3.10	Further unstable DSTATCOM	32
3.11	Correlated PIDs	33
3.12	Further correlated PIDs	33
3.13	Effect of P-controller as K_p increases	34
3.14	PI controller as T_i increases	35
3.15	PD controller as T_d increases	36
4.1	Generic closed-loop control system	39
4.2	Heuristic Z-N controller design	41
4.3	Intial FOPDT tuned responses	42
4.4	FPD-DSTATCOM control model	44
4.5	Scaling effects on performance	47
4.6	Error plot for:	48
4.7	Effects of scaling factors case 1	48
4.8	Effects of scaling factors case 2	49
4.9	Scaling effects on e and α	50
4.10	Scaling effects on overall performance	50
4.11	Uncertain parameters combination	51
4.12	Effect of nonlinear change in inductance	52
4.13	Effect of linear change in inductance	53
4.14	Effect of nonlinear change in resistance	54
4.15	Effect of linear change in resistance	54
4.16	Effect of nonlinear capacitance change	55

4.17	Effect of linear capacitance change	56
4.18	Linear vs. nonlinear model performance	56
4.19	Fuzzy PD control signal	57
4.20	Comparing conventional PD and fuzzy PD	58
4.21	Fuzzy PD error and error derivative curves	58
4.22	Conventional PD error and error derivative curves	59
4.23	Direct CAutoD fuzzy PD controller	60
4.24	Effect of average distance	62
4.25	Effect of higher mutation rate	62
4.26	CAutoD Interface	63
4.27	EA-FPD routine	64
4.28	Minimisation plot in 3D	66
4.29	Minimisation plot in 2D	67
4.30	Minimisation contour plot	67
4.31	Maximisation plot in 3D	68
4.32	Maximisation: α vs. \dot{e}	68
4.33	Maximisation contour plot	69
4.34	CAutoD by artificial evolution (Li, 2004a)	70
4.35	Evolutionary FPD vs. PD	72
4.36	Trade-offs between control objectives	73
4.37	Best PD controllers	73
4.38	Best FPD controller	74
4.39	Kpbest parameters	74
4.40	Kdbest parameters	75
4.41	Best switching signals	75
5.1	Basic MPC structure	79
5.2	General MPC Framework	81
5.3	Basic MPC idea	82
5.4	Changing horizons for unconstrained plant;	87
5.5	Unconstrained control signal:	87
5.6	Changing horizons for constrained plant:	88
5.7	Constrained control signal:	88
5.8	Raising control horizon for unconstrained plant:	89
5.9	Raised unconstrained control signal	89
5.10	Raising control horizon for constrained plant:	90
5.11	Raised constrained control signal	90
5.12	Lowering predictive horizon for unconstrained plant:	91
5.13	Lowered unconstrained control signal	91
5.14	Lowering predictive horizon for constrained plant:	92
5.15	Lowered constrained control signal	92
5.16	Plant with tuned filter coefficients case 1:	94

5.17	Control signal for case 1	94
5.18	Plant with tuned filter coefficients case 2:	95
5.19	Control signal for case 2	95
5.20	Unstable plant with raised FIR	96
5.21	Control signal (unsatble)	96
5.22	Stable plant with raised FIR	97
5.23	Control signal (stabilised)	97
5.24	Unconstarined further FIR tuning	98
5.25	Control signal of further tuning	98
5.26	Tuning FIR coeficients to unity	99
5.27	Control signal to unit tuning	99
5.28	Nonlinear feedback control loop	102
5.29	DF of frequency vs amplitude	105
5.30	Nichols chart for describing function	106
5.31	Model-free signal generator	107
5.32	Basic optimization routine	111
5.33	Step-up: 120 to 220 volts	115
5.34	Alpha: 0.0017 to 0.0031 rads	115
5.35	Step-down: 220 to 120 volts	116
5.36	Alpha: 0.0031 to 0.0031 rads	116
5.37	SPS DSTATCOM model	117
5.38	Single-line diagram	118
5.39	Closed-loop model validation	119
5.40	Dynamic response of DSTATCOM	120
5.41	Voltage support curves	121
5.42	Inverter voltage and current magnitudes	122
5.43	Flicker without DSTATCOM	123
5.44	Flicker with new DSTATCOM	123
5.45	MFPC-SPS DSTATCOM model	124
5.46	Mitigation of voltage sag/swell	126
5.47	Normal Operating Conditions	127
6.1	Automatic vs manual FPD tuning	132
6.2	Required control inputs	132
6.3	Nonlinear responses to step change	134
6.4	Step change in alpha	134
6.5	Responses to step change	135
6.6	Step change in alpha	135
6.7	MFPC in look-ahead mode	137
6.8	Control effort for MFPC look-ahead	137
6.9	MPC in look-ahead mode	138
6.10	Control effort for MPC look-ahead	138

6.11	Simplex cost function	140
6.12	CAutoD cost function	140
6.13	Pattern-search cost function	141
6.14	Simulated-annealing cost function	141
6.15	Simple GA cost function	142
6.16	Threshold-acceptance cost function	142
6.17	ITSE + ITSED performance	143
6.18	ISE + ISED performance	144
6.19	ISTSE + ISTSED performance	144
6.20	IAE + IAED performance	144
6.21	ITAE + ITAED performance	145
6.22	Time domain correlation of: e and \dot{e} with respect to α	145
6.23	Frequency domain correlation of: e and \dot{e} with respect to α	145
6.24	MFPC compensated	147
6.25	EA-FPD Compensated	147
6.26	PD Compensated	148
6.27	PI Compensated	148
A.1	Six-pulse DSTATCOM connected to distribution feeder	I
D.1	Outer loop voltage control	XX

Chapter 1

Introduction

1.1 Power Quality Control Problems in Distribution Networks

Rapid advances in more environmentally-friendly smart-grid technologies are influencing the 21st century leading economies such as the US, China, and Europe to shift from the 20th century electric grid. As these economies become flamboyant and so has the utility of electricity intensified as a catalyst for economic growth among these nations. With transmission and distribution networks still serving as critical link between electric generators and their consumers, the technological sophistication garnered so far does not match the consumer's power quality and reliability demands. Hence, it is about time to transform the current grid (often referred to as "dumb-grid") which has been around since 1930s into a smart-grid (Brown 2008).

A centralised grid for instance, aids much transmission and distribution congestion that makes it more inefficient and unreliable. Additionally, there is a contentious risk for failure to meet peak demand periods often served by inefficient power plants operating over a very short period of time (a few hours-per-year). These factors, added to increased power consumption due to population growth further stretch the traditional grid to its limits, raising serious concerns on economic impact of blackouts and interruptions being witnessed today. These have been estimated to costing the US's economy in excess of \$100 billion per annum as in (Partners 2009). While most recently (31st of July, 2012), the Indian grids failure which affected half of the country with hundreds of millions hit by power cut caused by excessive power absorption, leading to massive snags in rail transport and medical facilities.

In fact, the grid transformation stir has already begun with the emergence of a host of smart energy devices and systems, capable of dramatically enhancing grid efficiency, reliability and security at reduced tariffs, as well as promote green (clean) power generation. Smart energy, entails digital information technology application to electrical power network optimisation. Whereas, smart grid is the result of applying such technology to generate, transmit, and distribute electrical power to the customer through its various building blocks namely: conventional and cutting edge engineering facilities, smart meters, sensors and intelligent control devices, information technology, a two way communication system that enables the customer re-sale excess energy demand back to the grid, a rechargeable point for electric vehicles (EVs), and other features as characterized in (Amin & Wollenberg 2005). It has been estimated that, the potential benefits realisable from such transformation over the next 20 years would substantially increase productivity and GDP growth, cut carbon emission and improve national security, again (Partners 2009).

The distribution system is relatively perceived as an interface between the bulk and the custom powers, whose control objective is to strike a balance between the two for maintaining continuous healthy operation of the system. A good distribution control system is therefore expected to enhance the overall system efficiency through loss reduction and power quality control. Presently, distribution system equipment such as the tap changing transformers, synchronous machines, capacitor banks, static volt-ampere-reactive compensators (SVCs), and many other flexible ac transmission systems (FACTS) controllers at device level, including DSTATCOM are being applied for such control. However, there are numerous challenges facing the area at the moment in terms of the smart-grid de-centralizing functionality which include: voltage and reactive power compensation (now known as Volt-VAR optimisation); distribution system automation (DSA); power factor correction (PF); phase current balancing; integrate-able low loss transformers (to improve efficiency), distributed resources (typically, between 1kW - 50MW), and dispersed energy storage facilities (normally sited at consumer loads), which call for radical change in the type of controllers designed in these equipment for general system power quality improvement.

To understand this phenomenon, the losses regarding distribution lines and transformers have been classified into resistive and reactive components. While, resistive load losses are unavoidable, reactive load losses which emanate from capacitive and inductive circuit properties (cancelling each other) can be avoided. In a very large quantity, the reactive power increases distribution line currents being responsible for further energy losses. The distribution transformers often operate at efficiency higher than 98%, thus making their core losses negligible. However, transmission and distribution system losses together constitute 9% of the total from generation to the consumer's feeder. Out of this figure only 2 – 3% of the losses is attributable to the feeder lines and cou-

pling transformers. These are now generally regarded as the main causes of waveform deformations resulting into the so called power quality (PQ) problems.

There are various academic groups in the world presently researching into DSTATCOM control of power quality problems. In particular, with the current wave of smart grid evolution, a number of multinational electricity companies are actively investing into DSTATCOM technologies with the hope of integrating such within the smart grid context. These companies include Hitachi Europe, S & C Electric Company, ABB, Siemens, Schneider, and GE. Addressing the issue of the Volt-VAR compensation in relation to solving the PQ problem at the distribution network is the theme of this thesis.

The PQ problem has often been defined in relation to the deformations in sinusoidal waveforms of supply voltages or load currents given at fundamental frequency, whose amplitude is the same as the rated rms value in a three phase system. Where these deformations result in creating harmonics and interharmonics of the fundamental waves, they can cause serious deviations in system's normal behaviour as in (Dugan et al. 2003), (Chapman 2001*a*) and (IEEE 1993). The PQ phenomenon could also assume a combination of all possible scenarios in a multi-faceted manner, for instance, it could emanate from the utilities as voltage quality problem, normally triggered by integrating distributed resources (DRs) like wind turbine generators which produce incessant voltage and power fluctuations in a feeble grid (Bajpai & Gupta 2008). It may also emerge as current quality problems as a result of logging sensitive nonlinear loads onto the system such as, electric arc furnaces and computing devices which are capable of drawing non sinusoidal currents from sinusoidal source voltages. The third source could intrinsically appear from the inverter devices (e.g., DVR, DSTATCOM, UPFC, etc) meant to mitigate the PQ issue (IEEE 1993), (Thakare et al. 2009). A typical menace on the effects of PQ when sensitive computing equipment were first introduced, was reported to have infested early installations with haphazard failures. This paved the way for ANSI to come up with IEEE standard 446 defining the limits within which equipment should operate continuously without failure or interruption (Chapman 2001*a*).

This thesis will present a short list of power quality problems, their characteristics, and the traditional methods used to solve them in Table 1.1. The practical scope of this work is restricted to studying voltage sags, voltage swells, flicker and harmonic distortion. All these are solvable through DSTATCOM. Note that when DSTATCOM is inclusively used in harmonic correction it is often referred to as a shunt-active filter (Sannino et al. 2003).

It is observed from Table 1.1 that, the traditional solutions used to improve PQ are largely static. While these problems can vary from half of a cycle (0.01 sec) to one

Table 1.1: A Summary of PQ Problems: Nature and Solutions

(Chapman 2001*a*)

PQ Problems	Characteristics	Solutions
Impulsive Transients	Sudden change in voltage and current signals in steady state.	Filters, Isolation Transformers, and Surge Arresters.
Oscillatory Transients	Sudden change in voltage and current signals at (< 5 to > 500 kHz).	Filters, Isolation Transformers, and Surge Arresters.
Voltage Sags	0.1 – 0.9 Decrease in Per unit RMS Value at 0.5 cycles to 1 min.	DSTATCOMs, UPS, Ferroresonant Transformers, and Backup Generators.
Voltage Swells	1.1 – 1.8 Increase in Per unit RMS Value at 0.5 cycles to 1 min.	DSTATCOMs, UPS, Ferroresonant Transformers, and Backup Generators.
Over/Undervoltages	> 110% Increase and < 90% Decrease in RMS voltage for > 1 min.	Voltage Regulators and Ferroresonant Transformers.
Harmonic Distortion	Refer to IEEE Std 519 – 1992 for allowed THD ($\pm 5\%$) and TDD ($\pm 10\%$).	DSTATCOM as an Active Filter, Passive Filters and Ferroresonant Transformers.
Voltage Flicker	Variation in Magnitude with frequency.	DSTATCOMs and SVCs.

minute, the fastest solution should offer a bandwidth much lower than 0.01 seconds. This explains the reason for the failure of the static VAR compensator (SVC) which has been in operation at the distribution level since the 1930s. Although, they are still active at the transmission corridor where the span is much longer and hence requiring longer intervention speeds. Their application to both corridors actually continued until the 1980s with the introduction of the FACTS devices and their custom power devices (CPD) offerings from (Hingorani 1991).

The main problem of the SVC has been attributed to their slow response time, large footprints and high costs. Soon enough were the custom power devices introduced, the distribution static compensator (DSTATCOM) took over SVC's control functions at the distribution corridor for over three decades. The DSTATCOM can offer the needed bandwidth to cover the range for most of the PQ problems quoted above. However, one major drawback distinctive to DSTATCOMs has to do with the manually tuned linear control structures they are currently based on. To effectively improve the functionality of DSTATCOM to meet the demands of the 21st century grid, this thesis will investigate a set of challenges facing it with highlighted possible solutions.

1.2 The Challenges Facing DSTATCOM

Most of the techniques applied to curb PQ problems using DSTATCOM are designed upon trial-and-error tuning (i.e., Ziegler-Nichols) as in the proportional-integral-derivative (PID) control (Åström & Hägglund 2001). Although the methods have been successful over time, these however do not provide the control unification required to diversify a single controller and achieve unlimited multiple solutions (Li et al. 2004). The following section will identify challenges that need to be addressed before developing any meaningful solutions to the projected complexities of future distribution grid control.

1.2.1 Rating the DSTATCOM

This is a challenge for economic reasons from the manufacturers perspective, in that DSTATCOM ratings should be based on voltage deviations at the point of common coupling (PCC) rather than on the magnitude of the load. Equipment manufacturers often include a mismatch between equipment rating and the actual plant rating, so that compensation devices (i.e. DSTATCOM) would have to do extra amount of work to perform some mitigation functions. Consequently, control system designers can reverse this challenge through innovative control designs by trying to improve the ride-through capabilities of DSTATCOM.

1.2.2 Intrinsic Harmonic Generation

Self harmonic contribution nature of the DSTATCOM poses the other challenge. Modular design approaches have been successful in the past at the expense of space and cost to tackle this challenge. Similarly, the use of H-bridge and multilevel converters has also been used to manage the effect of total harmonic distortion (THD) and improve PQ control to considerable levels. However, they are disadvantaged mostly for their off-line implementation involving dedicated simulation studies based solely on approximated linear models. In order to reflect real-time characteristics of a distribution system, serious consideration of nonlinear model simulations has to be made, which must also include reasonable choice of a modulation index (M) that could substantially counter the switching effect of the commutative insulated gate bipolar transistor (IGBT) switches. As a known fact, a high value ($M \approx 1$) is normally recommended since it produces smooth output response which means low internal harmonics, but at the same time increases the system gain which causes overshoot. Therefore, there has to be some careful trade-offs while making the control decisions. Substantial reduction of the THD content must remain within the 5% allowed by the IEEE 519 standard.

1.2.3 Extrinsic Harmonic Generation

The fact that modern customer's loads are majorly becoming more sensitive and nonlinear in nature means these constitute one source of external harmonics generation. The integration of distributed-generation (DG) systems as renewable energy sources (RES) coupled with neighbouring operational equipment such as protective relays and circuit breakers constitute another. These components continuously keep shifting the operating points of the system and at the same time imposing model parameteric changes. Thus, the conventional controllers which are mostly designed upon linear modelling and manual tuning would not be able to reject all the disturbances at once. This trend would lead to steady state malfunctioning of the network. To reverse this challenge, tuning of DSTATCOM controller will be considered in this thesis.

1.2.4 Control of the Switching Angle

One most important challenge in DSTATCOM is the optimisation of its input control signal. Effectiveness of any control scheme applied is a measure of its ability to control desired variables with optimal and yet minimal control effort. This can be easily achieved in an open-loop approximated linear model control, if the plant and

its environment present no uncertainty. It rather becomes difficult in practice, as the power system being controlled is nonlinear, especially from an online perspective requiring regular updates. In this situation, a significant reduction in the magnitude of the control variable is assumed due to switching nonlinearities. Conversely, a larger control effort is often necessary to compensate for deficit in the desired output. To face this challenge, a fast optimisation algorithm needs to be sought through a carefully chosen performance index extensively designed to deal with the system error plus the derivative of the error to optimise the control output, i.e., the switching angle.

1.2.5 Heuristic Rule-Based and Other Solutions

Fuzzy logic controllers (FLCs) are rule-based systems which are applicable to poorly understood nonlinear systems, occasionally controlled by human operators without knowledge of their underlying dynamics. The major building block of an FLC system is fuzzy rule base (RB) related through an inference engine by means of a fuzzy implication and compositional procedure. The RB is normally formulated in linguistic terms, in the form of *if... then* rules, and there are various techniques for deriving them. Generally, the correct choice of membership functions for the linguistic variable plays a significant role in the performance of an FLC within the chosen universe of discourse, by providing perfect representation of the expert's knowledge through robust linguistic control rules (Herrera et al. 1995).

Manual trial-and-error design methods have been the first traditional ways of designing fuzzy controllers. The approach relies on the development of rule bases from the expert's knowledge data base. These schemes are normally indirectly (non-automated mode) used as supervisory controllers at high level (as in a distribution system), while low-level controllers are assigned to the plant's stabilization needs. Successful applications of assorted fuzzy controllers have been recorded after its discovery by Lotfi A. Zadeh in 1965. For example, (Li & Häule 1996) have used it in the area of fuzzy control in conjunction with PID, using genetic algorithm (GA) as well as simulated annealing (SA) based parameter tuning. Optimisation problems have also been respectively tackled via GA, SA and nonlinear model predictive control (NMPC) by (Li 1995) and (Li & Häule 1996). The work of Procyk and Mamdani, (1979); Yamazaki, (1994); Brown and Harith, (1994) and Noriega and Wang, (1998) have covered the implementation of self organising and self tuning adaptive neuro-fuzzy inference system (ANFIS). Other miscellaneous examples comprising of learning neuro-fuzzy controllers, classified systems, information retrieval and data base querying, pattern recognition and image processing have all been developed by Ichimura et al., (1995); Fukada et al., (1993); (Herrera et al. 1995); and Alexandra et al., (2008). However, in its application to power systems, a comprehensive overview presented in Tomsovic, (2000) has categorised the

scope to; power system stability (PSS), flexible ac transmission systems (FACTS) devices in the form of thyristor and static VAR compensator control, induction motor control, variable speed drive control, and PWM inverter control of a wind energy conversion system. Unfortunately, these solutions failed to deliver the required results in a distribution system which is ever increasing in complexity with contending nonlinear characteristics. This may be due to poor system designs or inherent inability to deal with such nonlinearities.

1.3 Proposed Solutions to PQ Problems

To properly account for these nonlinearities and overcome these challenges, this thesis advances two developments for DSTATCOM control.

1.3.1 Automation of Rule-Based Designs

Fuzzy logic can use linguistic or knowledge base to describe control surfaces in a continuous manner as against the bi-logical way of describing them in classical control methods, to tackle complex nonlinear control systems. An intelligent learning loop will thus be included as an outer supervisory loop in addition to the existing feedback loop for automation design as well as for online control. This will be achieved by extending the manual CAD simulator to computer-automated-design (CAutoD) designer in this thesis.

1.3.2 Model Predictive Control

Model predictive control relies on a dynamic model and online optimisation based on this model, instead of a rule base. This way, a complex nonlinear control problem can be simplified for online operation. A prediction scheme, however, can be integrated directly with the system I/O data and hence offer direct online control sequences without recourse to model presence. This scheme is thus termed “model-free predictive control” (MFPC) e.g., (Barry & Wang 2004). For PQ control applications, MFPC can be effective with a low control effort on the switching pattern of the converter IGBT switches at high switching frequencies. Given a right step-size, the method can also improve setpoint following performance and drastically reduce the THD on the output waveform. A new DSTATCOM control design scheme will be developed in the thesis to remove the need for costly multilevel implementations.

1.4 Contributions of the Thesis

1. This thesis investigates the viability of an improved conventional PD control design for DSTATCOM for the first time, and establishes that re-routing the derivative term through the feedback path produces a more efficient controller with a new value for the filter coefficient. Application of a number of manual tuning techniques during the design process accords the realisation of the initial control parameters needed for intelligent control implementation using fuzzy logic control in a nonlinear model.
2. The new PD scheme is then realised in a fuzzy controller based on a simplified Macvicar-Whelan matrix of a three-by-three ruled base. This is also the first time such design was applied in DSTATCOM control. Its closed-loop performance proved superior to both conventional PI and PD controllers in terms of setpoint following and disturbance rejection.
3. In the bid to automate the DSTATCOM controller design, the functionality of the manual CAD of FPD was extended to an EA based CAutoD scheme. The design engineer has an option of choosing between a set of multiple objectives and come up with controllers suitable for a control scenario at hand.
4. Finally, a novel model-free predictive controller is designed to overcome the system identification expenses experienced in conventional MPC schemes. In a direct online predictive scheme, the controller uses an a-priori simplex non-gradient algorithm in solving power quality problems with dispatch. Its model-free, non-gradient features make it unique from all other techniques in applying current control signals to predict future profile of the control variable.

1.5 Thesis Outline

In Chapter 2, a review of DSTATCOM control is performed. It covered applications of both conventional and artificial intelligence based techniques. It begins by laying a foundation on DSTATCOMs system configuration and model analysis in the steady-state before actually dealing with existing control challenges and their possible future solutions. Following a review on the tuning concepts of Zeigler-Nichols and Cohen-Coon in traditional PID control, explanations are given on the tuning methods used for rule-based, EAs in an adaptive setup, and model predictive control designs.

In Chapter 3, a working model is validated using neural network training tool where the model error is determined as a necessary step to efficient controller design. To achieve

an optimum system design, the nonlinear plant is first linearised and simulated in open-loop around a number of established operating points using its first order Taylor expansion upon which the current designs are based. A comparative analysis is performed on the traditional P-I-D structures in DSTATCOM and their effects presented. Several tuning methods aimed at improving the PID are also explored. Integrator wind-up and derivative-kick issues as well as known sources for concern in PID controllers are investigated. The derivative-kick is remedied by re-routing the derivative term with a filter coefficient through the feedback path to form the PI-D structure. By zeroing the integrator, the improved PD term is then used to develop a fuzzy PD controller for evolutionary designs in Chapter 4.

Chapter 4 studies and evaluates the practical viability of an off-line simplified three ruled-base fuzzy system design which will eventually have its parameters accessed and updated through an EA based CAutoD interface. With this arrangement, the DSTATCOM should be able to practically commute reactive power compensation with the network and reduce the THD from the waveforms online, which will be demonstrated in Chapter 6. By way of automating the procedure, the chapter presents a way of extending the CAD simulator to a CAutoD designer.

In Chapter 5, a novel model-free predictive controller for direct online DSTATCOM optimisation is developed as an optional smart solution to power quality problems. The new scheme is based on the operating principles of traditional MPC control used in a supervisory mode. The chapter also discusses the major advantages offered by such scheme which made it suitable to distribution system control application. Rigorous tests concerning some parametric tuning effects initially performed on the model-based technique leading to the new model-free design are fully discussed. An experimental model is also developed in this chapter from the SimPowerSystems software simulations.

Chapter 6 compares all the control methodologies advanced in the previous chapters in terms of their dynamic performance, i.e., setpoint following, rise time, and overshoots. In this chapter, a comparison of the performance of the chosen index with other measures of merit will be made, with correlations between time and frequency domain functions of the error and the error derivative inputs graphically established. The superiority of the novel MFPC technique will also be demonstrated and supported with tabular arguments. A final closed-loop system validation is performed to show a dramatic fit between the MFPC control scheme and the SimPowerSystems based simulation model.

In Chapter 7, conclusions of the thesis are presented with a highlight for further work. Particularly, the issues of integrating neural networks and fuzzy logic to the model-free concept are analysed. By way of conclusion, the chapter recommends the evolutionary

MFPC technique to the industry for its model-free reliance, fast computations, small foot-prints, low harmonics vis-a-vis low carbon emission, as well as cost effectiveness. Thus, giving an overall improvement in the ride-through capability of DSTATCOM to counter the major challenges surrounding it as listed in Section 1.2.

Chapter 2

Review of DSTATCOM Control for PQ Problems

2.1 Introduction

This chapter presents an overview on existing DSTATCOM technology and explores all the available control designs with their advantages and disadvantages in solving power quality problems. DSTATCOM system configuration coupled with its control challenges and trends have been extensively reviewed as relating conventional, rule based and modern control techniques. The chapter has also laid down a preamble to investigating modern and advanced intelligent controllers for optimal designs of DSTATCOM control used for this thesis. The difficulties of the existing techniques were subsequently evaluated and followed by recommendations on why evolutionary controllers are more suitable in solving PQ problems. A review table covering a ten-year period of various controllers applied to solving PQ problems through DSTATCOM has also been drafted in support of this research.

2.2 System Configuration

DSTATCOM is a shunt device configured through; IGBT switches with a range of frequencies between 2 – 4kHz, a coupling transformer, a dc capacitor link, and an external controller. Fundamentally, the voltage source converter generates controllable ac voltage source from stored energy in the dc capacitor link which appears behind the coupling reactance. Because the dc energy storage is shallow, it is thus not possible to exchange real power with the network. However, reactive power exchange is

accomplished by either injecting or absorbing reactive current at the point of common coupling (PCC) through the coupling reactance. Thus, the DSTATCOM can operate as an inductor when $|V_i| < |V_o|$ or a capacitor when $|V_i| > |V_o|$. But, there is no DSTATCOM action needed in a steady state operation for $|V_i| = |V_o|$. These exchanges improvise for any voltage deficiency that may have occurred as a result of dynamic reactive load demands or systemic disturbances. Despite lack of active power exchange, yet a small phase angle needs to be maintained between the ac supply and DSTATCOM output voltages to replenish the real power component necessary for guarding against losses (Singh et al. 2006). Through complicated electronic circuits based on for example, instantaneous power balance theory (Bukata 2010), measurements of current, voltage, and power are performed and fed-back for comparison with some pre-determined reference values as in appendix D. The differences, otherwise called error signals are passed on to the controller. The controller takes corrective decisions and then sends out a control command (α) onto the switching pattern of the DSTATCOM which issues a stabilised output voltage illustrated in Figure 2.1.

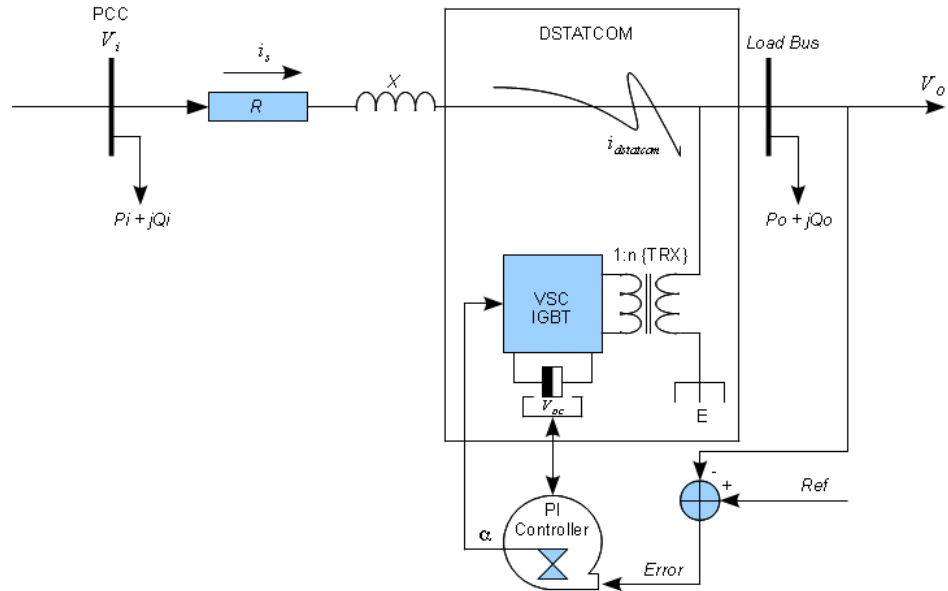


Figure 2.1: Shunt DSTATCOM with a PI controller

2.3 PQ Challenges and Trends

Superiority of DSTATCOM over the static VAR compensator as a practical solution to power quality issues cannot be overemphasized. Although both perform the same functions, DSTATCOM generates more reactive power at lower voltage ranges because its maximum capacitive power generation decreases linearly with system voltage. Thus, guaranteeing rapid response ($< 10ms$) to faults at higher capacitive reactive power and zero-delay. While, this variation goes proportional to the square of the voltage in SVC

and takes about $40ms$ due to thyrister switching. These advantages, added to small footprint and low cost, make the DSTATCOM practically more attractive than the SVC (Hingorani 1991).

Since its discovery as a custom power device (CPD) along with DVR and UPFC in 1980 by EPRI, DSTATCOM has gained wide applications (due largely to its commutative ability provided by the IGBT switches) at the custom and distribution voltage levels, and as a statcom at the transmission corridor (Hingorani 1991). Through the years, several schemes have been employed in DSTATCOM control using classical methods as in (Sanchez et al. 2009); (Ndubuka 2011); (Fan et al. 2009); and (George & Mishra 2009); and modern control theories, see for instance (Pal & Swarup 2008); (Jung et al. 2003); (Jouanne 2001); (Selvan & Anita 2011); and (Goyal 2008). A recent survey revealed that the proportional and integral (PI) controllers are now generally being applied for inner and outer DSTATCOM control loops (Bukata & Li 2011). The dominance is largely because bulk of industrial PID users appreciate more simplicity and short term profit maximisation objective rather than economies of scales and profit maximisation objectives in the long term (Ang 2005).

In challenging the survival of the traditional PI controllers in a smart grid setting, over 25 papers were recently delivered at a smart grid symposium at University of Strathclyde in Glasgow. Aimed at evaluating prospects of potential energy devices in terms of smart grids operations and control. With greater academic research attention now being focused in this area, research and development (R&D) projects towards this goal have been soaring since 2001 as initiated by EPRI Intelligrid (Brown 2008). Other recent contributors include some large corporations such as ABB, Siemens, S & C Electric Company, and Hitachi Europe. All in their bid to integrate distributed generation (DG) and renewable energy sources (RES) onto the distribution grid at a pilot scheme within the UK using DSTATCOM, in accordance with the EU 20 – 20 – 20 goals in climate change (Engineering 2011).

However, the design trend here, at which those corporations failed short to envision entails developing intelligent DSTATCOM module through evolutionary algorithms and advanced control methods for optimum voltage regulation at the PCC. This design must be able to automatically handle optimal reactive power exchange with the network to adequately resolve PQ issues as may be presented by integrating DGs and RES to it. The combination of these two tasks is currently being referred to as Volt-VAR optimisation in the smart-grid circle. As a central theme to my thesis, I intend to face the challenge through a ground-breaking research of advanced evolutionary algorithms (EA) based “ft3pak” developed at the University of Glasgow by intelligent systems group, and simulate the world’s first model-free predictive DSTATCOM controller.

2.4 Existing PQ Control Schemes

Static VAR compensators in conjunction with capacitor banks, recloser circuit breakers and surge arresters have for over sixty years been used to solve transient related PQ issues (Elnady & Salama 2005). The solution was improved by introducing DSTATCOM in 1980 to intervene in both transient and steady state network operations. The steady-state is one at which tougher PQ disturbances like sags, flicker and harmonic distortions tend to maximize network attacks. A detailed literature reporting on DSTATCOM control along other FACTS devices using standard simulation packages such as MATLAB, PSCAD, and EMTDC can be found (Singh et al. 2008). However, the soaring cost of PQ problems are becoming unbearable to the customers, utilities and other stake holders in the power sector. It has been reported that poor PQ annually costs EU industry and commerce, and the US economy about €10 and \$100 billion, respectively (Chapman 2001*b*). Hence, the search for more cost effective and robust DSTATCOM controllers capable of providing the required ride through for the future grid soon escalated. In the following sections, an overview of the control strategies applied in DSTATCOM for improving PQ and their undermining difficulties for the period 2001 – 2011 is presented. Altogether, 54 such references were reported (Bukata & Li 2011).

2.4.1 PID Control

The proportional-integral-derivative controller has gained popularity in industrial applications since the inception of Elmer's ship autopilot in 1911 (Ang 2005). This success was particularly attributed to its ease of implementation and accessible user friendly Ziegler-Nichols (ZN) tuning criteria. The reader is again referred to (Ang 2005) for a comprehensive list of patented PID tuning rules. As determinants of continuous system operation and its ability to reject disturbance, stability and robustness are the two most desirable tuning objectives to be realized in any control routine. Although these conditions may differ from linear to nonlinear systems, starting at no-load to full-load conditions. So far, the only PID application recently made in the open literature for studying control performance of the DSTATCOM was presented by (Xing-ping et al. 2009). In chapter 3, I revisited the use of some of these techniques in various PID design architectures with the aim of exploring their performances and lay a basis for my evolutionary designs. This makes the choice of an efficient tuning method prudent in this work, for which Table 2.1 is dubbed to give a summary guide on the efficiencies of these types of techniques.

Table 2.1: Summary Guide to Traditional Tuning Techniques

Chapman (2001*a*)

Tuning Technique	Advantages	Disdvantages
Manual	Possible online and requires no maths.	First-hand experience is required.
Ziegler-Nichols	Possible online and it is well proven.	Trial-and-error based, often very aggressive and causes process upset.
Cohen-Coon	Applicable on good process models.	Possible offline, restricted to first-order plants, and requires some maths.
Software Tools	Possible online or offline. Often incorporates sensor and actuator analysis. Simulation is possible before download	Very costly and involves training.

2.4.2 Fuzzy Logic Control

Fuzzy logic control is an aspect of computational intelligence which was first introduced as fuzzy set theory by Lotfi Zadeh in 1965. It was later applied by Mamdani to motor control in 1974. Since then fuzzy control has found significant application in various engineering capacity including the power industry. A bibliography on applications of fuzzy set theory in power systems from 1994 – 2001 is covered in (Bansal 2003). The ability to deal with time-varying or complex and nonlinear systems, in which human experience is significant gives it an edge over loads of conventional methods. Various regimes of fuzzy-PI, fuzzy-PD and neuro-fuzzy controllers have been successfully developed for the DSTATCOM to solve PQ problems, for example; (Bano et al. 2010), (Deniz et al. 2010), (Zhu et al. 2009), (Xu et al. 2010), and (Coteli et al. 2011). The reader is here referred to (Chowdhury 1998) for a list of successful applications of fuzzy control.

Despite these qualities, fuzzy controllers still suffer an inherently massive drawback due to manual tuning. This attracted proponents of fuzzy control applications to use various evolutionary techniques, particularly genetic algorithms (GAs) as a means for optimising fuzzy production rules and membership functions as demonstrated by (Ng 1995). However, a few exceptions like the neuro-fuzzy breed exhibits some automation features in the form of self-tuning mechanism. A more serious drawback evident in fuzzy systems application is in prohibitive computational burden to large rule base (RB). The RB tends to increase exponentially with increase in the number of inputs, especially in that all rules would normally have to fire (Passino 1998). These disadvantages rather made fuzzy control application to power system distasteful.

2.4.3 Artificial Neural Networks

Neural networks (NN) can be used as controllers through multi-layered or single-layered perceptron networks for function approximations. Back-propagation algorithm and its variants serve as the main basis for training the perceptrons. The configuration is placed in either feedback or feedforward loop of the desired control system. However, care must be taken during training to ensure that there is no mismatch between the network of the perceptron and the training data as it would hinder the system from being adoptive to new situation i.e., generalization. Neural networks are matured in power systems application as intelligent nonlinear emulators based on the popular black box concept of input-output relationships. They are equipped with training algorithms which enhances their learning capacity to perform as closely as possible, the set example, through fixed “weights” and “bias” terms from (Li & Häule 1996). They have particularly been used around the world in power systems for load forecasting function (Yang et al. 2007). Despite this wide applicability, NN exhibits a large permutation of training parameters which causes snag during feedforward time-series forecasting that is not conducive for “generalization”. This criterion increases the sensitivity of the network to a number of choices e.g. size of training sets as detailed in (Alvas da Silva 2002). Nevertheless, applications particular to power quality control using the DSTATCOM are reported in (Yang et al. 2007), (Karami et al. 2008), (Singh et al. 2005), and (Srivastava et al. 2009). However, the controllers designed using the NN scheme are often good for tolerating small perturbations only. Conversely, they have limited capacity to providing global control in a complex smart grid setting. Hence, the search for advanced control techniques such as the model predictive control (MPC) introduced below become imperative. Such a technique offers ideal responses to large perturbations and are reserved as the main contribution of this thesis.

2.4.4 Model Predictive Control

Model predictive control (MPC) has been recognised as the only more advanced control strategy than the well established PID control to be relevant for industrial applications. It has changed the ways industrial control systems were developed as well as conducting research activities in the area (Lawrynczuk 2007). Better known in slow petrochemical industry applications, the MPC is now gaining high penetration into other sectors as an advanced control technique due to the boost in modern high speed digital processors (Maciejowski 2002). Its unique features of low control update rates, handling actuator constraints and the ability to operate complex control systems closer to their limits makes it suitable for online applications. In PQ prediction, the current DSTATCOM outputs are subjected to some reference signal values based on past inputs in order to

calculate future outputs. This way, any waveform anomaly would have been anticipated and corrected before a disturbance occurs to the customers device. Although there was no serious application of the MPC throughout the literature for PQ control. However, the single application based on Smith predictor on harmonic prediction control for time delay realization and cancellation in DSTATCOM has been reported (Ruixiang et al. 2009).

Table 2.2 is presented at this point showing the pattern of control solutions applied to various PQ problems through DSTATCOM from 2001 – 2011 (Bukata & Li 2011). Based on its advantages and for the fact that it has never been used in the open literature for PQ control marks my motivation for using the MPC in this thesis.

Table 2.2: Controllers Applied to PQ Problems between 2001-2011

(Bukata & Li 2011)

(Refer to Table 1.1 for Details on PQ Problems)

PQ Problem \ Controller	PID	PI	PD	FPI	FPD	NN	MPC
Transients	✓	✓	✗	✓	✗	✗	✗
Interruptions	✗	✓	✗	✗	✗	✗	✗
Sags/Swells	✗	✓	✗	✓	✗	✓	✗
Over/Under Voltages	✗	✓	✗	✓	✗	✗	✗
Harmonic Distortion	✗	✓	✗	✗	✗	✓	✗
Flicker	✗	✓	✗	✗	✗	✓	✗

2.5 Summary

This chapter presented the working principle of DSTATCOM and its associated control methods. An exhaustive literature review concerning the control applications has been fully covered for the period 2001-2011. The literature shows that DSTATCOM has replaced the SVC as the most widely used among the custom power devices, it derives its universal acceptance for model flexibility, cost effectiveness, small footprint and rapid response characteristics. While the literature suggests a large amount of research work conducted using modern and artificial intelligence techniques, the DSTATCOM embellishes the simplicity and user friendly features of embedded PI controllers to its PQ functions. In other words, the PI controller is the only practically viable regime found today providing PQ solutions. This is particularly true because most of the other

schemes cited are poorly designed, and are either cost ineffective in implementation or have high computational burden problem.

Moreover, the PI currently in vogue, being a linear controller is quite inappropriate for an increasingly complex and nonlinear smart distribution grid application. This may explain the reason why the academic proponents of the smart grid concepts maintain that the 20th century grid can no longer fit the 21st century grid demands. The trend increases research activities focused towards the development of smart energy devices through virtual power plants (VPP) which will ensure delivery of optimum voltage profiles to the customer's equipment with increased system reliability and stability in the most cost effective way.

Chapter 3

DSTATCOM System Analysis

3.1 Introduction

In chapter 2, it is recognised that because of their common non-automated characteristics, the rule-based and existing PID controllers are deficient in handling nonlinear plants such as DSTATCOMs which have continually changing operating points. This fact encouraged research activity into the future of the PID from (Åström & Hägglund 2001). The Ziegler-Nichols tuning technique this is built upon has particularly served as a major disadvantage for its practical limitations. Consequently, several tuning methods were advanced towards ameliorating these limitations see for instance, (Ng 1995); (Li & Häule 1996) and (Feng 2000). In this chapter, a thorough analysis of the DSTATCOM and its associated control structures is performed, where a table of system parameters was constructed from calculations defining all the static and dynamic components used for the design. An attempt has been made to improve PID tuning capability in line with optimum control system design objectives. This is preceded by analysis on a working model validation using neural network training tool in which the model error is determined as a necessary step to efficient controller design. A comprehensive analysis of the system states is performed in the steady state to ascertain a congruent model behaviour that will match real system. Modest formulation relating all parameters pertaining to dynamic and static components in the system are outlined. The nonlinear plant was initially linearised and simulated in open-loop around some established operating points using its first order Taylor expansion. Consequently giving rise to the first PID parameter set needed for my future designs to be calculated via closed-loop system simulation. Further investigations confirmed the integrator wind-up and derivative-kick as another source for concern in PID control design (Li et al. 2004). Hence, I reconsidered the derivative-kick and proposed a remedy by re-routing the derivative term with a new filter coefficient through the feedback path to form the

PI-D structure as in (Banzhaf 2000). The improved PD loop extract which was found to be faster with lesser ripples has been adopted in developing my fuzzy PD controller for evolutionary designs in chapter 4.

3.2 Open-Loop Analysis

Reference to appendix Figure A.1, which assumes DSTATCOM connected to a stiff bus capable of handling distant load disturbances represented by R_{dc} . Whilst the dc capacitor C is responsible for generating dc bus voltage V_{dc} , a needed balanced three-phase ac voltage $V_{s(abc)}$ can be outputted by appropriately firing the IGBT switches $S1 - S6$. Thus, ensuring efficient control of the current I_{abc} flowing through the line impedance R_{abc} and L_{abc} . Moreover, the best method for analysing balanced three-phase circuits in synchronous systems is by using the well known Park's transform to convert the three-phase voltages and currents into their abc/dq rotating frames. The direct-quadrature-zero (dq0) or zero-direct-quadrature (0dq) transformation is the mathematical means for this kind of analysis. In the case of balanced three-phase circuits, application of the dq0 transform reduces the three ac quantities to two dc quantities. Simplified calculations can then be carried out on these imaginary dc quantities before performing the inverse transform to recover the actual three-phase ac results. This transformation conveniently simplifies the control problem by; 1) presenting the system variables as dc quantities, and 2) decoupling multiple system variables to allow application of the classical control methodology. Availability of the SimPowerSystems software resident in Matlab/Simulink enables a user friendly environment to meet these requirements as a real time representation of the power distribution system.

Firstly, the nonlinear mathematical model of Eq. 3.1 is very common to the literature e.g., (Rashid 2001). This model characterizes the dynamics of the DSTATCOM (see appendix A for derivation). However, the reference used here defined the dq0 transform with respect to the rotor axis by first representing the quadrature axis current (i_q) rather than the direct axis current (i_d) as shown in the equation. Conversely, Eq. 3.1 can be simplified into Eq. 3.2 whenever $\alpha \Rightarrow 0$. That is, small values of α will make $\sin(\alpha) = 0$ and $\cos(\alpha) \approx 1$. Other assumptions made towards linearising this equation are zero harmonic generation and presence of an infinite parallel resistance.

$$\frac{d}{dt} \begin{bmatrix} i_q \\ i_d \\ v_{dc} \end{bmatrix} = \begin{bmatrix} -\frac{R}{L} & \omega & 0 \\ \omega & -\frac{R}{L} & \frac{m}{L} \\ 0 & \frac{m}{C} & 0 \end{bmatrix} \begin{bmatrix} i_q \\ i_d \\ v_{dc} \end{bmatrix} + \frac{V_s}{L} \begin{bmatrix} -\sin \alpha \\ \cos \alpha \\ 0 \end{bmatrix} \quad (3.1)$$

The system input applied to DSTATCOM is recognised as the switching angle α in radians. The output to the system is a voltage leading a reactive current component. The plant parameters used in simulation are specified a-priori according to Table B.1.

Model comparison was carried out in section 3.3.1 using the data obtained from the linearised model of Eq. 3.2 and compared against a first-order-plus-delay-time (FOPDT) model data implemented in simulink.

$$\begin{aligned}\mathbf{X} &= \mathbf{A}\mathbf{X} + \mathbf{B}\mathbf{U} \\ Y &= \mathbf{C}\mathbf{X}\end{aligned}\tag{3.2}$$

where

$$\mathbf{X} = \begin{bmatrix} i_q \\ i_d \\ v_{dc} \end{bmatrix}, \quad \mathbf{A} = \begin{bmatrix} -\frac{R}{L} & \omega & 0 \\ \omega & -\frac{R}{L} & \frac{m}{L} \\ 0 & \frac{m}{C} & 0 \end{bmatrix}, \quad \mathbf{B} = \begin{bmatrix} -\frac{V_s}{L} \\ 0 \\ 0 \end{bmatrix}, \quad \mathbf{U} = \alpha,$$

and

$$\mathbf{C} = \begin{bmatrix} -V_s & 0 & 0 \end{bmatrix}$$

The characteristics Eq. 3.3 of the system is given by the transfer function model comprising of three eigenvalues with a real negative pole and two negative complex poles. Positions of these poles confirmed DSTATCOM as a damped and stable system that can successfully be controlled using linear controllers as suggested in the literature.

$$s^3 + 2s^2 + s \left[w^2 + \frac{R^2}{L^2} + \frac{m^2}{LC} \right] + \frac{R}{L^2C} m^2 = 0\tag{3.3}$$

3.2.1 Power Exchange at the PCC

Appropriate level of power exchange (injection or absorption) at the point of common coupling is a function of the model's accuracy. There are linear and nonlinear modelling procedures available for determining this accuracy as illustrated in (Tewari 2002). However, for online control needs, application of the nonlinear model is made to represent most of the practical system's nonlinearities, and to isolate any involvement

of linear model approximations responsible for creating modelling errors between the models. The mathematical expressions relating the system current (I), real power (P), reactive power (Q), and the power or load angle (φ) to the system voltages used for this study are described as (Bukata & Li 2009).

$$I = \frac{V_i - V_o}{jX} \quad (3.4)$$

$$P = \frac{V_i V_o}{X} \sin \varphi \quad (3.5)$$

$$Q = \frac{V_i V_o}{X} \cos \varphi - \frac{V_o^2}{X} \quad (3.6)$$

where V_i is the input source bus voltage, V_o is the DSTATCOM output bus voltage, X the system impedance, and φ is the power or load angle between the input and output bus voltages measured in degrees.

Regarding this phenomenon, a preliminary study in Figures 3.1 to 3.4 is presented depicting the input-output relationships and the system states in determining how nonlinear actually is the DSTATCOM. The figures also provide us the chance to see the interaction between active and reactive power and the way they exchange at the PCC. By using the specifications of Table B.1 through Eqs. 3.4 - 3.6, the active and reactive powers are noted to relate according to a *sine – cosine* dynamic range shown in Figure 3.1. The DSTATCOM first acted in the capacitive mode by injecting positive VARs attaining its maximum (0.024 MVar) at a switching angle of -16 degrees.

The active power at this point (intersection) is seen discharging as the reactive support retrogresses until zero, whence the DSTATCOM changes to inductive mode (absorbing negative VARs) to a minimum of -0.024 MVar. At this time, the active component begins to build up by recharging the dc side capacitor to avoid total voltage collapse. This cycle repeats itself when the capacitor has been replenished and the reactive component turns capacitive ready for the next exchange support. As a consequence of this reactive exchange, the voltage is being supported throughout the operation cycle of DSTATCOM at the PCC as shown in Figure 3.3, which presents a progressing voltage from minimum to its maximum values, i.e., -220 to 220 volts, for a sinusoidal excitation. The Figure also potrays the somewhat linear relationship existing between output voltage and the switching input (α) in DSTATCOM (see Table 3.1). The trend is shown in Figure 3.4 where some selected switching angles are varied against time, the

voltage curves are seen to vary accordingly in a monotonic pattern. The relationship of the three system states (i_q , i_d , and v_{dc}) with α can be seen in Figure 3.2. Where i_q tends to decrease linearly with α as Q changes from capacitive to inductive mode in the range 100 to -100 amps. Similarly, v_{dc} also decreases considering the ac voltage magnitude as its initial value, spanning between 220 to -220 volts (in the opposite direction to v_{ac}). Thus, It can be inferred from the on-going that DSTATCOM is a small power device at its currently rated parameters.

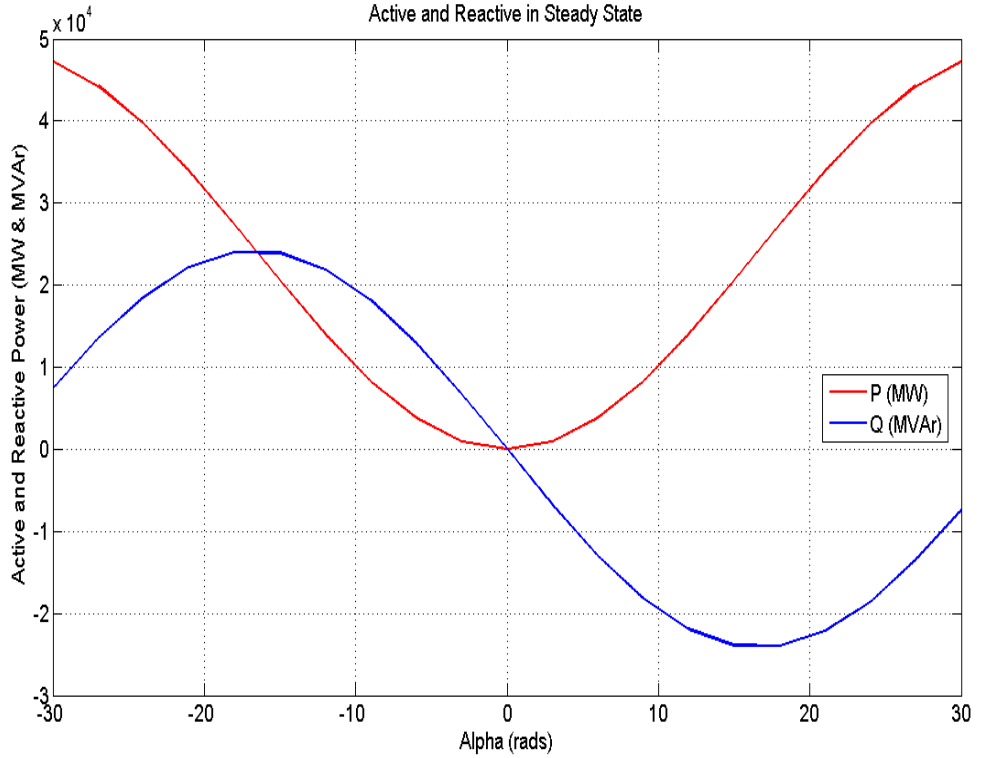


Figure 3.1: Active and reactive power in steady state

3.2.2 Steady-State Analysis

The steady state analysis of the power system is often conducted by studying the network interactions at the point of common coupling (PCC). In this direction, the use of trigonometric function is firstly made to eliminate the phase angle (φ) from Eqs. 3.5 - 3.6 (Larsson 2000), so that

$$\left(Q + \frac{V_o^2}{X}\right)^2 + P^2 = \left(\frac{V_i V_o}{X}\right)^2 \quad (3.7)$$

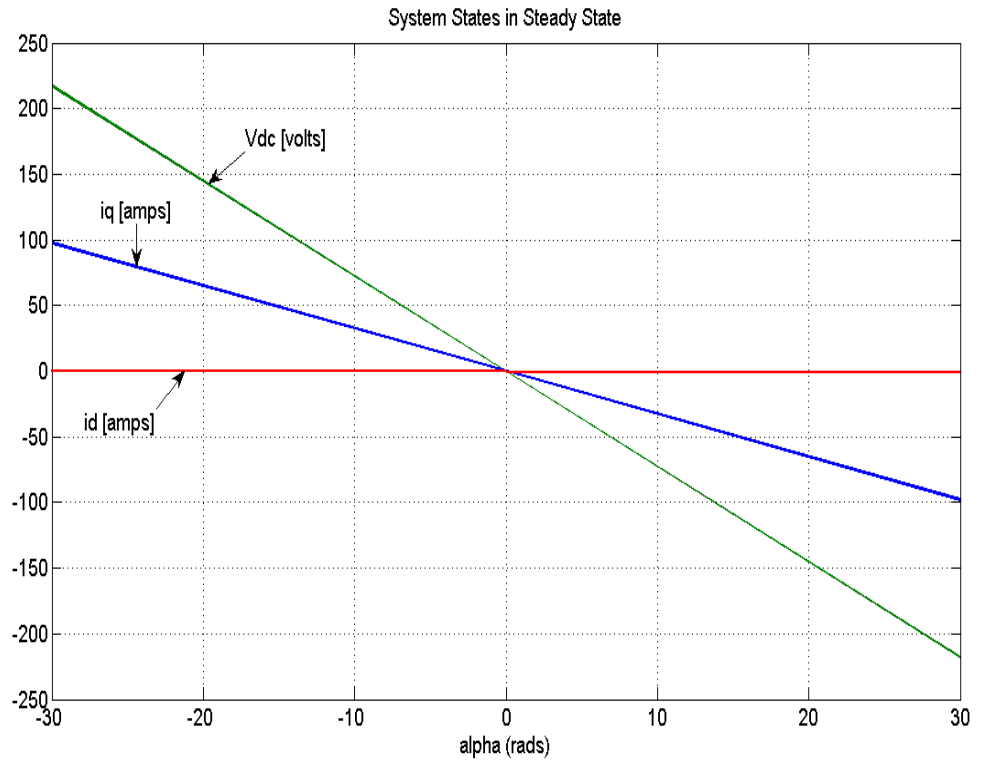


Figure 3.2: i_q , i_d , and V_{dc} in steady state

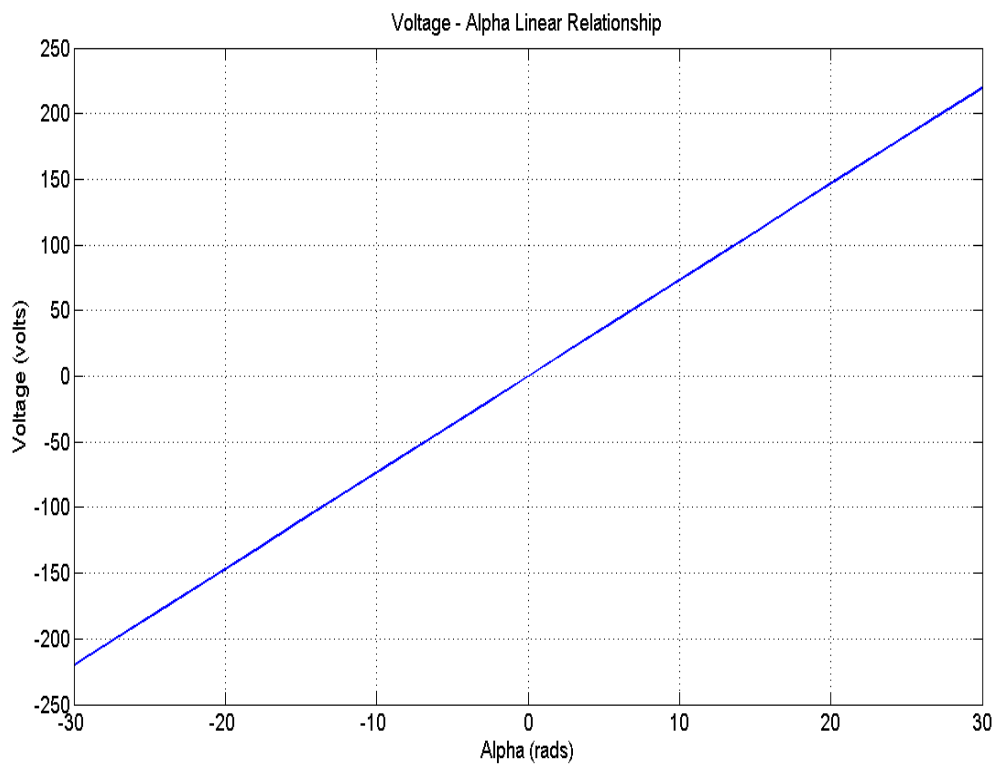


Figure 3.3: Linear alpha-voltage relation

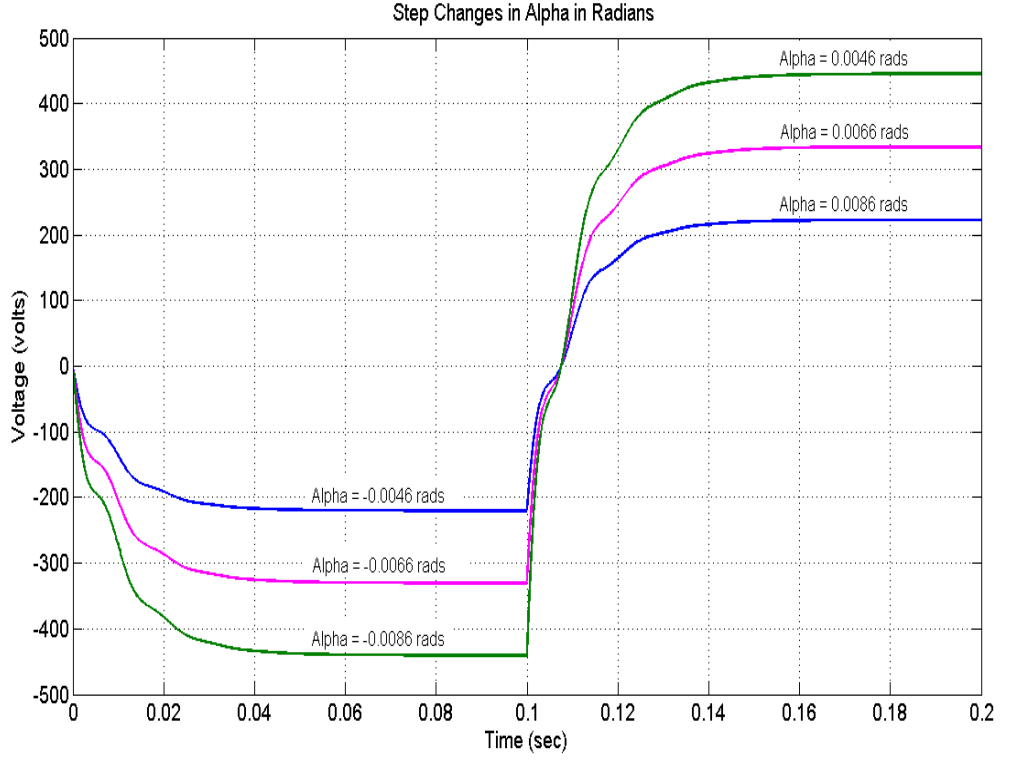


Figure 3.4: Step cahnges in alpha [rads]

Solving for V_o^2 gives

$$V_o^2 = \frac{V_i^2}{2} - QX \pm X \sqrt{\frac{V_i^4}{4X^2} - P^2 - Q \frac{V_i^2}{X}} \quad (3.8)$$

The solution has real positive parts if

$$P^2 + Q \frac{V_i^2}{X} \leq \frac{V_i^4}{4X^2} \quad (3.9)$$

Where the inequality represents the mode of the required reactive power at the PCC i.e., capacitive (injecting) or inductive (absorbing). Replacing the short-circuit power $P_{sc} = \frac{V_i^2}{X}$ at the PCC (receiving end), yields

$$P^2 + Q P_{sc} \leq \left(\frac{P_{sc}}{2} \right)^2 \quad (3.10)$$

It can be observed from 3.10 that

- The condition for maximum reactive power transfer occurs at $\frac{P_{sc}}{4}$ when $P = 0$.
- The condition for maximum active power transfer occurs at $\frac{P_{sc}}{2}$ when $Q = 0$.
- The voltage at the PCC (V_i) and the line admittance (G) are both proportional to the transfer limits.
- The transfer limit is increased by injecting reactive current into the PCC at $Q < 0$.

Since there is no active power exchange at the PCC due to line inductance, then the task reduces to the transfer of reactive power alone, which by implication also influences the line to accommodate active load. In order to obtain a positive solution to 3.8, the load is assumed characterised by an admittance (G) with active and reactive power receiving capacity given as, again (Larsson 2000)

$$P + jQ = V_o^2 G(1 + j \tan(\delta)) \quad (3.11)$$

where the angle δ denotes the power factor angle.

Thus, reactive current is injected into the system whenever $\tan(\delta < 0)$ i.e., leading power factor and reactive current is absorbed by the DSTATCOM when $\tan(\delta > 0)$ i.e., lagging power factor. By normalizing Eqs. 3.8 and 3.11 through

$$p = \frac{P}{P_{sc}}, \quad q = \frac{Q}{P_{sc}} \quad (3.12)$$

$$v = \frac{V_o}{V_i}, \quad g = \frac{G}{1/X} \quad (3.13)$$

The positive solution of 3.8 after normalization may be deduced as

$$v = \frac{1}{\sqrt{g^2 + (1 + g \tan(\delta))^2}} \quad (3.14)$$

The solution suggests that the line voltage ($v = 1$) is unity for any admittance ($g = 0$), and the load voltage approaches zero as the load admittance approaches infinity. This was achieved by setting the LHS side of Eq. 3.1 to zero, yielding

$$0 = \begin{bmatrix} -\frac{R}{L} & \omega & 0 \\ \omega & -\frac{R}{L} & \frac{m}{L} \\ 0 & \frac{m}{C} & 0 \end{bmatrix} \begin{bmatrix} i_q \\ i_d \\ v_{dc} \end{bmatrix} + \frac{V_s}{L} \begin{bmatrix} -\sin \alpha \\ \cos \alpha \\ 0 \end{bmatrix} \quad (3.15)$$

Assuming no reactive power compensation at the PCC, then a pure active load can only receive half the short circuit power as its maximum from the line according to 3.10. Figure 3.5 was derived by normalizing 3.11 showing the voltage/reactive-power dependency during steady-state operation after 40 samples. Output constraints imposed for this kind of operation within $\pm 10\%$ of nominal voltage (e.g., 220V), can be observed.

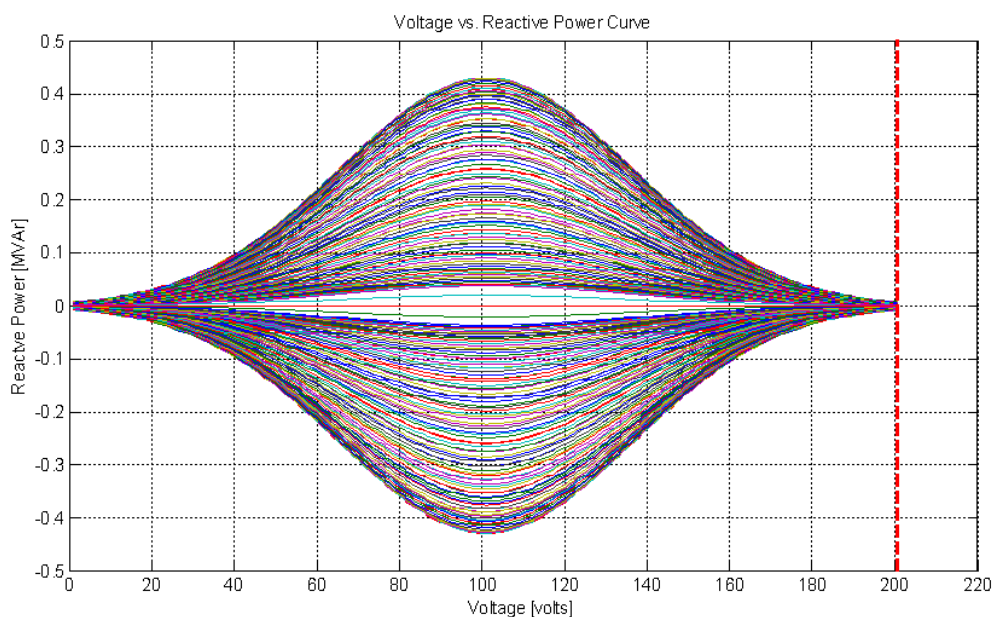


Figure 3.5: Receiving end voltage transfer Limit

The Figure shows a theoretical transfer limit of approximately 91.8% or 202V (red line), which is rather unacceptable for practical purposes (Larsson 2000). Thus, the need for robust reactive power compensation device at the load end to meet the practical transfer limit is obvious. This until now, is being supplemented locally by connecting capacitor banks at the load end. Unfortunately, capacitor switching is in itself another source of PQ problems. Well known standards, such as the IEEE 519 – 1992, IEEE 446 and IEC 61000 – 4 – 30 exist for controlling total harmonic distortion (THD) levels within the 5% range for continuous equipment operations (IEEE 1993).

3.3 Open-Loop Simulations

3.3.1 Model Comparison

Linear and nonlinear DSTATCOM model computations can be validated against simulation or experimentation model responses to check for mismatch through either time or frequency domain data. Here, a neural network training tool is used with 116 epochs to graphically fit and compare the mathematical plant model against an approximated first-order-plus-delay-time (FOPDT) model in Figure 3.6. Neural networks have been trained to accurately perform complex functions in various fields, including pattern recognition, identification, classification, speech, vision, and control systems (MathWorks 2009a).

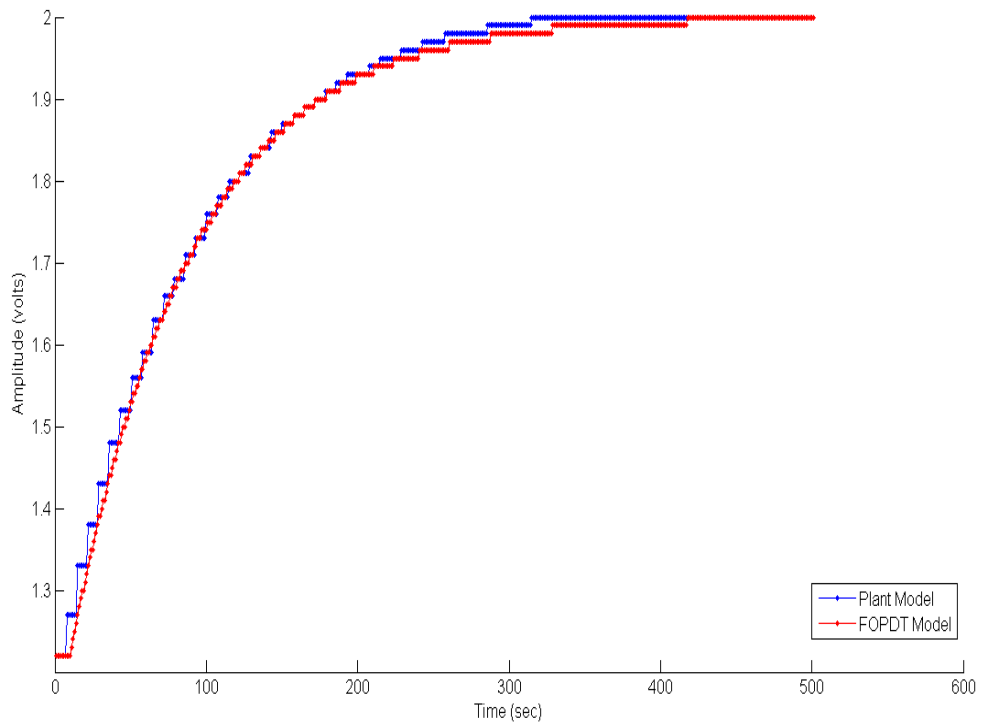


Figure 3.6: Model comparison

Basically, this method statistically correlates the coefficient of determination (R^2) of the fitness through model errors. High values of R^2 denote poor model fitness which does not guarantee good control predictions or other engineering surveys. A residuals analysis was performed at each combination of the fitted model, and the corresponding response was calculated from the n^{th} observations of the data set which was initially generated from the PIDEasyTM software as

$$e_n = r_n - f(x_n; k) \quad (3.16)$$

where r_n is the n^{th} response in the data set and x_n is the vector of variables at time vector \mathbf{k} . It is observed from Figure 3.6 that the residuals yielded a reasonable reduction of the random errors.

3.3.2 Locating Operating Points

The nonlinear DSTATCOM model was simulated in the open-loop to gain more insight into the input-output relationship of the system. A step input signal sampled at 5μ seconds was applied aimed at producing a response in consonance with the IEEE std $\pm 10\%$ of the nominal consumer's nonlinear load voltage. After 10 such runs, the result was compiled in Table 3.1 showing an almost linear relationship between the input switching angle (α), and the output voltage (V).

The response in Figure 3.7 shows the dynamic behaviour between the two models around some established operating points. It can be observed that the DSTATCOM is not absolutely nonlinear and the linearization process is a powerful means of analysing the nonlinear plant in helping better understanding of its dynamics. This way, optimisation of a custom voltage profile within the quoted international standard range of $\pm 10\%$ volts can be relatively achieved through suitable control regimes.

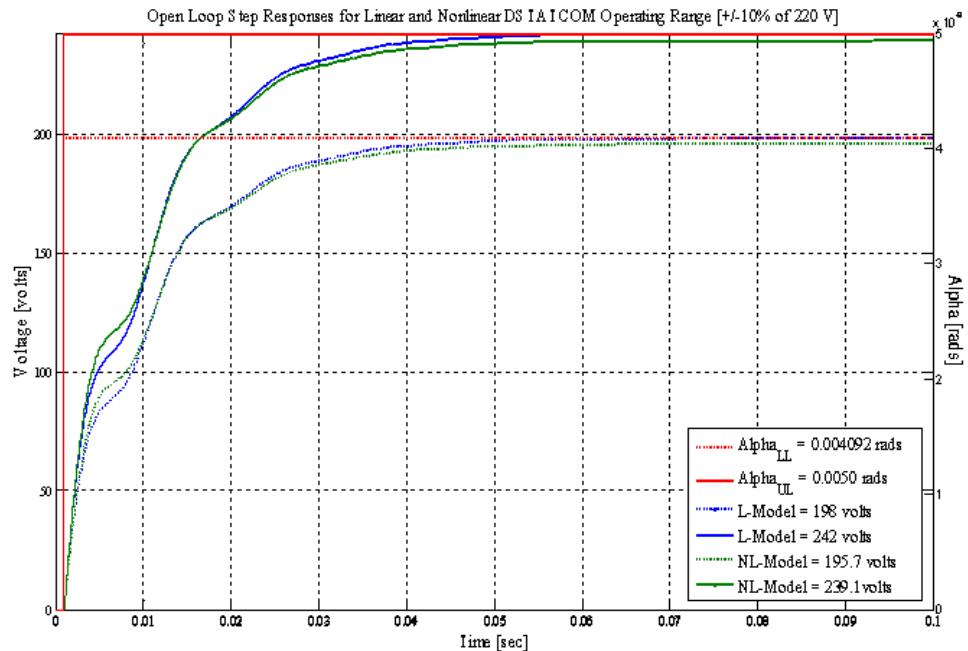


Figure 3.7: System operating points

Table 3.1: Voltages with varying alpha inputs

$\alpha(rads)$	0.0046	0.0066	0.0086	0.0106	0.0126
$V(volts)$	220	320	416	513	610
$\alpha(rads)$	0.0136	0.0156	0.0176	0.0196	0.0216
$V(volts)$	658	755	850	948	1044

3.4 Analysis for DSTATCOM PID Control

Reference to the generic closed-loop circuit in Figure 3.8. Simulating the circuit using a fixed structure PID controller with 13 samples, produced the results presented in Table B.8 establishing the best design for the value of ρ . Correlation between the feedforward positioned derivative and feedback re-routed derivative is made in terms of system error, overshoot and the rise-time with variable filter coefficient ρ . It has been observed that the system becomes unstable for any value of $\rho < 3$ as shown in Figures 3.9 and 3.10. Observations revealed that the percentage overshoot is maintained at 29% and 34% throughout from $\rho = 3 \sim 30$ while the system is stabilised. However, the rise-time exhibits some ringing transients in the conventional case at $\rho = 3, 4,$ and 5 as in Figure 3.11, although it is shown to improve in the new scheme in Figure 3.12. On the other hand, the error in both cases was zeroed, but seemed to jump above the unit magnitude before settling after about 27 seconds. The speed then starts to depreciate with $\rho \geq 6$ in the conventional scheme and begins to appreciate in the new scheme until $\rho = 11$ (when it reaches its best), again as revealed in Figure 3.12, achieved through a 220 base voltage. Thus, confirming $\rho = 11$ as the new best value offering the fastest rise-time of 0.896 seconds.

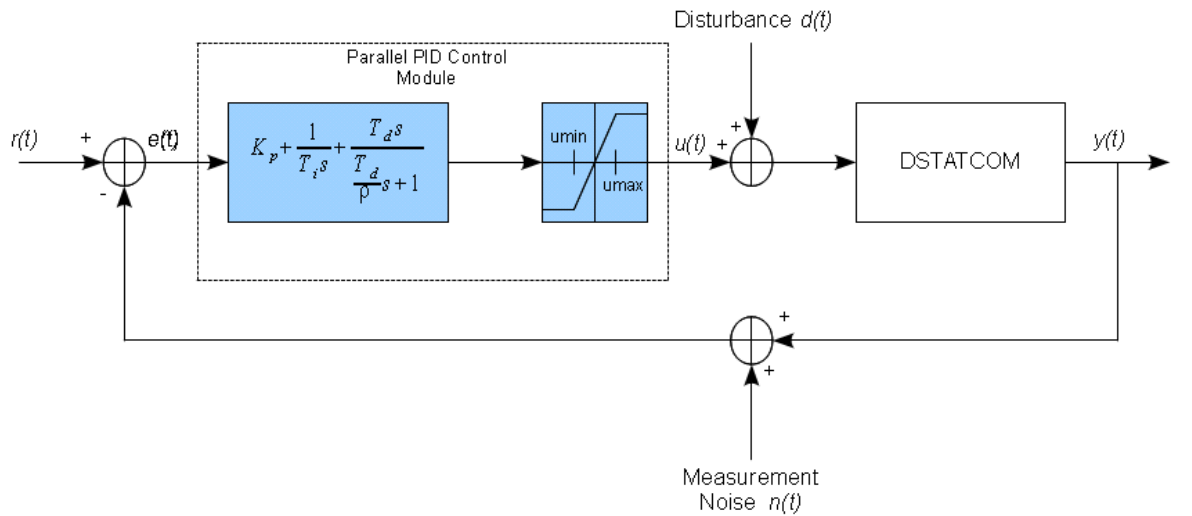


Figure 3.8: Closed-loop circuit

The PI controller is commonly used for voltage regulations in DSTATCOM (Wenjin

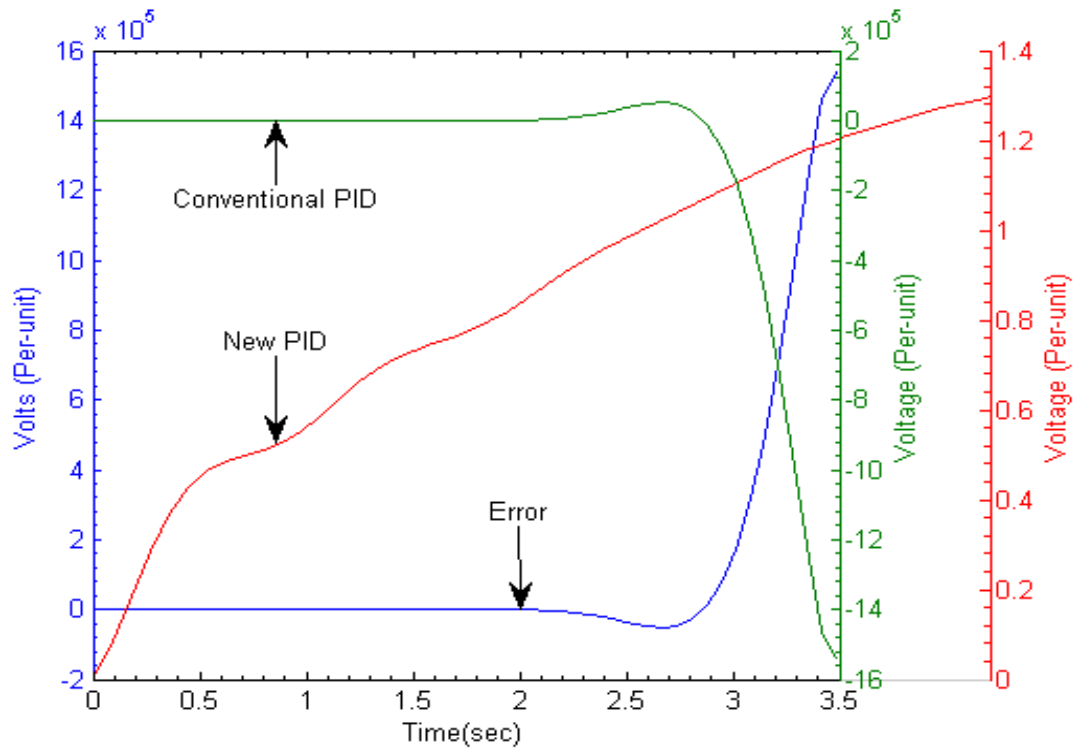


Figure 3.9: Unstable DSTATCOM
 $\rho = 1$

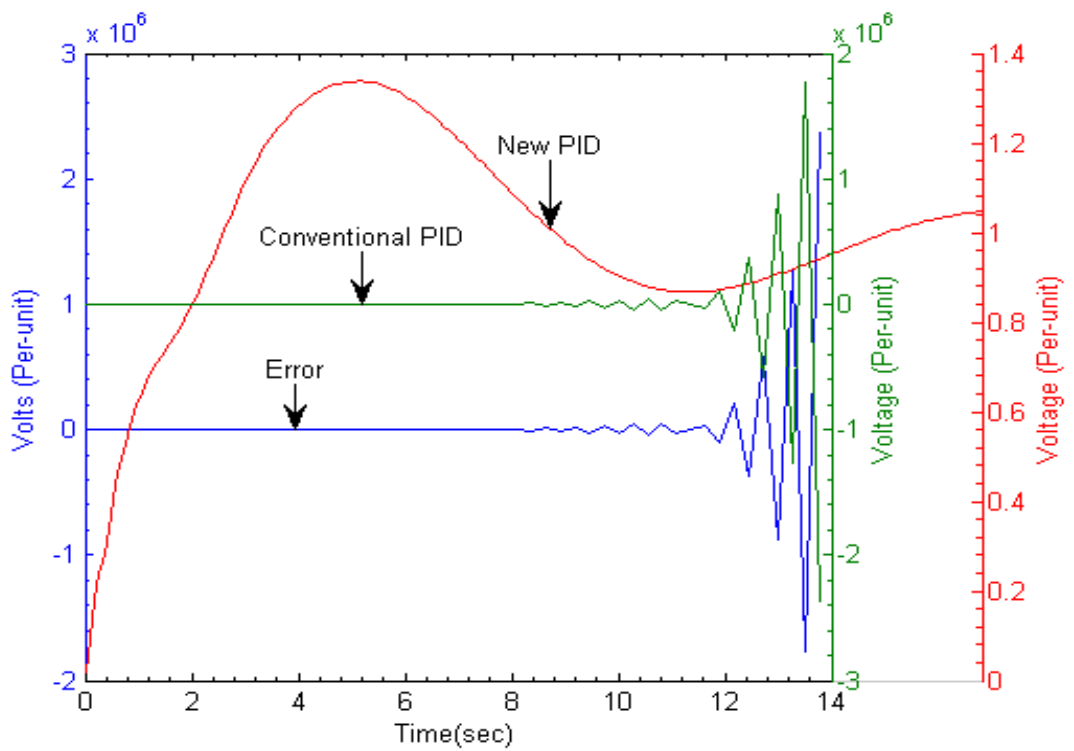


Figure 3.10: Further unstable DSTATCOM
 $\rho = 2$

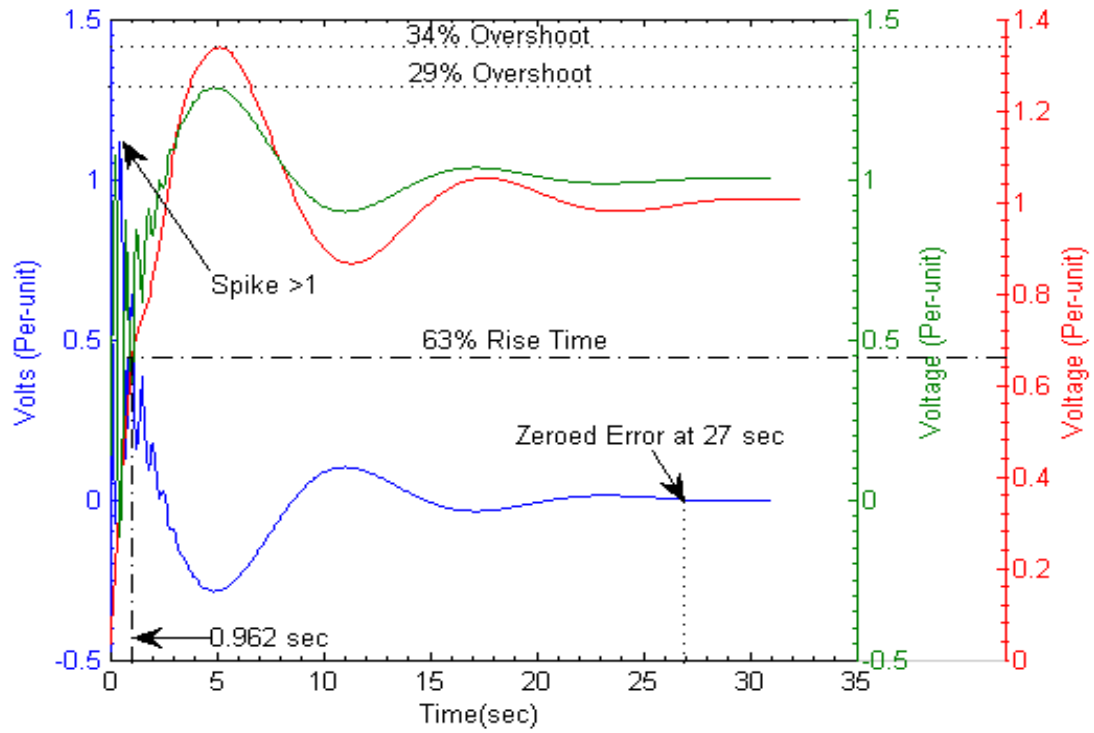


Figure 3.11: Correlated PIDs
 $\rho = 3$

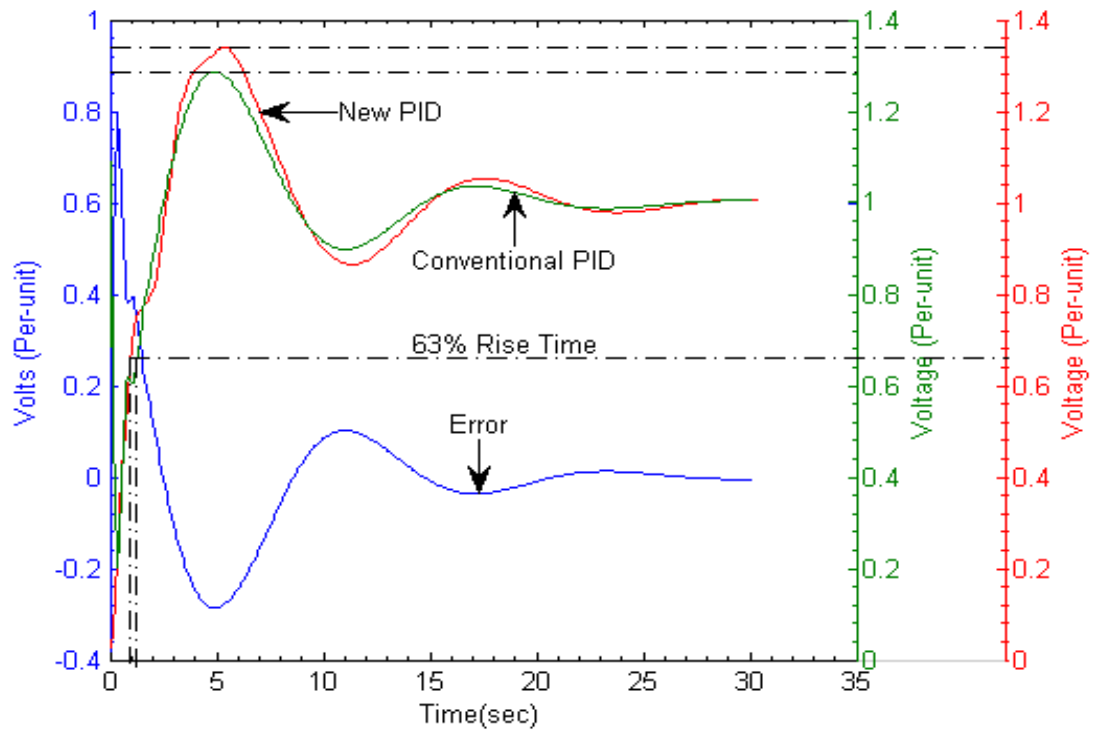


Figure 3.12: Further correlated PIDs
 $\rho = 11$

2010) and (Singh et al. 2005). Yet, using such a linear controller does not always account for the unobserved system states and changing operating conditions of the nonlinear system. Moreover, the integral action always introduces a phase lag which slows down loop recovery due to disturbances, and causes actuator saturation known as “windup effect”. Remedies to these type of problems already exist, see for instance (Li et al. 2004). Close observations revealed that, the near-zero real pole suggests the system is at the brink of an integral action and hence the steady-state enhancement via a PI integrator can as well be omitted.

3.4.1 Effect of the Proportional Term

Presence of the proportional (P) term increases overall system gain and reduces steady state error at the expense of large overshoots. During PID design, the parameter K_p is continually tuned manually in closed-loop, till it is just large enough to destabilise the system as $T_i \Rightarrow \infty$ and $T_d \Rightarrow 0$. This effect is investigated in the closed-loop response of Figure 3.13, as K_p varies from 0.1 to 1.0.

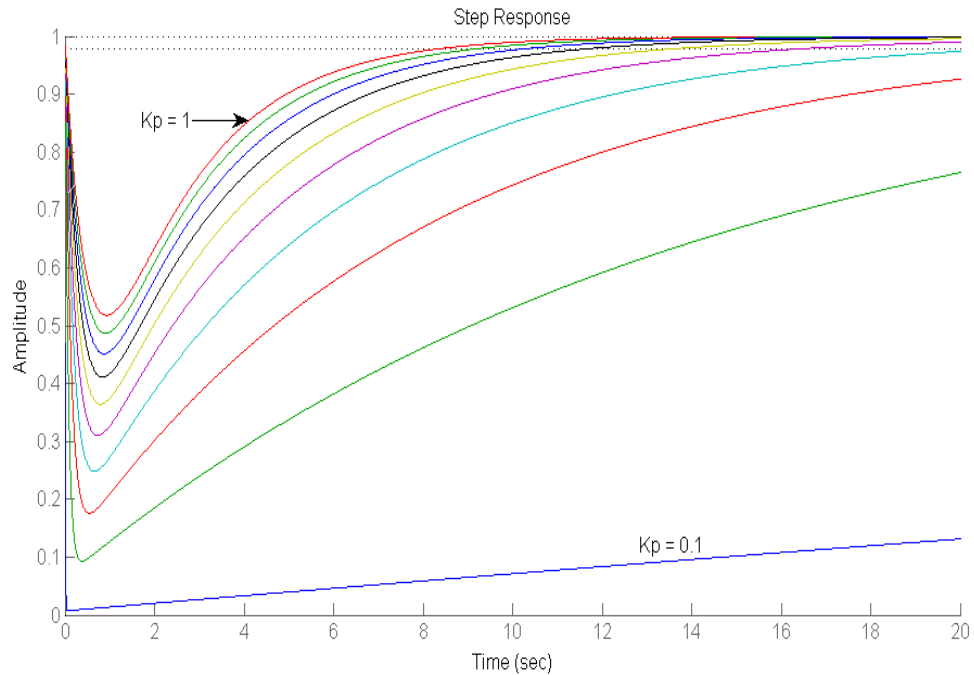


Figure 3.13: Effect of P-controller as K_p increases

It is observed that when $K_p = 1$ (large enough), the magnitude of the output variable steadily rises at high speed as a non-minimum phase plant (typical of power system network as it transits from one mode to another) with large phase margin.

3.4.2 Effect of the Linear PI Terms

In order to remove the error and reduce the overshoot, an integrator is added to the proportional term to implement the PI controller in the expression

$$C(s) = K_p \left(1 + \frac{1}{\tau_i s} \right) \quad (3.17)$$

while still keeping $K_p = 1$ and applying different values of τ_i in the range $[0.15 \sim 1.5]$ as shown in Figure 3.14. It was observed that any value of $\tau_i < 0.15$ would throw the system out of stability. Conversely, the overshoot and steady state error are reduced by raising the values of τ_i .

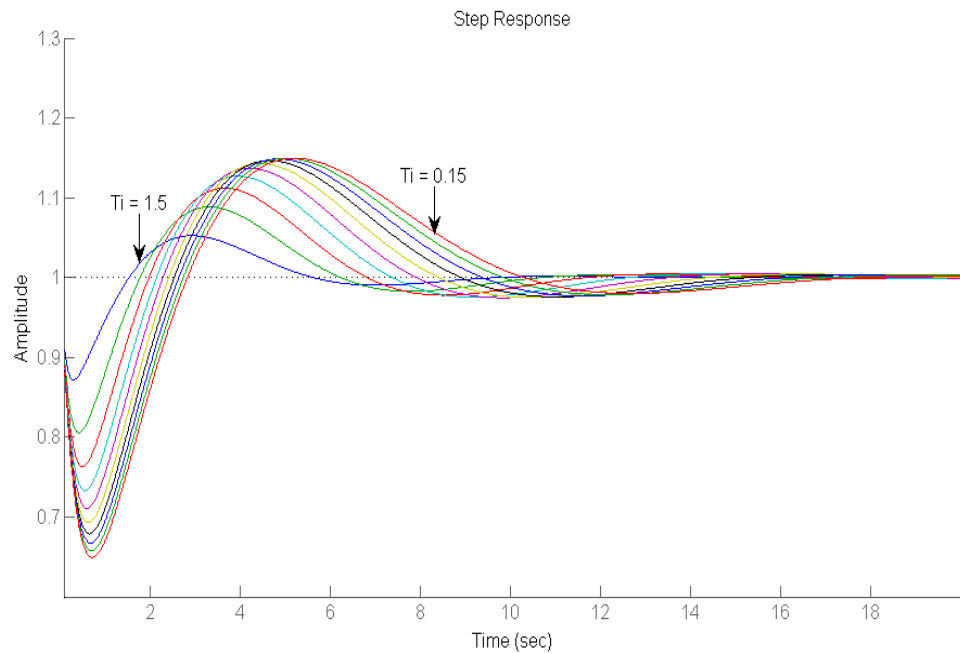


Figure 3.14: PI controller as T_i increases

3.4.3 Effect of the Linear PD Terms

Further, if a nonlinear PD controller is used, it is shown that such an integrator as added above, is unnecessary in eliminating steady-state errors (Li et al. 2006). In this section, we investigate proportional-derivative control so as to accelerate disturbance rejection by providing a phase lead. The effect of which is evident in Figure 3.15, providing damping and removing overshoots. Through the known Taylor's series expansion, the continuous time PD control law is given by

$$u(t) = K_p \left(e(t) + T_d \frac{de(t)}{dt} \right) \quad (3.18)$$

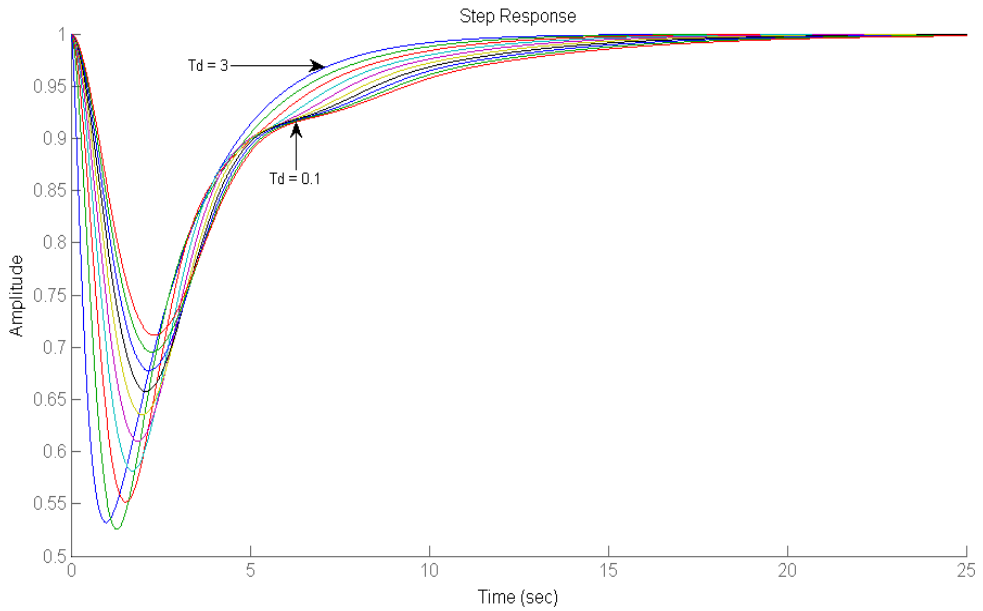


Figure 3.15: PD controller as T_d increases

3.5 Summary

In this chapter, preliminary stages towards PID control design methodologies are presented. Determination of the model error as an important design objective, was carried out during model validation exercise. The operating points of the system were then established to serve as a beacon to the current design as well as to future control designs in this thesis. These were based on some underlining international standards governing operations and control of the distribution power network. Based on these presumptions the PID, PI and PD controllers were re-designed for setpoint regulation for my DSTATCOM model. The initial parameters to these controllers were firstly defined through the traditional Ziegler-Nichols (1942) methods, and later compared with the refined Ziegler-Nichols, Cohen and Coon, and Chien-Hrones-Reswick tuning rules using an approximated FOPDT plant model under appendix B. Two closed-loop circuits were then analysed for investigating the most effective size and location of the derivative filter (ρ) to counter derivative-kick for use in my fuzzy PD design in Chapter 4. Individual effects of P, PI and the PD controllers on the system were then reported, and it is found that the PID controllers designed in the feedback path offer smoother and faster ride-through to the setpoint at $\rho = 11$, better than in the feedforward loop setting which showed $\rho = 10$ from (Ng 1995).

Chapter 4

CAutoD of Fuzzy Controllers for Improved PQ

4.1 FLC for PQ Applications

In this chapter, a new detailed online automation procedure of the system through evolutionary fuzzy PD designs, search and optimisation is presented. The literature has shown recent successes achieved from such combination typically committed to off-line Computer-aided design (CAD), e.g., (Ng & Li 1994). Although in most of these approaches, the FLCs were applied in dynamic control of GA parameters (such as population size, mutation rate and crossover rate) rather than the other way round (i.e., GA parameters to control FLCs). Such approach has a significant negative impact on the performance of the GA, especially when the parameters are poorly selected. For example, it could lead to premature convergence problem where the search gets trapped in a local minima as often experienced, thereby causing overall deterioration in the GA's performance. A reverse engineering attitude is employed here to solve that problem by using a "genetic-fuzzy amalgam" (instead of the traditional fuzzy-genetic one), to acquire and automatically tune the fuzzy PD parameters online during system operation. The benefits offered by this kind of tuning include reduced computational burden posed by heavy rule-bases and membership function density from (Ng & Li 1994), (Hoyle 1996) and (Chowdhury 1998). To implement the idea, a well established computer-automated-design (CAutoD) simulation package from (Li et al. 2004) is made to extend the existing computer-aided-design simulator in an adaptive feedback manner introduced in section 4.8.1. The three design stages involved include an off-line manual fuzzy PD controller design to serve as foreground for investigating and comparing the performance of the conventional linear controllers analysed in Chapter 3 with the new CAutoD scheme. An online CAutoD based fuzzy PD routine

is then designed through a chosen performance index to automatically evolve optimum fuzzy PD controllers. Finally, online application of both designs to an experimental DSTATCOM model developed from SimPowerSystems in Simulink was used to analyse its dynamic response and monitor the total harmonic distortion (THD) reduction in power quality (PQ) studies and for Volt-VAR optimisation at the PCC. Although it is conventionally recognised that optimisation routines are to be practically utilised off-line, because actual DSTATCOMs usually rely on pre-defined control schemes as found in PI controllers, often offering simple *if...then* control procedures with request for low memory space and slow computation facilities. Therefore, in order to improve the performance of the intended fuzzy PID controllers from the design stage, I adopted the examples set out in a phd thesis from (Ng 1995) and proved that my online design can offer the needed economic computational resources to make CAutoD-FPD based DSTATCOMs competitively faster, more stable and more reliable in solving PQ problems. Here, a number of simulation studies using Matlab/Simulink environment involving different scenarios in testing the robustness of FLCs were carried out to prepare the ground for transiting from manual to automated design of the FLCs through a well chosen performance index. Since the FPD design has to be built on the behaviour of a conventional PD controller, a thorough presentation of a generic PID control paradigm was initially established through a given example in section 4.2.

4.2 Generic PID Control Paradigm

A generic PID closed-loop control system is presented in Figure 4.1 with the control rule u_{PID} , defined in terms of the controller coefficients and the system error as

$$u_{PID} = K_p \left[e(t) + \frac{1}{T_i} \int_0^t e(t)dt + T_d \frac{de(t)}{dt} \right] \quad (4.1)$$

where $e(t) = r(t) - y(t)$, and $r(t)$ is the reference signal. The disturbance $d(t)$ normally is associated with the control output and transferred back into the system along with the reference input. It is noted in this Figure that the filter coefficient ρ was incorporated in the feedforward-loop to tame the high frequency gain associated with the measurement noise $n(t)$. However, Xue et al., suggested relocating ρ in the feedback-path rather, as it would remove the integrator and fasten the response. Based on this philosophy, I investigated its effect and developed a conventional PD controller for my nonlinear fuzzy PD control.

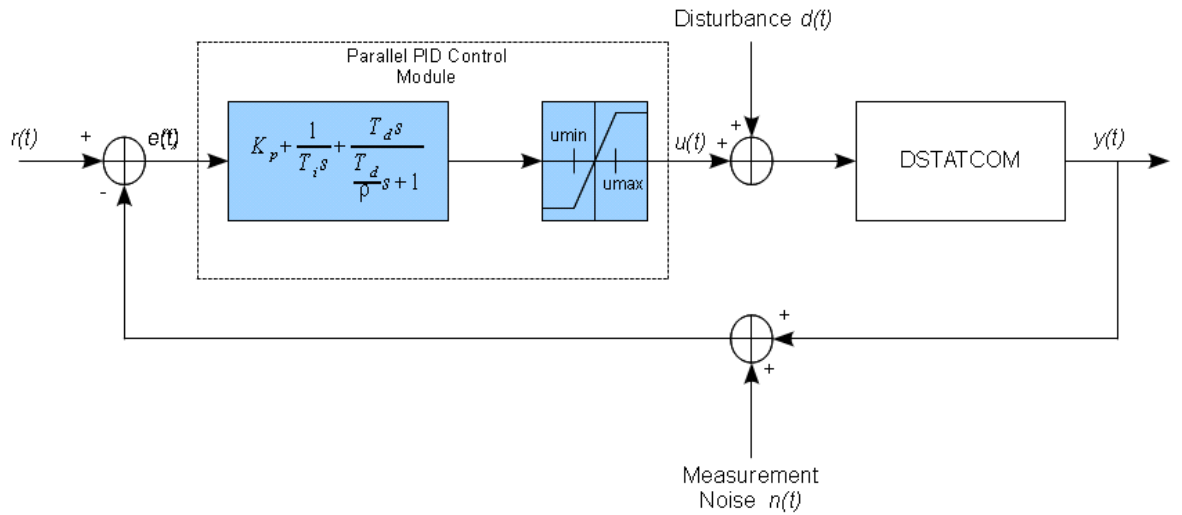


Figure 4.1: Generic closed-loop control system

4.2.1 PID Tuning Methods

Practical PID tuning is basically done through integral and derivative time constants as the main drivers of the control action, and Ziegler-Nichols method as the vehicle. This method has been used for long time to determine the process dynamics based on both time and frequency domains. The result was several commercial autotuners flooding the market from the early 80's to the recent autotuner sensing of optimal PID parameters (Zhuang & Atherton 1993). Although, Z-N method has been sharply criticized for being too sensitive to measurement noise, which application was reduced to slow processes with large time constants requiring close monitoring, as they have to be operated closer to their stability limits (Levine 2011). Yet, several tuning techniques were developed around its principles for its simplicity, with improved robustness. In this section, we explored and re-examined the accuracies of some of these methods listed below, in order to investigate the way they affect the performance of my design model.

- AMIGO Tuning Rules (the PID parameters were calculated using Table B.3)
- Weighed-Setpoint Ziegler-Nichols Tuning Rules
- PIDeasyTM Tuning Rules (used with neural net tool in section 3.3.1 for model comparison)
- CHR Tuning Rules (The initial tuning parameters for both setpoint and disturbance rejection needs can be obtained using the values for a , L and T from the Tables B.4 and B.6, and displayed in Tables B.5 and B.7, respectively)

By way of comparison, the variation between the initial parameters in all cases suggests a very close fit, each of which comfortably provides good closed-loop setpoint following.

4.2.2 Design Specifications

Setpoint regulation and disturbance rejection are two major control objectives I am concerned with here in relation to power quality problems. And these can be determined through careful evaluation of some limiting factors which can off-set system's controllability, such as: measurement noise, external disturbances, model uncertainties and nonlinearities. Therefore, It is customarily considered a good design practice in the control community to focus on realising the following specifications towards accomplishing my intended designs from (Li & Häule 1996), (Åström & Hägglund 2001), and (Feng 2000).

- Setpoint following (Regulation problem)
- Sensitivity to measurement noise
- Good disturbance rejection
- Robustness to model changes
- Stability

4.2.3 Linear Model Identification

The use of the well known Ziegler-Nichols approach was made to identify the equivalent first-order-plus-delay-time (FOPDT) model needed for approximating the initial PID controller parameters according to (Xue et al. 2007). Parameters of interest like, system gain k , time delay t and the time constant T are easily read off from Figure 4.2. The negative intercept $a = kL/T$, suggests the nonminimum phase characteristics of the DSTATCOM. Since it is difficult to deal with a real distribution network, the input-output data was extracted from the open-loop step response simulation of the linear mathematical plant model defined earlier, to produce the FOPDT model in Eq. 4.2.

$$H(s) = \frac{ke^{-sL}}{1 + sT} \quad (4.2)$$

Tuning algorithms can simply then be formulated for time domain response from Table B.2. The frequency domain response (not considered here) is also attainable using similar table for frequency response parameters. Some tuning methods are briefly discussed under section 4.2.1 and more details about them can be found (Feng 2000); (Xue et al. 2007).

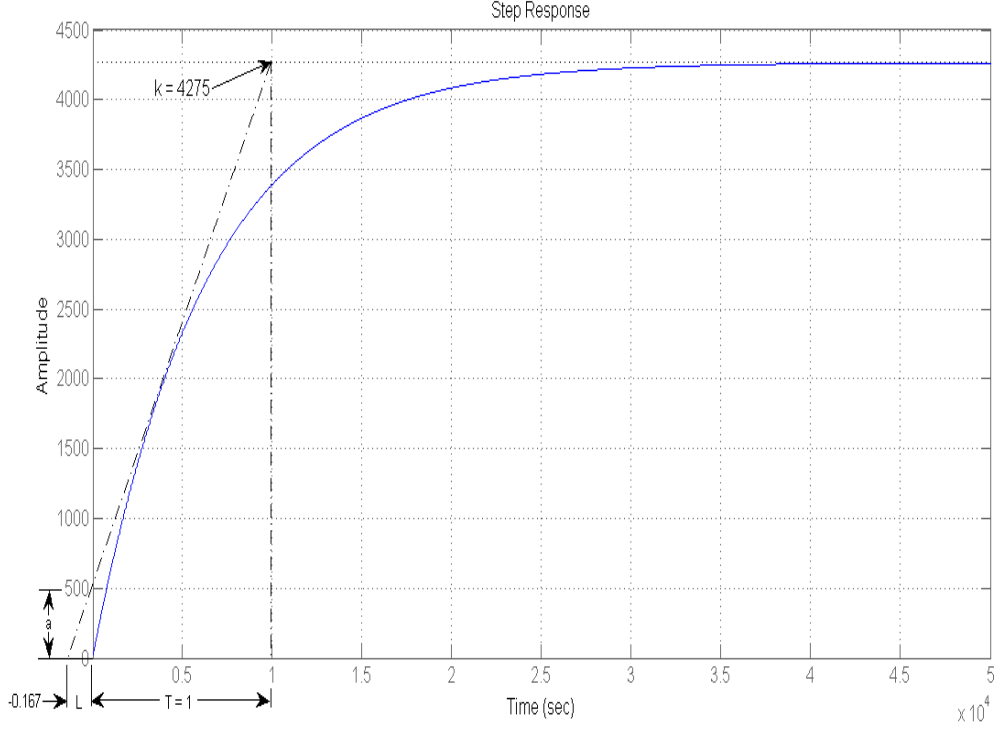


Figure 4.2: Heuristic Z-N controller design

From the closed-loop simulation, it is observed that the integrator introduced by the controller has been eliminated and thus reduced G_c to a simple proportional-derivative system shown in Figure 4.3. The effectiveness of the initial control parameters can vividly be seen from the error plot tending to zero, indicating their sufficiency in the case of a stable and damped system under discuss. I further investigate its performance on unstable plants as well as to plants with integrators enforced by uncertainties during steady state operations.

The numerical values of the parameters can thus be determined directly from the Table as the initial PID tuning rule with $a = kL/T = 714$. And the resulting closed-loop control system obtained using these values is $G_c(s)$ with controller $H(s)$ and the original plant $G(s)$ defined as

$$H(s) = \frac{0.00012s^2 + 0.0014s + 0.0028}{s} \quad (4.3)$$

$$G(s) = \frac{161300s^2 + 161300s + 1.516e005}{s^3 + 2s^2 + 224700s + 35.56} \quad (4.4)$$

$$G_c(s) = \frac{HG}{1 + HG} = 0.00012s + 0.0014 \quad (4.5)$$

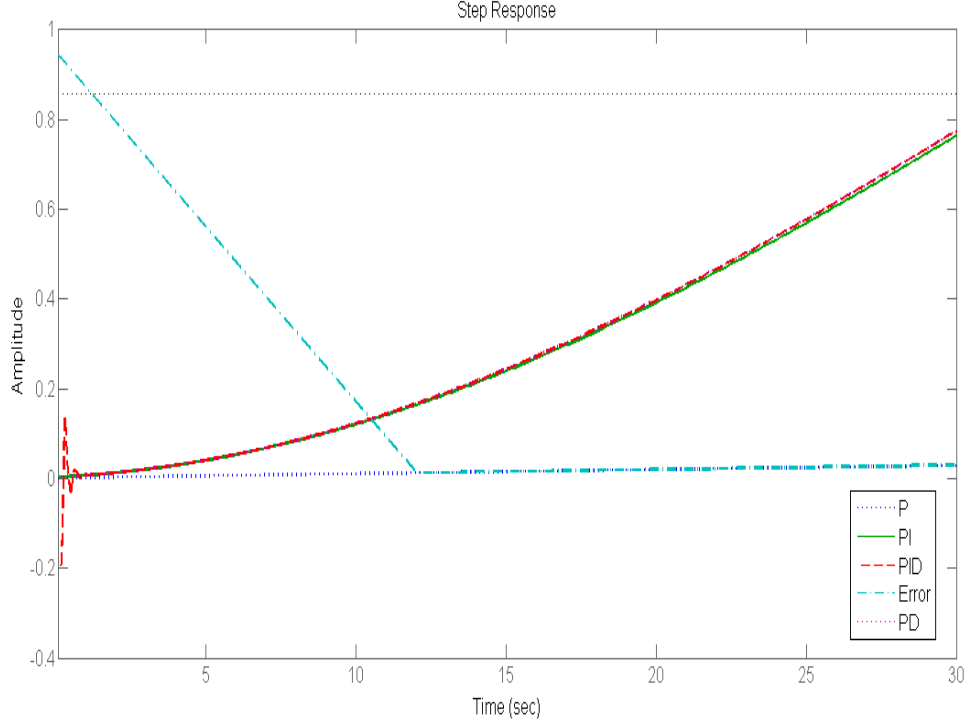


Figure 4.3: Intial FOPDT tuned responses

4.3 PID Design Case Study - a Linear DSTATCOM Plant

Consider the third-order nominal plant representing my DSTATCOM model given by

$$G(s) = \frac{161300s^2 + 161300s + 6.884e^{10}}{s^3 + 2s^2 + 224700s + 35.56} \quad (4.6)$$

which has a characteristic equation identified through specified parameters, defined as

$$s^3 + 2s^2 + s \left[w^2 + \frac{R^2}{L^2} + \frac{m^2}{LC} \right] + \frac{R}{L^2C} m^2 = 0 \quad (4.7)$$

It is apparent that the solution to Eq. 4.6 yields three roots comprising of a real pole and a pair of complex eigenvalues. These roots have negative real parts suggesting a damped and stable DSTATCOM which can conveniently be represented by a first-order plus delay time (FOPDT) plant. The desired goal for this application is that a step input produces a closed-loop output signal with an:

- Overshoot of 20%
- Rise-Time of at most 1.05 seconds
- 27 seconds settling time
- Zero steady state error

This kind of plant is referred to as a Type-1 system (Tewari 2002), and thus does not exhibit steady state error with constant inputs because of infinite positional error constants. Therefore, it must be equipped with a free integrator in the forward loop to cancel the zero before it could effectively be controlled.

4.4 A-Priori Tuning of FPD Controllers

Prior to applying the CAutoD interface, there is need at this point to investigate on the tuning effects of the factors influencing some specified closed-loop performance indices of the system in manual mode as shown in Figure 4.4. In this Figure, the fuzzy controller block consists of a pre-processor, fuzzification, rule base, inference engine, defuzzification, and a post-processor blocks. In practice, the tuning procedure involved in fuzzy systems offer great flexibility in tuning the nonlinear function implemented by the fuzzy controller. But, generally there is no guarantee that performance specifications and system stability can easily be attained through proper tuning of the desired fuzzy systems. Moreover, nonminimum phase systems (such as being dealt with here) can impose fundamental limitations from achieving set control objectives no matter how well the fuzzy controllers are tuned. However, a reasonable choice of control inputs and output usually provide a good tuning premise on the scaling factors. This section makes proper investigation of each of these factors and the way they influence fuzzy controller response.

4.4.1 Input-Output Scaling Factor Tuning

Reference to Figure 4.4, the scaling factors S_e , $S_{\dot{e}}$ and S_{α} , are set of notable tuning factors that largely influence fuzzy decision process at the system's input and output ports in accordance with the chosen inferencing procedure. The tuning process is

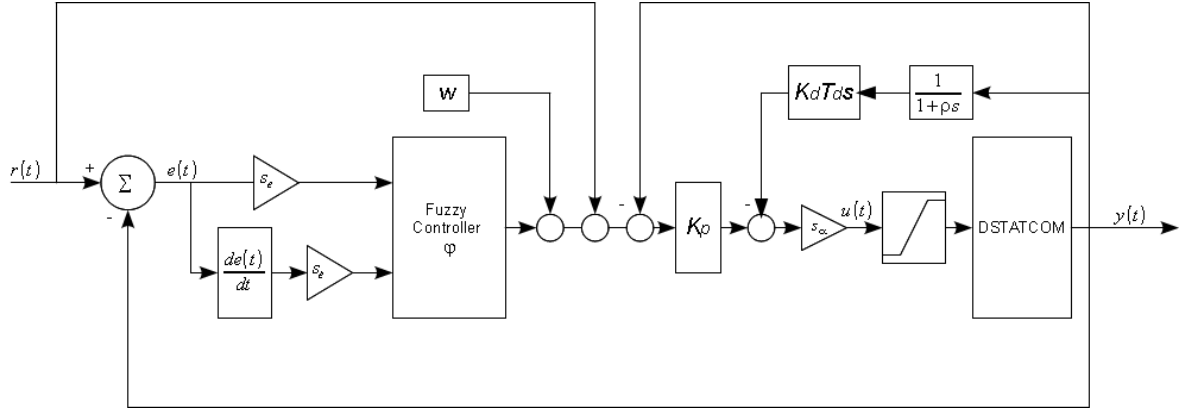


Figure 4.4: FPD-DSTATCOM control model

initialised by arbitrarily setting the first input scalar (S_e) as an inverse of the setpoint value from (Ng 1995) as

$$X_e = \frac{22}{e_{max}} e(k) = S_e e(k) \quad (4.8)$$

where e_{max} represents the step size of the error signal which in this case is $\pm 10\%$ of 220 volts (i.e., ± 22 volts), measured against the distribution feeder standard nominal supply normally supplied to the consumer's terminal in Nigeria. X_e is the fuzzified set of the error variable. Note that Eq. 4.8 is similar to the traditional proportional controller $u_P(k) = K_p e(k)$. Then, the second input scaling parameter for the error derivative S_d given as Eq. 4.9, is continually modified through an empirically acquired value of \dot{e}_{max} from the process dynamics. This action is suppose to normalise the fuzzy set X_d of the derivative input calculated from the gradient of the original error curve in the range ± 0.5 volts/sec.

$$X_d = \frac{0.5}{\dot{e}_{max}} \frac{\Delta e(k)}{\Delta t} = S_d \frac{\Delta e(k)}{\Delta t} \quad (4.9)$$

Meanwhile, the output scaling factor S_α is linearly varied from zero to its maximum value as a singleton function such that

$$\alpha_c = \frac{\alpha_{cmax}}{X_{cmax}} X_c = S_\alpha X_c \quad (4.10)$$

where α_c is the crisp control output (plant input) and α_{cmax} its maximum value. The action of the control output due to fuzzifying a fuzzy set (i.e. Low) in the universe

of discourse and its maximum values are denoted by X_o and X_{omax} , respectively. The control output is issued as a switching angle (α) designed to saturate beyond some threshold in the dynamic *sine-cosine* operating range of the DSTATCOM established as $\pm 30^\circ$ or ± 0.5236 radians. The main benefit of the dynamic range is seen where the DSTATCOM can be applied in high voltage zones at the transmission corridor as a statcom.

To exemplify the procedure illustrated above, I assumed the scaling factors a priori by setting $w_{1-3} = (0.879, 0.12, 0.5)$ and fixed $\alpha = 0.5$ while fixing the number of rules to $R = 3$, and applied them in Eq. 4.10 to yield

$$\alpha_{crisp} = \frac{(0.879 \times 0.5) + (0.12 \times 0.5) + (0.5 \times 0.5)}{(0.5 \times 3)} = 0.4996 \quad (4.11)$$

Then we made $\alpha = 1$, and by retaining the values of w and R , a new value for α_{crisp} is found as follows

$$\alpha_{crisp} = \frac{(0.879 \times 1) + (0.12 \times 1) + (0.5 \times 1)}{(1 \times 3)} = 0.4996 \quad (4.12)$$

In both cases, the result approximately produced the same expected crisp control signal of 0.5, which means “medium or zero” in linguistic terms. It also shows that the chosen method directly depends on the weighting factors as is demonstrated by varying $w_{1-3} = (0.345, 0.9, 0.07)$ and setting $\alpha = 1$ while maintaining $R = 3$, yielding

$$\alpha_{crisp} = \frac{(0.345 \times 1) + (0.29 \times 1) + (0.07 \times 1)}{(1 \times 3)} = 0.235 \quad (4.13)$$

It is observed that with lower weighting factors, the resultant control signal is also lowered. However, care should be taken not to make the sum of the numerator equal to zero, which means there has to be conclusions to all possible control decisions taken. Conversely, a zeroed denominator would saturate the actuator and cause system malfunction. Now, I can assert that the crisp control value of $\alpha = 0.4996$ or 0.235 radians makes a lot of sense, because it lies within the dynamic operating range ($-0.5236 \leq \alpha_{crisp} \leq 0.5236$) earlier quoted for the DSTATCOM’s input signal. Again, Table C.1 presents the preliminary results obtained from this procedure. Better results can be achieved by reducing the value of γ at each iteration.

4.4.2 Deficiency of the A-Priori Tuning

The decision on the parameters to be used for optimal tuning is a vital one which could jeopardise fuzzy system design when wrongly made. As previously mentioned, the current fuzzy parameter tuning involved is manually based on trial-and-error. Although, the trend shows a huge increase in the use of neural networks and genetic algorithms to automate fuzzy rule-bases and membership functions (Cheong & Lai 2000); (Visioli 2006); and (Homaifar & McCormick 1992). Such techniques still require pre-specification of the rule base structure which is often too large. Another disadvantage is that disordered membership functions often arise, resulting in sub-optimal interpolation. In trying to solve the problem, I adopted the technique from Tang et al., in which optimal tuning of the fuzzy PD parameters is accorded through an evolutionary algorithm based CAutoD tool. The CAutoD technique has not in the past been applied to assess fuzzy PD parameters in power quality problems. However, the closest studies applied simple GA in a multi-objective genetic algorithm to solve generic fuzzy PID problem (Tang 2011). The success of CAutoD applications in providing robust optimisation solutions to engineering and business related problems is well documented (Li et al. 2004).

4.5 Prelims to CAutoD Tuning

The common design objective in this project is to regulate DSTATCOM's output voltage to a setpoint accurately and as fast as possible during disturbance, in accordance with some specified performance indices. A direct fuzzy control scheme has been adopted for this purpose where the error and the error-derivative inputs are measured and fuzzified, and the resultant fuzzy variables are passed to the inference engine of *if then* rules to make the control decisions. The ensuing classified fuzzy decisions are then defuzzified into crisp value as a control force driving the actuator of DSTATCOM. In a typical regulation problem, load disturbances are of low frequencies and are thus prototyped along with the setpoint following as step commands for simulating closed-loop system's specifications. For example, suppose that for a given step input, a stable response with $P^*\%$ overshoot, a bandwidth of T_r^* seconds, and a settling time of T_s^* seconds are required. The performance index that can simulate the closed-loop setpoint following of the control system's objectives by way of minimising J , provided the specific values of P , T_r , T_s , and ω_i where $i = 1, 2, 3, \dots$ are positive weighting factors, is given by

$$J = \omega_1(P - P^*)^2 + \omega_2(T_r - T_r^*)^2 + \omega_3(T_s - T_s^*)^2 \quad (4.14)$$

In such optimisation routine, when the gradient of the function $J = \frac{\delta F(x)}{\delta x} = 0$, i.e., system error has been zeroed, the response should then show that the control system has closely satisfied its performance specifications. Prioritization of achieving any of the specifications can be met by allotting a high value to its respective weight, like if the rise time specification is more important to meet than the remaining two specifications, then ω_2 is made higher with respect to the others accordingly.

4.5.1 Effect of Scaling Factors

In this operation, the DSTATCOM model is simulated in closed-loop using integration step size of $5 \mu\text{seconds}$. By arbitrarily assigning input-output scaling gains to the system using the procedure described in subsection 4.4.1. Again, closed-loop simulation of Figure 4.4 produced the plots in Figures 4.5 and 4.7. A stable response was achieved by setting $S_e = S_{\dot{e}} = 1.0011$ and $S_\alpha = 0.9998$ with an error plot dropping to zero, depicted in Figure 4.6. To demonstrate the effect of changing the gains, I raised $S_e = 100$. Formation of ripples is immediately observed from Figure 4.8, causing serious overshoot. This is akin to speeding up the system by raising the proportional gain in control engineering sense. Similar effect was also observed by slightly raising $S_\alpha = 1.1$, while preserving $S_e = S_{\dot{e}} = 1.0011$.

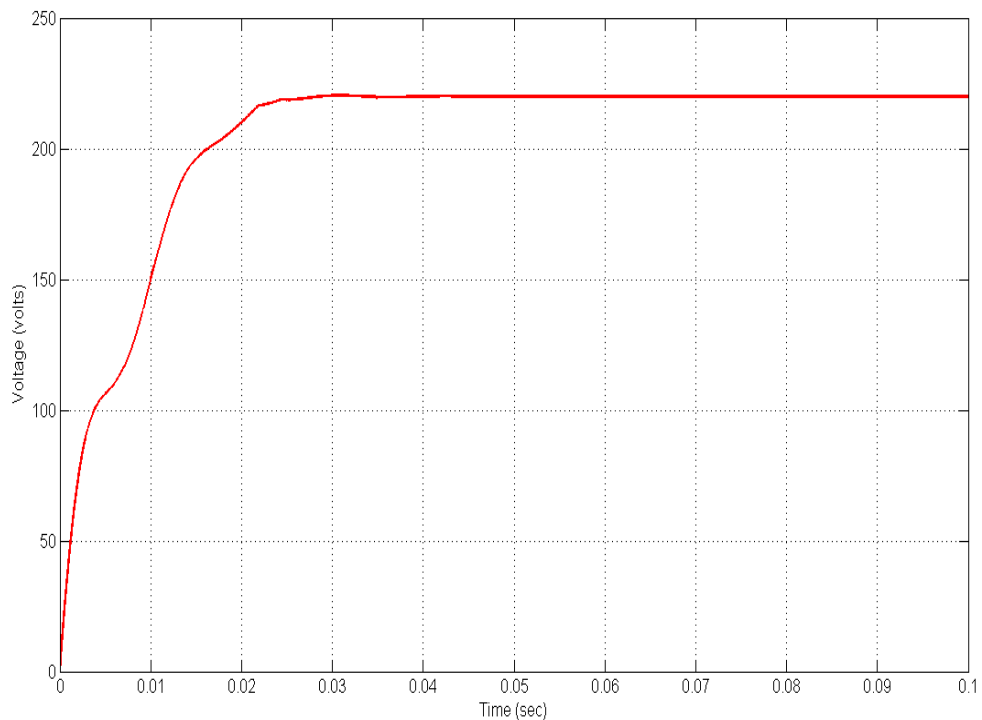


Figure 4.5: Scaling effects on performance
 $S_e = S_{\dot{e}} = 1.0011; S_\alpha = 0.9998$

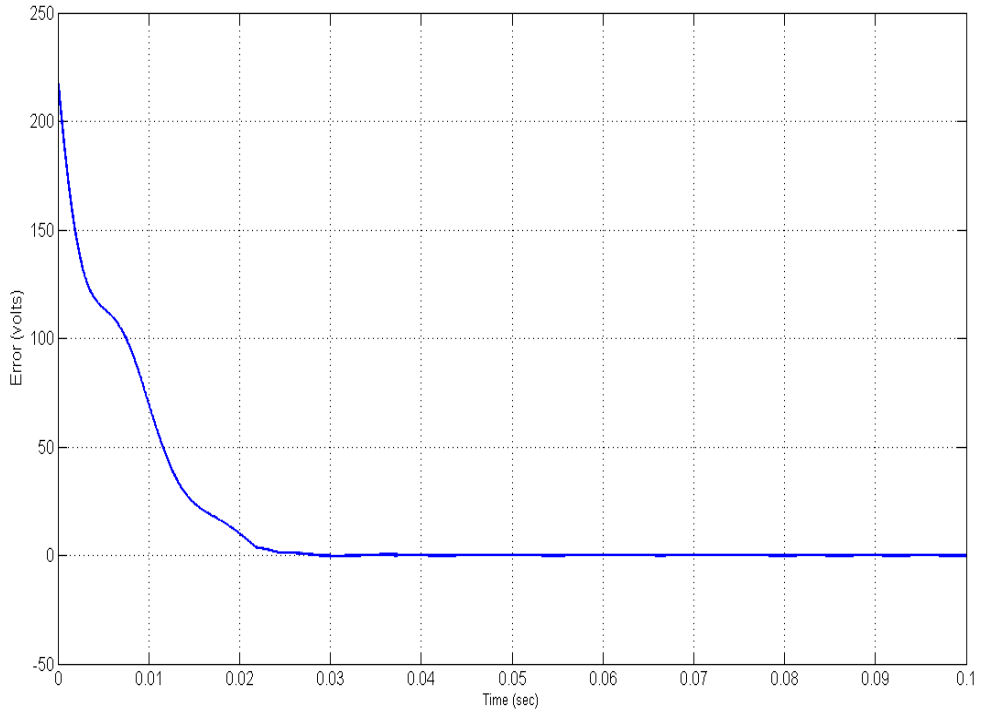


Figure 4.6: Error plot for:
 $S_e = S_{\dot{e}} = 1.0011; S_{\alpha} = 0.9998$

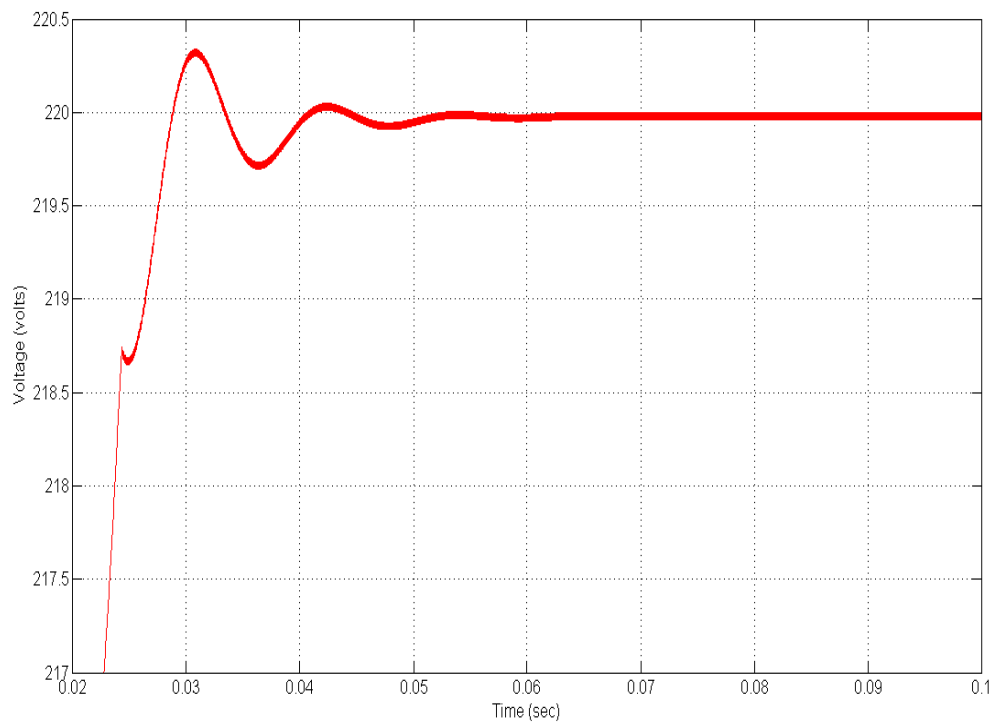


Figure 4.7: Effects of scaling factors case 1
 $S_e = 100; S_{\dot{e}} = 1.0011; S_{\alpha} = 0.9998$

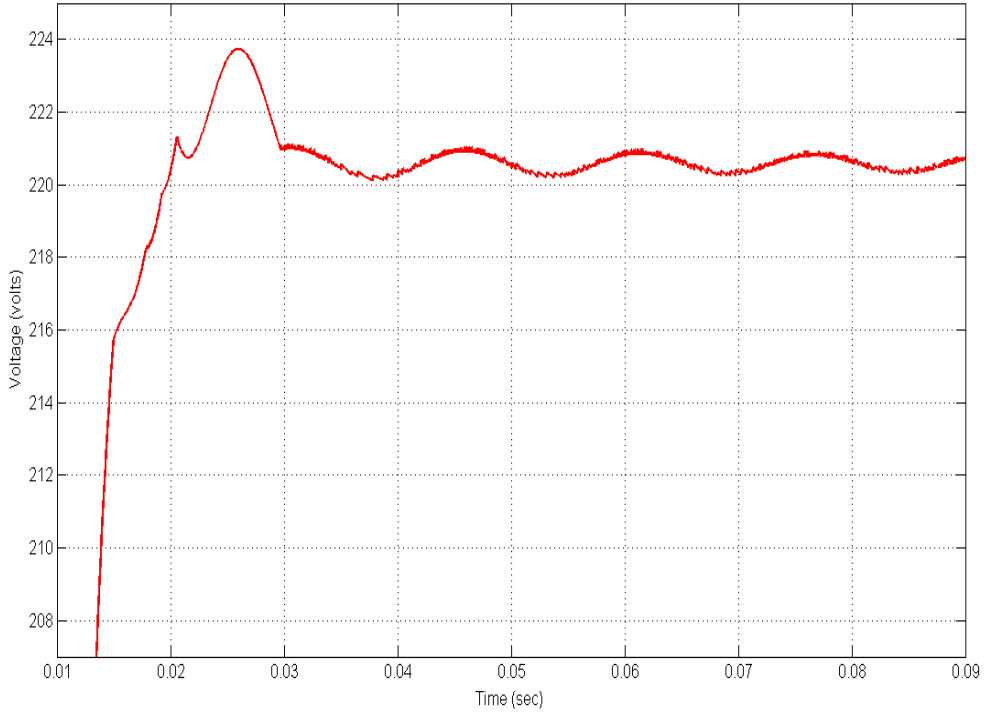


Figure 4.8: Effects of scaling factors case 2
 $S_e = S_{\dot{e}} = 1.0011; S_{\alpha} = 1.1$

However, increasing output scaling factor can easily stretch the system to its unstable region as shown in Figure 4.8. It can thus be deduced that, higher scaling values increase system response at the expense of large control inputs causing undesirable practical actuator saturation. It is also noted that S_e influences the controller's performance in determining the steady state error through rules activation. While $S_{\dot{e}}$ (especially in small values) affects the transient stability and the system convergence. This has been graphically demonstrated in Figure 4.9, where the error is seen zeroed as its rate of change is confined within the band $-0.5 \leq \dot{e} \leq 0.5$. The control signal (α) is noticed also to settle at the 0.5 value after transients that lasted for 0.005 seconds. The observed effect, including the DSTATCOM output voltage response at 220 volts, are also depicted in Figure 4.10.

4.5.2 Robustness to Model Changes

Robustness is related to that behaviour of a real control system that has been excluded from the mathematical model of the control system, which accounts for the model sensitivities to the unmodelled dynamics. Steady state and transient stability are the two most important issues considered in power system control, operation and planning. These maintain the system's synchronism in the event of inadvertent disturbances such

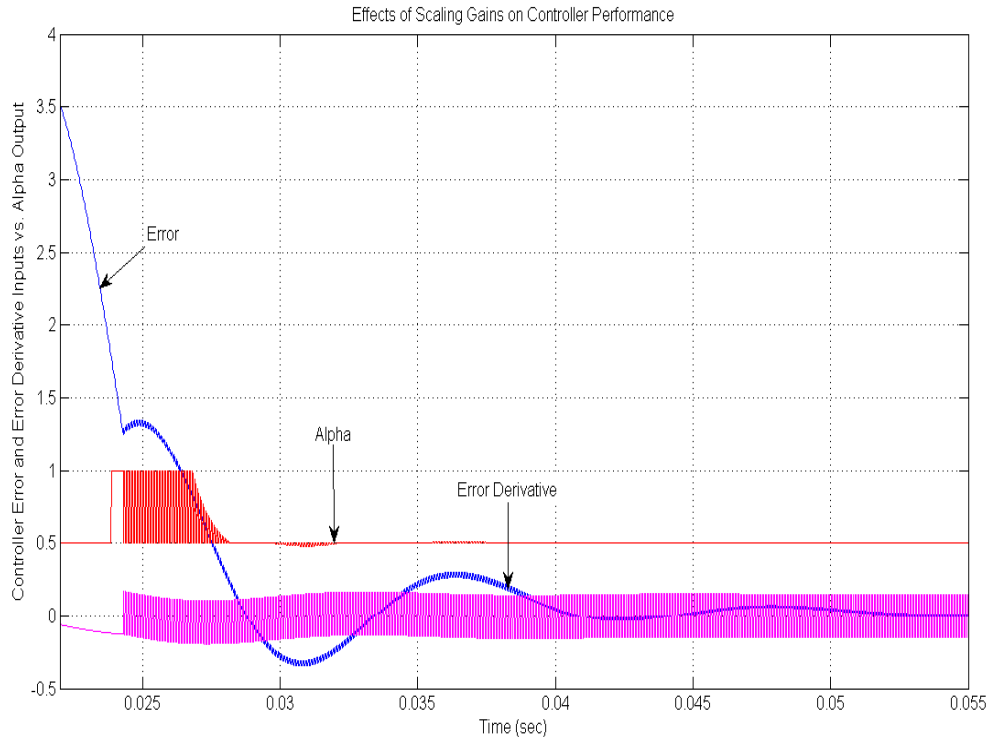


Figure 4.9: Scaling effects on e and α
 $S_e = 100; S_{\dot{e}} = 1.0011; S_\alpha = 0.9998$

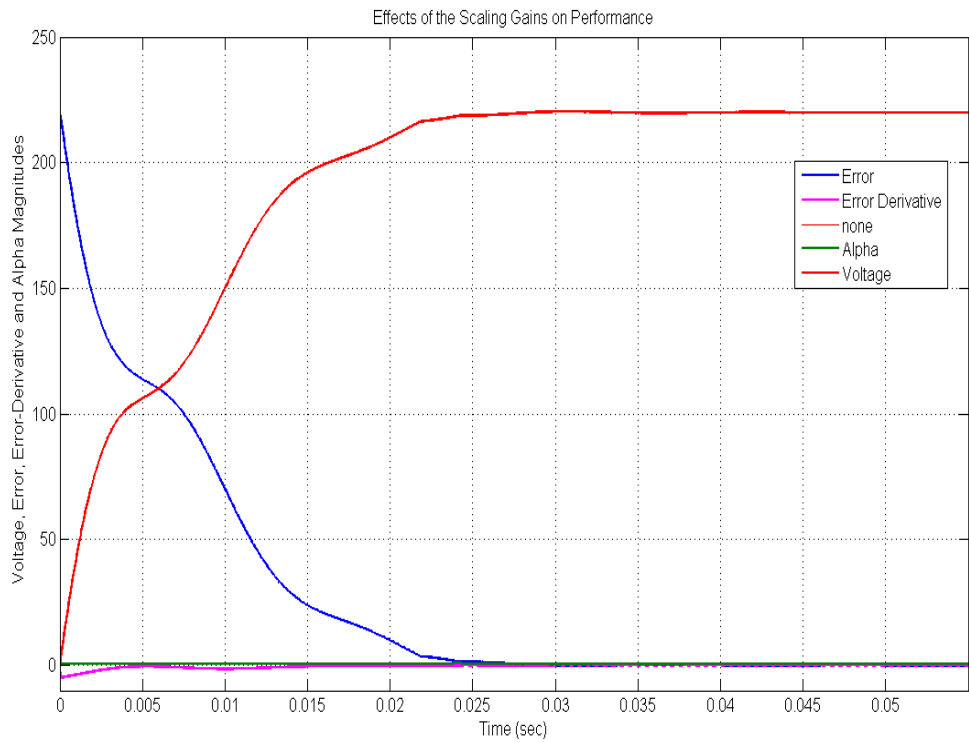


Figure 4.10: Scaling effects on overall performance
 $S_e = 100; S_{\dot{e}} = 1.0011; S_\alpha = 0.9998$

as sudden load changes, faulty line switching, and generator outages which often give rise to uncertain model parameter changes. Thus, it is imperative to consider the effects of these disturbances during any control system design before implementation. Typical model uncertainties would often emerge as changes in parameter gains, shift in pole-zero locations, and complex parameter variations (unstructured uncertainties) within specified operating ranges. Here, I looked closely at the steady state operations in a distribution system, considering changes in various circuit parameters such as resistance, inductance and capacitance as they occur during plant control cycles. I begin by considering the nonlinear closed-loop uncertain DSTATCOM model given as

$$P = \text{feedback}(G * K, 1) \quad (4.15)$$

where K is the controller, and G is the uncertain state space DSTATCOM having three uncertain parameters namely; resistance (R), inductance (L) and capacitance (C) with $1 \pm 10\%$ variation uncertainty each. Twelve step responses of four combinations of these three uncertain parameters are shown in Figure 4.11. This kind of uncertain system is robustly stable within tolerable amount of parameter uncertainty of up to 115% of the modelled uncertainty. This assertion has been verified comparing three controllers in the following scenarios for each of the uncertain parameter.

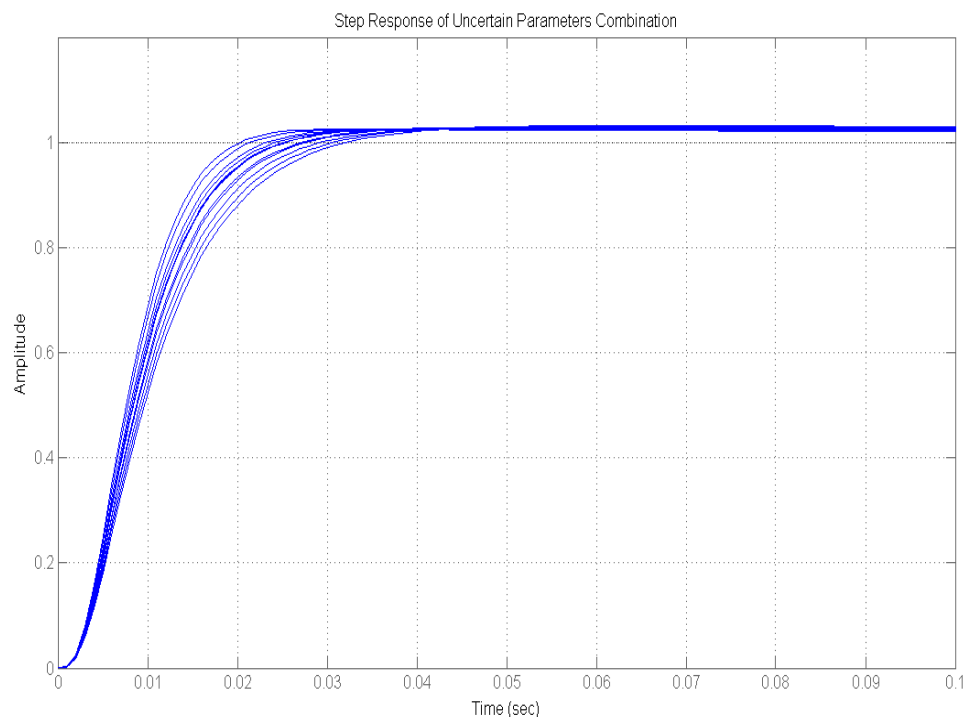


Figure 4.11: Uncertain parameters combination

4.5.3 Scenario No. 1: Changes in Circuit Inductance

For a situation where a nonlinear DSTATCOM model is equipped with one or more extra zeros at the numerator, the control action would need to place some poles (pole-placement) in order to supplement for zero cancellations. Figure 4.12 and 4.13 depict the respective scenarios in a nonlinear and linear model, where the fuzzy PD stabilises the steady state error as $t \Rightarrow \infty$ in a closed-loop operation, given a setpoint following of 220V command. The failure of the PD and PI controllers is vividly seen when sudden drop in the magnitude (180V) occurred at $t = 0.65$ and $t = 0.66$ seconds, respectively. These changes were introduced into the system through some parametric alterations shown in Table C.3.

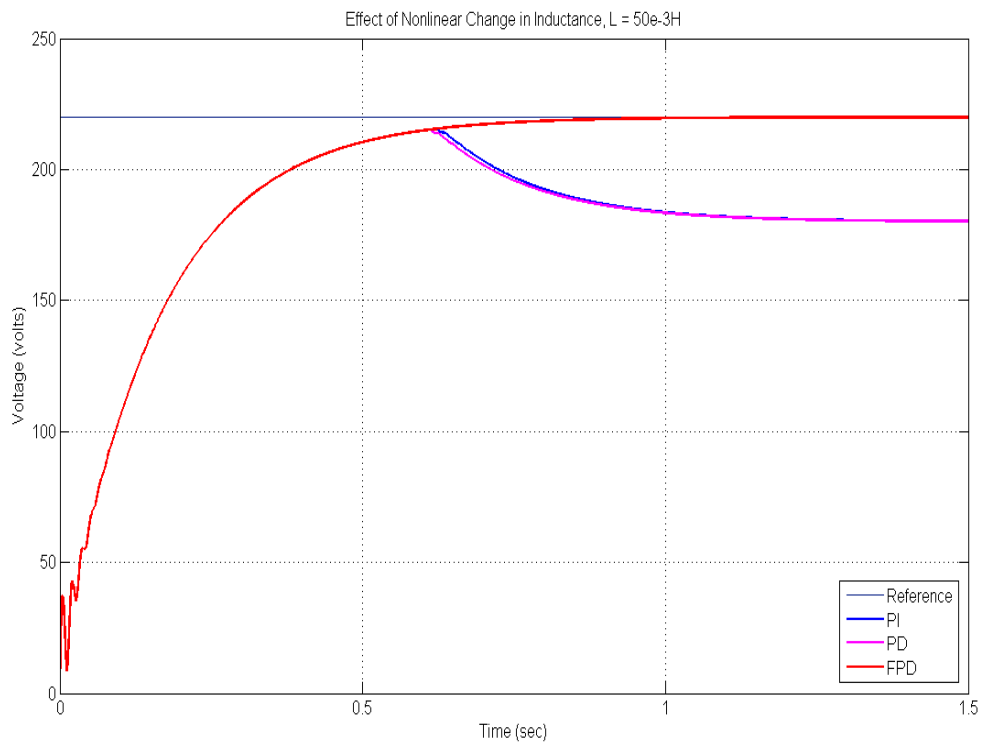


Figure 4.12: Effect of nonlinear change in inductance
Nonlinear model: $L = 50 \text{ mH}$

4.5.4 Scenario No. 2: Changes in circuit Resistance

The change in circuit resistance is akin to uncertain parameter gain changes which is bound to raise the gain margin by introducing a transfer zero capable of speeding up the system and causing overshoot. This situation has been depicted in Figure 4.14 when the circuit resistance was changed from 1Ω to 3Ω . By applying a step signal of 220V to the nonlinear DSTATCOM in a closed-loop, the responses from the PI and PD

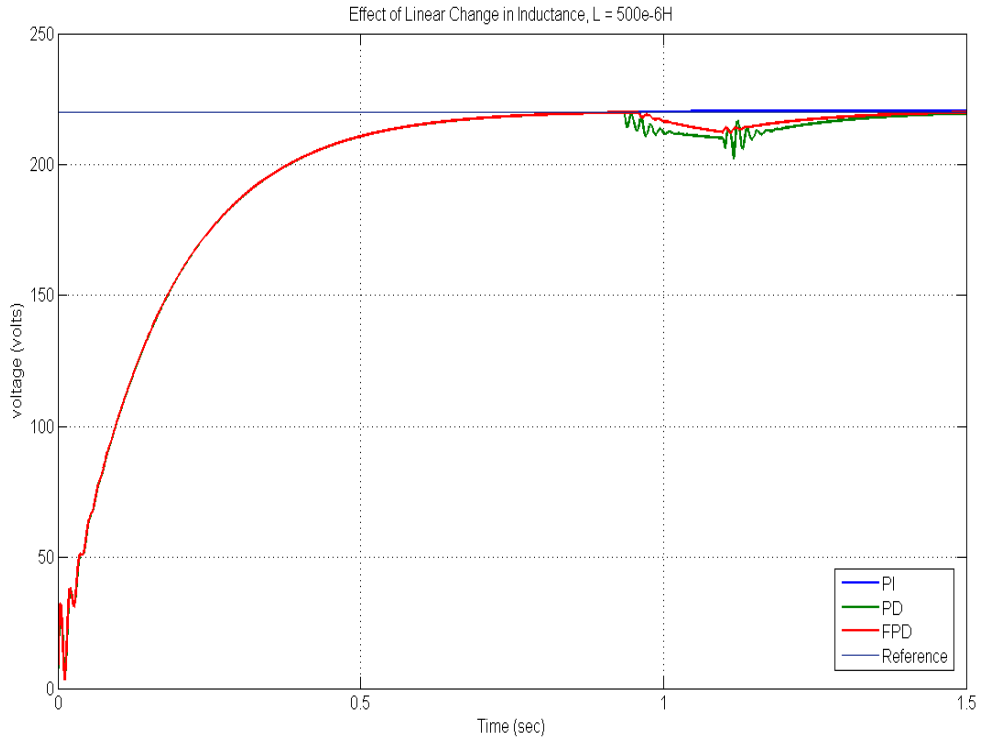


Figure 4.13: Effect of linear change in inductance
Nonlinear model: $L = 50 \text{ mH}$

controllers are noticed to stagnate at 180V with vivid traces of overshoots. While with the same control effort of 0.01129 radians, the fuzzy controller stabilizes the system at zero error and zero overshoot. However, the linear DSTATCOM responses for the PI and PD controllers produced no overshoot as in Figure 4.15, although the magnitude of the outputs drop to 200V , again the fuzzy controller maintains its grip at 220V through a control effort of 0.01364 . The details of the system parameters used for this simulation are listed in Table C.4.

4.5.5 Scenario No. 3: Changes in Circuit Capacitance

This is a case of “type 2” nonlinear DSTATCOM with an extra pole at the origin. The circuit capacitance was raised to $1500\mu\text{F}$ from $500\mu\text{F}$, while retaining the original circuit resistance and circuit inductance values. Step response closed-loop simulation of the nonlinear plant shown in Figure 4.16 depicts a PI controlled system infested with overshoot to the tune of 95.7% , rising at 0.0125 seconds and settling at 0.18 seconds. Although its performance is better than the PD controller which exhibits a speed of 0.013 seconds, yet offers settling time of 0.17 seconds at 82.82% overshoot, lower than the PI. The fuzzy PD can be seen to offer smaller settling time (0.14) and 0% overshoot at a little slower speed of 0.016 seconds. Similar observations are made when

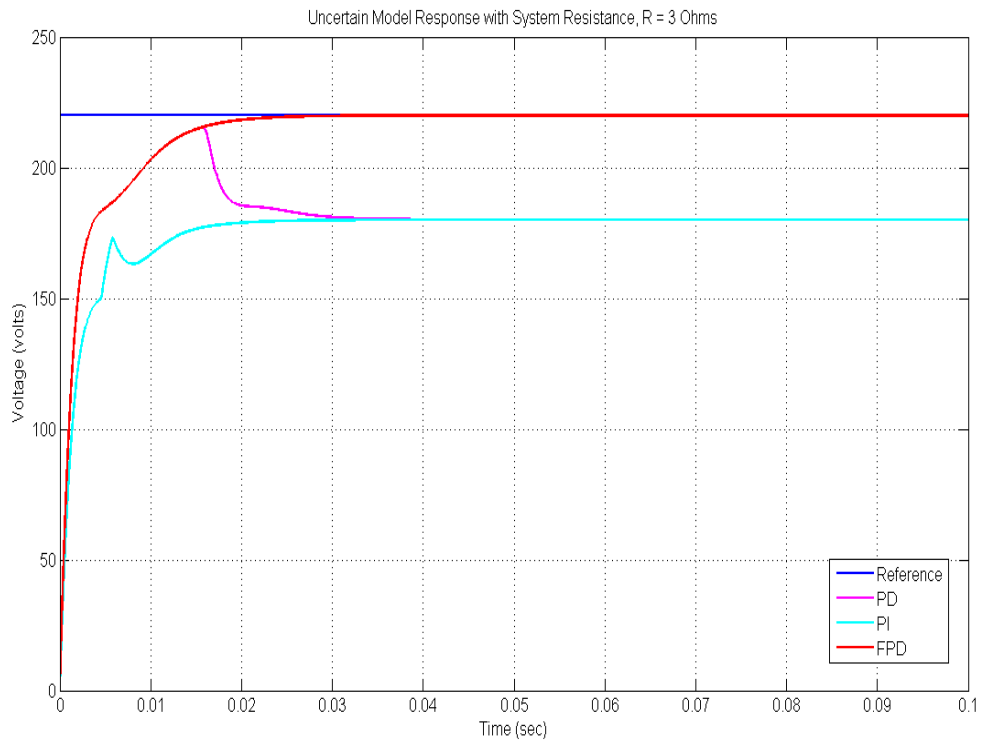


Figure 4.14: Effect of nonlinear change in resistance
Nonlinear model: $R = 3\Omega$

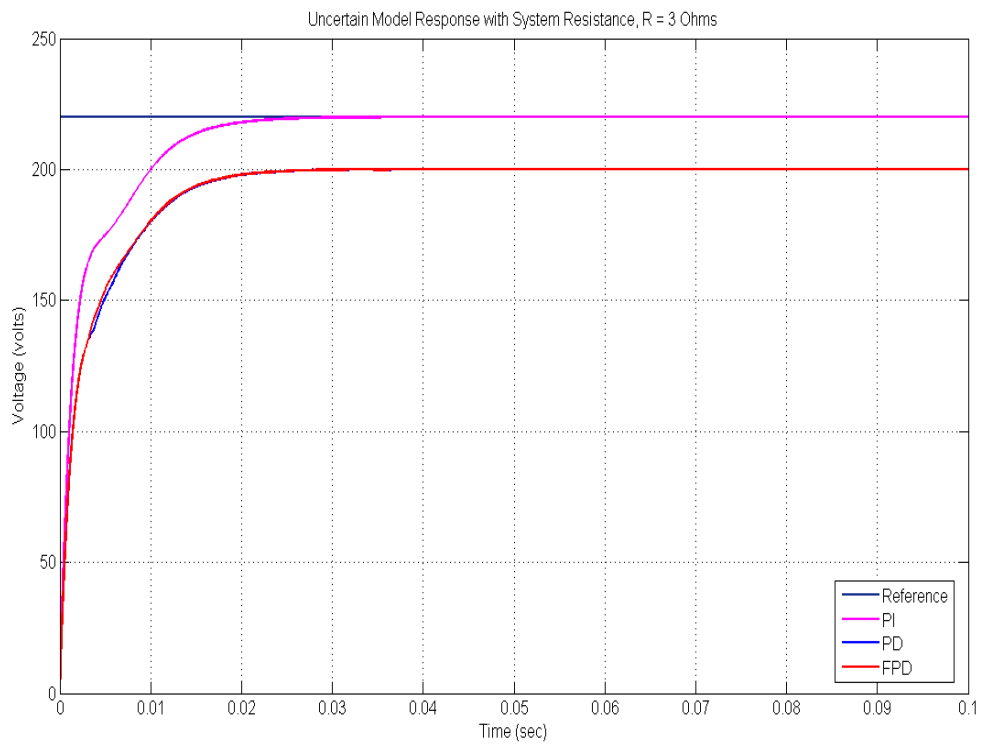


Figure 4.15: Effect of linear change in resistance
Linear model: $R = 3\Omega$

the linear system in Figure 4.17 is simulated, in which the performance of both FPD and the PD controllers are well behaved withing reasonable speed, with restrained 0% overshoot limits. However, the PI controller characterises a 59% overshoot, pointing to its unsuitability even in the linear model, where it is ubiquitous today. The circuit parameters used for describing this scenario are presented in Table C.5.

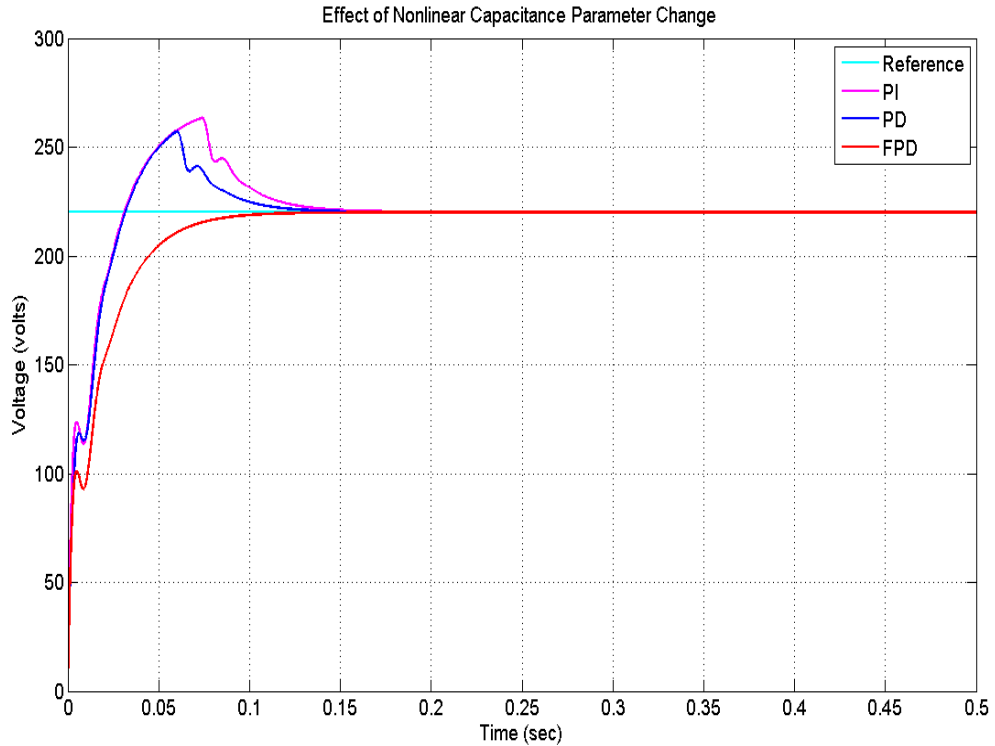


Figure 4.16: Effect of nonlinear capacitance change
Nonlinear model: $C = 1500\mu\text{F}$

4.5.6 Setpoint Following

Closed-loop performance based on CAD simulation targeted at a 220 volt feeder was investigated. Figure 4.18 shows step responses to both linear and nonlinear models controlled by PI, PD and the fuzzy PD. It is observed that the nonlinear fuzzy PD offers a faster response and a shorter settling time with no overshoot against both linear PI and linear PD controllers. Despite oscillations observed in the linear PD, yet it is faster than the linear PI controller justifying our earlier claim.

The subscripts L and NL, denote linear and nonlinear model respectively. It is noted that the nonlinear FPD model offers optimum control effort of 0.0046 rads. The results are displayed in Table C.6. It is interesting to note the linear PI model overshoot kept at 0% and its nonlinear PI counterpart rose to 12.55%. This actually is a pointer to the huge success of the PI control application to DSTATCOM found in the literature.

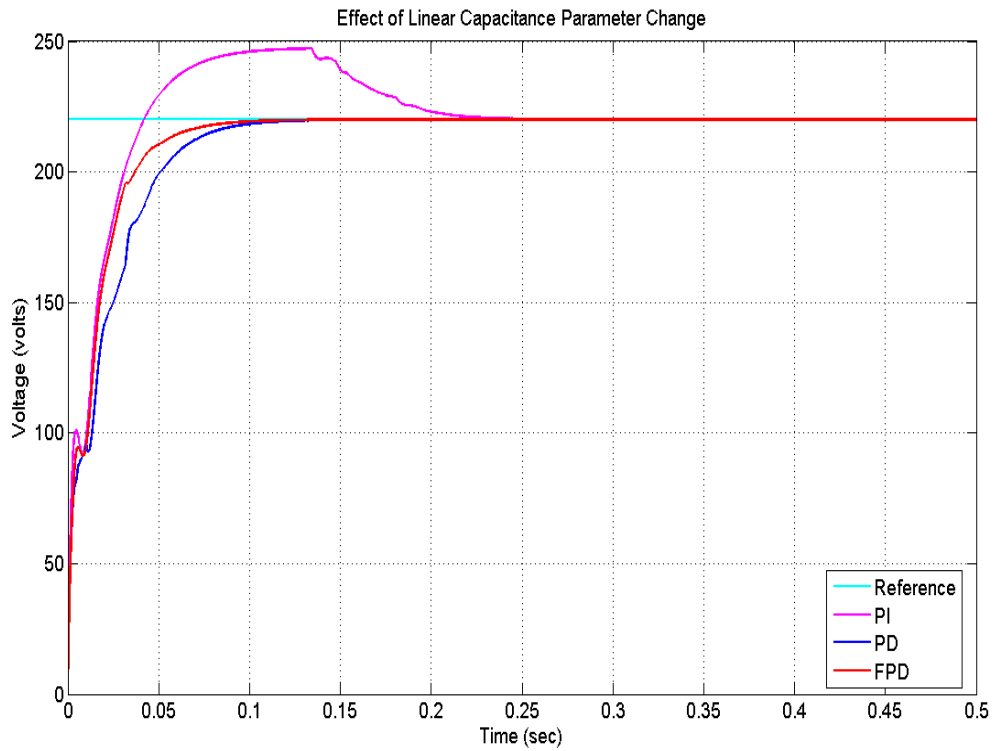


Figure 4.17: Effect of linear capacitance change
 Linear model: $C = 1500\mu\text{F}$

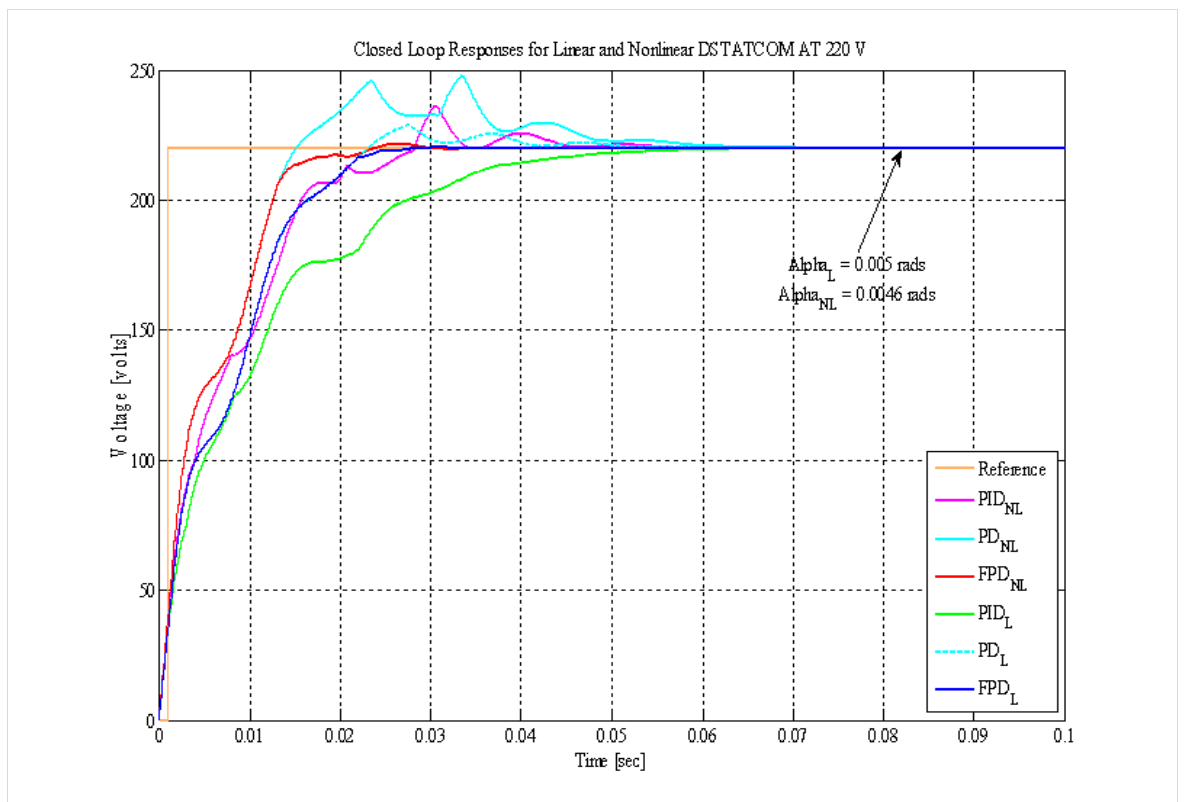


Figure 4.18: Linear vs. nonlinear model performance

However, its behaviour in the nonlinear model suggests a re-think for real-time application. Better alternatives are yet found in the linear and nonlinear FPD models reflecting 0.17% and 0.74% overshoot, respectively. Although the linear model looks more promising, the philosophy behind this work is automating a control system that captures the nonlinearities of the distribution system online. Therefore, the nonlinear FPD model is chosen for the CAutoD simulation interface.

4.5.7 Test for Step Changes

To further test the performance of my design, the controllers are subjected to time domain step changes and the error variation monitored as indicated in the following Figures. Applying a control signal traversing between $\pm 30^\circ$ shown in Figure 4.19, produces the result depicted in Figure 4.20, respectively showing the responses from conventional PD and fuzzy PD against a set value of 45 units. With a step change applied at 1500 seconds, it is immediately observed that the FPD follows swiftly with no overshoot and at a faster response time. The error and error derivative plots for the fuzzy and crisp PDs are each represented in Figures 4.21 and 4.22. It is interesting to note how the fuzzy PD error plot adopts a continuous trend, when that of the crisp PD conformed to a sharp break as in every bi-logic controller following a step change.

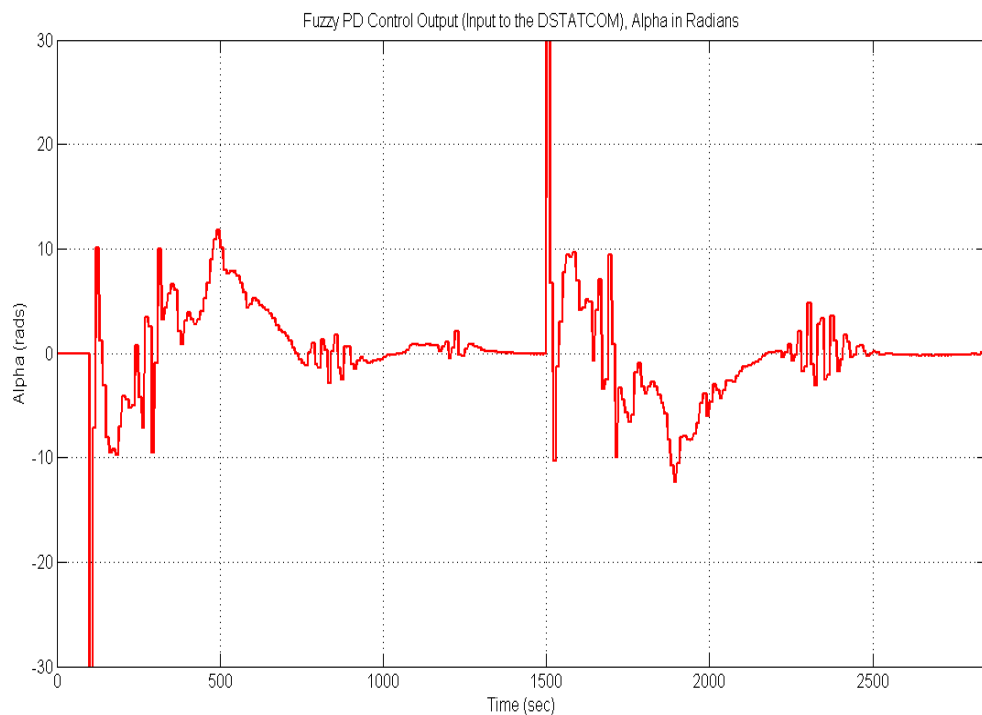


Figure 4.19: Fuzzy PD control signal

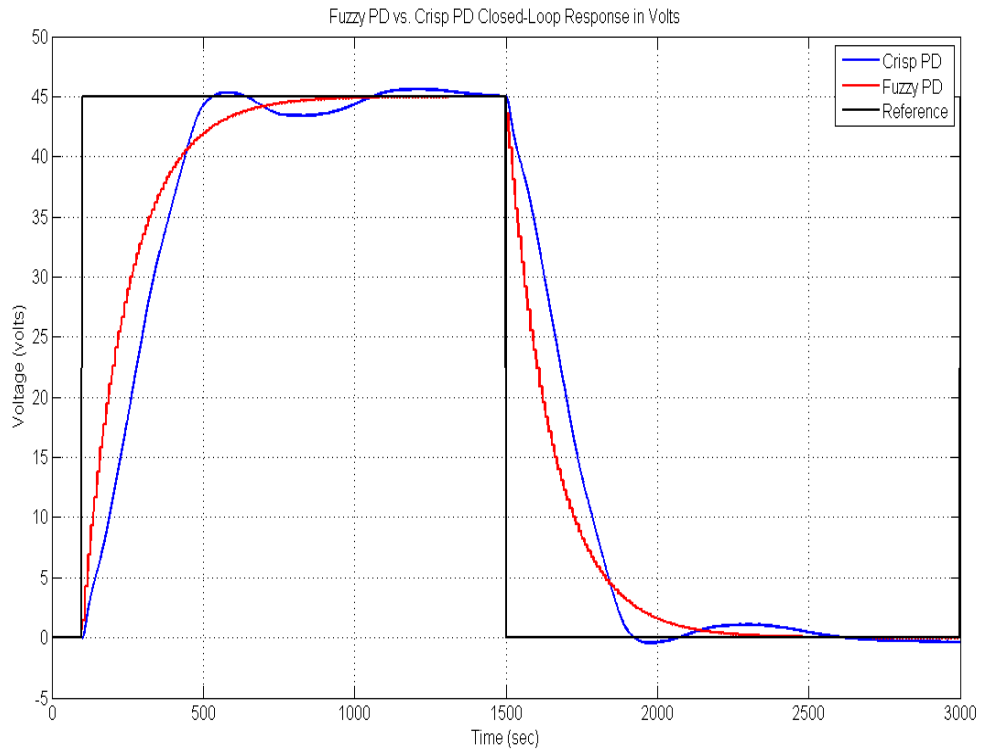


Figure 4.20: Comparing conventional PD and fuzzy PD

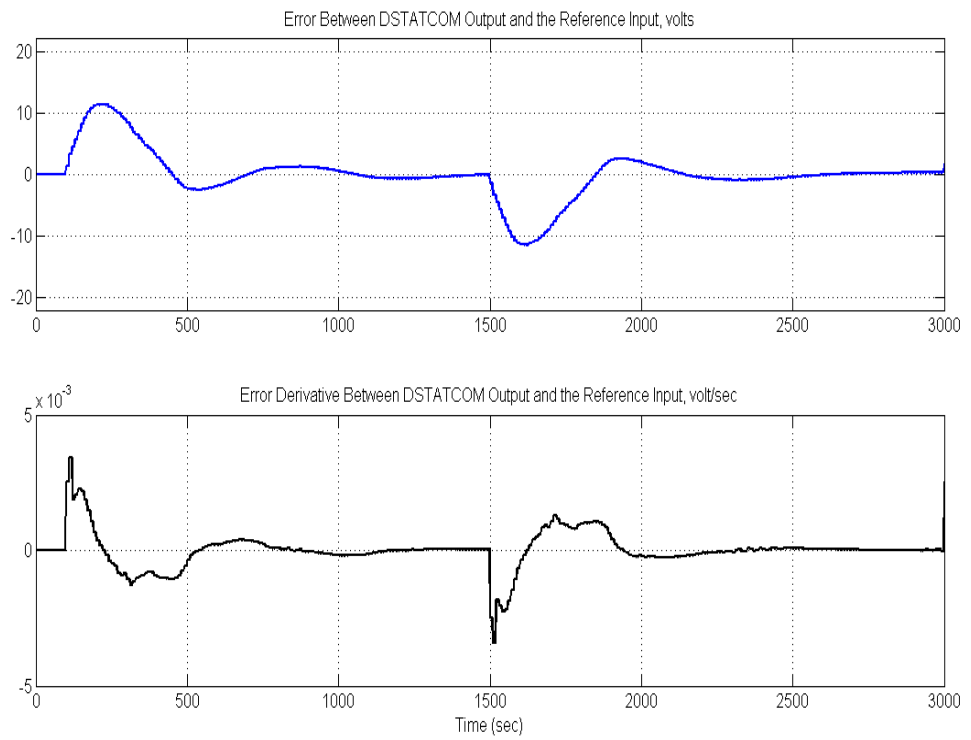


Figure 4.21: Fuzzy PD error and error derivative curves

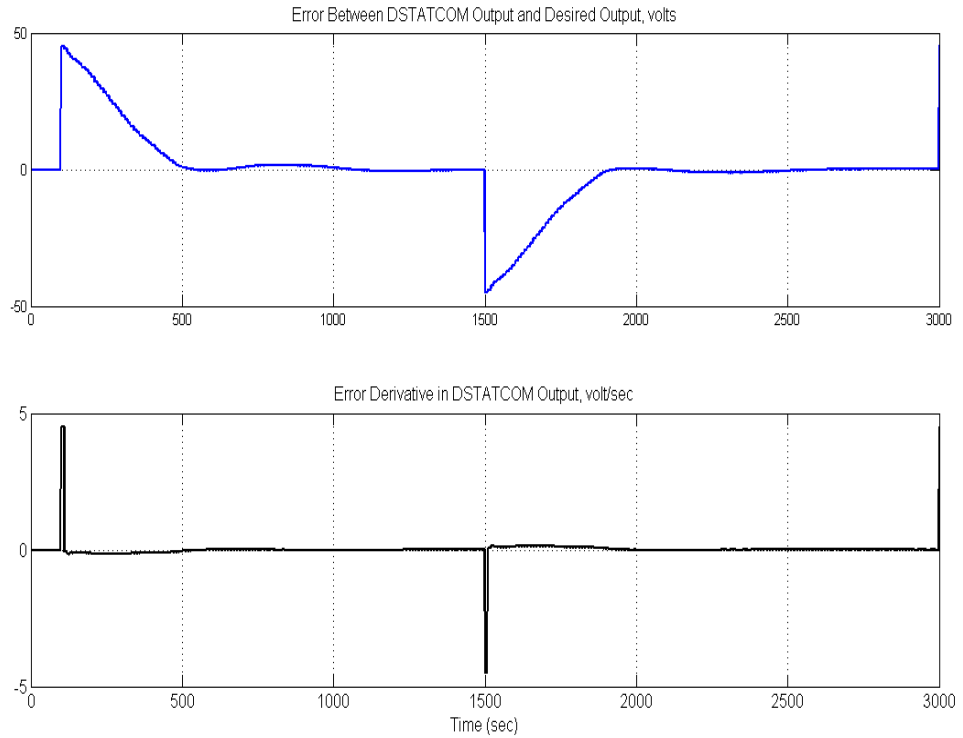


Figure 4.22: Conventional PD error and error derivative curves

4.5.8 Benefits of the CAutoD Scheme

Contrary to the existing manual CAD fuzzy PD design simulations described in section 4.4, the “intelligent” CAutoD evolutionary approach automatically evolves the fuzzy PD parameters to meet all performance specifications without going through the rigorous design procedures explained in that section. It also reduces the computational burden associated with huge rule-bases often resulting in poor loop-shaping found in changing DSTATCOMs during controller synthesis. Another powerful characteristic of the evolutionary fuzzy PD design is that; it enables online verification of various trade-offs among conflicting specifications by modifying current objectives, and searching through the projected space for selecting the best set of final controller for real time implementation. The main differences of the EA from the traditional optimisation techniques can be listed as follows:

- EA relies on objective functions whose corresponding fitness level directs the search progress rather than on derivative knowledge used by the traditional techniques
- EA is a nondeterministic optimiser whereas the traditional method is deterministic

- EA searches so many points at once in parallel rather than a single point search in the traditional method
- EA works indirectly by encoding the parameter sets rather than working directly on the parameters in the traditional method

4.6 From Manual to Automatic Design

The next subsections will describe the methods of my automated design procedure transiting from the manual design techniques. As previously mentioned. This extension is accorded through one of the component powers of the EA, particularly the genetic algorithm (GA). GA is a nondeterministic optimisation search method that always forces its way out to a global minimum from a seemingly domineering local minimum without getting stuck in the search space. Basically, it emulates the evolutionary philosophy of genetics in natural biological selection to simulate computer evolution. It performs parallel and directed search to evolve the fittest population in a given generation. The method I describe below is developed from the genetic model reference adaptive controller proposed on page 460 in (Passino 1998), depicted in figure 4.23. Next, I explain how GA is used to design and tune fuzzy PD parameters online via the CAutoD package.

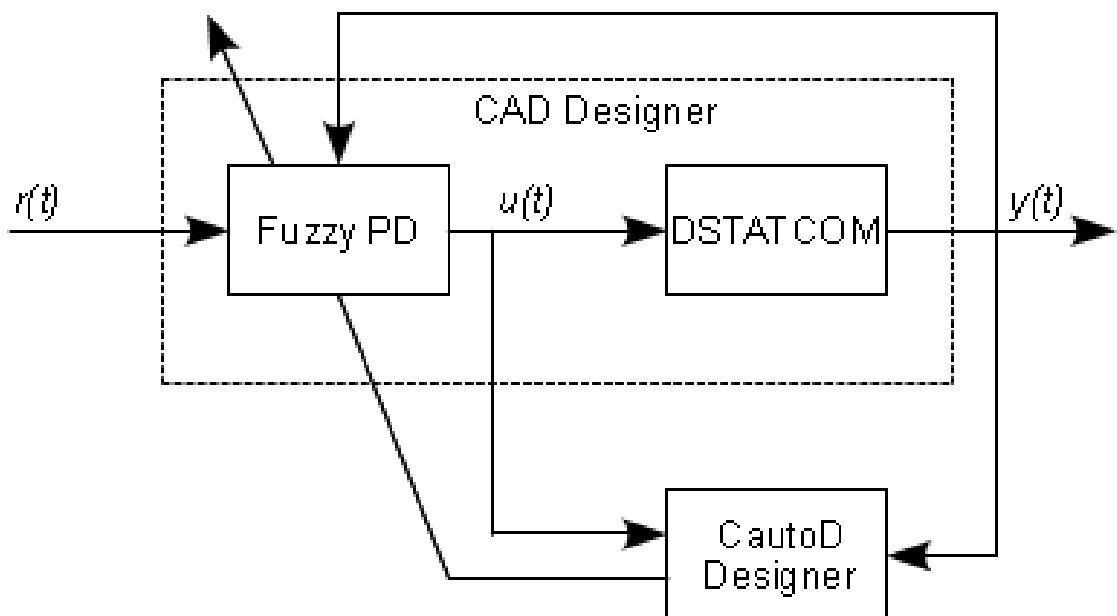


Figure 4.23: Direct CAutoD fuzzy PD controller

4.6.1 Evolutionary Stage

A pseudo-code structure of a simple genetic algorithm (SGA) is shown below from (Goldberg 1989). The population at time t is represented by the time-dependent variable P , with the initial population of random estimates being $P(0)$. I used this structure to hypothesize my optimisation problem in the remainder of this Section. The evolutionary process begins as $P(t)$ in equation 4.22, often termed as the “generation”, shifts from time t to time $t + 1$ to form a new generation of population $P(t + 1)$ through the well known genetic operators namely; selection, crossover, and mutation (Tan 1997). An initial population size $P(t) = 31$ at $t = 0$ was set a-priori over 60 generations. I set a high initial population size as a matter of priority at this point.

Algorithm 1 Simple genetic algorithm procedure (SGA)

Ensure: $t = 0$;
Require: initialize $P(t)$;
Require: evaluate $P(t)$;
 while not finished **do**
 Ensure: $t = t + 1$;
 Require: select $P(t)$ from $P(t - 1)$;
 Require: reproduce pairs in $P(t)$;
 Require: evaluate $P(t)$;

Setting the right amount of diversity of the population guarantees that GA will produce better results as it searches for more points, yet it can hamper the performance of the GA. Diversity is directly connected to the average distance between individuals such that; the higher the distance the larger the diversity and vice versa. This is described in Figure 4.24, where the diversity is shown higher at about 15% of the total number of generations. The trend seems to produce the best fitness value at my desired minimum, i.e., $\alpha \approx -0.0046$. GA being non-deterministic in its search criteria, it tends to produce a different result each time, irrespective of the number of generations run. The most important element however is the population size which was set at 20 (instead of 31), used to obtain this Figure.

Another factor directly impacting the average distance between individuals is the mutation rate (the higher the better) as is demonstrated in Figure 4.25, where a rate of 0.87 produced best fitness at exactly -0.0046 . This lead to setting the probability that one string will mutate per generation to $p_m = 0.001$. The probability and the number of crossover points are set to 0.8 and 40, respectively. The two input parameters (the individuals) are specified as error and error-rate. The “tournament” selection scheme is used for its efficiency and deterministic size variability advantage (Tan 1997). Thanks to the “ft3pak” flex-tool embedded in Matlab, depicted in Figure 4.26 that provides a suitable interface for the needed extension from CAD to CAutoD simulations during the automation process.

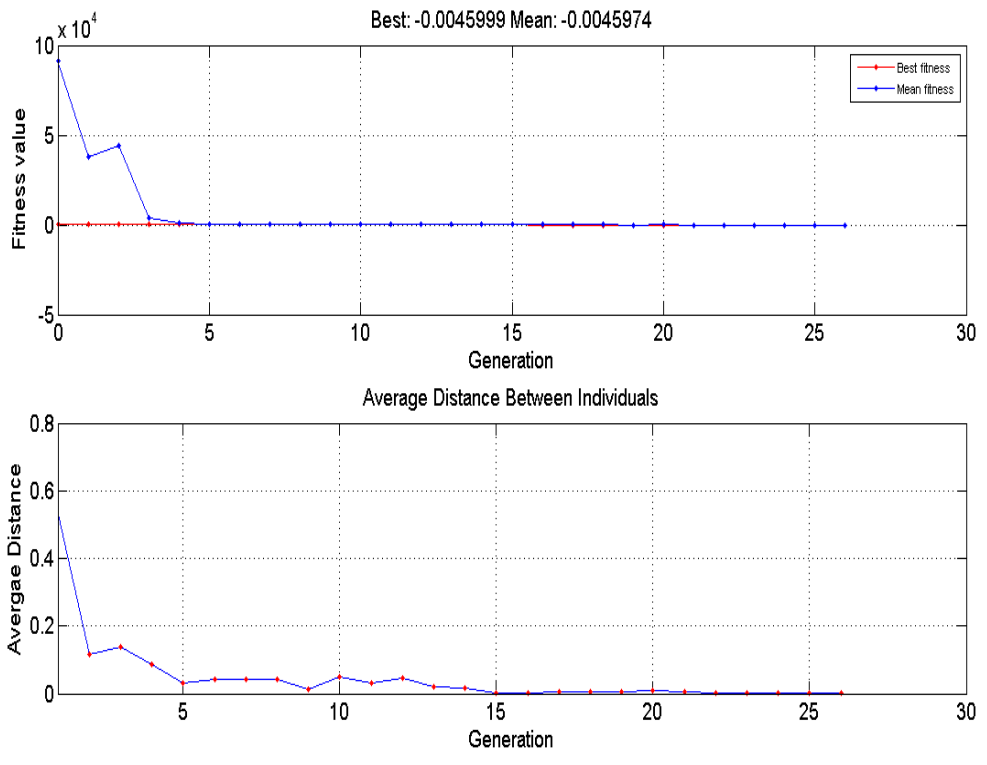


Figure 4.24: Effect of average distance

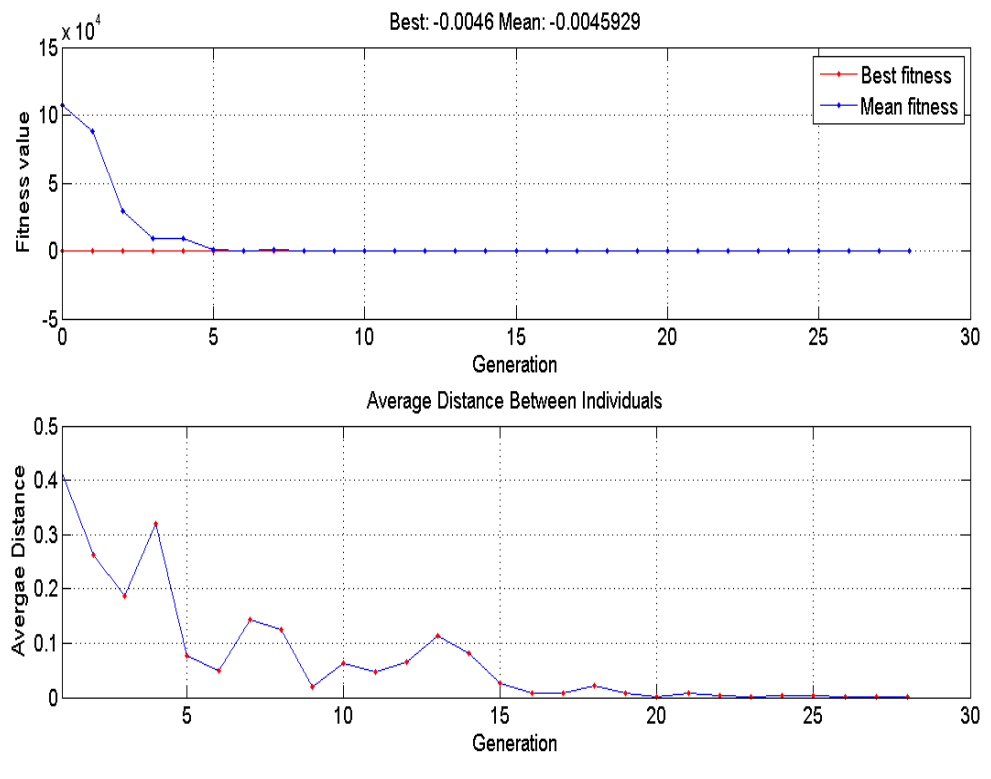


Figure 4.25: Effect of higher mutation rate

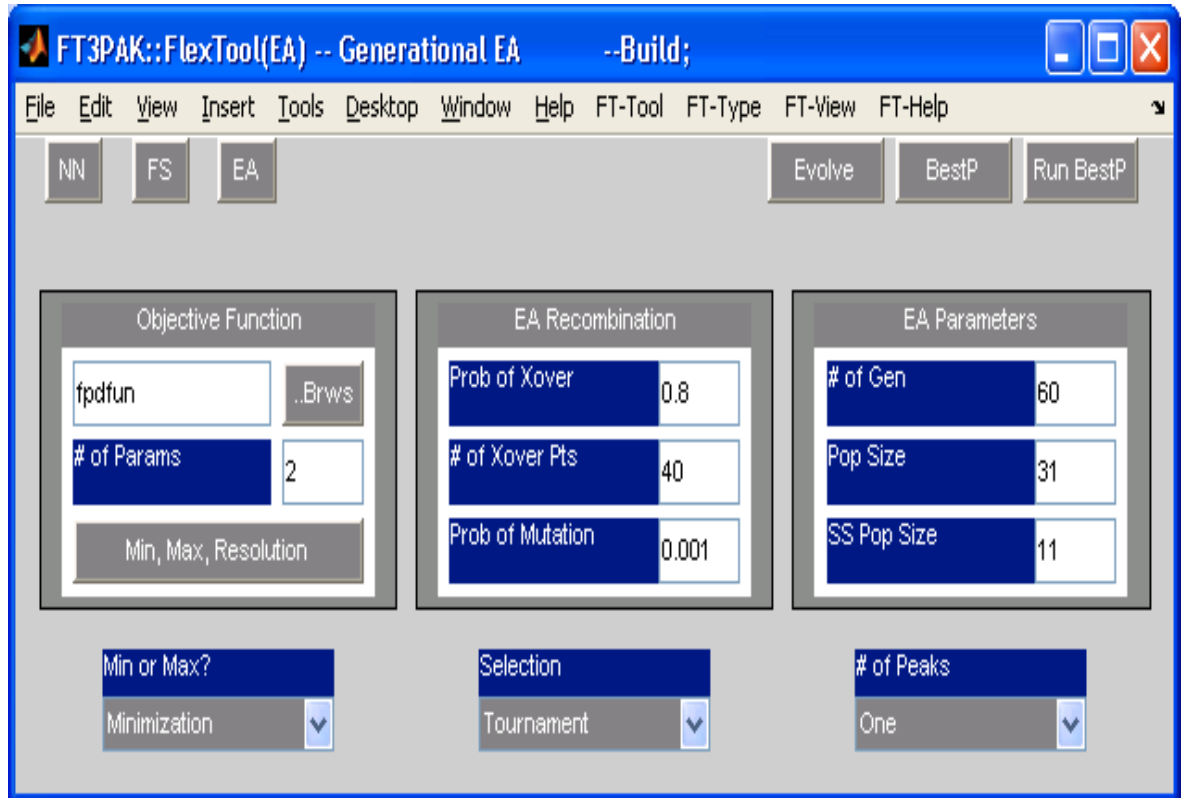


Figure 4.26: CAutoD Interface

4.6.2 Genetic-Fuzzy PD Encoding

At this stage, a genetic-fuzzy PD fusion is realised based on the genetic settings made above, plus an appropriate choice of a performance index to be made in subsection 4.6.4. The EA generates a population of strings representing individual candidates of controllers through the routine described in Figure 4.27. After initialisation, the EA accesses and obtains the input-output data from the model at each time step via the CAutoD interface during simulation, so that fitness of each emerging controller from the population may be evaluated. While this is happening, a new fitness function is being calculated from the error resulting between desired and actual model outputs. Optimal solutions are estimated whenever the error is driven to zero, otherwise the EA propagates to the next generation of controllers through crossover and mutation until optimal solution is achieved. The fittest controller (string) in the population is then chosen for the system control. This allows automatic evolution of the controllers through generations in time steps, thereby tuning the controllers in response to model changes.

4.6.3 Problem Formulation

Optimum customer's voltage profile also known as integrated Volt-VAR control (IVVC) at the point of common coupling (PCC) can be formulated as a minimisation problem.

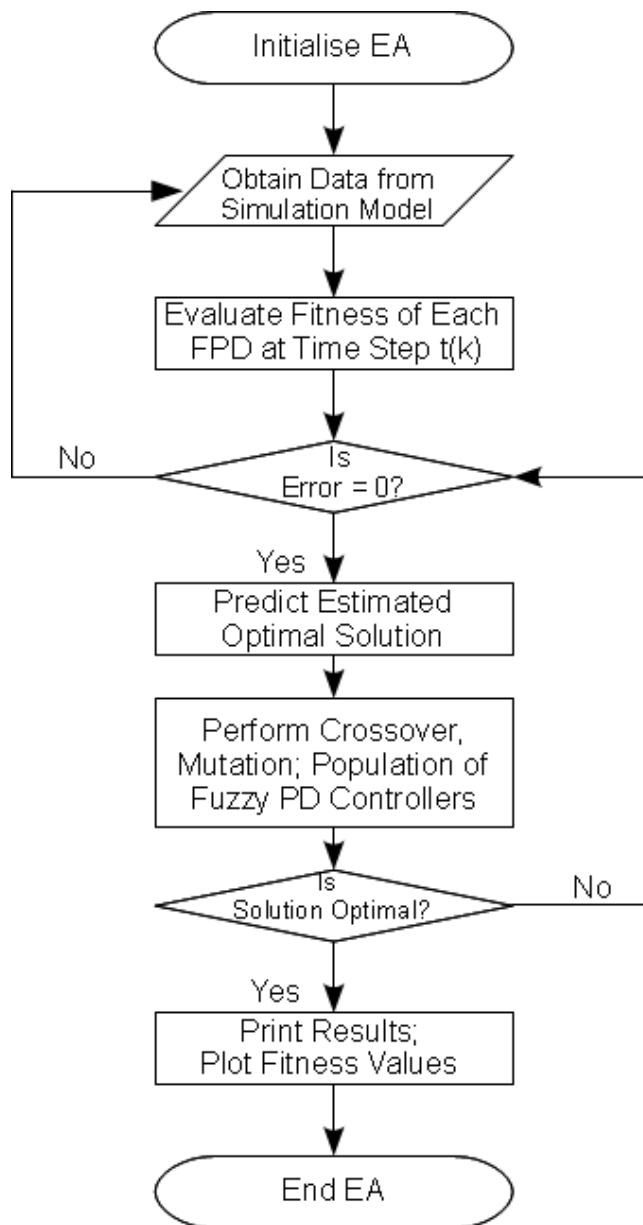


Figure 4.27: EA-FPD routine

Again, the objective is to regulate DSTATCOM's input (control output) by forcing the control error to zero. The algorithm for computing the minimum cost function for the DSTATCOM's input α within the time interval t in a closed-loop fashion is expressed as:

$$F_{cost}[\alpha(t)] = \min_J [e_{cost}(t) + de_{cost}(t)] \quad (4.16)$$

Contrary to my earlier formulation in Eq. 4.14, where the index was based on traditional performance measures. I inclined to deal directly with the parameters of the fuzzy PD through the measure of its error index from Eq. 4.16 using EA to minimise the function \bar{J} as set out in (Feng 2000). It is understood EA can easily convert a minimisation problem to a maximisation one by simply transposing cost function to fitness function through $J \Rightarrow \bar{J}$ in the Euclidean space $f : \mathfrak{R}^+ \rightarrow \mathfrak{R}^+$. Thus, the following fitness function can be used to minimise \bar{J} , such that

$$J = \frac{1}{\bar{J} + \epsilon} \in (0, 1) \quad (4.17)$$

and $\epsilon > 0$ is a small positive integer. J can thus be maximised by minimising \bar{J} to yield the desired response. Here, the error (e) and its rate of change (\dot{e}) between the setpoint and the actual plant output are considered as fitness (individuals).

4.6.4 Choice of the Performance Index

To enhance my choice, I looked beyond the traditional ITAE and IAE indices normally found in CAutoD package and added the derivative of the error (\dot{e}) to the basic index, as a requirement for high accuracy and low chattering at the steady state, and constructed the following performance index in the time domain.

$$J = J_{ITASE+ITASED} = \sum_t^n t|e^2(t)| + \sum_t^n t|\dot{e}^2(t)| \quad (4.18)$$

where J_{ITSE} and J_{ITSED} are the costs of the respective model components; $e(t)$ and $\dot{e}(t)$ are the same as above under no-load condition, referred to as the individuals; and n is the final-time. The chosen performance index is expressed through the individuals consisting of real-valued vector of two parameters each, normalized around [1 -1] and

[0.5 -0.5]. Illustration of the minimum and the maximum values of the combination of the individuals portrayed in 3D, 2D and the contour plots are shown in the following Figures. The plots demonstrate how well behaved the chosen function is, while converging to a single global minimum which occurs at the point [0 0] in the x - y plane. And the maximum is also noticed to converge at 1 in the same plane.

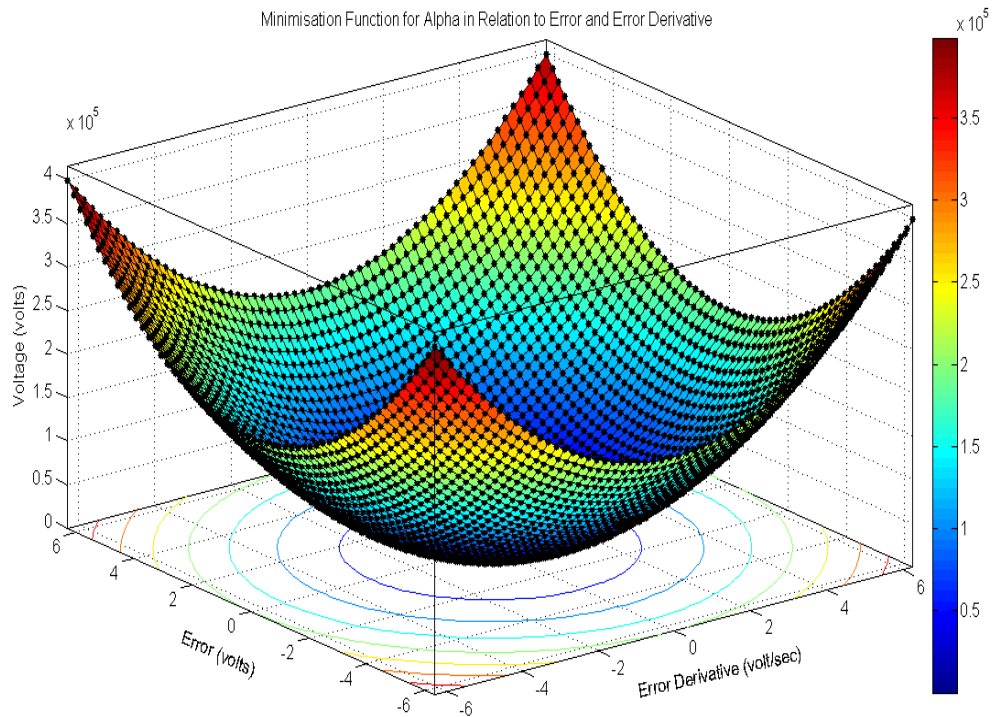


Figure 4.28: Minimisation plot in 3D

4.7 Conventional Optimisation Tools

The application of optimisation techniques to the sectors of the power system, especially the area of operation and planning, which is often a large scale problem has seen tremendous improvement over the last three decades. A detailed survey on particle swarm optimisation (AlRashidi & El-Hawary 2009) and evolutionary computation applications in general power systems are respectively given (Alvas da Silva 2002) and (AlRashidi & El-Hawary 2009). Notwithstanding, their particular application to solve PQ problem in DSTATCOM is still limited. Thanks to the optimisation toolbox available in Matlab environment, through which numeric computing power of matlab is extended to enable me use other optimisation techniques to compare my non-gradient to gradient methods presented in chapter 6. In this chapter, two evolutionary methods for DSTATCOM control have been proposed and detailedly described for solving power quality problems.

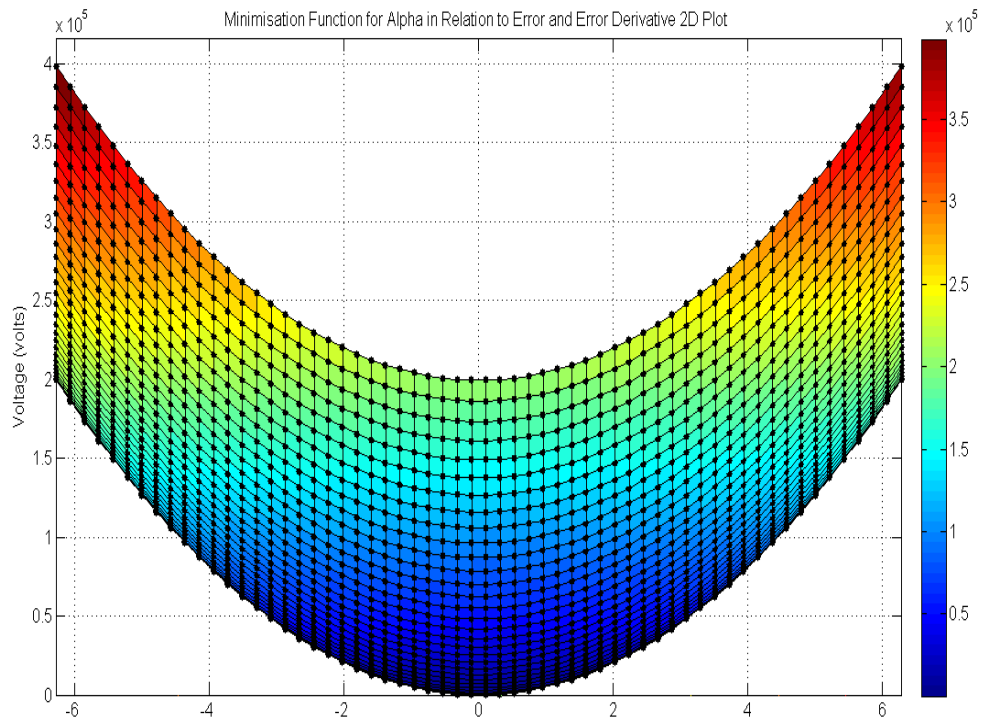


Figure 4.29: Minimisation plot in 2D

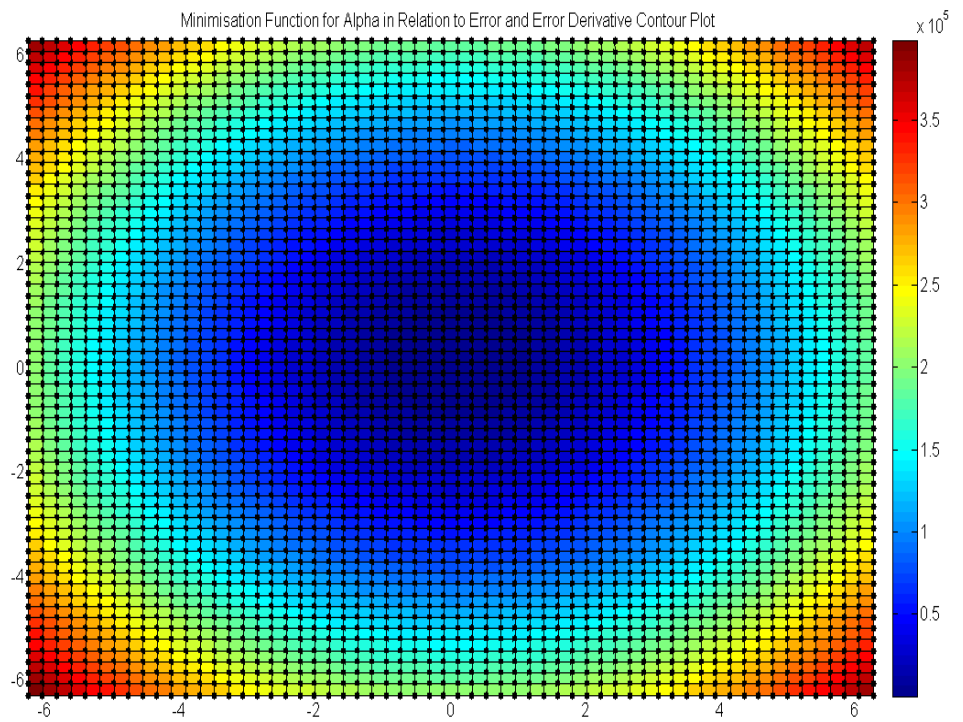


Figure 4.30: Minimisation contour plot

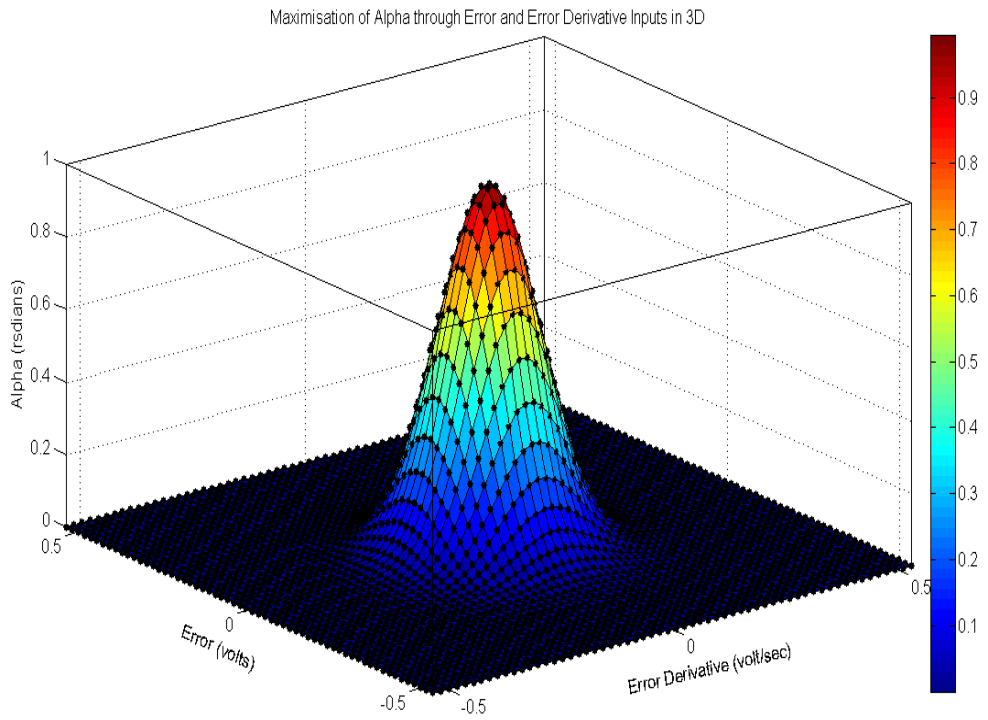


Figure 4.31: Maximisation plot in 3D

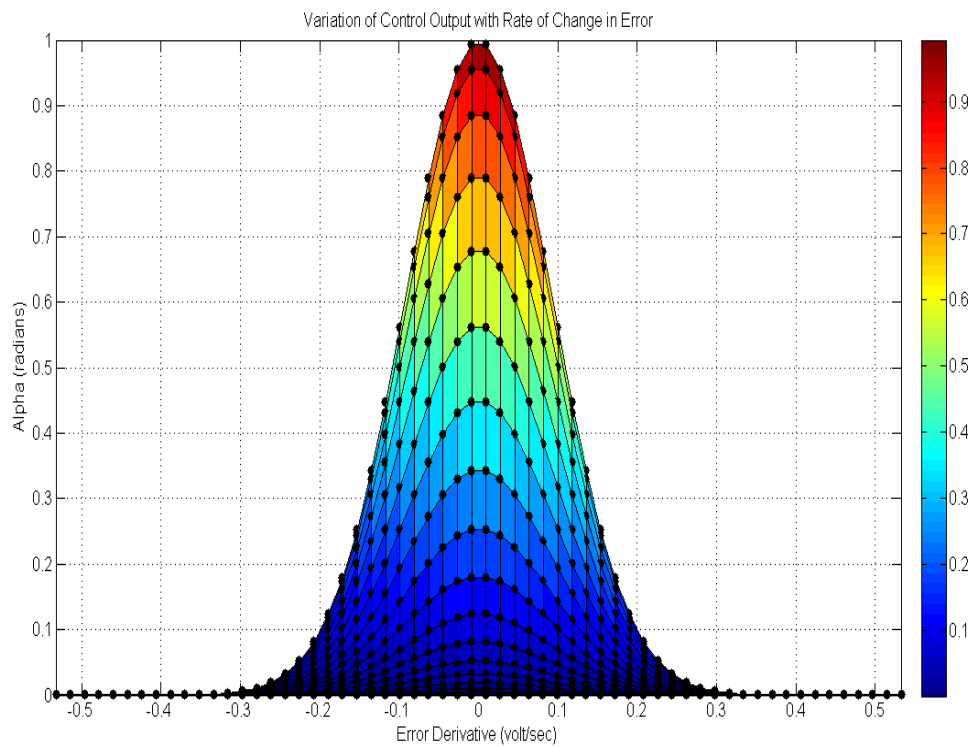


Figure 4.32: Maximisation: α vs. \dot{e}

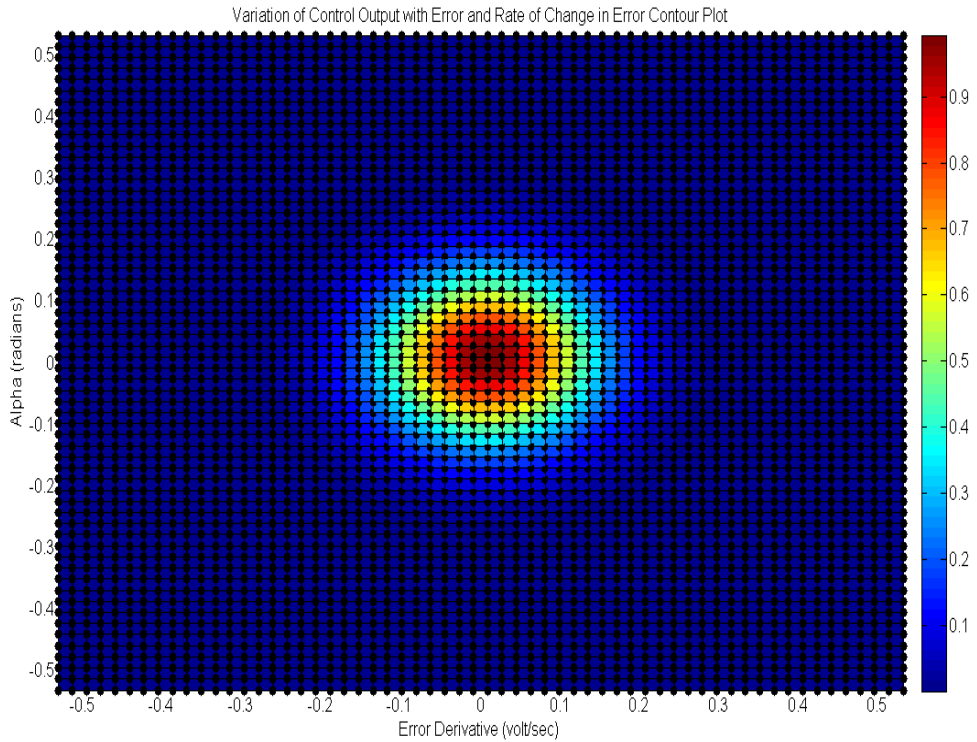


Figure 4.33: Maximisation contour plot

4.8 Methods for PQ Control System Design

I proposed two novel solutions to the DSTATCOM problems. Both of which are based on evolutionary computer-automated-design interface. The first method designed an evolutionary fuzzy PD control algorithm in this chapter (explained below), while the second is based on evolutionary model-free predictive control algorithm presented in chapter 5.

CAutoD for FLC

The concept of CAutoD perhaps first appeared in 1963, in the IBM Journal of Research and Development as a written computer program to search for hardware constraints on logic circuits (Kamentsky & Liu 1963). It is now possible to transform traditionally CAD simulation into CAutoD through biologically-inspired machine learning or search techniques like evolutionary computation (Clune & Lipson 2011); (Li et al. 2004); and (Hornby 2003).

These biologically inspired evolutionary algorithms offer reduced search time in solving multi-objective problems by encoding non-numerical design parameters. The search process is accomplished through three well known stages namely; selection, crossover

Computer-Automated Design by Artificial Evolution

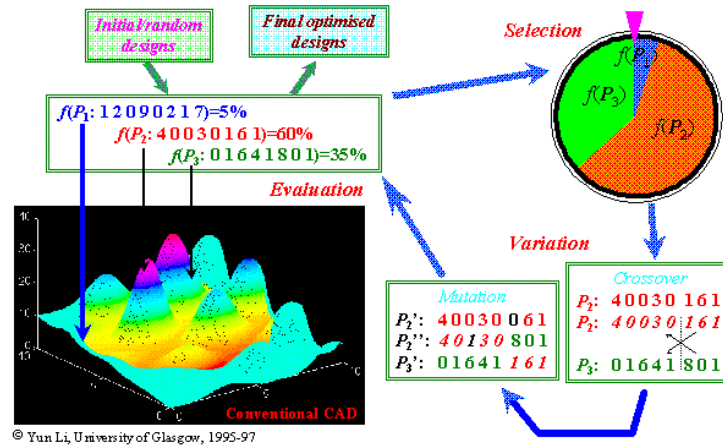


Figure 4.34: CAutoD by artificial evolution (Li, 2004a)

and mutation, using survival-of-the-fittest a-posteriori learning, refer to (Li et al. 2004) for details. Optimal designs often begin by sourcing initial generation of candidate at random from an existing designer’s database. Final evolution would include the fittest candidates representation of automatically optimized digital prototypes. Figure 4.34 depicts the “ft3pak” representation of the CAutoD package as a non-deterministic polynomial optimisation technique. For this work, the DSTATCOM is loaded in the feedback with a simplified three-ruled fuzzy-proportional-derivative (FPD) controller as an adaptive mechanism whose parameters are assessed continuously in order to update the control variable as explained in section 4.8.1.

4.8.1 Automated Fuzzy Control System Design

Evolutionary algorithm based adaptive mechanism is planned to be used for this case as a CAutoD designer. It observes control signals from the fuzzy PD controller and adapts its parameters, whilst updating them continually under plant parameter uncertainties. In such case, the desired performance may be characterised as that of a reference model which the controller tends to emulate in a closed-loop fashion as described in chapter 4 via Figure 4.23 from (Passino 1998). The use of CAutoD in this context invokes the capabilities of artificial evolution to become “computer-automated-design” which can “intelligently” guide the performance of the candidate controllers to tune those parameters in meeting the system’s specifications.

4.8.2 CAutoD Tuning of FPD Control Systems

Since the EA works by trying to maximise a fitness function $J(\theta)$ in selecting the individual denoted by θ (4.6). The computer representation of EA can be achieved by

making θ a string, or “chromosome” in a biological sense. While in a computer sense, the string comprises of digit locations or “genes” to encode different values or “alleles” from a number system, e.g. alleles from the base-2 covers the set $\{0, 1\}$ and those from base-10 covers the set $\{0, 1, 2, 3, 4, 5, 6, 7, 8, 9\}$. Thus, a binary chromosome would have zeroes and ones in the gene locations. Therefore, optimising parameters given in base-10 number line needed to be encoded to binary through the known standard base-2 conversion procedure before being decoded back to base-10 again. In order to avoid the encoding/decoding computational cost for online applications, I based all my EA designs on base-10. Since I am committing EA to fuzzy PD tuning, I need to represent the K_P and K_D parameters for any given PD controller as individuals. I use my pre-calculated PD controllers from chapter 3 as an example, where $K_P = 0.100$ and $K_D = 0.300$. Then the chromosome representation can respectively be cited as +010000 and +030000. Note the concatenation of the digits to form chromosomes for which I assumed six digits plus the sign digit for each parameter. The decimal point’s position is left for the computer to track. Each chromosome has its unique structure biologically referred as “genotype” and also represents a unit point of the EA in the search space called “phenotype”. I can now assign a syntax to represent a population of individuals (i.e., a whole set of PD controllers) by setting the k^{th} chromosome to be defined as

$$\theta^k(t) = [\theta_1^k(t), \dots, \theta_M^k(t)]^T \quad (4.19)$$

where θ^k denotes a single parameter of a fixed string length at time t , and M represents the “traits” of all the parameters in k . Note the concatenation of elements to form a vector which I will use to base my computer algorithm instead of concatenating the elements to form strings as I did before. So that, the population of individuals at time t can be defined as

$$P(t) = \{\theta^k(t) | k = 1, 2, \dots, N\} \quad (4.20)$$

where N stands for the number of individuals in the population. This number is chosen to be big enough in order to minimise the number of computations and enable elements in the population to cover the entire search space as detailed in chapter 4.

4.8.3 CAutoD for Fuzzy PD Systems

Table C.7 presents the best controllers obtained by randomly evolving fuzzy PD parameters for different EA runs in a DSTATCOM designed for some medium distribution

voltage range between $318V - 1.1kV$. The quality of the scheme is tested and demonstrated in the following Figures.

Figure 4.35 compares the performance of an EA based Fuzzy PD and EA based crisp PD controllers. The effectiveness of the EA-FPD scheme is readily seen converging much faster than the EA-PD. The existing trade-offs resulting from the design objectives for 31 emerging controllers at the end of the evolutionary CAutoD routine is also depicted in Figure 4.36. Five different combinations of the “best” PD and FPD controllers depicted respectively in Figures 4.37 and 4.38, produced the “best” and “worst” case scenarios for the fitness function of the EA-FPD controllers at any one of the five runs plotted in Figure 4.39. In this respect, the design engineer can quickly choose from the table a resulting controller to suit particular function for implementation, e.g. $KP_1 + KD_1 = J_1$ is a standalone implementable PD controller, and so on. The method also gives the engineer an advantage for diverting the evolution to focus on special trade-off decisions during conflicting engineering objectives which are ordinarily too difficult to make.

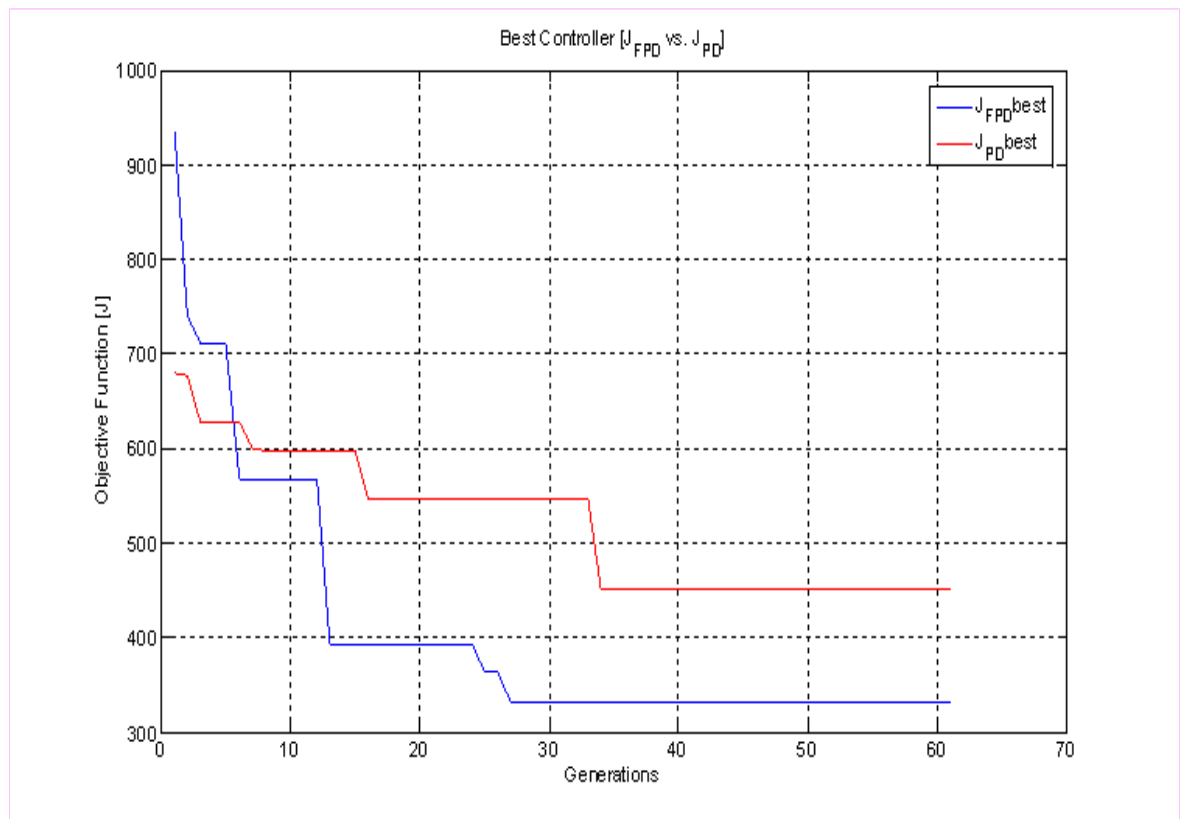


Figure 4.35: Evolutionary FPD vs. PD

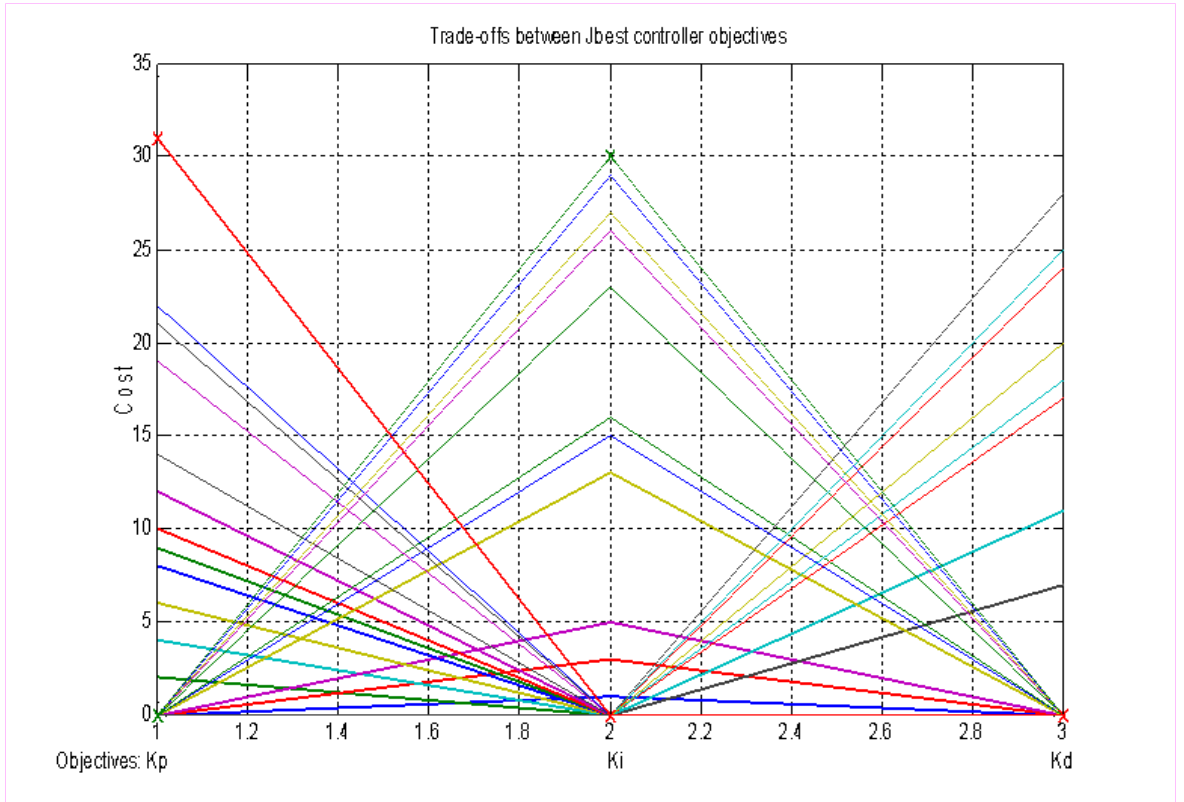


Figure 4.36: Trade-offs between control objectives

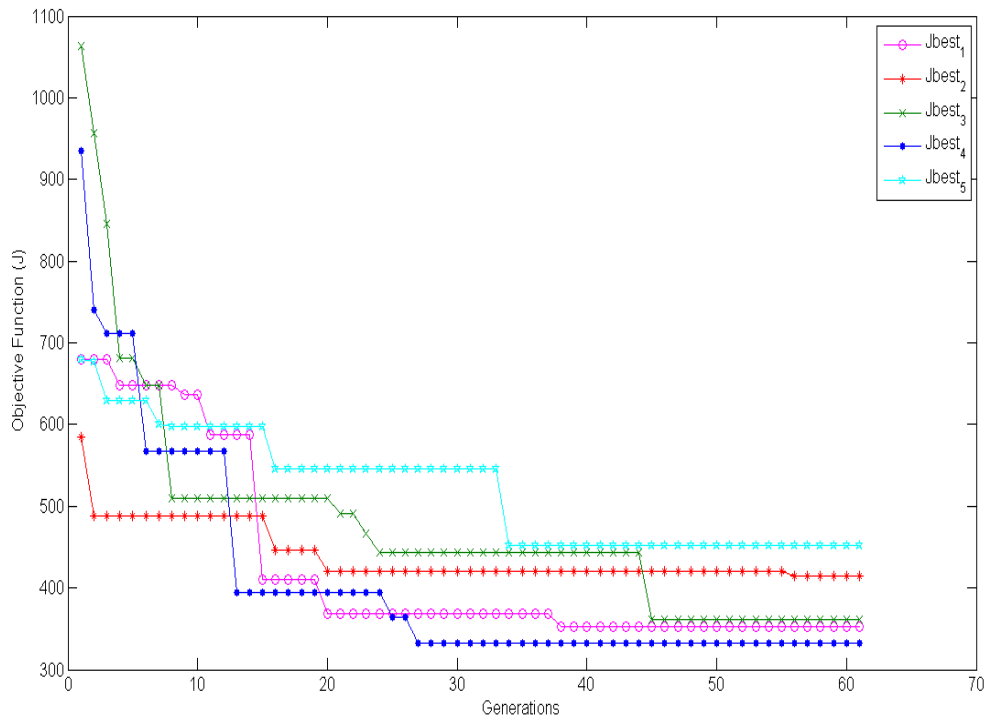


Figure 4.37: Best PD controllers

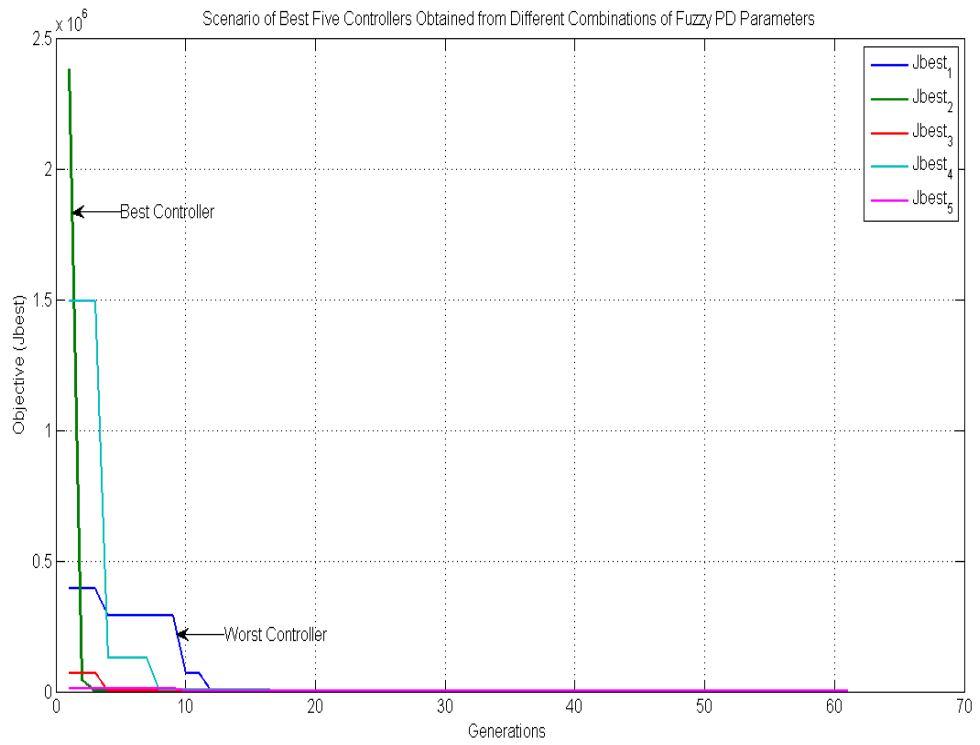


Figure 4.38: Best FPD controller

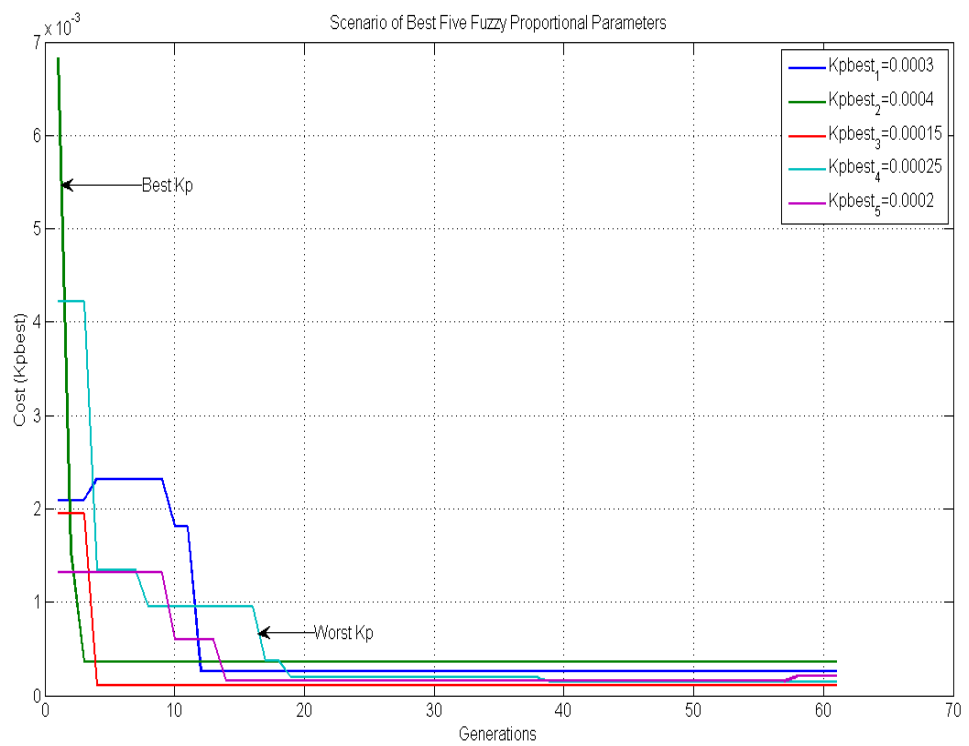


Figure 4.39: Kpbest parameters

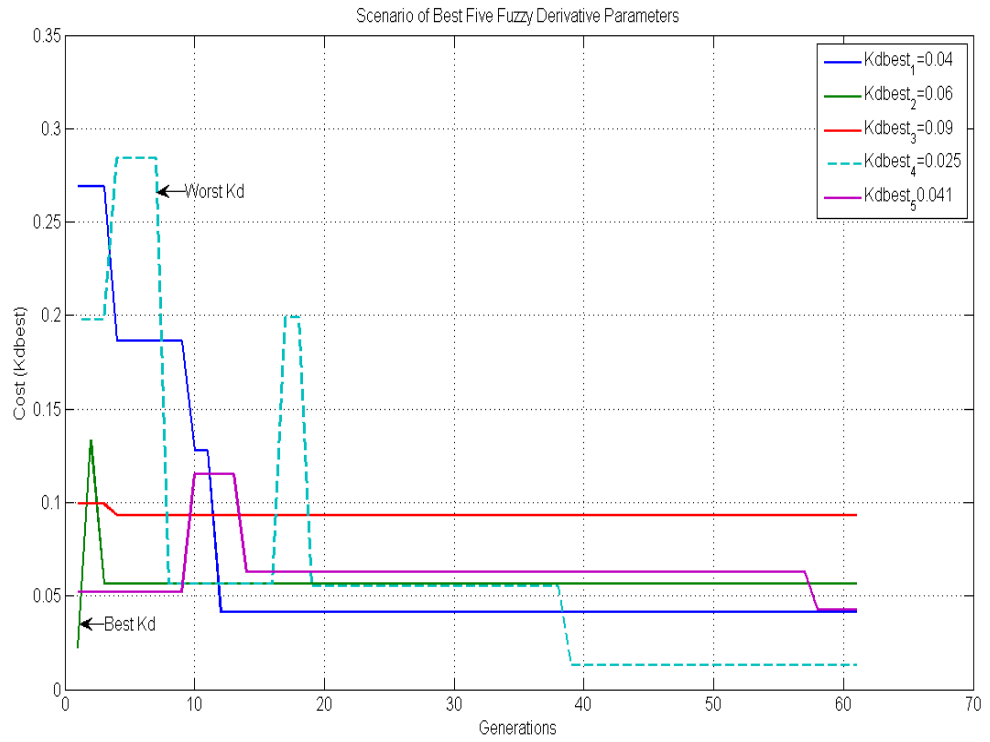


Figure 4.40: Kdbest parameters

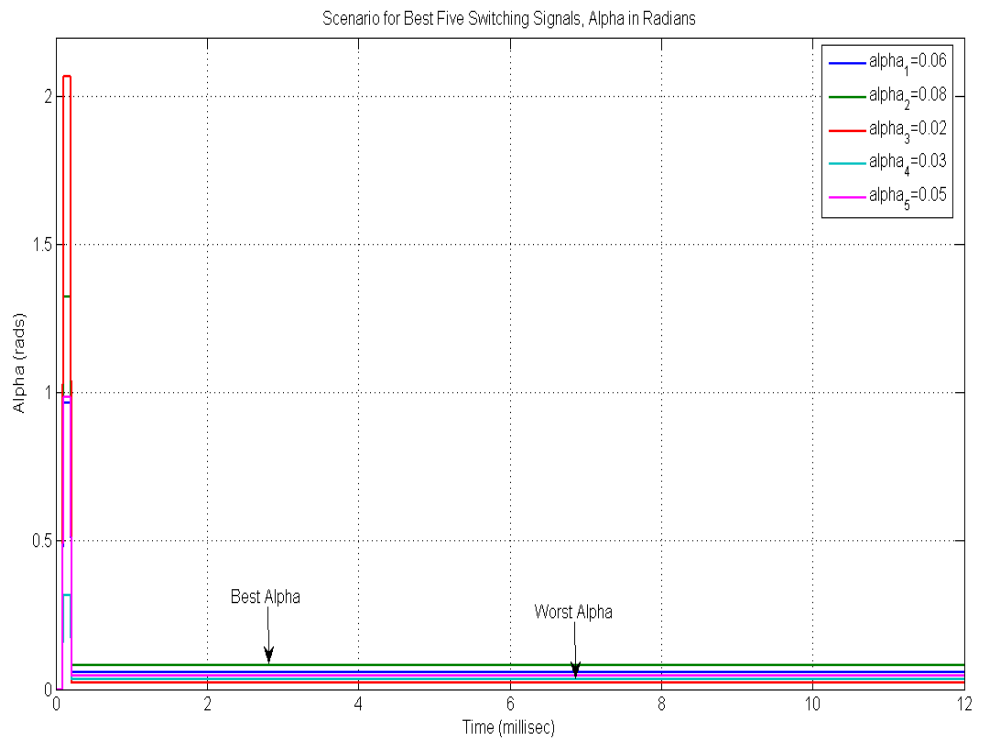


Figure 4.41: Best switching signals

4.9 Summary

This chapter studied and evaluated the practical viability of an off-line simplified three-rule base fuzzy system design which eventually had its parameters accessed and updated through an online EA based CAutoD interface. Having presented a detailed off-line computer-aided-design based Fuzzy PD scheme, this chapter has also developed a robust online CAutoD-Fuzzy PD algorithm for practical DSTATCOMs application in section 4.6. The first part of the chapter was pre-occupied by rigorous manual tuning performance evaluation of the fuzzy PD controller based upon TSK model. The fuzzy PD overcomes the robustness and steady state performance tests when applied to both perturbed and unperturbed plants as compared to crisp PD and PI controllers. However, the second part was dedicated to automating the manual design through CAutoD package as a way of extending the CAD design from (Li & Häule 1996). A robust online evolutionary algorithm procedure has been studied, and a tournament selection was proposed to avoid the added computational cost involved at each generation during interpolation, chromosome sorting and fitness averaging as in (Tan 1997). Also in this chapter, the diversification of single control problems to multiple solutions has been demonstrated through continuous evolution. This lead to the satisfaction of all desired specifications with interactive trade-offs between control scenarios automatically generated and tabulated without having to perform any re-design task as would have been the case in a manual setting. Finally, comparison between automated and manual design performances presented in chapter 6, has shown the uniqueness of my technique by intelligently converging at higher speeds. However, the major disadvantage with the technique is huge memory resource requirement which will make it uneconomical for real time implementation. Therefore, I decided to use the chapter to serve as a basis for comparison with my main contributory work which deals with model-free predictive controller (MFPC) design for DSTATCOMs, presented in chapter 5.

Chapter 5

Evolutionary Design of Model-Free Predictive Control Systems

5.1 Methodologies

In chapter 4 we have seen how manual computer-aided-design (CAD) of a fuzzy PD controller was automated by way of extension through CAutoD-fuzzy PD amalgam. The CAutoD scheme was shown to supersede its CAD counterpart in terms of steady state performance and robustness to model changes. However, despite these abilities, it still remains doubtful as to whether the combination could favourably compete in terms of cost savings and computing memory resource allocations which in real-time applications would be very unattractive for utilities. More importantly, the question which has not been properly addressed by this combination is that of safety and equipment constraints. Saturation at the output may have been automatically taken care of, but issues arising due to natural limitations which could be imposed on the model's input-output ports have not been discussed anywhere in the literature, and this is a significant drawback which needs be addressed. For this reason, this chapter proposes a novel model-free predictive controller for direct online application in DSTATCOM as an optional smart solution to power quality (PQ) problems. The new scheme is based on the operating principles of the traditional model-based predictive (MPC) control. With 30 years of chemical industrial presence, the MPC has grossly been under-utilised particularly in the academic community where its chief advantage, the potential to inherently handle constraints (removing the need for anti-wind-up due to integrator presence in the PI controller) was hardly acknowledged, and therefore renegaded its role to slow industrial processes. The literature has quite recently suggested the application of the MPC in nonparametric and nonlinear systems with higher bandwidth, see for example, (Kashiwagi & Li 2004); (DoyleIII et al. 1995). It has additionally

been regarded as the only advanced control technique to have significantly impacted the industrial process on a wider scale for the following reasons from (Maciejowski 2002):

- The only generic control technology consistently dealing with equipment and safety limitations
- The same basic formulation applies to both single and multi-variable plants
- It is easy to understand and implement
- It is more powerful than PID at all levels and easier to tune even in complex loops containing long delay constants

Briefly described, the MPC uses its power of prediction to solve online optimal control problem in the open loop. While closed loop performance is achieved through measurements in the next time-step to update the optimisation problem. The underline principle is to assume a linearised model of the plant and implement the first control sequence at each time-step receded over a finite control horizon. Some of its earlier successful strategies were built upon step response, impulse response and state-space linear models including, for example, model algorithmic control, extended horizon control and generalised predictive control. The reader is referred to (Nikolaou 2001); (Barry & Wang 2004) for detailed survey on the MPC theory and practice. Nonetheless, most of the applications reported therein were strictly restricted to slow linear and not-too nonlinear processes.

Research activities enhancing MPC technology rapidly expanded when its ability to operate plants closer to the limits while dealing at the same time with real-time constraints became apparent. This resulted in a variety of faster schemes in linear approximation of nonlinear processes being developed as in (Zanma & Asano 2010); (Wang & Boyd 2008); (Stenman 1999); and (Trulsson & Ljung 1985). I have in the previous chapters learnt that point-wise online linearization requirement in an environment riddled with missing algorithmic gradient information makes the PI unsuitable for smart control systems (Canale et al. 2006). While, heavy rule-based computations slow down the system and lack the credible stability criteria for assessing the system. The model approximation errors and heavy computational burden caused by slow online optimisation routines tend to make model-based designs even more unattractive in the wider industrial application.

In this contribution, the possibilities of applying model-free predictive control (MFPC) methods in distribution static compensator (DSTATCOM) have been explored. I began

with augmenting a saturation element in nonlinear modeling of DSTATCOM through describing functions. Then, a Nelder-Mead simplex optimiser is incorporated in the MFPC as a non-gradient routine rather than the usual gradient or linear quadratic programming (LQP) solution offered in (Johnson & Moradi 2005). The idea is to bypass the model-based computational burden and predict the presence of limit cycles for enhancing stability in order to support efficient practical online tuning in the simplest possible way. Finally, simulation exercises carried in Matlab/Simulink environment confirmed the superiority of my novel MFPC scheme over the previously presented control methods as well as over other optimisation techniques.

5.2 Revisiting the MPC Structure

In this section, I highlighted on the concept and the basic structure of the model-based scheme as a preamble to my model-free design. The concept of the MPC is built upon the idea of generating process inputs (control actions) online, serving as solutions to a practical optimisation problem which is solely dependent on the process model and process measurements. The process measurements construe the MPC's feedback and/or feedforward element. The basic structure of a typical MPC is described through Figure 5.1 from (Nikolaou 2001).

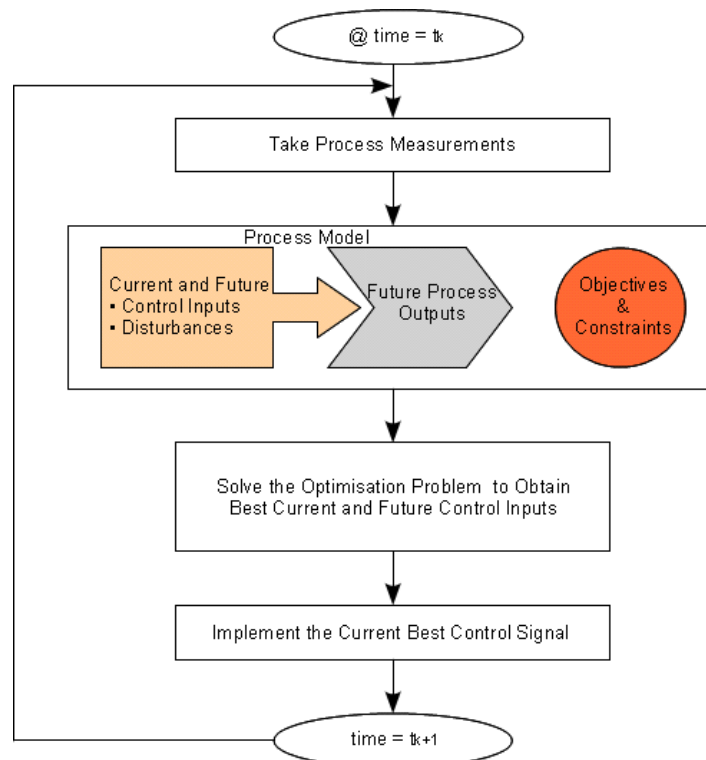


Figure 5.1: Basic MPC structure

Realisation of the MPC has been straightforward especially in slow dynamic plants like the chemical process, in which online optimisation is readily feasible. In such situation, the MPC solves a receding open-loop real-time optimal control problem over finite time horizon, with the first control of the resultant control series being executed on the process (Perez 2008). Rather inappropriately, most of these designs were based on linearised process models, whereas the majority of systems practically available are nonlinear. Hence, using nonlinear models with robust optimisers such as the non-gradient simplex algorithm proposed in this thesis is the only way to meet all the required system's performance specifications.

5.2.1 Description of the Basic Principle

A general framework notation of the MPC is presented in Figure 5.2 showing the internal model (Q) assumed to be linear for calculation simplicity, which is used in predicting the behaviour of the DSTATCOM model (P) starting from current time (t) through a future prediction horizon (M). The predicted behaviour is a function of an input trajectory dependent on the condition at the current time stated as $u(t+i|t)$; for $i = 0, 1, \dots, H - 1$, applied over the entire prediction horizon with the aim of finding which input produces the best prediction. The filter (F) located ahead of the setpoint $r(t)$ may be designed as a first-order low-pass with unit gain and small time constant or a critically damped second-order with high natural frequency. Its purpose is to add robustness to the model following by providing smooth reference signal through soft-start. The DSTATCOM is modelled as P: $\mathfrak{R}^N \mapsto \mathfrak{R}$ subjected to disturbance $d(t)$, where N represents the degree of freedom in the control input $u(t)$ requiring online optimisation. And the controller block (K) is responsible for issuing the control signal of length N by minimising the error between y_r and the predicted plant output y_m over a finite future horizon acquired through current output of the plant $y(t)$ (Perez 2008). As in other control formulations, the MPC design objective also poses a minimisation problem of a cost function, J: $\mathfrak{R}^N \mapsto \mathfrak{R}^+$ subject to some specified constraints which I will still maintain in my model-free design. The reader may refer to (Maciejowski 2002) for details.

5.2.2 Model-Based Formulation

Two basic approaches to model-based predictive control designs are available i.e., state-space model-based scheme, and the input-output model-based scheme. I adopted the former in the first part of this chapter, as it is the commonest framework where designed controllers have specified terminal reference conditions. That is, at the end of horizon

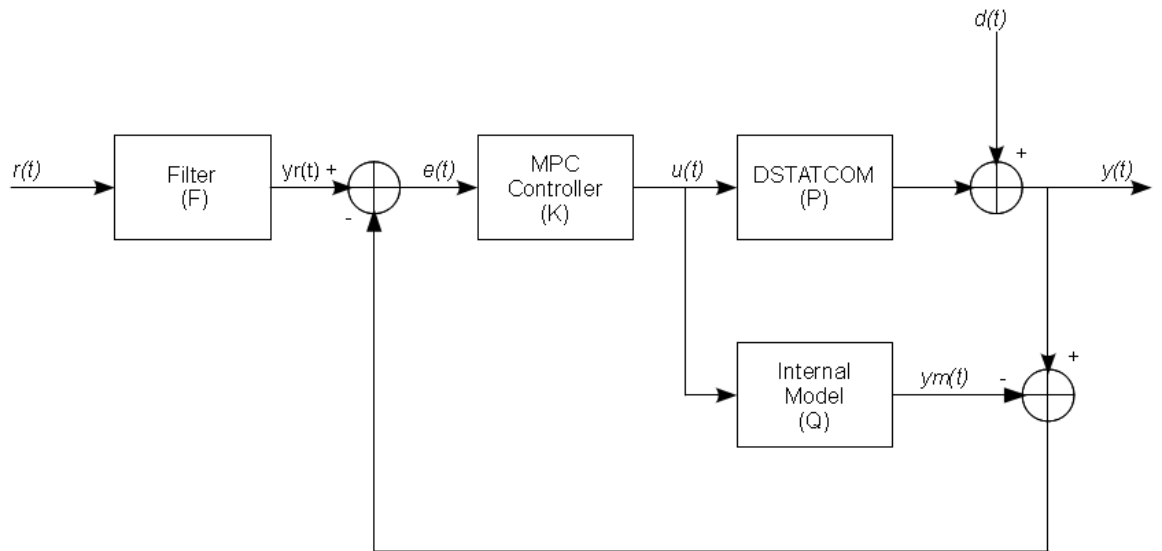


Figure 5.2: General MPC Framework

$t + M$, the control $u(t)$ should be calculated in a recursive manner backwardly to the present time. In the latter scheme, the control is aimed at achieving the predicted performance of the plant as specified, which I applied in the second part of the chapter (model-free design), because of its ability to deal with real-time control problems as they emerge.

The discrete feature of the MPC according real-time control through simple quadratic programming over finite horizons seems to have boosted its applicability. Leading to its basic formulation being built upon certain universal assumptions given in the literature. Such as a linear time-invariant plant model with a quadratic cost function which penalizes changes on the input vector ($\Delta u(t) = u(t) - u(t - 1)$) rather than penalising the input vector ($u(t)$) values directly; and that all constraints are in the form of inequalities (Maciejowski 2002).

Figure 5.3 demonstrates the internal working principle of the MPC which has been simulated using a response from my DSTATCOM's model over one cycle for $2\frac{1}{2}$ time-constants, sampled at $T_s = 0.002$ seconds. I begin by assuming a discrete-time setting represented by the current time t , while the current plant output is regarded as $y(t)$. The plant output should follow the setpoint trajectory $s(t)$ at the current point in time when a disturbance occurs. And it is supposed to be guided by a distinct reference trajectory $r(t)$ of a pre-calculated time constant $\tau = 0.008$ seconds, approaching the setpoint exponentially.

This way, the MPC quadratic routine can solve the minimisation problem over the two

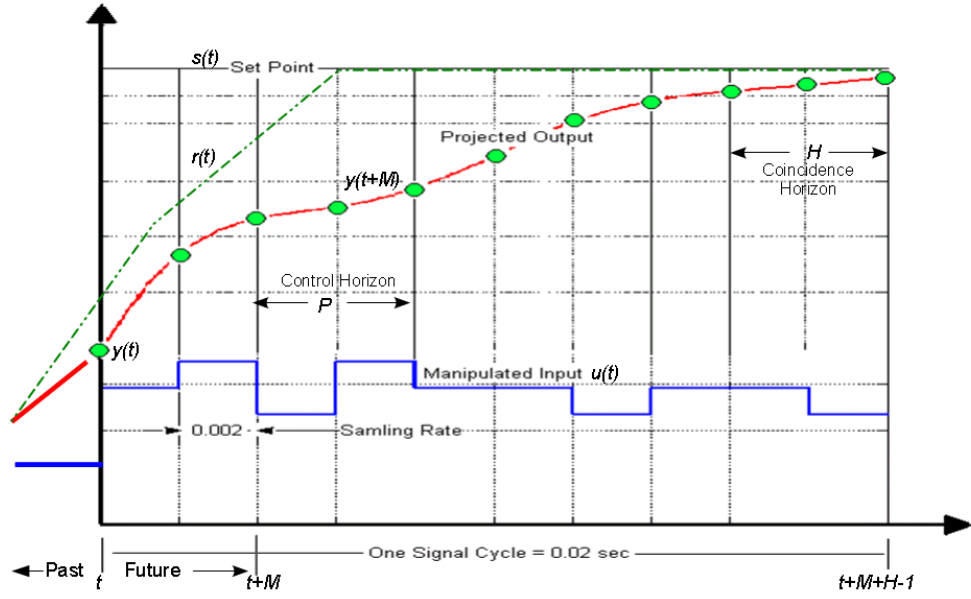


Figure 5.3: Basic MPC idea

horizons N and M in a receding manner through the following objective function:

$$J(u) = \min_{u(t+1), \dots, u(t+N)} \left\{ \sum_{k=M}^{M+H-1} |y_r(t+k) - y(t+k)|^r \right\}^{\frac{1}{r}} \quad (5.1)$$

where $y(t+k) = y(t+k|t) = y(t) + [y_N(t+k) - y_N(t)]$, $\forall k$, is estimated based on measurements from the model up to the current time t , for all $j \in M, M+1, \dots, M+H-1$ with $M \geq 1$ being the minimum allowed prediction step; $r = 1, 2, \dots, \infty$ is evaluated over the finite horizon of k as a metric norm and may take any of the known norms like; mixed, M_1, M_2, M_∞ or weighted, provided it allows online minimisation of the objective function (J). the Euclidian norm with $r = 2$ is normally used in quadratic programming (QP) to solve the online optimisation problems in which the first control signal $u = t+1$ is always applied to the plant in the following sequence till optimum solution is attained.

$$u = [u(t+1)u(t+2) \dots u(t+N)] \quad (5.2)$$

Note that the control horizon is often given the same value as the coincidence horizon (i.e., $N = H$), while $N \leq M$ from Perez (2008).

5.2.3 Step Response as a Model

Here, I considered step response design of a linear DSTATCOM model to enable me study the generic dynamic behaviour of the MPC. The step response concept is simple in the sense that a step input can directly be applied on the controlled variable (actuator) of the plant to yield subsequent output variables as time t approaches infinity (i.e., until stability). However, the technique has its drawbacks, see for example page 108 of (Maciejowski 2002). Among these drawbacks, I am particularly interested in converting the feature of the step inputs often disrupting the plant's normal operation in real time to practical usage for my new model-free design. Because of the model linearity, I can determine the response to an arbitrary input vector via a *convolution* integral which is defined as

$$y(t) = \sum_{j=0}^t V(t-j)\alpha_j \quad (5.3)$$

I can then apply a unit pulse at time $t = 0$ to one of the inputs k such that, $\alpha_l(0) = 1$: $\alpha_l(n) = 0$ for $n > 0$, in my DSTATCOM model operating at a steady-state with all initial conditions (for input and output variables) set to 0. So that, the order of the output response k given as $(v_{kl}(0), v_{kl}(1), \dots)$ can be represented as a vector of all the output responses at time (t) as $[v_{1l}(t), v_{2l}(t), \dots, v_{pl}(t)]^T$. From this I can develop a matrix showing the response of each output to a unit pulse applied to an input as:

$$V(T) = \begin{bmatrix} v_{11}(t) & v_{12}(t) & \dots & v_{1q}(t) \\ v_{21}(t) & v_{22}(t) & \dots & v_{2q}(t) \\ \vdots & \ddots & & \vdots \\ v_{p1}(t) & v_{p2}(t) & \dots & v_{pq}(t) \end{bmatrix} \quad (5.4)$$

Although it is theoretically feasible to acquire a pulse train response matrices through pulse response tests of the form: $\{V(0), V(1), \dots, V(N)\}$. It is however almost practically impossible to perform such tests due to the enormous pulse amplitudes required to excite the plant to give meaningful results. And the sequence should be long enough to make $V(N) \approx 0$ even if the test was carried out. In such situation, the plant's initial steady-state condition is never zeroed and the convolutional information resulting from the impulse differences $(y(t) - y(-1))$ which in practice replaces $y(t)$, can never be accounted for. That is why I revert to using the concept of unit step input in conjunction with the convolution integral below.

For a unit step input $l : \alpha_l(t) = (1, 1, 1 \dots)$, the plant's output response k is obtained as

$$y_l(t) = \sum_{j=0}^t v_{kl}(t-j)\alpha_l(j) = \sum_{j=0}^t v_{kl}(t-j) = \sum_{j=0}^t v_{kl}(j) \quad (5.5)$$

and yields the following step response matrix.

$$M(t) = \sum_{j=0}^t V(j) \quad (5.6)$$

The matrix $M(t)$ is often referred to as the dynamic matrix, from which dynamic matrix control (DMC) may have been coined. Hence, the sequence $M(0), M(1), \dots, M(N)$ can be used as the model of the plant, wherefore a large value of N , $M(N+1) \approx M(N)$ (Maciejoweski, 2002). The output ensuing from the arbitrary input sequence can thus be expressed using the step response matrix $M(t)$ and the changes of the input vector $\Delta u(t)$, instead of the pulse response matrix $V(t)$ and the actual input $u(t)$ given in Eq. 5.2. Hence, the transformation of this (pulse response) equation via the convolution integral into its step response counterpart can be accomplished by

$$y(t) = \sum_{j=0}^t M(j)\Delta u(t-j) \quad (5.7)$$

I can now relate this equation to the state-space model of the DSTATCOM as a necessary prediction design step. The model used is recognised to be of the following order.

$$x(t+1) = Ax(t) + Bu(t) \quad (5.8)$$

$$y(t) = Cx(t) + Du(t) \quad (5.9)$$

where x is a 3-state vector, y is the measured output, A is 3×3 matrix, B is a column vector, C is a row vector, and ($D = 0$) as already defined in chapter 2, and the initial state is assumed known as $x(0) = 0$. By first applying the impulse response and

then transforming it to the step response using the convolution integral as before, the following linear model parameters were obtained.

$$\mathbf{X} = \begin{bmatrix} i_q \\ i_d \\ v_{dc} \end{bmatrix}, \quad \mathbf{A} = \begin{bmatrix} -220 & 0 & 0 \\ -200 & -377 & 0 \\ 377 & 200 & 129.3 \end{bmatrix}, \quad \mathbf{B} = \begin{bmatrix} -4.4e + 004 \\ 0 \\ 0 \end{bmatrix}, \quad \mathbf{U} = \alpha,$$

and

$$\mathbf{C} = \begin{bmatrix} -330 & 0 & 0 \end{bmatrix}$$

But, as I have noted that the system has 3 states ($x(t)$) which are responsible for storing the history of the system, so that by knowing $x(t)$ there is no need to know what happened before time t to predict the system's behaviour in the future. Unfortunately, the step response model I want to incorporate for prediction does not have a state. Which means I cannot access the state, and will therefore have to reasonably use the 'past' available information about the system's behaviour long before time t . The prediction sequence can thus be accomplished through the optimisation process earlier described.

5.3 Preliminary MPC Simulations

Again, using DSTATCOM model of Eq. 3.1, I performed closed-loop MFPC simulations based on different values of the control and predictive horizons with the aim of investigating their influence on the new model-free technique.

5.3.1 Tuning Effects on MPCs

As I have experienced in the first part of chapter 4, where manual tuning through trial-and-error techniques of some specific parameters became an element of the design problem. In MFPC design too, there are a number of adjustable parameters that need be tuned to achieve the desired performance specifications. And these would normally include filter coefficients, input and output weights, control and prediction

horizons, and disturbance dynamics. In this section I shall investigate the effects of changing such parameters under uncertainties and changes in a model operating under feedback condition. Although it has been argued that feedback can itself destabilise a stable system, it is also believed to reduce the effects of unmeasurable disturbances and restrain the uncertainties due to model changes being transferred into the model behaviour. Such investigations are necessary for guiding my model-free design.

5.3.2 Effects of Tuning Horizons

By selecting direct form symmetric FIR filter coefficients [0.5 0.05] from the MPC in Matlab, a model-based design simulation was performed by setting the input weight to 0, and the input rate weight to 0.1. Recall that, I will be changing the rate of change of the input instead of changing the input directly. The control signal shown in Figure 5.5 was sampled at a control interval of 0.002 seconds. Setting the output weight to 1, the control signal produced the response shown in Figure 5.4 at predictive and control horizons specified as $P = 20$ and $C = 2$. Both unconstrained and constrained MPC models were considered for this exercise. Constraints were enforced as depicted in Figure 5.6 where the response showed remarkable improvement from overshoot at lower cost depicted in Figure 5.7. To further gain insight into this phenomenon, I fixed the predictive horizon value and raised the control horizon to 4. It is observed that the overshoot has reduced with improved settling time at virtually the same cost as in Figures 5.8.

By enforcing constraint as in Figures 5.10 with its associated control signal in Figure 5.11, the overshoot is suppressed and converted to an undershoot with improved settling time. However, this condition is also not healthy for equipment operation. Observations showed that changing the predictive horizon down stream can significantly affect the system's response, especially with applied constraints which produced oscillatory response with prolonged settling time. This scenario has been demonstrated in Figures 5.12 to 5.15, where the predictive and control horizons were dropped to 10 and 2, respectively. Therefore, predictive horizon values are more desirable if pegged at about 5 : 1 ratio to control horizon. Yet, higher predictive values (above 20) occasionally lead to loose control with large overshoots. Additionally, my investigation revealed that, the closer the control horizon is to the predictive horizon, the tighter is the response, agreeing with $C \leq P$ earlier noted.

5.3.3 Effects of Tuning Filter Coefficients

The direct form FIR filter used here is meant to guide the output trajectory, and its coefficients play a significant role in ensuring close-tracking of the reference trajectory.

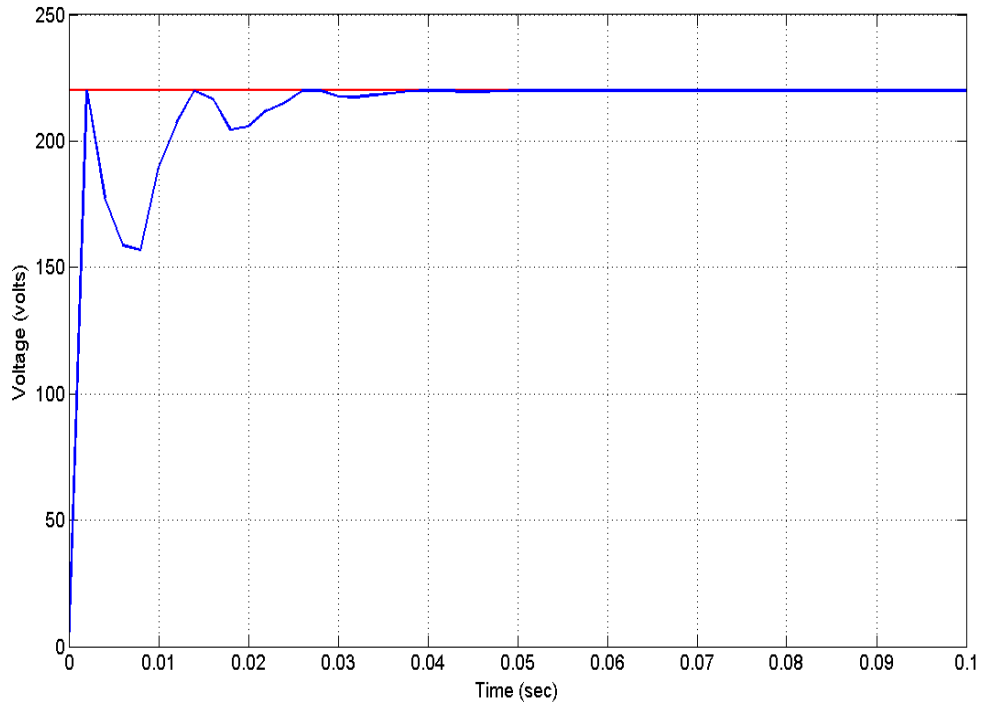


Figure 5.6: Changing horizons for constrained plant:
 $P = 20; C = 2$

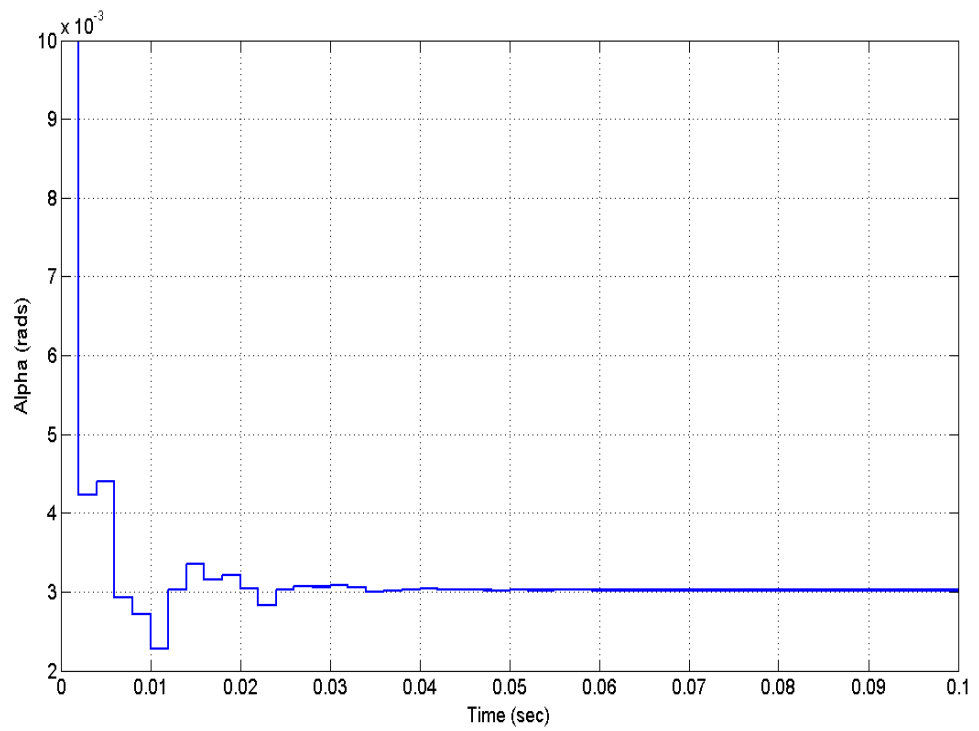


Figure 5.7: Constrained control signal:
 $\alpha = 0.003050$ rads

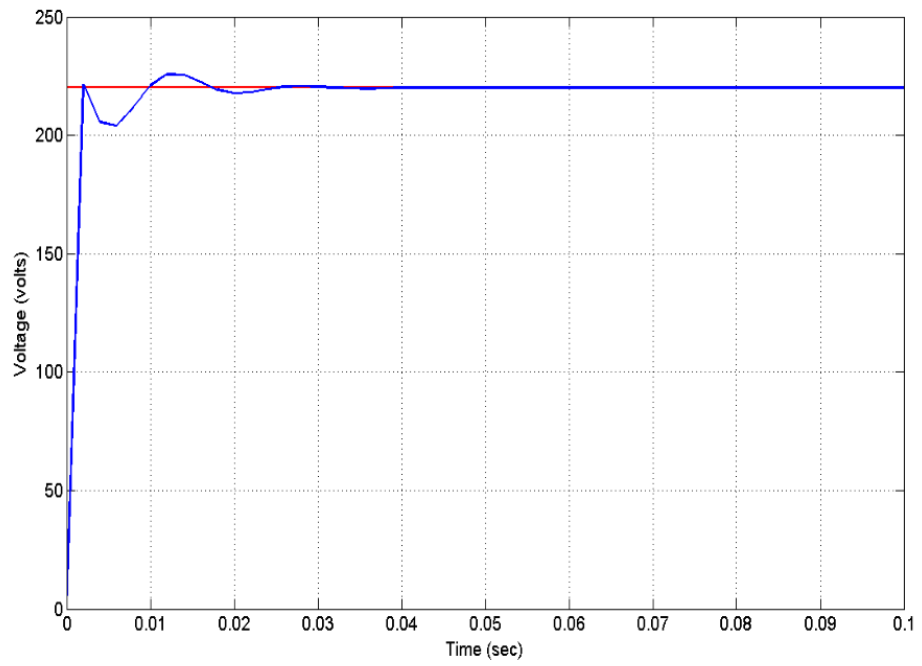


Figure 5.8: Raising control horizon for unconstrained plant:
 $P = 20; C = 4$

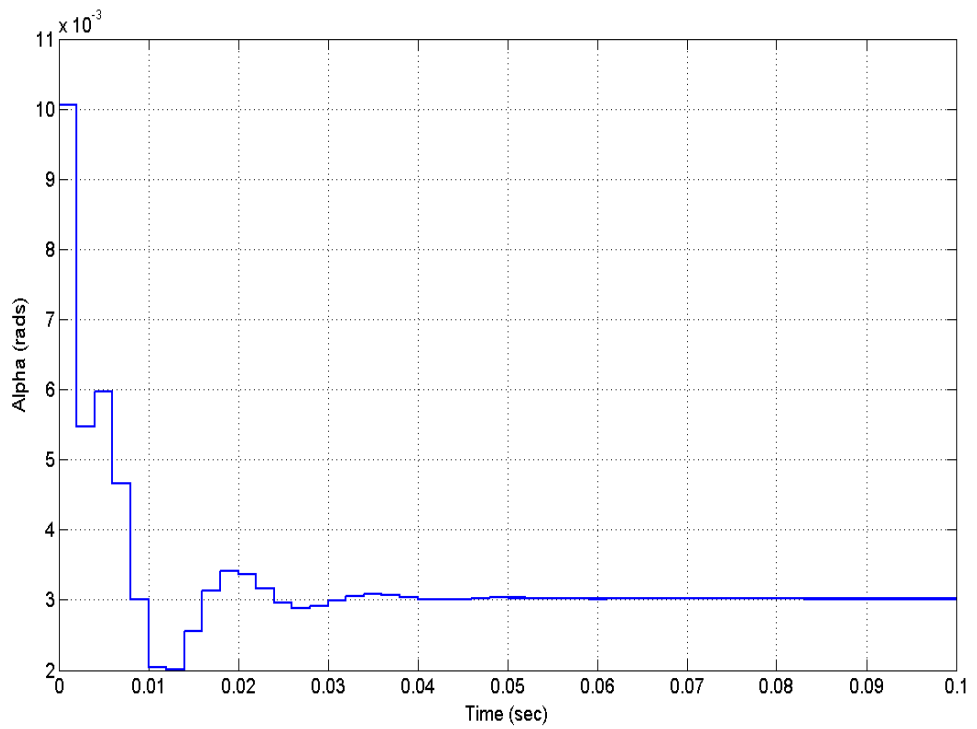


Figure 5.9: Raised unconstrained control signal
 $\alpha = 0.003020$ rads

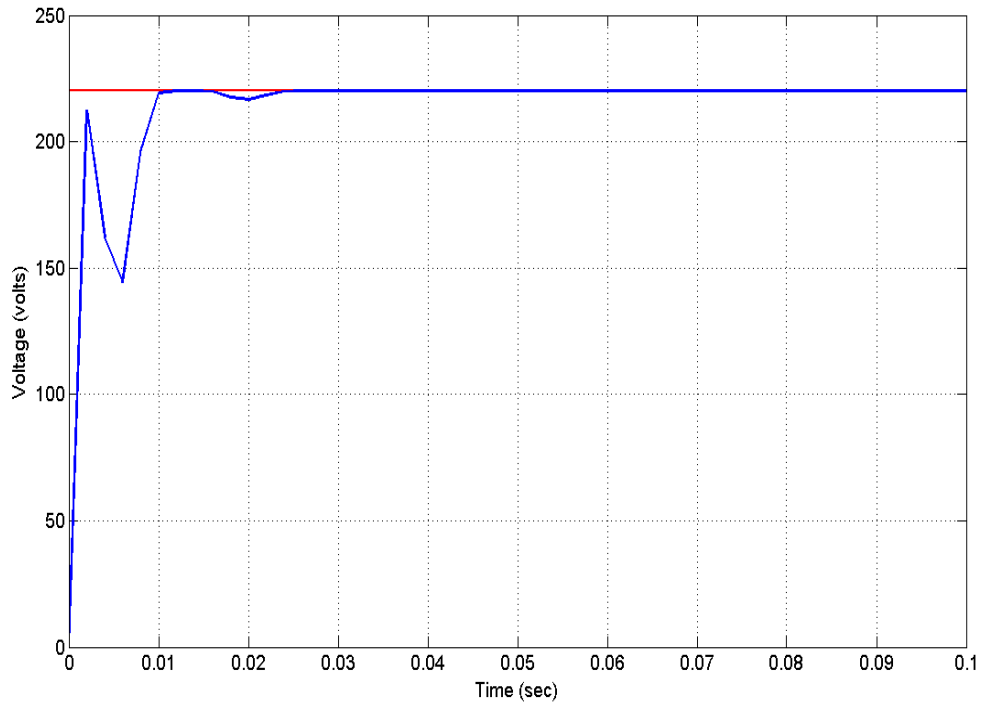


Figure 5.10: Raising control horizon for constrained plant:
 $P = 20; C = 4$

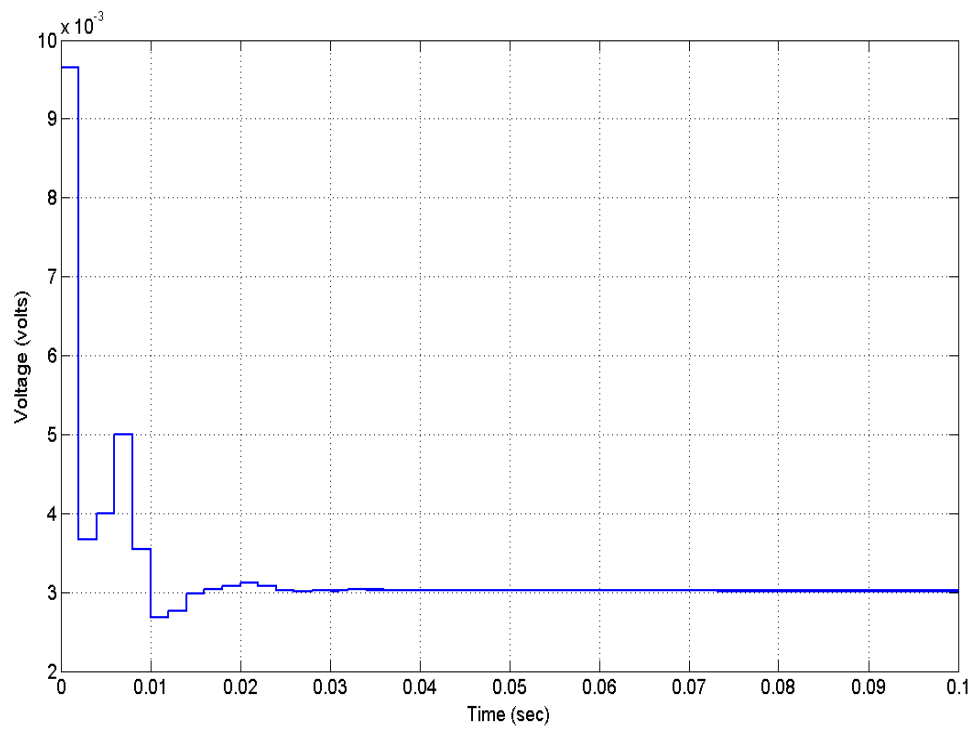


Figure 5.11: Raised constrained control signal
 $\alpha = 0.003050$ rads

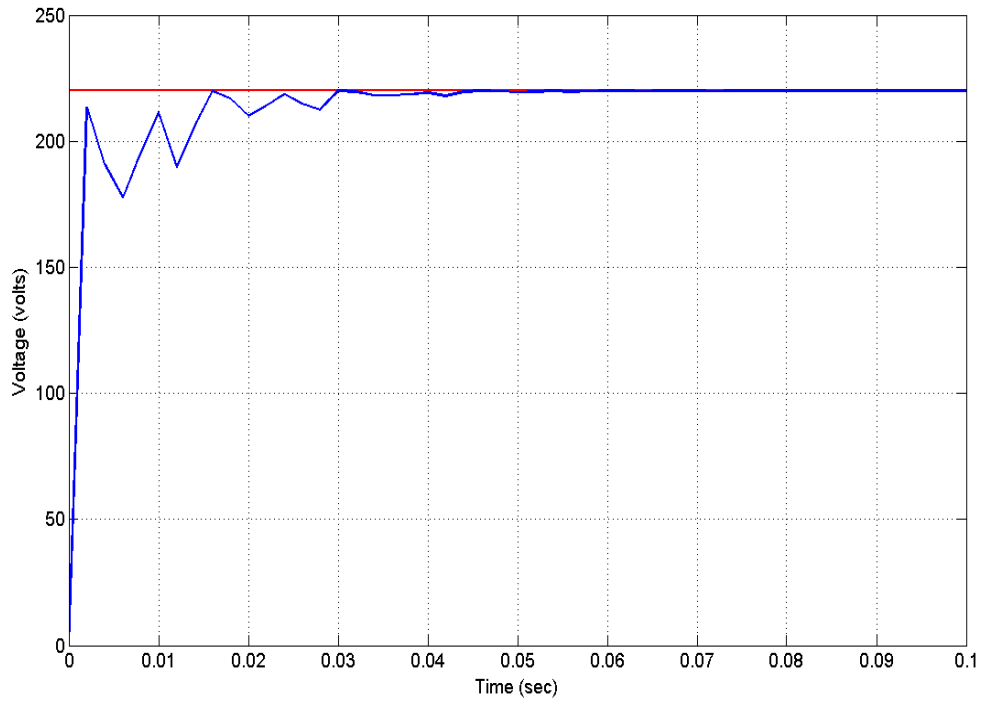


Figure 5.14: Lowering predictive horizon for constrained plant:
 $P = 10; C = 2$

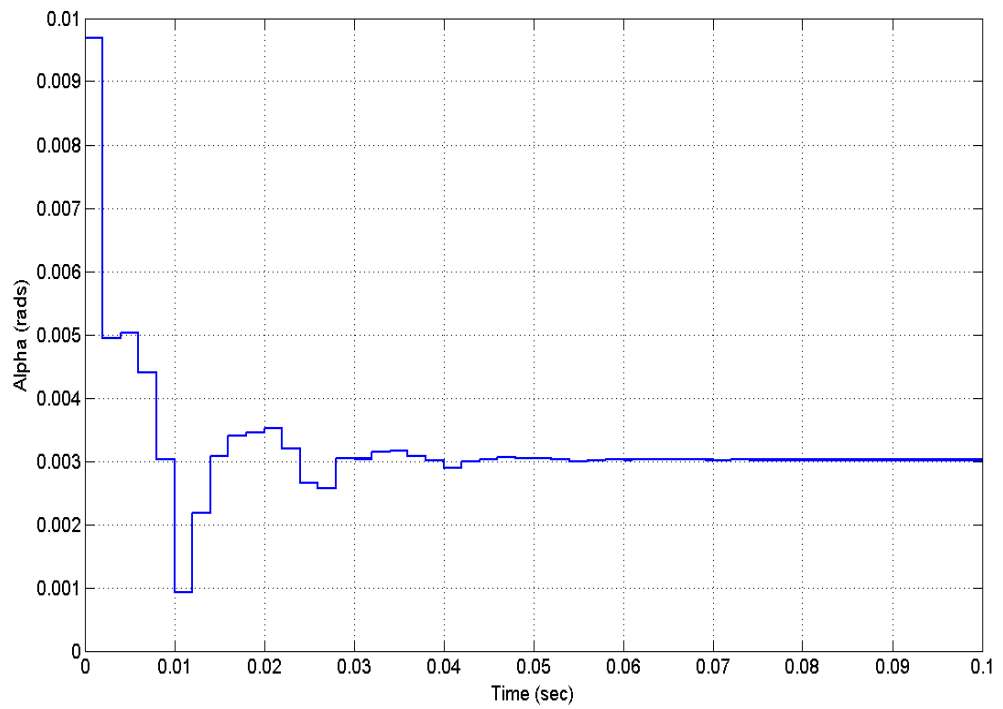


Figure 5.15: Lowered constrained control signal
 $\alpha = 0.003050$ rads

Since data is the summation of signal information and noise contamination. It becomes paramount to employ an appropriate filtering and smoothening (interchangeably used) device to remove noise from the signal before the data is used for predictive control. By removing the high frequency signal from the data (enhances prediction performance), the chances of damaging the real-timeliness of the data is eliminated (no time-delay introduced). Smoothening simply means estimation of past values based on available information until the present time. Two methods have been identified towards this process viz; optimal smoothing, and bidirectional (low-pass) filtering from (Kanjilal 1995). For simplicity, I used bidirectional approach to introduce the concept of real-time bidirectional filtering for the model-free design application, in section 5.5. I chose it because, off-line model-based method discussed in this section is incapable of processing terminal data.

Figure 5.16 demonstrates this effect through FIR's numerator coefficients $[0.5 \ 0.05]$ by applying a step setpoint trajectory $s(t) = 220$ volts in an unconstrained plant, where the output trajectory ($y(t)$) is observed to follow the reference trajectory ($r(t)$) at a rather wide pace with successive ringing. The control effort which was sampled at 0.002 seconds interval is shown in Figure 5.17. A completely different trend is found in Figure 5.18 as the first coefficient A is lowered to equal B , building a pair of coefficients as $[0.05 \ 0.05]$. Although the ringing has been eliminated from the responses, but the magnitude of $r(t)$ has dropped to 200 volts. However, there is improvement in the output $y(t)$ which rouse from 115 volts to 175 volts, at a high cost of 0.003720 rads in Figure 5.19.

Consequently, an opposite effect was produced when the coefficient A was raised to 5 while keeping B fixed. Figures 5.20 and 5.21 clearly show the system thrown into instability by this action. However, further lowering coefficient A to 0.005 and raising B to say 0.5 has actually stabilised the system once again and improved the reference following as the magnitude appreciates as indicative in Figure 5.22 and 5.23.

As a final test on the effects of filtering, I created another scenario by lowering the value of coefficient B to 0.005 while fixing $A = 0.5$, and applied horizons of $P_H = 20$ and $C_H = 4$ to an unconstrained system. Sampling time remains as before i.e., (0.002) seconds. The reference response ($r(t)$) seems massively overshoot, and repelled the output trajectory ($y(t)$) which also is forced far below the setpoint trajectory ($s(t)$) as depicted in Figure 5.24. The control effort is shown to go through several cycles before settling at 0.0024 radians as in Figure 5.25. To further verify the filter tuning characteristics, I raised both coefficients to a unit value and observed that the responses even grew further apart and adorned in overshoots as presented in Figure 5.26. While Figure 5.27 represents the control effort that produced the change at 0.00174 rads.

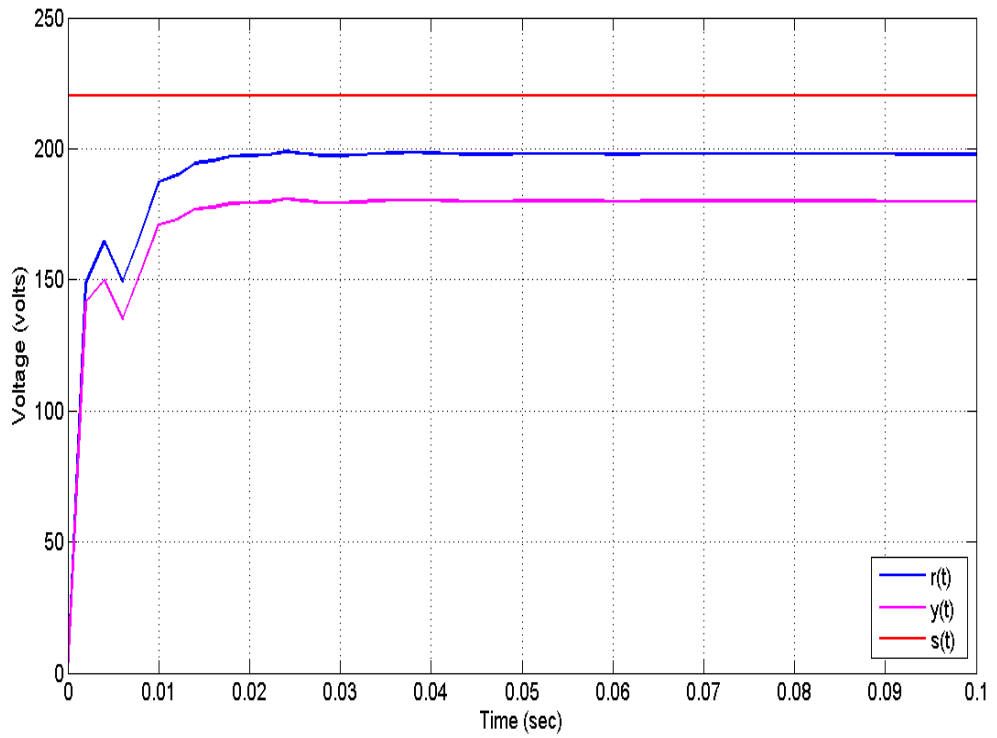


Figure 5.18: Plant with tuned filter coefficients case 2:
 $A = 0.05; B = 0.05$

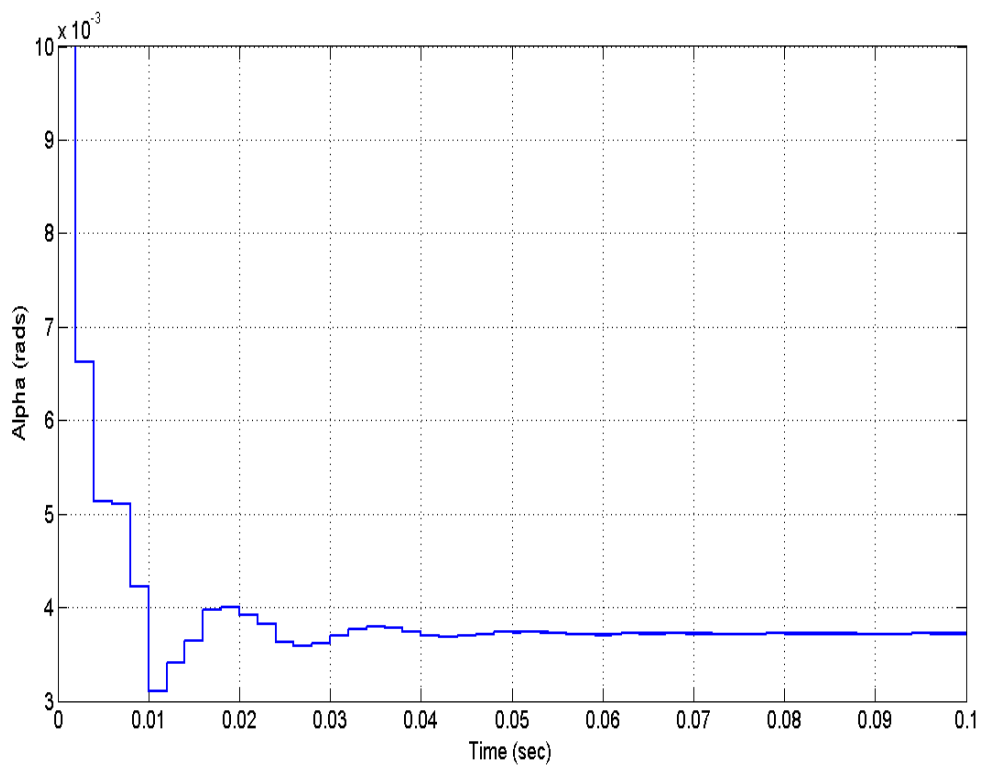


Figure 5.19: Control signal for case 2
 $\alpha = 0.003720$ rads

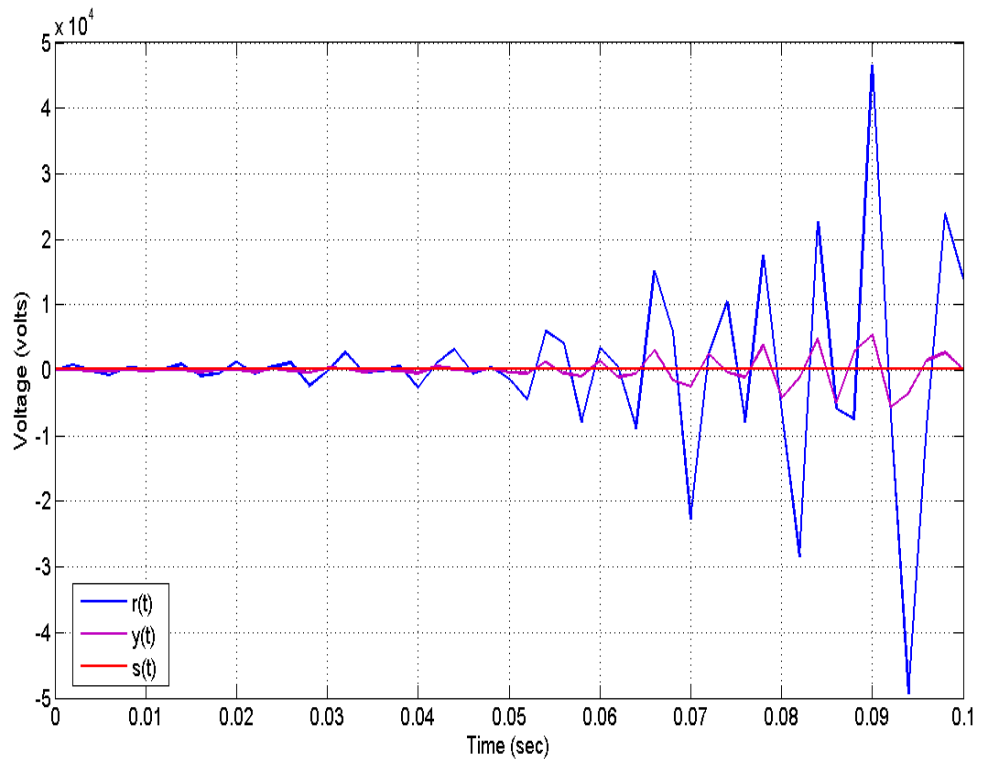


Figure 5.20: Unstable plant with raised FIR
 $A = 0.5; B = 0.05$

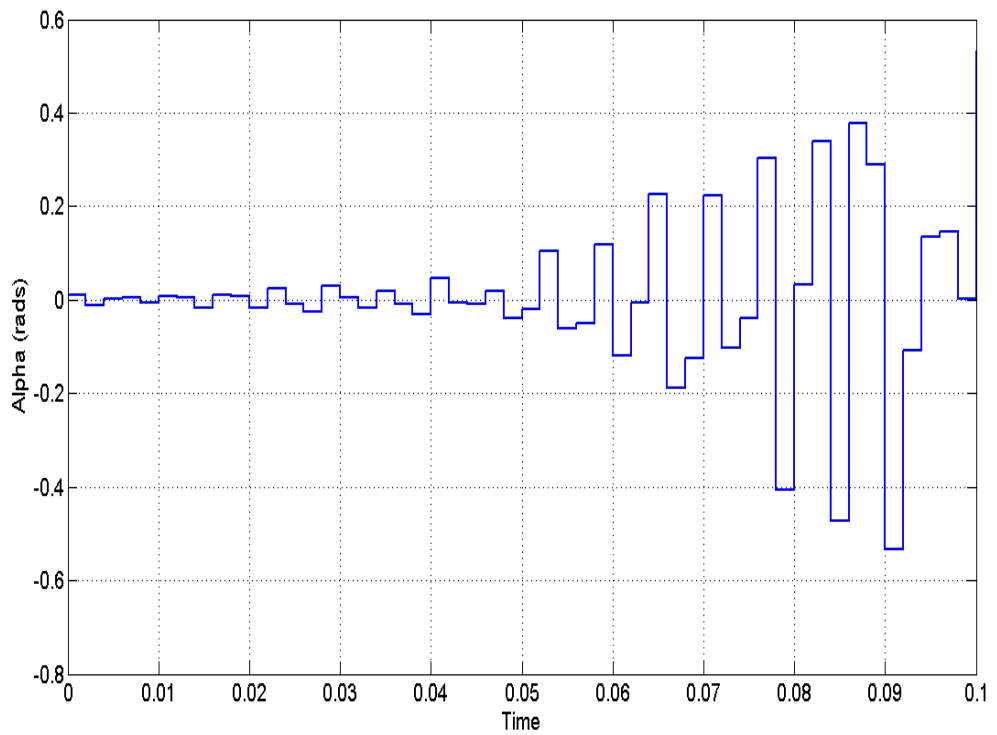


Figure 5.21: Control signal (unsatble)
 $\alpha = \text{undefined rads}$

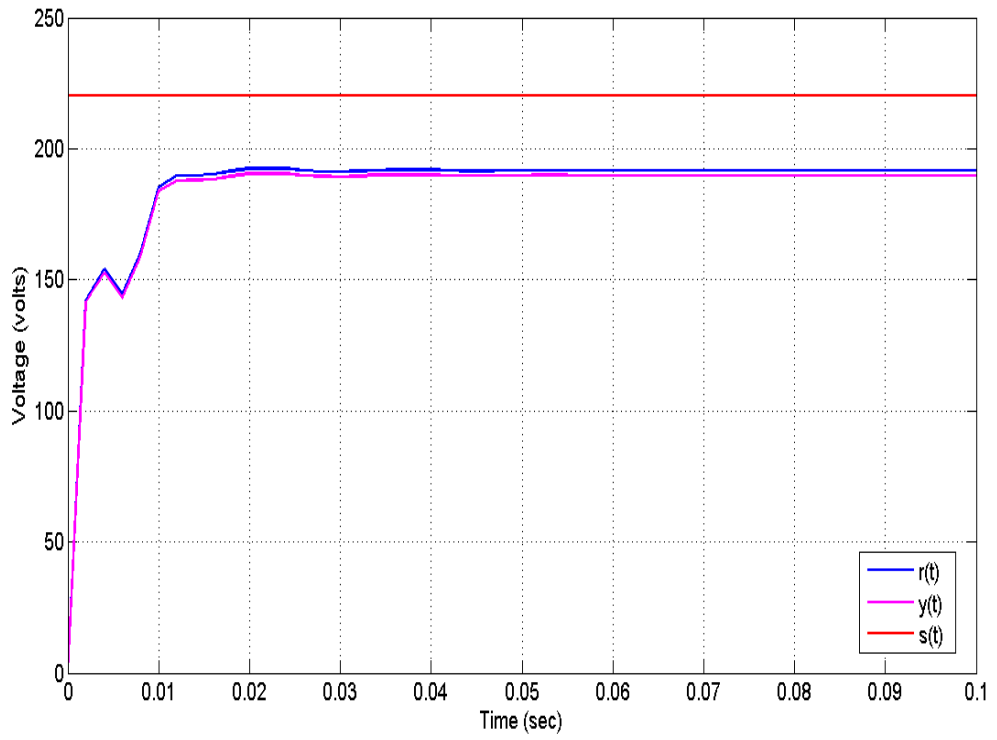


Figure 5.22: Stable plant with raised FIR
 $A = 0.005$; $B = 0.5$

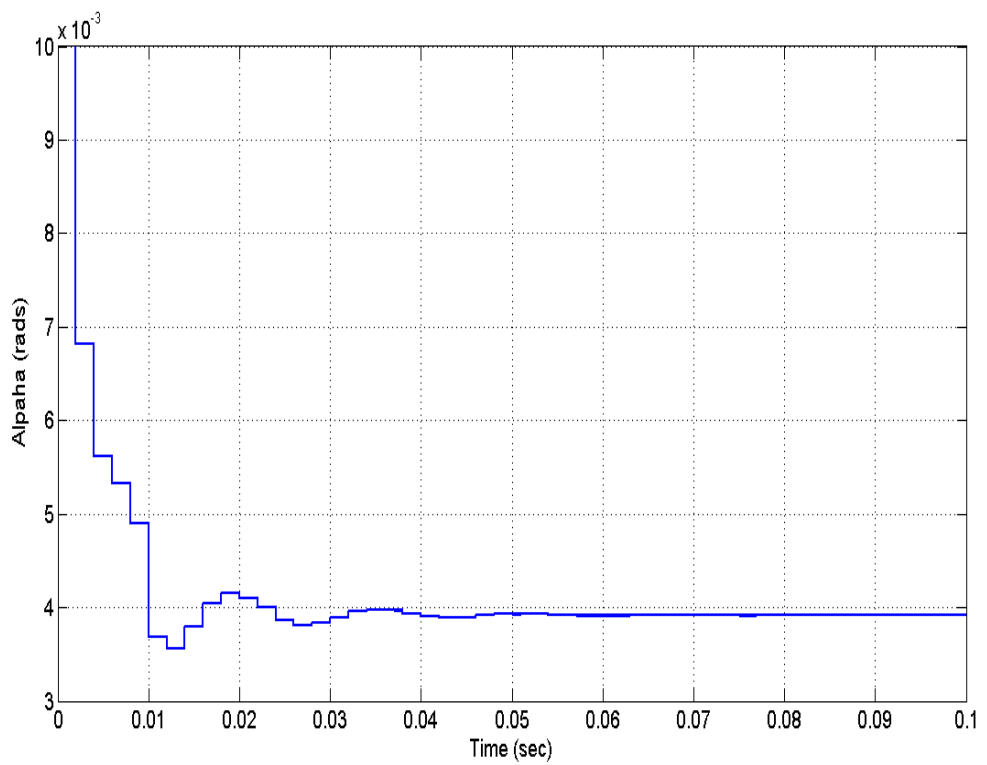


Figure 5.23: Control signal (stabilised)
 $\alpha = 0.003900$ rads

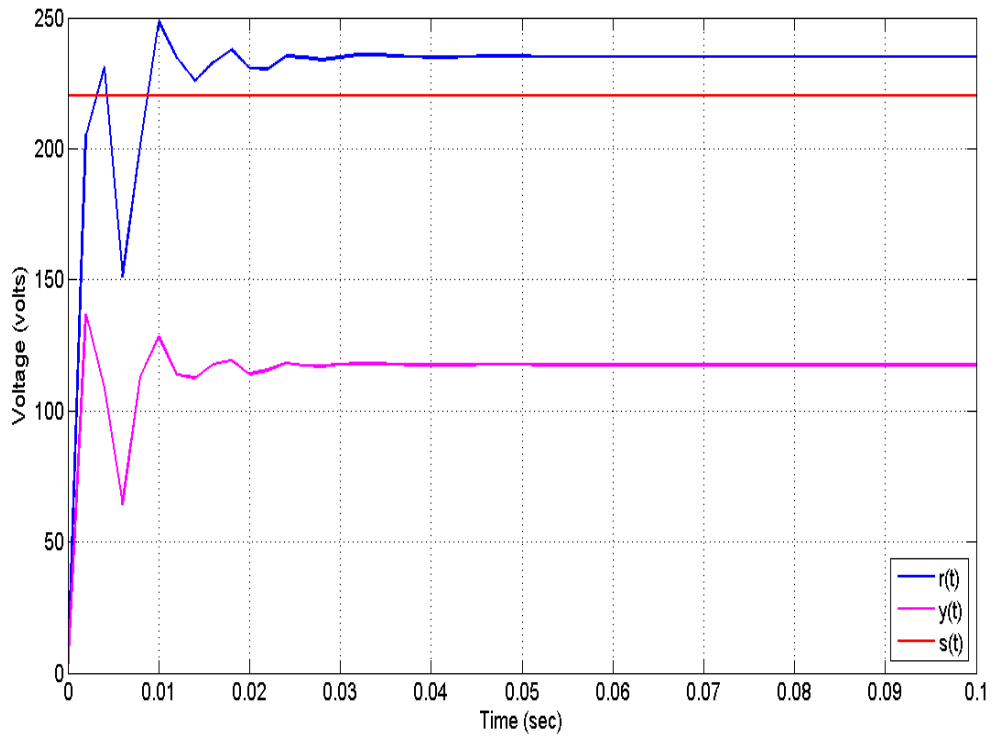


Figure 5.24: Unconstrained further FIR tuning
 $A = 0.5; B = 0.005$

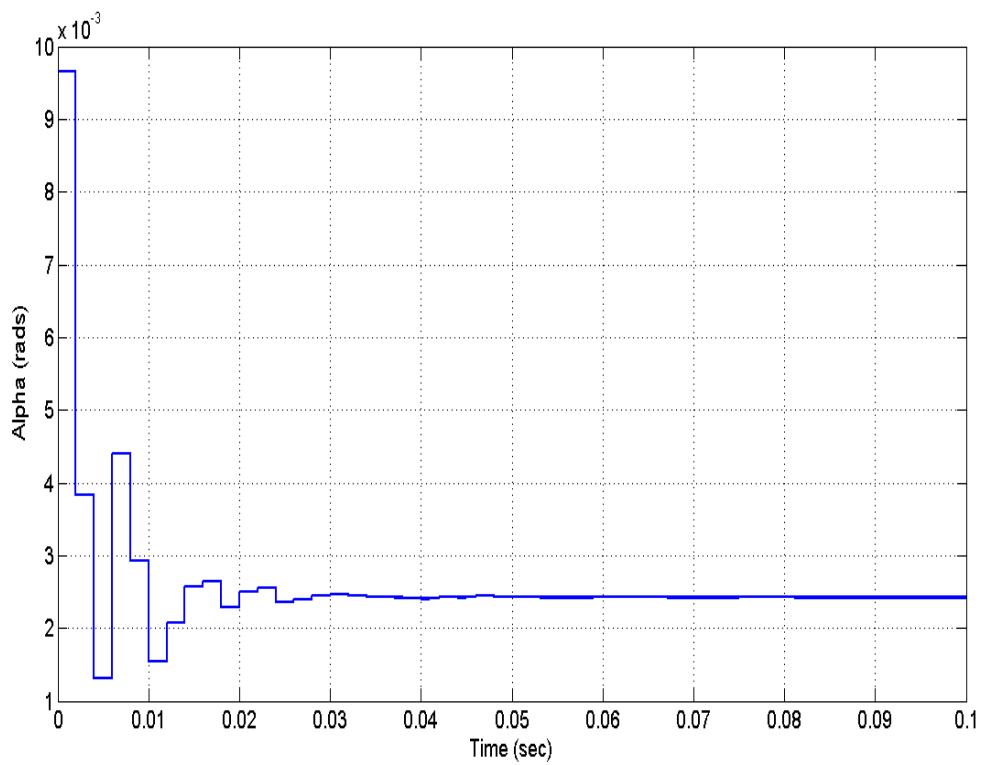


Figure 5.25: Control signal of further tuning
 $\alpha = 0.0024$ rads

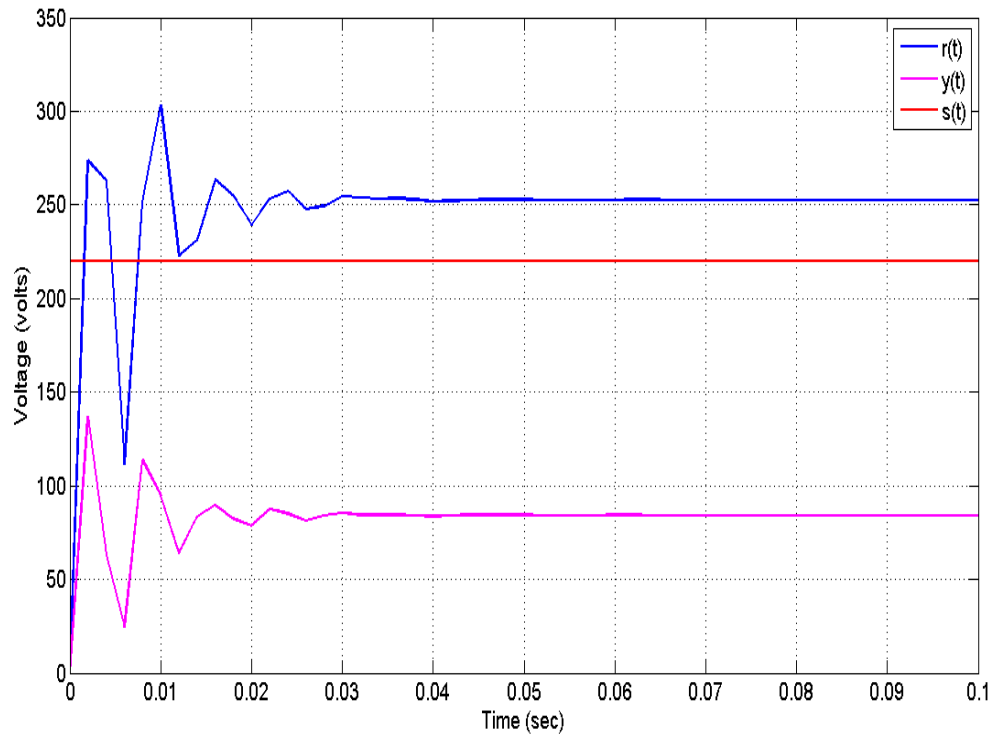


Figure 5.26: Tuning FIR coefficients to unity
 $A = 1; B = 1$

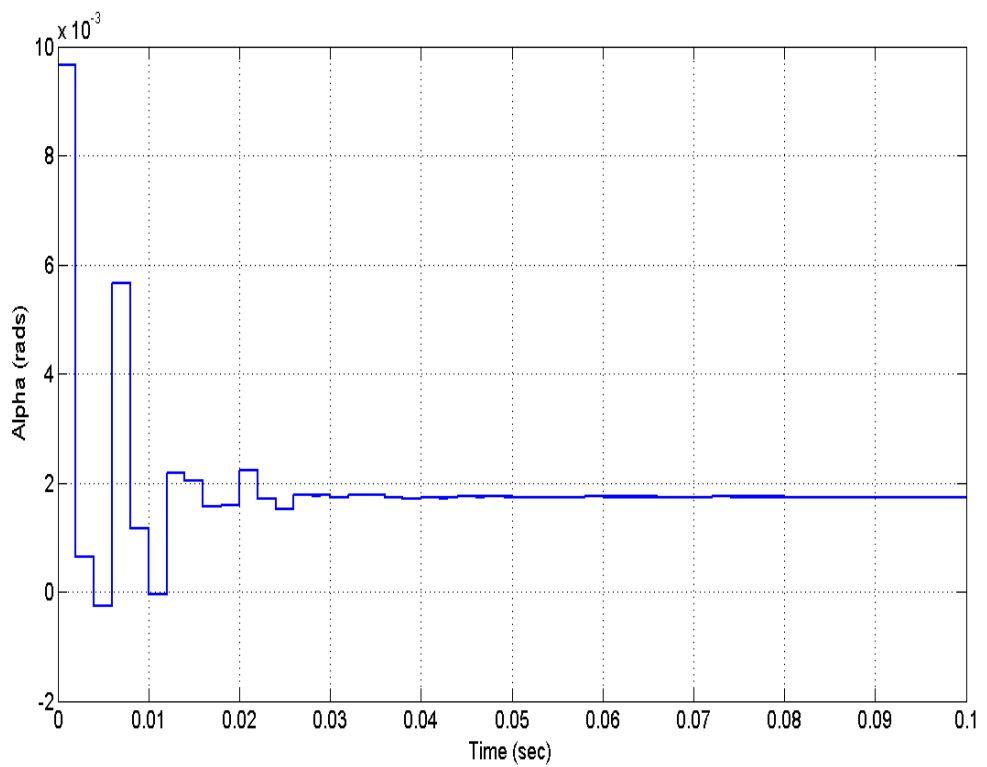


Figure 5.27: Control signal to unit tuning
 $\alpha = 0.00174$ rads

5.3.4 Effects of Weight Tuning

Three types of weights are involved in MPC tuning i.e.; input, change of input, and output weights. As before, I set the input weight $u(t)$ to 0 and set its rate of change $\Delta u(t)$ to 0.1, while the output $\alpha(t) = 1$ for this simulation. In order to meet the desired performance specifications, five measures of merit were compared, namely; *ISE*, *ITE*, *ITAE*, *ITSE*, and *ISTSE* as often found in the MPC control design. Considering a two degree of freedom system earlier depicted in Figure 5.2, showing the command signal passing through a pre-filtering stage before assuming a closed-loop reference ($r(t)$) position. Two important transfer functions fundamental to feedback theory, in addition to the system's existing transfer functions are; sensitivity function and complementary sensitivity function which relate all other inputs and outputs within the system according to (Maciejowski 2002). In a good feedback design practice, it is normal to have the sensitivity function as small as possible. This would guarantee best setpoint following and suppress the effect of disturbance at the output to the barest minimum. Since both sensitivity functions complement each other in time domain design, I am going to assume a single figure for them for simplicity. Table 5.1 is the result of simulating the system with pre-assigned tuning weights. The sensitivity indices indicate that the *ITSE* index performs better than the other three at the lowest set of sensitivities for change in input, input, and the output weights.

Table 5.1: Performance Index Based MFPC Tuning

PI	Parameters	Weight (W)	Sensitivity (S)
ISE	Input	0	0
	Input Rate	0.1	$1.011e - 005$
	Output	1	$-3.42e - 006$
IAE	Input	0	0
	Input Rate	0.1	$2.973e - 007$
	Output	1	$2.251e - 007$
ITSE	Input	0	0
	Input Rate	0.1	$1.023e - 009$
	Output	1	$1.751e - 009$
ITAE	Input	0	0
	Input Rate	0.1	$8,213e - 009$
	Output	1	$3.002e - 008$
ISTSE	Input	0	0
	Input Rate	0.1	$1.102e - 005$
	Output	1	$-5.39e - 005$

5.3.5 Problem of the Model-Based Prediction

Excessive model reliance is the main disadvantage of model-based predictive controllers, especially in models driven full of model errors from the first principles. This may often require huge computation costs before reasonable solutions are attained. At times the solutions are even hardly achievable if applied to nonlinear systems with stochastic dynamics of varying operating points at short time constants. One other concern about the MPC also is the need for Kalman's filtering for state estimation which also adds to its computational complexity. Notwithstanding its successful applications in slow dynamics linear practical systems, the success needs be extended to fast dynamics nonlinear ones. The extension may be applicable in one of the following three categories. One, a case of model characterised by unavailability of the quantitative knowledge of the plant often referred to as "black box problem". In such case, the plant may have either too many complex dynamics or the physical process may have been poorly understood. Two, a case where the knowledge of the plant is available but inaccurate, such as in engine combustion control dealing with for example, fuel level changes. This type of problem is referred to as "gray box problem". Three and the simplest of the two models is the "white box problem", in which the quantitative knowledge of the plant is readily available and can easily be controlled through established control methods and tools including the MPC. To solve this problem, in section 5.4 I devised a new means of boycotting the model with its associated Kalman's filter and use online input-output data of the system in an adaptive manner to perform prediction control in a model-free environment. This will tackle the black, gray, and white problems especially, the gray problem with which most industrial applications are identified.

5.4 Switching to Model-Free Prediction Control

The concept of the model-free control is built around the model-on-demand theory described in (Cleveland & Devlin 1988), which was presented as an alternative polynomial modelling to conventional modelling techniques the likes of wavelets, radial basis and neural networks. The idea is to perform modelling around unique operating points on the input-output data by directly storing it in pairs such that for every modelling requirement around that operating point, a subset of data is made available from the data base for modelling operation, instead of indirectly adapting the global process model. This scheme offers the advantage of realizing a congruent model free from linearized operating point dispersions. To achieve this, I adopted the three stages prescribed for a model-free method realization from (Hsu & Meyer 1968). These stages include a restrained control structure, an optimization criteria, and an optimization routine all of which have been discussed under section 5.5. The DSTATCOM was first

augmented through a saturation describing function (DF) to account for nonlinearities and establish the system's stability criterion for the model-free approach as explained below.

5.4.1 The Describing Functions

Describing functions theories represent a powerful mathematical means for evaluating the behaviour of nonlinear systems, see details on description of some nonlinearities in (Ushio 2002). The motivation behind this is based on the fact that all real systems are nonlinear except within a limited operating range. Also the control engineer is relieved of having to linearise a nonlinear model from first principle techniques. This fact is also true for DSTATCOM in which the benefits of nonlinearity can easily be tapped to generate desirable periodic signals.

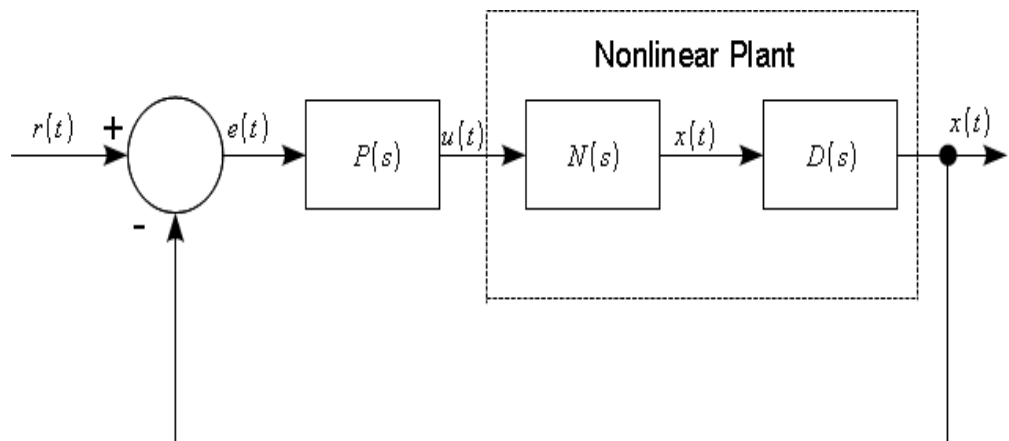


Figure 5.28: Nonlinear feedback control loop

The stability analysis of nonlinear feedback control systems such as fuzzy controllers whose theory remains illusive can now be readily analysed using describing functions as explained (Wang & Boyd 2008). Conversely, the stability of an off-line design of predictive controllers in open-loop mode is simply realized through parameter tuning while formulating the problem provided that the plant model is accurate as I have demonstrated above, see also (Bhende et al. 2006). Therefore, my proposed online model-free design uses the capabilities of describing functions to sense the presence of limit circles (oscillations) in closed-loop. This way, the same parameters are used to tune the controller for optimality as in the model-based, except that optimality is very difficult to realise in the case of model-based tuning.

Figure 5.28 shows the general notation of a closed-loop control system for nonlinear DSTATCOM plant $D(s)$, augmented with describing function of a saturation element

$N(s)$. The augmented describing function will be deduced in section 5.4.2. The decoupled controller $P(s)$ is an unrestricted structure type, e.g., a model-based predictive controller generating control sequence $u(t)$ based on error signal $e(t)$, which is produced by the difference between the setpoint $r(t)$ and the controlled variable $y(t)$. In this work, only $u(t)$ and $y(t)$ generated online data is required to implement the model-free predictive control. (Ushio 2002) has shown that, choosing the error as $e=a \cos \omega t$ would simplify extracting the control signal such that,

$$u = ue = u(a \cos \omega t, -a\omega \sin \omega t) \quad (5.10)$$

Since ωt has a minimum period of 2π with e as a trigonometric function, then u is a piecewise smooth function of the same period. Similarly u can be expanded by considering the fundamental component of a Fourier series such that $u = a_1 \cos \omega t + b_1 \sin \omega t$ while ignoring the sub-harmonics and subjecting all the even components to zero, so that

$$a_1 = \left(\frac{2}{\pi}\right) \int_0^\pi u(a \cos \omega t, -a\omega \sin \omega t) \cos \omega t d\omega t \quad (5.11)$$

$$b_1 = \left(\frac{2}{\pi}\right) \int_0^\pi u(a \cos \omega t, -a\omega \sin \omega t) \sin \omega t d\omega t \quad (5.12)$$

the describing function, DF may thus be deduced as

$$N(a, \omega) = \frac{a_1 - jb_1}{a} \quad (5.13)$$

5.4.2 Augmented DSTATCOM

The nonlinear DSTATCOM model can be given in the following ordinary differential equation

$$\dot{x} = f(t, x, u) \quad (5.14)$$

$$y = g(t, x, u) \quad (5.15)$$

where the variables f and g can be evaluated using any analytical solver, while u and y are the external control input and output signals to the DSTATCOM.

For the model-free design, all limit cycles in linear systems are assumed to be periodically sinusoidal whose period and amplitude can be predicted by describing functions through the nonlinear feedback control system described above. This assumption is only valid since the transfer function of the nonlinear plant $D(s)$ is a low pass filter of reasonably small time constants, actually less than 0.008 seconds as I have earlier established from the linear plant in chapter 2.

The augmented DSTATCOM model based on Eq. 5.13 can be represented as a saturation nonlinearity which has the following sinusoidal input describing function:

$$N(a, \omega) = -1, \quad \text{if } \omega \leq -1 \quad (5.16)$$

$$N(a, \omega) = \frac{2}{\pi}(\sin^{-1}(\omega) + (\omega\sqrt{1 - \omega^2})), \quad \text{if } -1 < \omega < 1 \quad (5.17)$$

$$N(a, \omega) = 1, \quad \text{if } \omega \geq 1 \quad (5.18)$$

where $\omega = 0.5/a$, defined over saturation within the range of 0.5 and -0.5 , and a is the amplitude of the sinusoidal input.

I can thus compute what is referred to in the literature as the sine input describing function (SIDF) $N(a, \omega)$ for any varying range of amplitudes x against the frequency ω . For example, taking the range from 0.1 to 21 at step size of 2.1, as in Figure 5.29 showing a decaying frequency with amplitude growth. Note the expression for SIDF is just a modification of the linear transfer function representing the LTI system $G(j\omega)$ as an approximated quasi-linear system whose response to sine wave is not purely sinusoidal. In this type of system most of the output energy is assigned to the same frequency (ω) as in the input. Therefore, does not require the customary external harmonic filter as they intrinsically tend to behave like a low or band-pass filter. For this advantage, SIDF technique is invariably applied in estimating oscillation (limit cycle) amplitudes in sinusoidal electronic circuits. Generally, DF methods are more important in the analysis of systems which are not too nonlinear, such as the DSTATCOM.

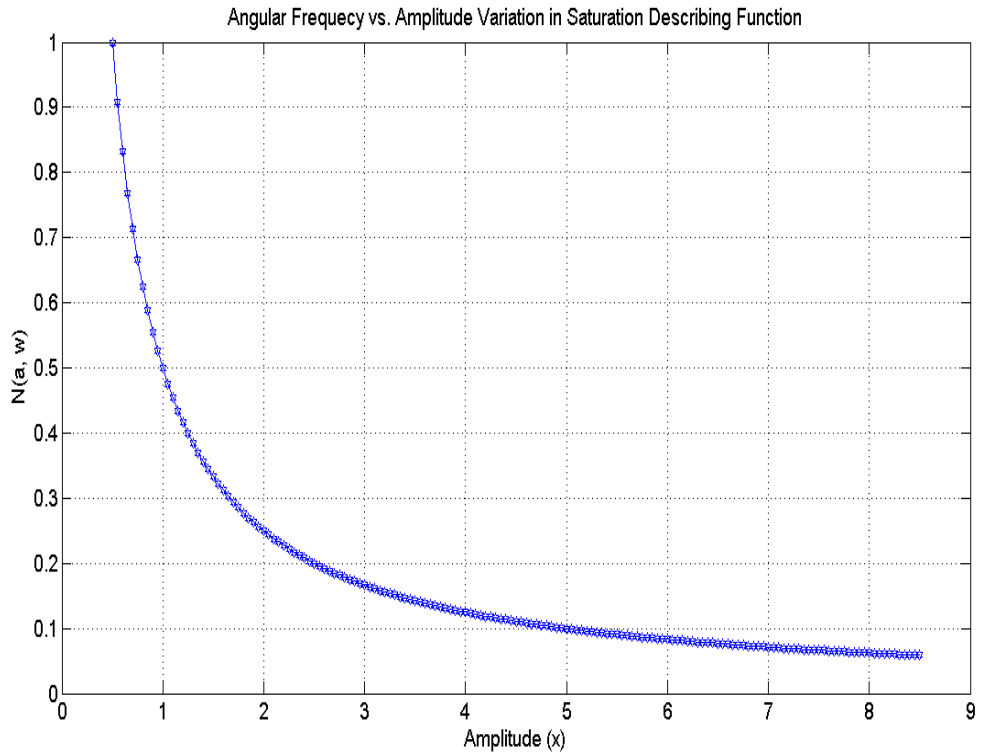


Figure 5.29: DF of frequency vs amplitude

The condition for the existence of a limit cycle in the system's response is defined as (Hsu, 1968),

$$G(j\omega) = -P(j\omega)D(j\omega) = \frac{-1}{N(a)} \quad (5.19)$$

and

$$G(a, \omega) = N(a, \omega)D(j\omega) = -1 \quad (5.20)$$

satisfies the condition for the closed-loop system from Figure 5.28 to oscillate, assuming its linear and steady state stable. In such case, the system is behaving as a low-pass filter in which the equation is used to predict self-oscillations. The stability analysis of this kind of system is described below.

Equation 5.19 can be solved analytically and it is easy to determine the presence of a limit cycle that causes instability at each intersection of the right and the left hand terms of the equation using Nichols curve. The right hand term gives the amplitude of the limit cycle which depends on the saturation droop, while the left hand term gives its

frequency that is independent of the droop size. The describing function maps between the lines, irrespective of the droop size, at $(0\text{dB}, -180)$ and $(\infty, -180)$ as illustrated by the Nichols chart in Figure 5.30. Thus, existence of limit cycles is not affected by changes in droop size. But changes in time constants due to, for example, load recovery time can significantly affect $P(jw)$ which is a “gain” value, by longitudinally shifting $G(jw)$ across the Nichols chart. Moving the curve below $(0\text{dB}, -180)$ inevitably changes the amplitude and removes any limit cycle present without altering the stability of the closed-loop system.

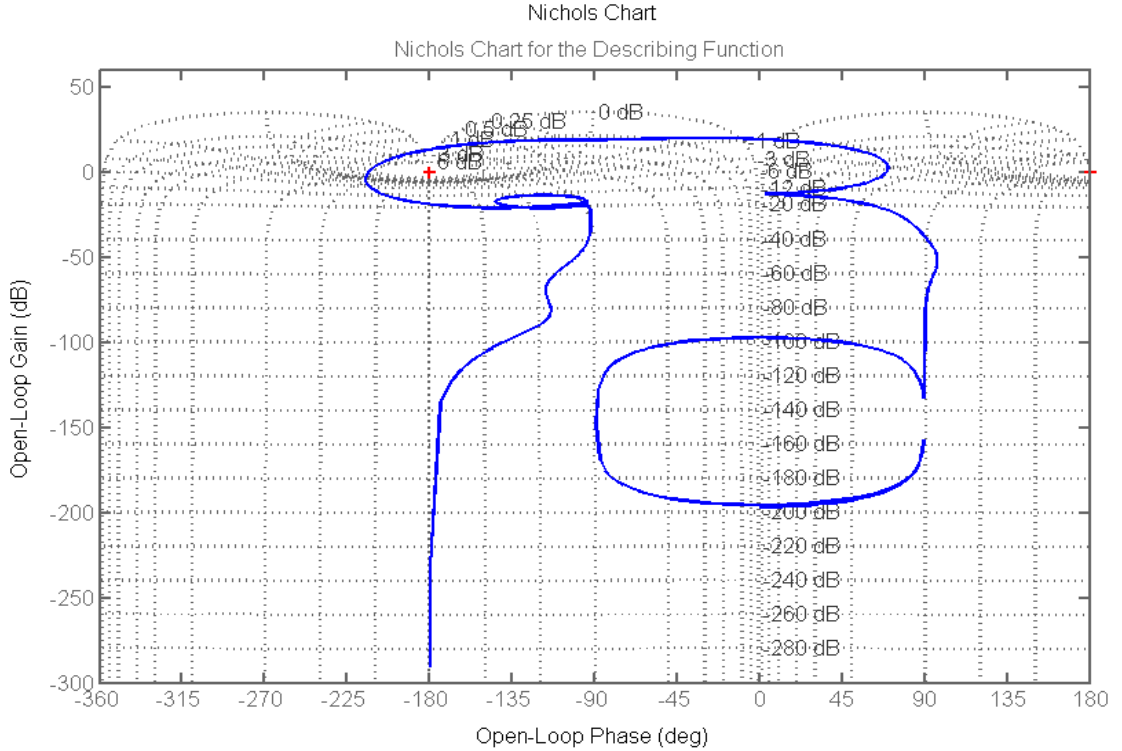


Figure 5.30: Nichols chart for describing function

5.5 MFPC Direct Online Design

As earlier explained, the simplex version of the iterative feedback tuning introduces the concept of computing a gradient-free cost function in our model-free design. The template of the algorithm in subsection 5.5.1 is required for the vector of control parameter $\beta(k) \in \mathfrak{R}^l$ to perform online control optimization through gradient extension of 5.21 as

$$\frac{\delta J}{\delta \beta}(k) = \frac{1}{T_f} \int_0^{T_f} \left\{ e(t, \beta(k)) \frac{\delta e(t, \beta(k))}{\delta \beta} + \mu^2 u(t, \beta(k)) \frac{\delta u(t, \beta(k))}{\delta \beta} \right\} dt \quad (5.21)$$

The aim is to compute the closed-loop system signals at varying operating points. This way, real system data is made available to the optimal routine at all time via the

database storage formed by the closed-loop signals namely; reference $r(t)$, error $e(t)$, manipulated variable $u(t)$, and the control variable $y(t)$, again prescribed as per Figure 5.28 in the time domain. The reader is once more referred to (Kashiwagi & Li 2004) for details on such computations. From the on going, implementing the model-free routine of 5.21 clearly requires processing the actual plant data to obtain all the signals in 5.22, that is:

$$e(t, \beta(k)), \frac{\delta e(t, \beta(k))}{\delta \beta}, u(t, \beta(k)), \frac{\delta u(t, \beta(k))}{\delta \beta} \quad (5.22)$$

as shown in Figure 5.31. It is obvious from the figure that two set of responses due to $r(t)$ and $e(t, \beta(k))$ are injected at the reference entry points. The current error $e(t, \beta(k))$ and the control signal $u(t, \beta(k))$ at each iteration are stored while the error signal $e(t, \beta(k))$ is again fed back into the reference point to generate new signals $e^1(t, \beta(k))$, $u^1(t, \beta(k))$, and $y^1(t, \beta(k))$. This process is repeated until optimal solution is attained. It is clear from that no model is required for the procedure, validating my claim of a model-free design.

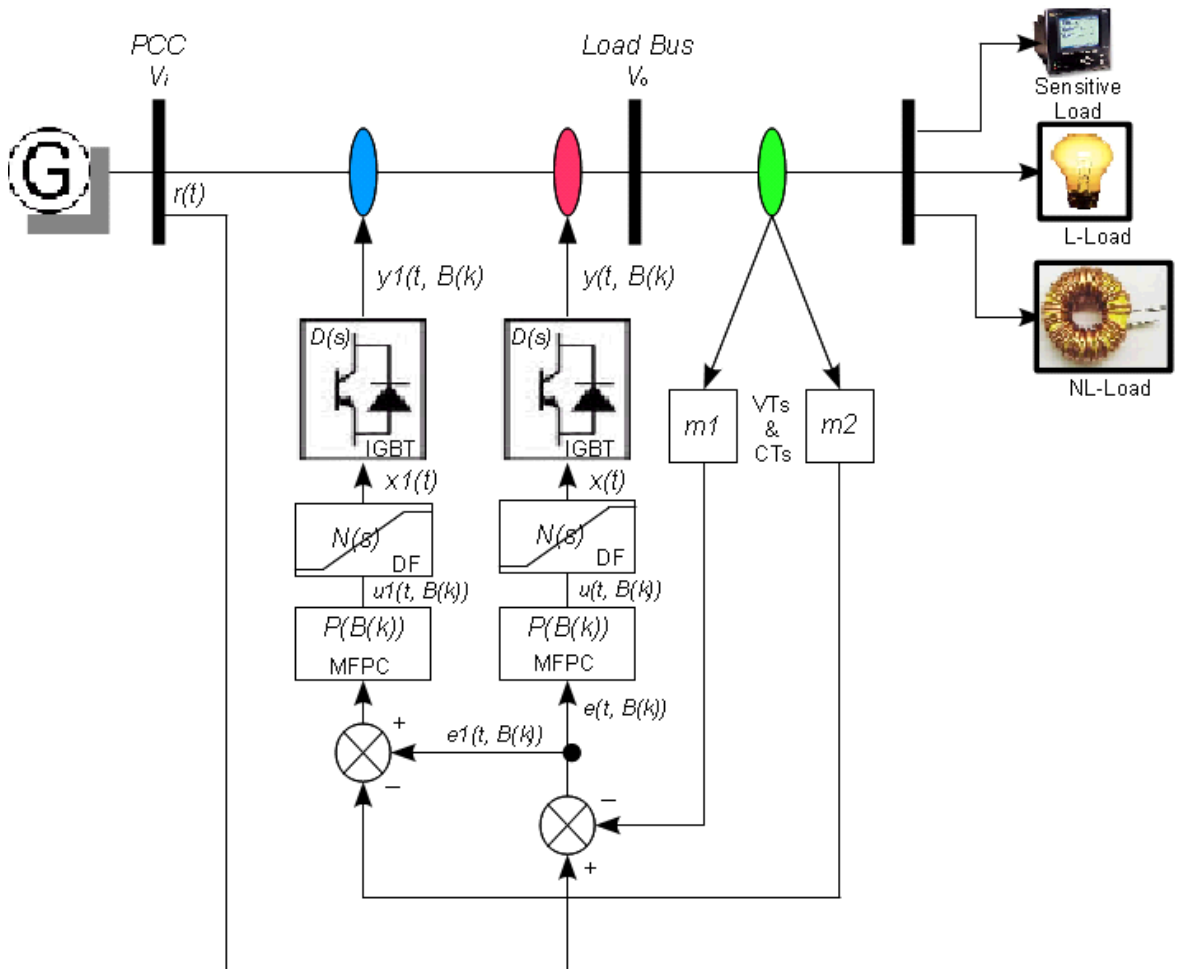


Figure 5.31: Model-free signal generator

5.5.1 Model-Free Predictive Control Paradigm

The concept of model-free control presented in chapter 5 is built around the model-on-demand theory described in (Cleveland & Devlin 1988) which was presented as an alternative polynomial modelling to conventional modelling technique the likes of; wavelets, radial basis and neural networks. Nonetheless, the literature suggests that model-free prediction was triggered by Van Overschee and De Moor's approach of using a normal MPC fundamental principle to usurp past input, past output, and future input signals in predicting the future process output (Barry & Wang 2004). In the same token, researchers like (Stenman 1999); (Kadalia et al. 2003); and (Barry & Wang 2004), were motivated to design an MPC that directly used subspace identification based on system matrices later to be known as MFPC . While the the idea of using describing functions in nonlinear control techniques emerged from (Åström & Hägglund 1985). It has been understood that the majority of the subsystem identification based MFPCs are only good for slow process applications due to their reliance on system matrix data, as in the MPC. Unfortunately, the gradient algorithms mostly used in the scheme is deficient for the difficulties often encountered while seeking analytical solution of Ricatti equation in more complex systems. For this reason, I proposed a-posteriori Nelder-Mead simplex method for online MFPC application in DSTATCOM discussed in chapter 5.

In a model-based design the states $i_q(t)$, $i_d(t)$ and v_{dc} in Eq. 3.1 cannot be measured directly and therefore are predicted through a state estimator such as Kalman filter which is often designed around an internal model of the plant using gradient methods for flexibility. However, the idea of such prediction in the model-free concept is built with the intent of boycotting the model and replacing gradient algorithm with a much faster simplex algorithm. This section describes the stages involved in achieving such model-free technique.

Restrained Control Structure

This is the first of the three steps involved towards the new model-free design introduced in section 5.5. This stage is akin to implementing output constraints on the system and is accomplished through the following way. Online operations of the nonlinear model in Figure 5.28 generates a database and delivers a pair of manipulated input u and control variable y around an operating point such that

$$g(t) = n(\psi(t)) + \xi(t), \quad t = 1, \dots, N \quad (5.23)$$

where $g(t)$ is a nonlinear model updated at every new operating point, $n(\cdot)$ is an undefined model's nonlinear mapping and $\psi(t)$ is a white noise term.

A decoupled predictive controller with a high gain factor and an integrator can be replicated and included in the feedback as a conventional proportional-integral scheme in the following way.

$$P(\beta) = \beta_1 + \frac{\beta_2}{s} \quad (5.24)$$

where the controller parameters are represented by

$$P(s) \Rightarrow P(\beta), k_p \Rightarrow \beta_1, k_i \Rightarrow \beta_2, \text{ and } \beta_i \in \Re, \quad i = 1, \dots, l.$$

and the vector of the parameters expressed as $\beta_i \in \Re^l$, and l represents the total number of parameters.

Including an integrator at this stage enables attainment of the stability boundary known as limit cycle, in the nonlinear DSTATCOM control during steady state operations. Conversely, introducing a large gain factor guarantees system stability by appropriately adjusting the time constants as explained in subsection 5.4.2.

Gradient Optimization Criterion

The decision about optimisation criterion is the second step, which was initially performed through gradient information based cost functions for solving optimization problems since the 1960's (Hsu & Meyer 1968). This technique works best in slow processes with large time constants. As high speeds are particularly desirable in systems with small time-constants and with continuous shifting operating points. Then, a robust direct optimization criterion is required to access an established database regardless of gradient information to solve the online optimization problem. The simplex algorithm is a direct search method proposed in the next subsection to perform online synthesization of the controller properties, as a final step to the new model-free design procedure.

To better understand the inner working of the scheme, I first analyse the algorithm through a working template given in Figure 5.32. The Figure describes a basic deterministic objective function routine ideal for localising weighting indices for error, control, and process output signals expressed in the continuous time domain as

$$J(\beta) = \frac{1}{2T_f} \int_0^{T_f} [R_y e(t, \beta)^2 + \mu^2 S_u u(t, \beta)^2] dt \quad (5.25)$$

where R and S are weighing filters, T_F is the final time, t is time instant, e is the system error, δe is rate of change of the error, u being the control signal, δu is the rate of change of the control signal, μ is the weighting cost, and β is the vector of control parameters as given in the following equations.

For simplicity, the weighting filters in 5.25 are set to $R = S = 1$, then the gradient cost function formulation becomes

$$J(\beta) = \frac{1}{2T_f} \int_0^{T_f} (e^2(t, \beta) + \mu^2 u^2(t, \beta)) dt \quad (5.26)$$

this formulation leads to the generation of four control parameters based on the vector $\beta \in \mathfrak{R}^l$ shown to achieve a steady state as $T_f \rightarrow \infty$ in following manner:

$$\frac{\delta J}{\delta \beta} = \frac{1}{T_f} \int_0^{T_f} \left\{ e(t, \beta) \frac{\delta e(t, \beta)}{\delta \beta} + \mu^2 u(t, \beta) \frac{\delta u(t, \beta)}{\delta \beta} \right\} dt \quad (5.27)$$

Evolutionary Non-Gradient Simplex Scheme

The simplex algorithm was first published in 1965 as “Nelder Mead simplex” algorithm (Lagarias et al. 1998). Since then, it has been widely applied as direct search method for nonlinear unconstrained optimization. The algorithm utilises a simplex of $k + 1$ points of k dimensional vectors p by making unidirectional move over the initial guess p_0 and adding 5% of each component $p_0(i)$ to p_0 . It then uses the k vectors as elements of the simplex in addition to p_0 . When $p_0 = 0$, i is assigned as 0.00025 and the simplex is then modified repeatedly by the algorithm in the following sequence: *order*, *reflect*, *expand*, *reflect*, *calculate*, *contract – outside*, *contract – inside*, and *shrink*. Interested readers are referred to optimisation toolbox in Matlab for a detailed description of this phenomena. It is implemented here through the gradient of Eq. 5.27, which was traditionally noted for slowing down the routine and increasing computational count when used in nonlinear systems. Hence, The simplex algorithm is incorporated as an iterative feedback tuner (IFT) within the restrained prediction space to search for optimal control solution with dispatch, in the following minimization problem (5.28).

$$\min_{w.r.t. \beta \in \mathfrak{R}^l} J(\beta) \quad (5.28)$$

The motivation behind the use of simplex IFT is that they are gradient-free functions which are practically capable of accessing online closed-loop data by bypassing the

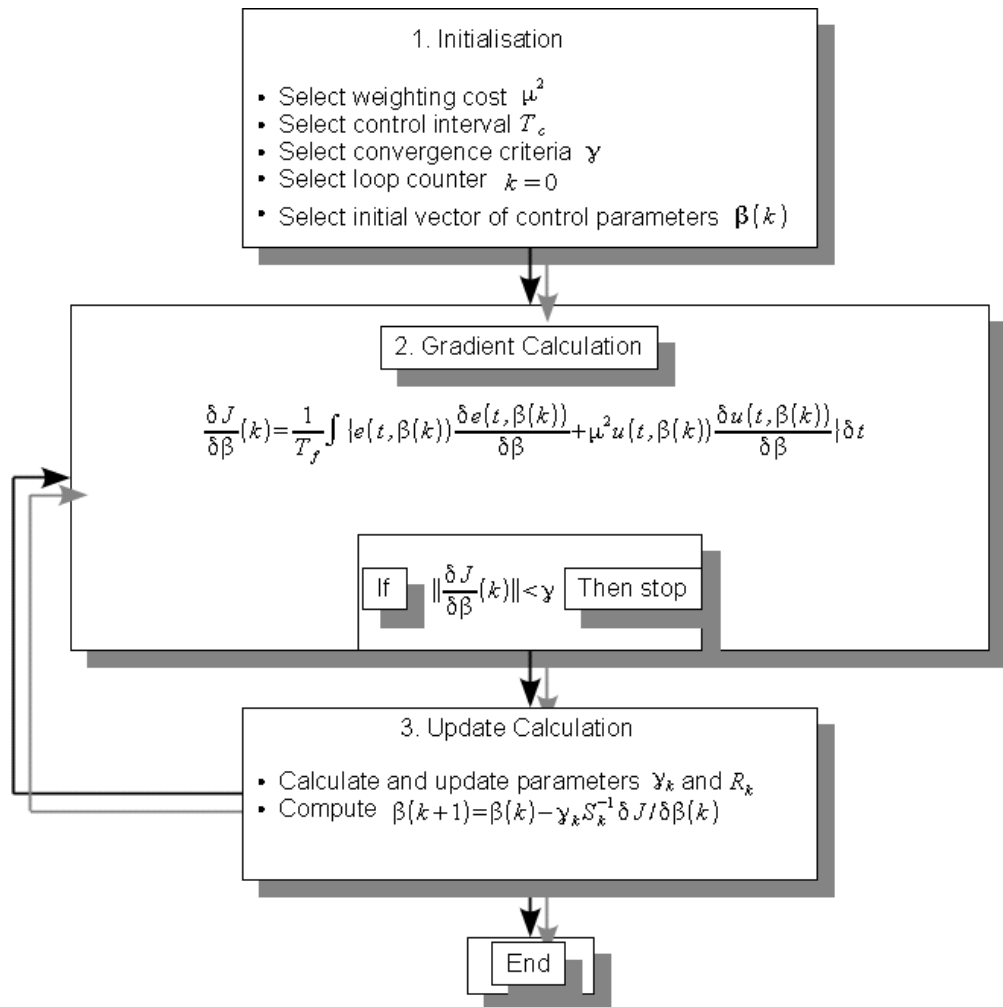


Figure 5.32: Basic optimization routine

intermediate models occasionally encountered in model-based designs due to changing operating conditions. And the technique can be realised by decomposing the gradients in (5.27) to a simple quadratic problem solvable over finite coincidence horizon C and control horizon M in a direct online MPC formulation described in (Kashiwagi & Li 2004). I then replaced (5.28) with a new design objective $J : \mathfrak{R}^M \mapsto \mathfrak{R}^+$ to synthesize the MPC to solve for $Q : \mathfrak{R}^M \mapsto \mathfrak{R}$ such that

$$J(u) = \min_u \|e\| \quad (5.29)$$

subject to constraints imposed by the describing function saturation on the actuators and its rates of change given by

$$u_{min} \leq u(t) \leq u_{max} : \Delta u_{min} \leq \Delta u(t) \leq \Delta u_{max} \quad (5.30)$$

and

$$e = r - y \quad (5.31)$$

is the error to be minimized, while y is the predicted output at the current time t estimated from the model and actual output information. Numerical minimization is preferred in practice as analytical zeroing of J means setting infinite control gains which threatens the system's stability (Kashiwagi & Li 2004). Thus, the new online formulation of 5.29 taking 5.31 into consideration yields:

$$J(u) = \min_{u(t+1), \dots, u(t+M)} \left\{ \sum_{k=L}^{L+P-1} |r(t+k) - y(t+k)|^r \right\}^{\frac{1}{r}} \quad (5.32)$$

The objective becomes clear from 5.32, of minimizing the control effort with respect to the error. To realise this with a given setpoint value $s(t)$, a reference trajectory $r(t)$ will be traced by the plant output $y(t)$. Such a desired trajectory is normally obtained from the response of a first-order low-pass pre-filter in (Kashiwagi & Li 2004). However, low-pass filters are occasioned with an 'input leakage effect' in a one-pole one-zero transfer configuration that flattens out the cross over frequency leading to implementation difficulties and overall performance degradation. To combat the effect, I replaced this filter with a finite impulse response (FIR) filter which is inherently stable and requires

no feedback. This means that, all its poles are located at the origin within the limit cycle, an essential condition for stability. The impulse response $f(n)$ is then calculated by feeding the FIR filter input with the Kronecker delta $\delta(n)$ impulse signal to yield a response of a set of coefficients or tap weights b_n using

$$f(n) = \sum_{i=0}^l b_i \delta(n - i) = b_n \quad (5.33)$$

for $n = 0$ to l .

The discrete implementation is realized in Z-plane as

$$F(z) = Z \{f[n]\} = \sum_{n=-\infty}^{\infty} f(n)z^{-n} = \sum_{n=0}^l b_n z^{-n} \quad (5.34)$$

The reference trajectory $r(t)$ is also defined in the continuous-time domain as

$$r(t) = s(1 - e^{-\frac{t}{\tau}}) \quad (5.35)$$

In order to compute J through (5.32) discrete-time domain to conform with (5.34), a difference equation is derived from 5.35 as

$$r(t + 1) = \alpha r(t) + (1 - \alpha)s \quad (5.36)$$

for a chosen control interval $T(\mu s)$;

$$\alpha = 1 - \frac{T}{\tau} \quad (5.37)$$

Hence, iterating 5.36 yields

$$r(t + 2) = \alpha r(t + 1) + (1 - \alpha)s = \alpha^2 r(t) + (1 - \alpha^2)s \quad (5.38)$$

Generally, the reference trajectory ($r(t)$) is iterable k-steps ahead, such that

$$r(t+k) = \alpha^k r(t) + (1 - \alpha^k)s \quad (5.39)$$

Similarly, it is possible to estimate from the plant model $D(t)$ the output $y(t+k)$ by iterating $yM(t)$ k-steps ahead. As the objective function is being formulated, its minimization can be applied online to obtain an optimal control sequence of the form

$$u = [u(t+1)u(t+2), \dots, u(t+M)] \quad (5.40)$$

Thus, accomplishing the new model-free predictive control sequence.

5.6 Test for Step-Change

In this section, the dynamic behaviour of the new MFPC scheme is tested against step changes occasioned by overvoltage and undervoltage conditions. An overvoltage condition is caused by a number of factors such as single load or a group of load dropping out of the system, leading to a sudden rise in the source voltage or current. This phenomenon is the same as the voltage swell situation treated in subsection 5.8.3 through the simulation model. In a similar way as the voltage sag has been treated in the same section, the undervoltage condition is a voltage drop phenomenon caused by a source outage or due to some feeder fault. We have been able to demonstrate both these conditions through our control model in Figure 5.33 to 5.36.

A step-up change is applied in the first case following a drop of 120 volts in Figure 5.33 which is required to be raised to 220 volts. The action has been accomplished by the MFPC where an initial control output of 0.0017 radians is transformed to 0.0031 radians to produce the required change in voltage as depicted by Figure 5.34. The dynamics of the system were then changed to mimic a step-down situation with an initial voltage state at 220 volts, a sudden drop was introduced at 0.1 seconds to 120 volts as shown in Figure 5.35. The control effort responsible for upholding the change came down to 0.0025 radians from 0.0045 radians and is shown in Figure 5.36. Clearly, the control model demonstrates the flexibility to accommodate any kind of change with an intact reference following through the Figures.

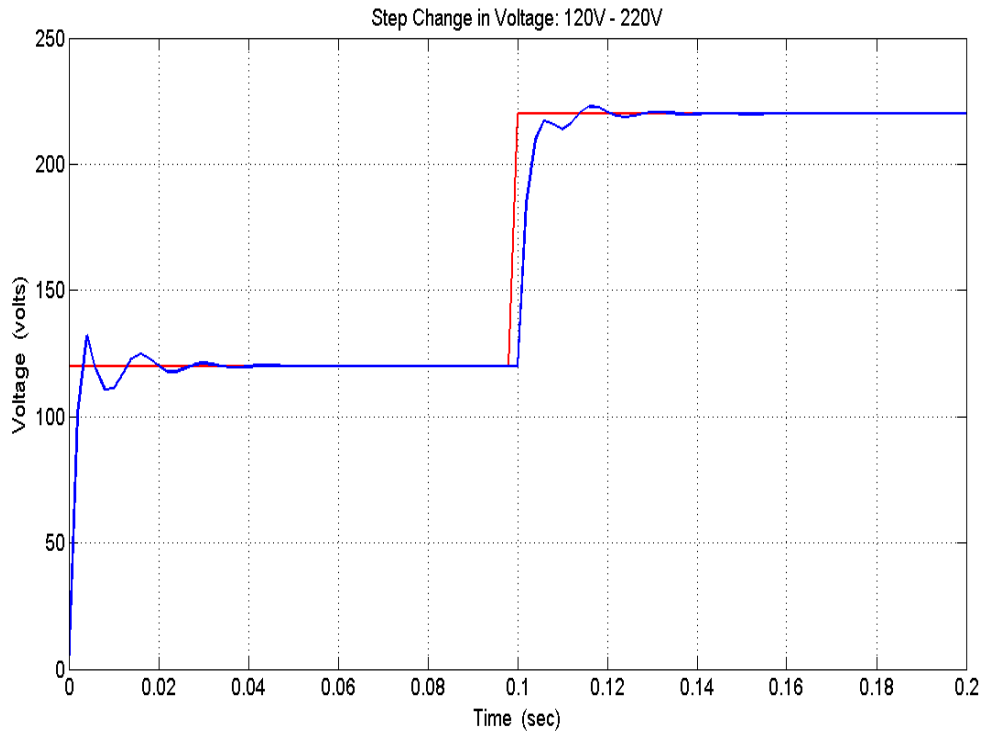


Figure 5.33: Step-up: 120 to 220 volts

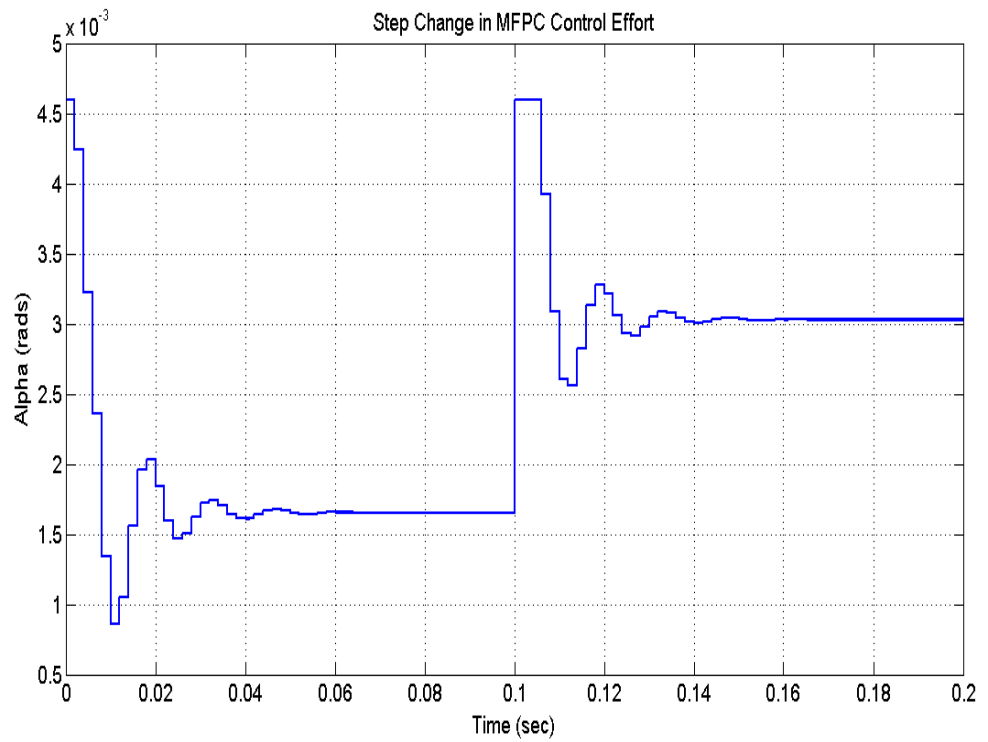


Figure 5.34: Alpha: 0.0017 to 0.0031 rads

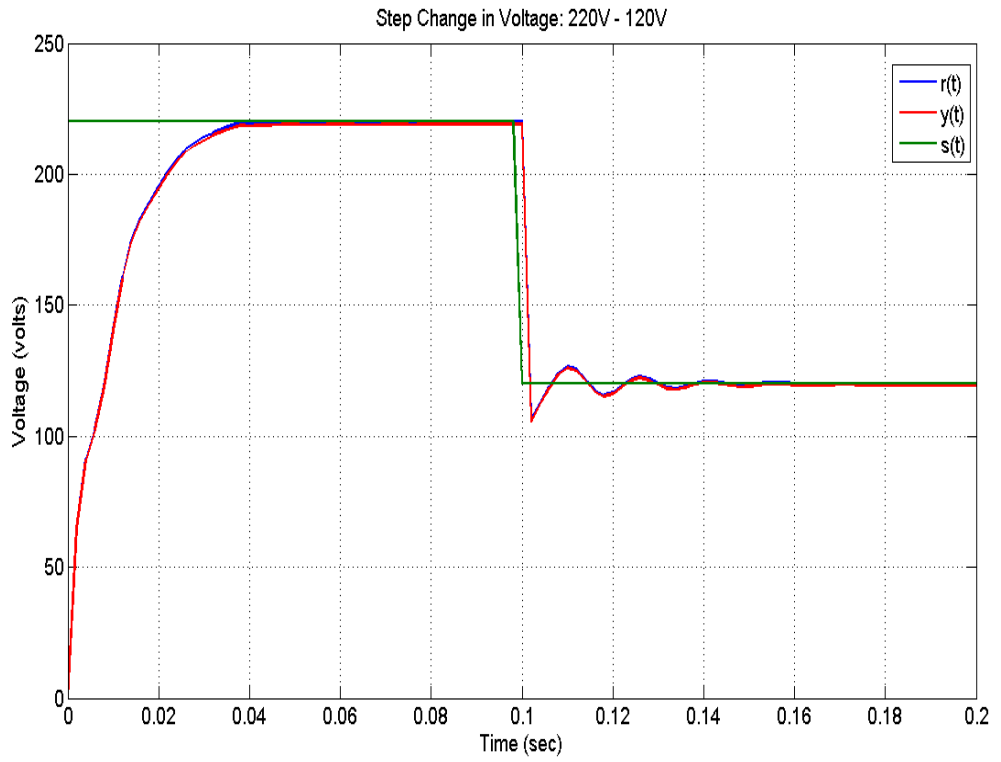


Figure 5.35: Step-down: 220 to 120 volts

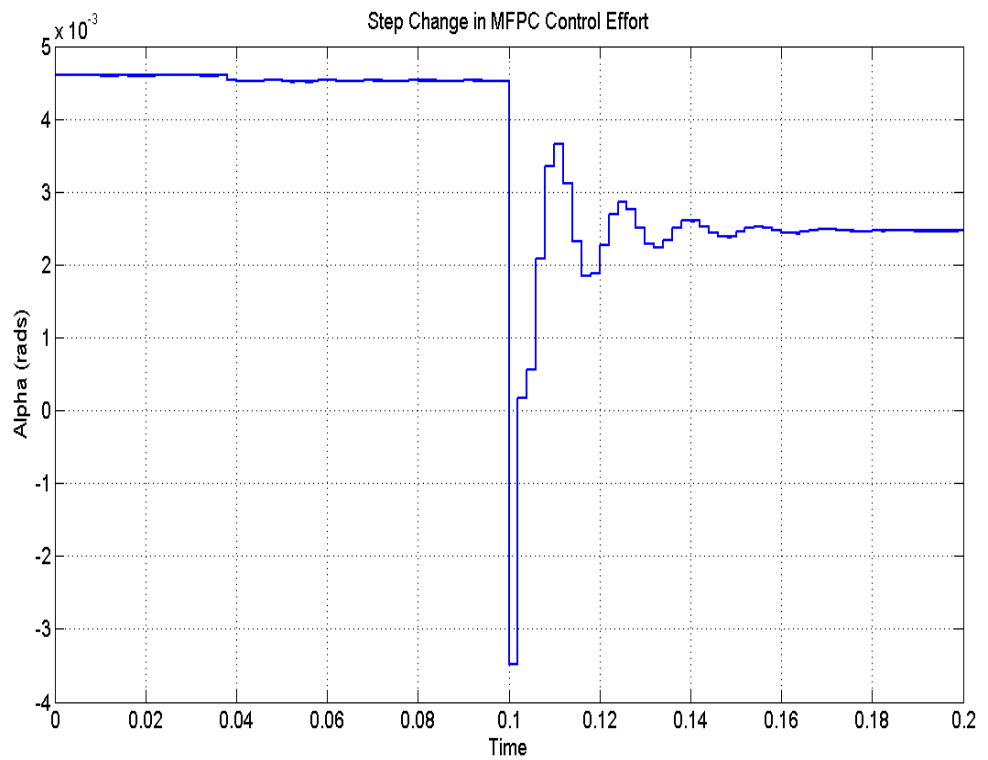


Figure 5.36: Alpha: 0.0031 to 0.0031 rads

5.7 Experimental DSTATCOM Model

With the difficulty envisaged for testing my design on a real power system, the SimPowerSystems (SPS) software provides me with the required simplicity and relative analytical power to rapidly design, implement and simulate nonlinear control systems. Equipped with sophisticated power electronic devices and other electrical, electromechanical as well as control systems libraries, the software performs better than conventional analysis tools. It contains textbook proven models which have been validated against the experience of the Power Systems Testing and Simulation Laboratory of Hydro-Quebec, a large North American utility sited in Canada. A detailed test model shown in Figure 5.37, with an accurate representation of two IGBT based voltage-sourced PWM inverter bridges has been developed. The SPS has been proven as an ideal platform for the realisation of complex, self contained power systems as found in application to power utilities, aircraft, automobiles, and manufacturing plants (MathWorks 2009a). Coupled with Simulink, SPS provides the necessary domain for multi-modelling and efficient control design environment.

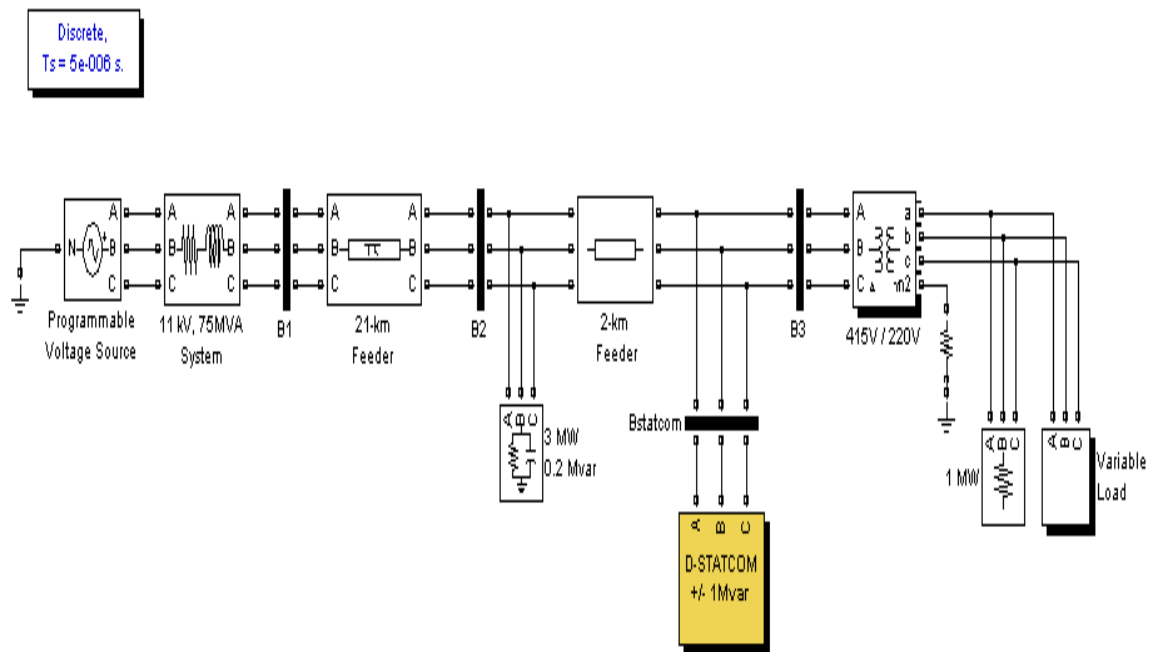


Figure 5.37: SPS DSTATCOM model

A single-line representation of the test system is depicted in Figure 5.38 illustrating the various components and their ratings involved in the simulation model. The shunt DSTATCOM device can be seen rated at 1 MVar, 11 kV and connected to the PCC (B2) through 11 kV/415 V coupling transformer.

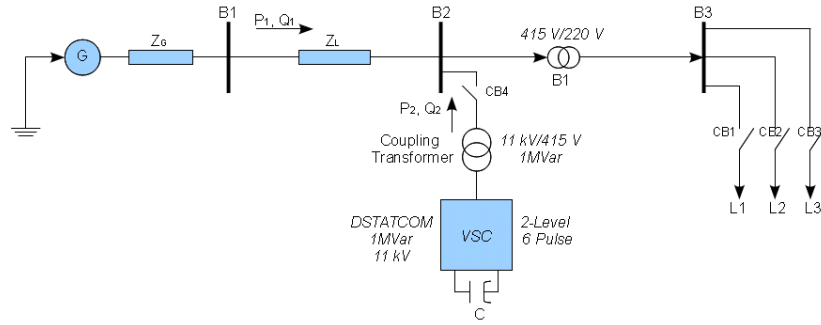


Figure 5.38: Single-line diagram

The circuit is based on a fixed-step discretized sampling time of $T_s = 5 \mu\text{seconds}$ at a switching (modulation) frequency of 1400 Hz. And the controller is fitted with larger sample time of $(32 \times T_s = 160) \mu\text{seconds}$. A $500 \mu\text{F}$ capacitor determined from calculations in the design stage, acts as the DC voltage source for the inverter, while the inverter output is fitted with LC damped filters (resistances connected in series with capacitors) to give a quality factor of 30 at 50 Hz. Voltage and current acquisition is enabled by anti-aliasing filters. This type of model is ideal for studying power quality related issues such as harmonics and other control system dynamics typically within the range of hundreds milliseconds to one second (Giroux et al. 2001).

Further closed-loop validity correlation between the control model and the simulation model designed through the SimPowerSystems software presented in chapter 5 is shown in Figure 5.39. This affirms the closeness of my derived control model to the simulation model and hence its suitability for practical applications, despite the presence of minor unavoidable modelling errors. However, trends shown from the simulation model data (red) indicates clearly that initial conditions in practical DSTATCOMs starts way above zero (in fact at 0.47 pu). Conversely, the control model data curve (blue) shows the initial condition to begin in the vicinity of 0.07 pu. Despite bearable overshoots that can be observed in both models, the settling times are remarkably set almost at the same phase, although my control model exhibits a much faster rise time trend. But in the overall the correlation can generally be said “acceptable” for practical viability.

5.8 Power Quality Simulations

The traditional distribution system design parameters would normally include analysis of the system’s voltages, currents, active and reactive power rms quantities at the PCC through ordinary control systems. The approach of this research is based on automated intelligent designs to rapidly integrate optimisation of the related parameters to the customer using modelling and simulation. In this section, a selected number of specified

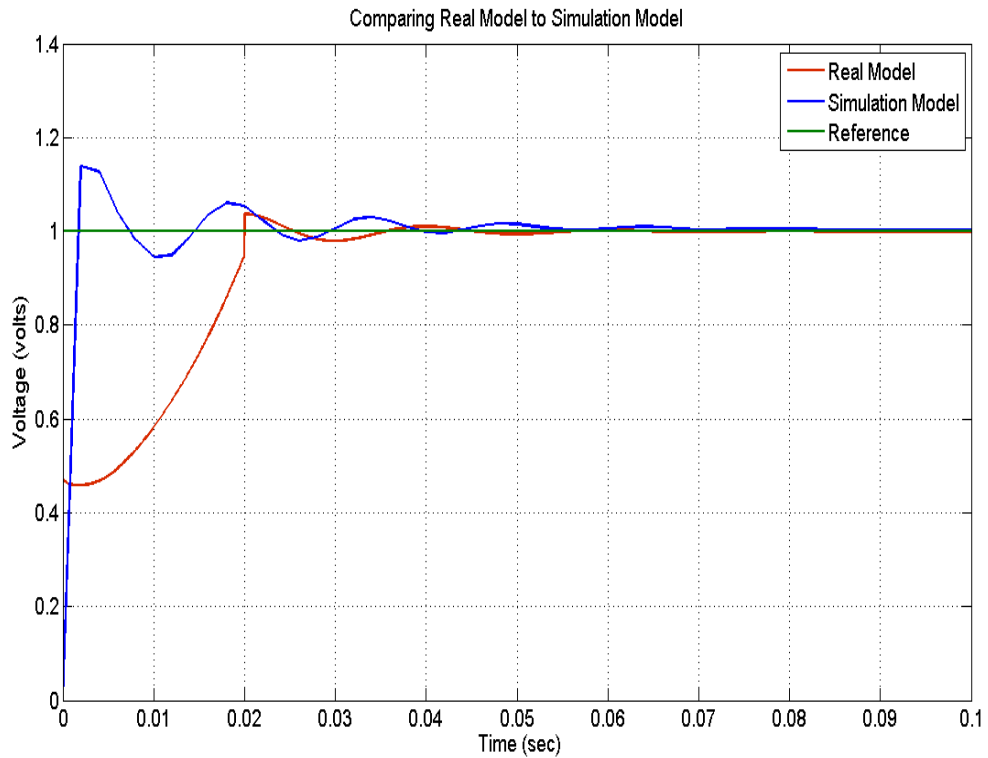


Figure 5.39: Closed-loop model validation

PQ problems are simulated and controlled by my novel model-free design placed in the feedback with the SimPowerSystem (simulation) model described above.

Identification of PQ issues is basically done either from the perspective of the disturbances caused by the supply voltage quality or load current quality. Voltage sag or voltage swell represent an example of the first category. These kind of disturbances can lead to tripping of sensitive computing and medical equipment, which often translate into industrial shut-down costing the operators an enormous amount of money (Acha & Anaya-Lara 2002). As such mitigating devices are installed at the appropriate position to quell them. The second category involves a phenomenon of poor quality current absorbed by the load. Current and voltage harmonics normally ingested by disturbed loads in, for example, switching action in a converter, or unbalanced currents and voltages drawn by unbalanced loads. A more intricate example is a 'flicker' which is normally caused by voltage variations due to rapidly changing load dynamics attached to a feeble grid (Sannino et al. 2003). This section designed two simulation closed-loop model topologies of the new MFPC from the SimPowerSystems Tool for studying the effects of these faults.

5.8.1 Dynamic Performance Test

During this test, a single phase simulation of the programmable source block from Figure 5.37 was used to modulate the internal voltage of a 11 kV source. The system was in initial transient state that lasted for about 0.13s shown in Figure 5.40, trace 1, as it eventually reached the steady state when DSTATCOM was activated. Exactly at 0.4s, the source voltage is increased by 10%. The DSTATCOM compensates for this voltage increase by absorbing reactive power from the network at $Q = -1.55$ Mvar shown in PQ plot (red), of the same Figure. At $t = 0.5$ s, the source voltage is decreased by 10% from the value corresponding to $Q = -1.5$ MVar. Shown in a closer view on Figure 5.41 at this point, the DSTATCOM must generate reactive power to maintain a 1 pu voltage in which Q changes from -1.55 Mvar to -1.45 MVar. All this was taking place while the active power, $P = 0$, shown in blue in the PQ trace.

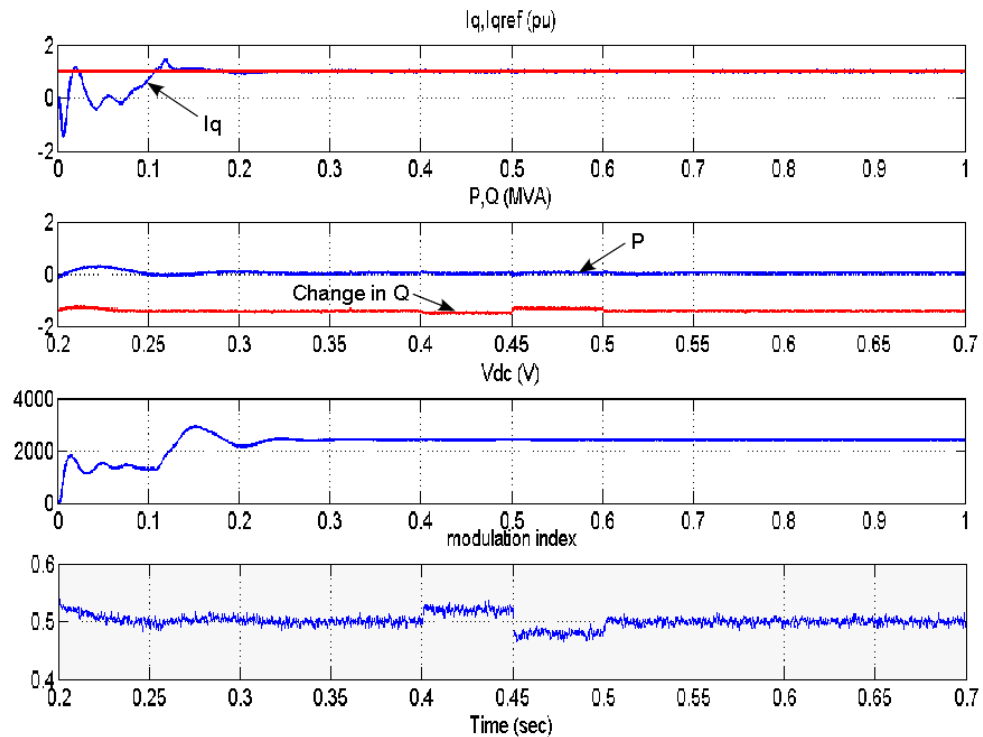


Figure 5.40: Dynamic response of DSTATCOM

It should be noted that when the DSTATCOM changes from inductive to capacitive operation, the inverter modulation index m shown in Figure 5.40 (trace no. 4), is increased from 0.5 to 0.52 and then decreased to 0.48, corresponding to a proportional increase in inverter voltage of Figure 5.42, V_a Inv trace (no. 2). Also, a capacitor dc side voltage is shown in trace no. 3 of Figure 5.40 as 2500 volts. It has been produced by the ac side voltage serving as its initial condition. The simulation was performed using a discrete step time ($T_s = 5.8$) μ s, and the dynamic response of DSTATCOM to step changes in source voltage following is observed depicted as V_{B1} and V_{B3} in Figure

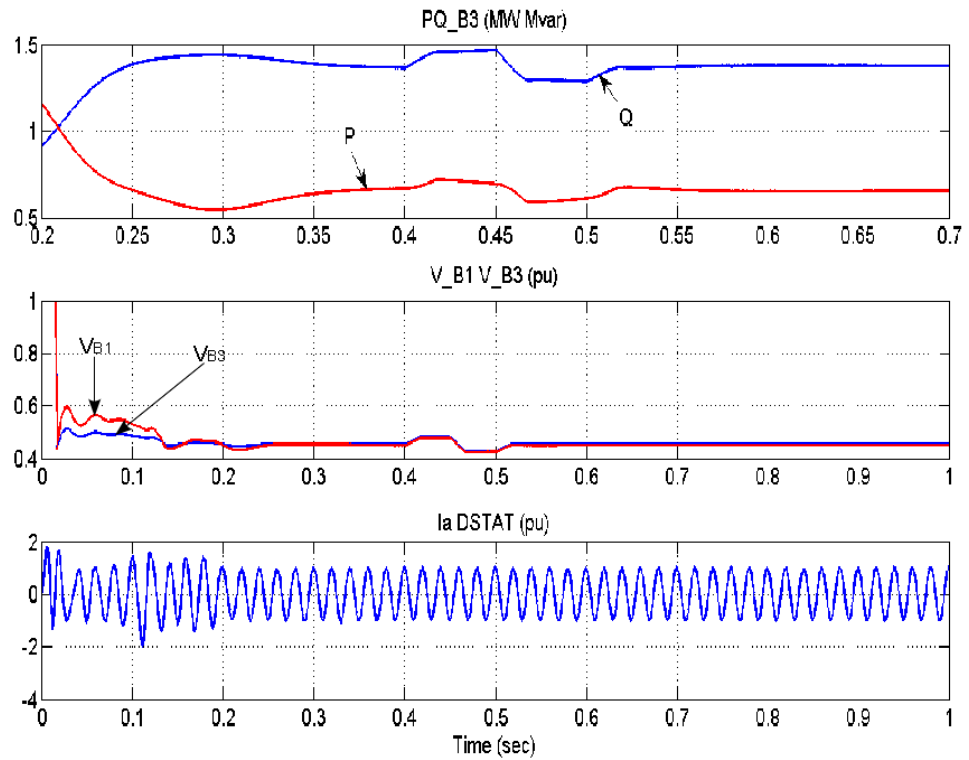


Figure 5.41: Voltage support curves

5.41. The relative single phase inverter voltage and current wave forms are presented as in Figures 5.42.

5.8.2 Flicker Control

Recently, interconnection of wind turbines in addition to arc furnace operations at the transmission and distribution voltage levels have been identified as the chief causes of flicker. A number of methods for flicker control with associated cost implications have been introduced (Sannino et al. 2003). The new DSTATCOM designed for custom Volt-VAR optimisation at the outer control loop in this work was as specified earlier. Note that, current control schemes are usually employed in the inner control loop to cater for load balancing problems. However, I use the outer voltage control loop as most appropriate for solving power factor, harmonic distortions as well as other power quality related problems such as sags, swells and flicker. The details on the control strategy of the DSTATCOM can be found in Appendix D.

The plant is as in Figure 5.37, comprising a 11kV/415V/220V; 3-phase ($\Delta - Y - Y$) transformer unit connecting 220V linear and 415V variable loads via B3. The nonlinear load is assumed to be constantly absorbing changing reactive currents analogous to an arc furnace generating voltage flicker. Note that flicker simulation would require

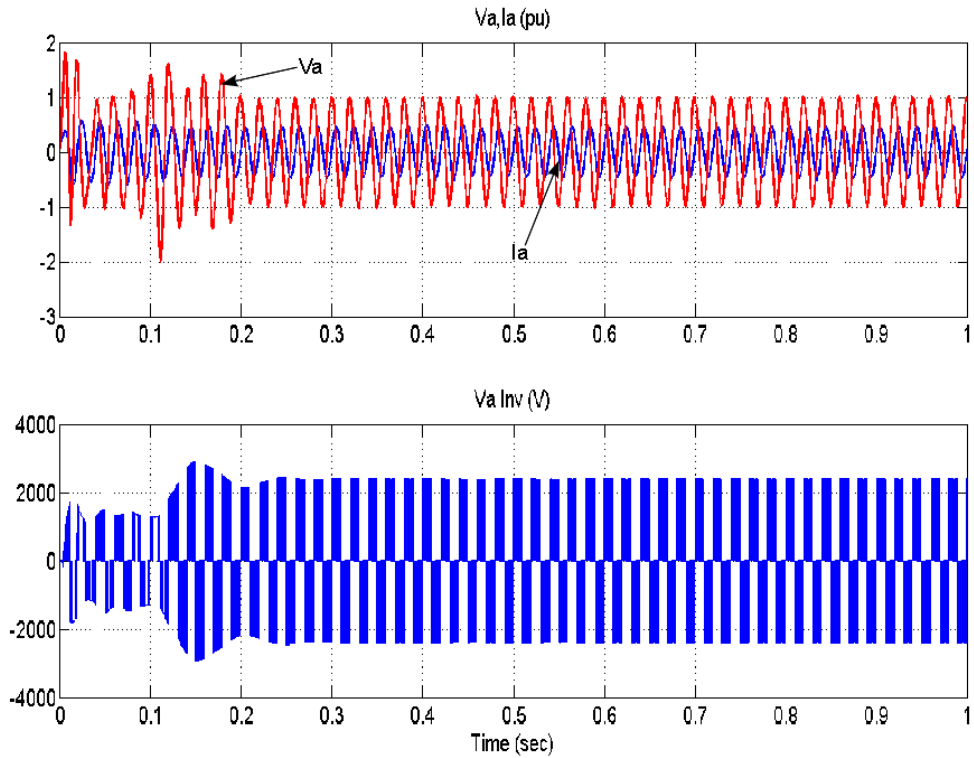


Figure 5.42: Inverter voltage and current magnitudes

maintaining a high lagging power factor ($\Phi \approx 0.9$), while the magnitude of the nonlinear load current is modulated at 5Hz to keep its apparent power approximately ranging between 0.01 to 0.14 MVA.

To exemplify the use of the model to mitigate a voltage flicker problem, the voltage at the programmable voltage source was kept constant and the modulation of the variable load was enabled. Following simulation, the DSTATCOM is said to be floating while in Q regulation mode i.e. it performs no voltage correction as can be observed from the plots of Figure 5.43. The inverter current I_a (trace no. 3) at this scenario has not been injected, i.e., it remains constant at zero. Massive variations are observed in both P and Q at B3 (trace 1), while there is no proper following between voltages at B1 and B3 (trace 2), in fact the voltage at B3 (purple) tends to vary between 0.93 per unit (pu) and 1 per unit, about $\pm 7\%$ variation. Re-running the simulation with DSTATCOM controller now changed to voltage regulation mode, it can be seen in Figure 5.44, trace 2, that the voltage fluctuation at B3 shown in purple, has now reduced to 0.945 pu to 0.955 pu corresponding to $\pm 1\%$ reduction. This is due to the inverter current injection observed in trace no. 3 of the Figure. Fluctuations between the reactive and the active power components is also observed to narrow down in trace no. 1. This test reveals that DSTATCOM can in fact be operated under two modes i.e. the voltage or automatic mode, and the reactive power or manual mode. The voltage mode uses the current as a control variable to affect reactive power compensation into

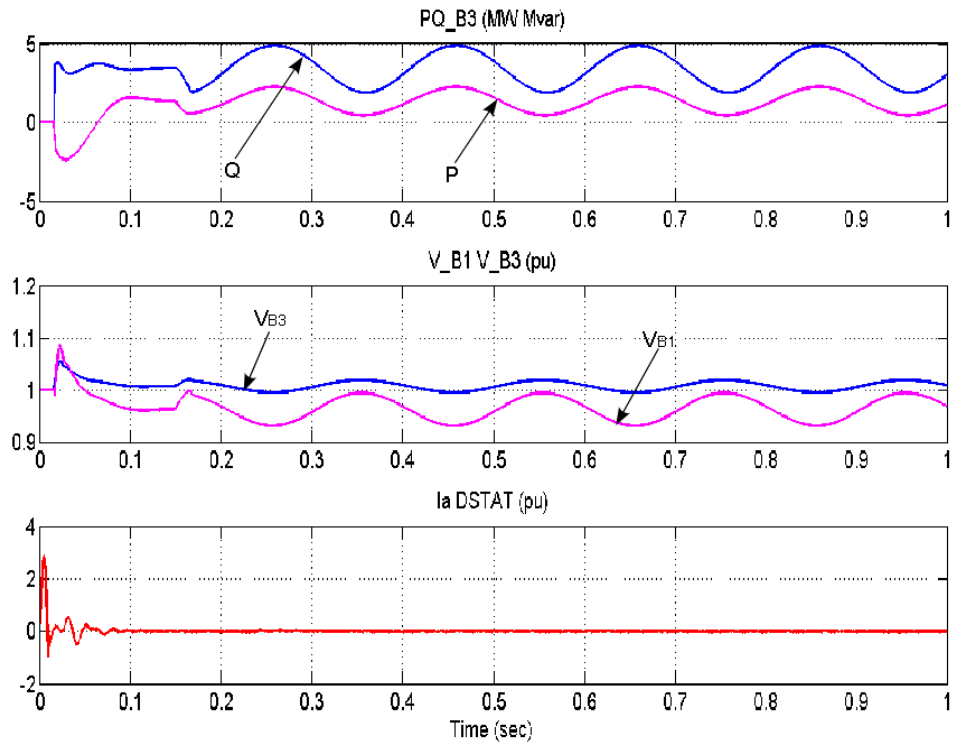


Figure 5.43: Flicker without DSTATCOM

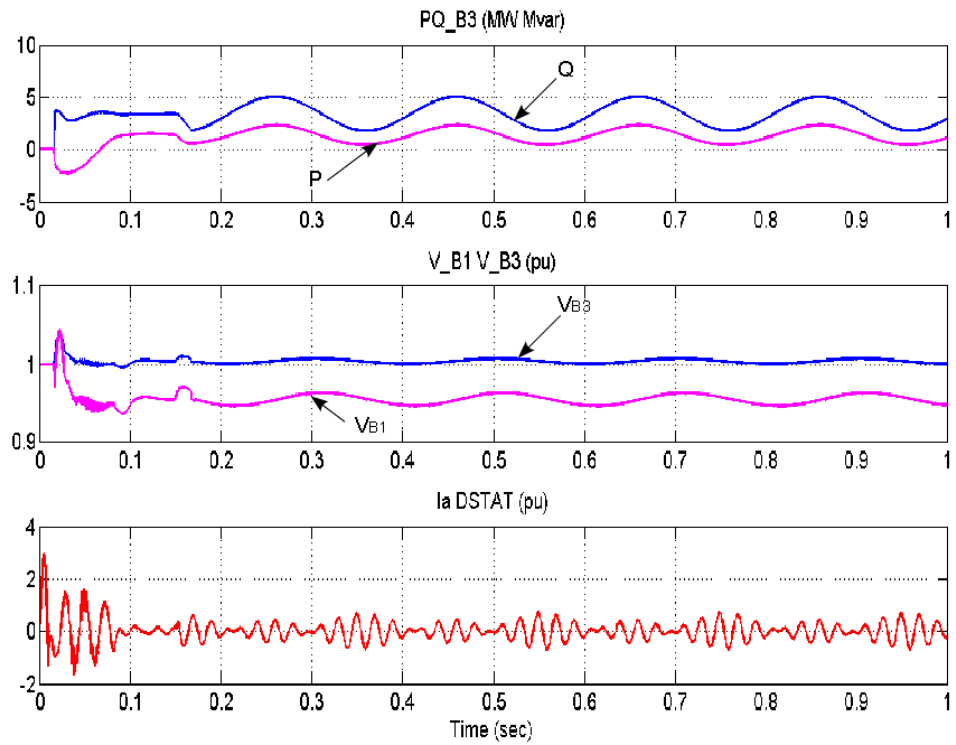


Figure 5.44: Flicker with new DSTATCOM

the system for overall system voltage support. The reactive power mode, on the hand, uses the amplitude or phase angle of the system voltage as a control variable to meet the reactive power demand of nonlinear loads and for power factor correction as well as for voltage or load unbalances.

5.8.3 Sag and Swell Control

Voltage sag and voltage swell have been respectively defined, according to Table 1.1, as decrease (0.1 – 0.9) or increase (1.1 – 1.8) in per-unit RMS values from a duration ranging 0.01 seconds to 1 minute (Chapman 2001a). The model of Figure 5.45 was used to investigate these effects where a sag-laden distant load located at the consumer’s premises is firstly considered and demonstrated in Figure 5.46. To create sag (undervoltage) condition, an induction motor load is connected in series to a three phase circuit which is being excited by a sinusoidal input. A heavy current drawn due to the motor direct-online (DOL) starting ability, has initiated a sag as demonstrated in Figure 5.46a (system current is shown at the inset of the Figure). Hiding trasients and taking a closer look at the Figure reveals the little variation in the current responsible for causing the sag between (0.4 – 0.5) seconds. In this case, the MFPC equipped DSTATCOM is required to minimise sag strength when operated.

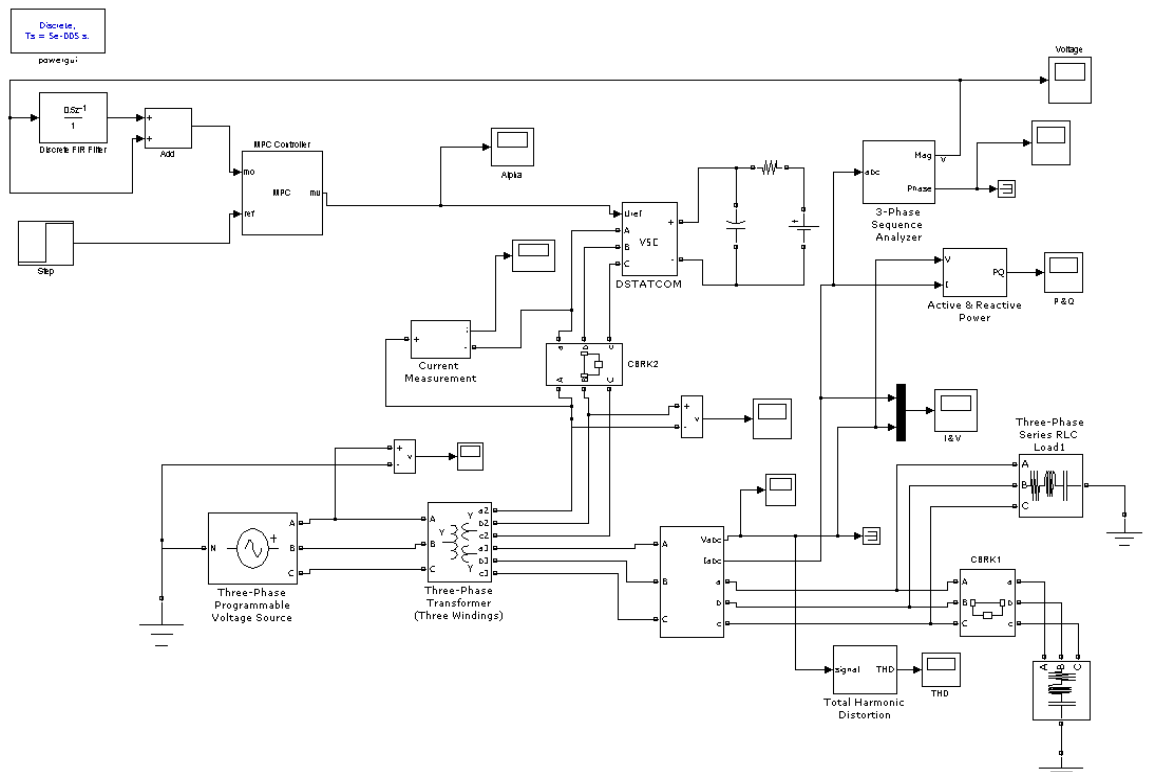
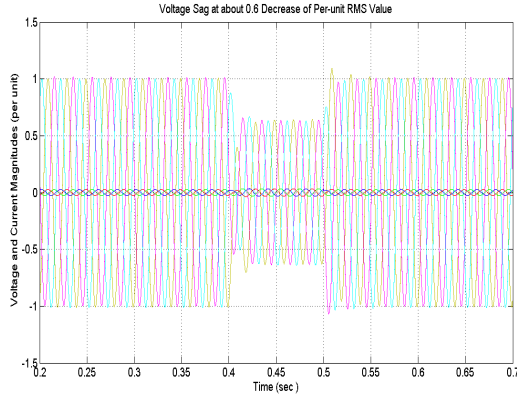


Figure 5.45: MFPC-SPS DSTATCOM model

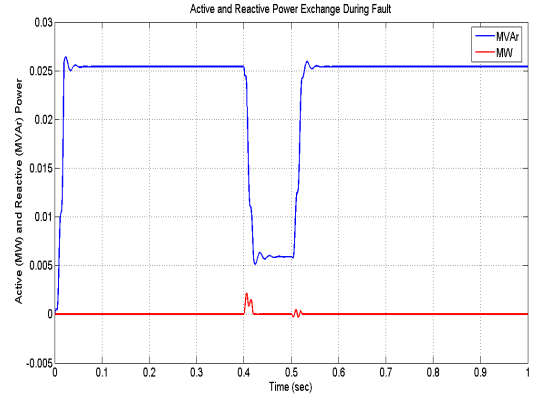
Figures 5.46b and 5.46c display the step responses to the active and reactive power exchange, as well as the steady state voltage at the PCC during the sag creation. As before, since there is virtually no active power exchange taking place between DSTATCOM and PCC, its magnitude can be seen to be maintained at zero, except for little variations due for replenishing the stored energy lost between the sag duration quoted as (0.002 MW) and (0.00067 MW). But the reactive component can be seen to reach its maximum 0.0252 MVAR before the instant of the sag during which it was suddenly depleted to 0.0052 MVAR. This phenomenon also applied to the step voltage during sag which was forced to drop to 0.68 per-unit. Operating the MFPC in a closed fashion, ended the sag condition at 0.5. At this point, all the active, reactive and voltage components regained their constant magnitudes.

Similarly, a swell condition is created by connecting another distant load in parallel as depicted in the same model Figure 5.45. As earlier, a swell is the reverse form of a sag. However, the chief causes of swell may be regarded as high-impedance neutral connections, abrupt drops in large load, and a single-phase fault on a three phase system. The consequences of such abnormality can be diverse ranging from erroneous data to electrical contact erosion and damage to sensitive semiconductor devices. The new MFPC scheme has also been instrumental in solving this problem as presented in Figure 5.46d. A closer look of the overvoltage (swell) condition is vividly shown to occur as usual between 0.4 and 0.5 seconds, before the DSTATCOM is brought into operation. A current rush of 0.125 amps magnitude responsible for the swell is observed almost doubling its original value (0.067 amps), i.e., an increase of 50%.

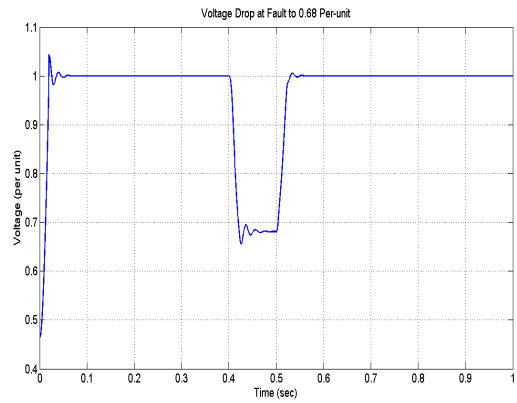
The power exchange involved during the swell condition reversed the glitches of the active component before the swell is quenched by the new DSTATCOM shown in Figure 5.46e. And the amount of reactive power demand caused by the current rush can be seen shooting from its nominal 0.013 MVAR to 0.055 MVAR at the end of the swell. The voltage growth due to the sag has been depicted in Figure 5.46f where an increase in PCC voltage is raised to 46% of its nominal per-unit value during the scenario. The swell condition is also seen to normalise following the intervention of the new DSTATCOM. This operation is clearly depicted in Figure 5.47a showing the no-fault voltage and current quantities at the PCC in a close-look (ignoring transients). Both Figures 5.47b and 5.47c also present the step responses to active and reactive power, as well as the no-load voltage at the PCC. The active power is maintained at zero, while the reactive power reaches its maximum value of 0.0128MVAR for unit input signal. The current injected by the DSTATCOM during the sag condition is represented in Figure 5.47d. Note the current boost generated in tackling the deficiency before restoring normal operation.



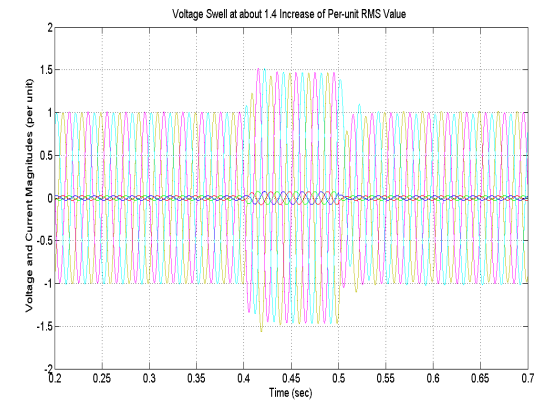
(a) Voltage at 0.6 per-unit decrease of RMS



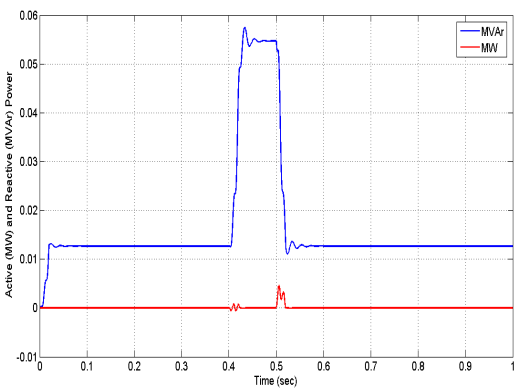
(b) Power exchange at the PCC



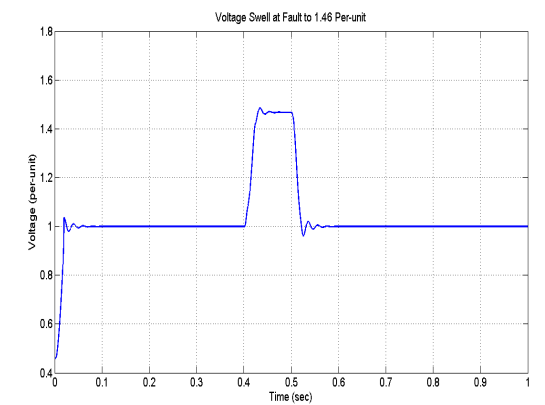
(c) Voltage drop due to sag



(d) Voltage at 1.4 per-unit increase of RMS

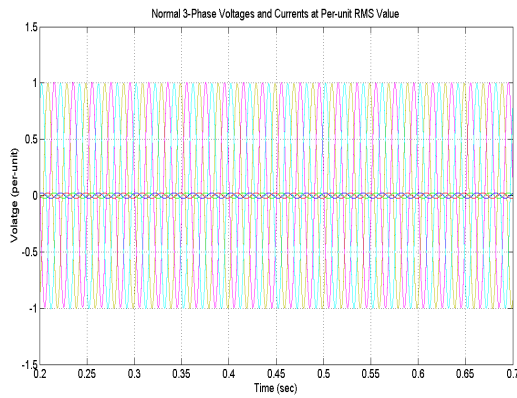


(e) Power exchange at PCC during swell

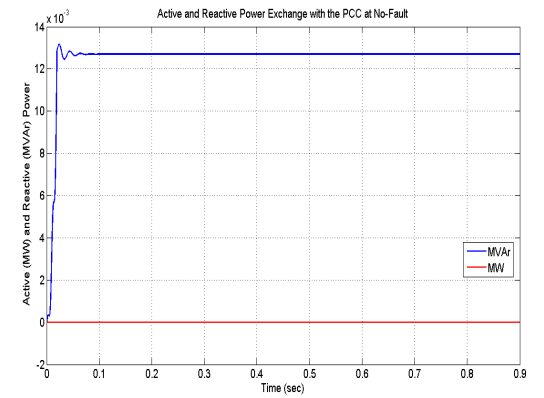


(f) Voltage growth due to swell

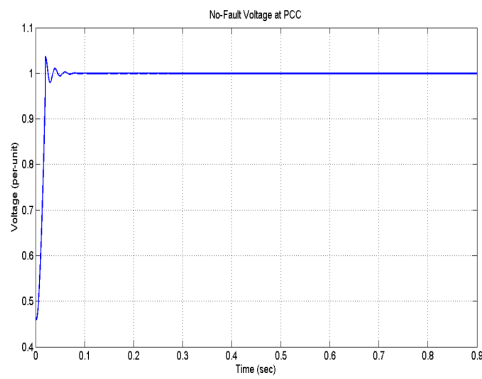
Figure 5.46: Mitigation of voltage sag/swell



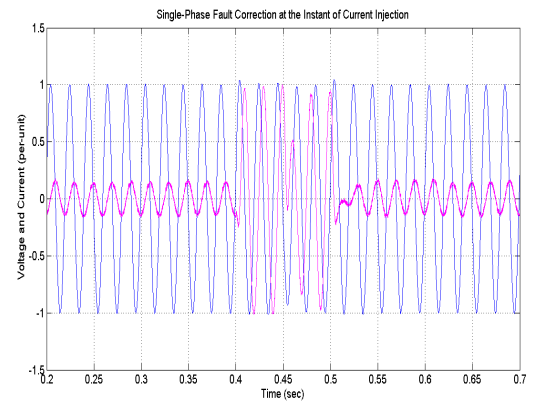
(a) Normal Quantities at No-Fault Condition



(b) Power exchange at the PCC



(c) No-fault voltage at the PCC



(d) Current injection

Figure 5.47: Normal Operating Conditions

5.8.4 Harmonics Control

Grid harmonics control has frequently been offered by passive (series LC) filters and DSTATCOMs often referred to as active shunt filters when used for the purpose. Since passive filters tend to provide current harmonics with low impedance paths, the application of the DSTATCOM as an active shunt filter would serve in absorbing and disallowing the harmonics flowing back to the source. Thus, giving DSTATCOM an edge over the passive filtering which so much depends on the wavering distribution and load structures. Hence, the DSTATCOM employed here is expected to neutralise the harmonic content of the feeder involved by injecting reactive current in phase with the harmonics induced by the load current in accordance with the level allowed in IEEE Std. 519 – 1992 (IEEE 1993). Refer to subsection 6.2.6 for a comparison of all my design paradigms in terms of total voltage harmonic reduction.

5.9 Considerations for Practical Implementations

Most of my designs presented in the previous chapters and this one alike, were implemented in Matlab/Simulink environment. The capabilities of this environment can be extended to real-time workshop to automatically generate *C* or *C(++)* codes from Simulink for executing continuous and discrete-time models directly on a vast range of computer applications. The Real-Time Workshop in Simulink can provide the design engineer with the following practical capabilities with details available from (MathWorks 2009a):

- As a rapid prototyping tool, it enables designs implementation quickly without resort to manual coding and debugging. Thereby originating graphical Simulink blocks and automatically generating the codes needed for control implementation and other dynamic algorithms.
- Embedded real-time control, once a Simulink system design has been designed accomplished, the code for real-time controllers can be generated, and linked ready to be downloaded onto the selected target processor. The Real-Time Workshop supports lots of commercial hardwares, embedded controllers and microprocessor boards.
- Real-time simulation code can be created and executed for an entire system or specified subsystems for hardware-in-the-loop simulations. Typical applications include training simulators (pilot-in-the-loop), real-time model validation, and testing.

- Stand-alone simulation can be run directly on a host machine or transferred to other systems for remote execution. Because time histories are saved in Matlab as binary or ASCII files, they can be easily loaded into Matlab for additional analysis or graphic display. In conclusion, Real-Time Workshop provides a comprehensive set of features and capabilities that provides the flexibility to address a broad range of applications. Refer to (Zhang 2008) for details.

5.10 Summary

This chapter presented a novel model-free predictive controller for direct online application for DSTATCOM as a smart solution to power quality (PQ) problems. The new scheme is built upon operating principles of the traditional model-based predictive (MPC) control which is intended to be deployed as a supervisory controller. Clear exploration was made of its advantages over existing controllers as an advanced control methodology with safety and constraints handling ability with regards the way it was grossly under-utilised by the academic community. Consequently, an extensive study of the dynamic behaviour of the MPC was first carried out. Particularly, the tuning effects of some specific parameters were initially established to guide my new design and the ways these influence the design process. These comprise of weights, filter coefficients, and horizons.

The chapter also utilises the power of an a-priori non-gradient simplex algorithm for its simplicity and search rapidity to implement the online model-free template. The nonlinearity of the DSTATCOM prior to this, was re-enforced through a saturation describing function which locates the limit cycles needed in real time stability analysis.

Resultant simulations from the design model were then performed and compared against PI, PD, EA-FPD as well as conventional MPC, in which the new MFPC proved superior by offering a control effort of 0.0045 radians for a 220 volt step change shown in subsection 6.2.2. A SimPowerSystem model was finally developed in order to check the practical validity of the new technique. Four power quality cases were hypothesised and treated. In each case my method set a time record standing to be broken. For example, total harmonic reduction (THD) was achieved at its record lowest of 0.04% and 0.05% from respective methods (see chapter 6. Thereby almost reproducing the original fundamental signal. Other cases treated include flicker and voltage sag/swell mitigation, which were also shown to be effectively controlled.

Chapter 6

Comparison and Discussions

6.1 Methods and Schemes Studied

This chapter discusses and compares the results of all the control methodologies advanced in the previous chapters in terms of their performances such as, setpoint following, rise time, as well as overshoots. The automated evolutionary FPD scheme is particularly verified to perform better than its manual counterpart. In this chapter, a comparison of the performance of the chosen index with other measures of merit has also been presented. In which the correlations between time and frequency domain functions of the error and the error derivative inputs are graphically established. The superiority of my novel MFPC technique is graphically demonstrated and supported with tabular arguments. Its performance in the simulation (SimPowerSystems) model with respect to harmonics reduction has been compared to other control paradigms. The MFPC routine is tested in simulink for the steady state operation where it is compared to other designs in closed-loop path of a nonlinear DSTATCOM. Responses from the PI, PD, FPD, MPC and MFPC schemes are presented. The plots clearly show the extent to which overshoots and oscillations manifest in other controllers have been swiftly labelled by the new model-free method. The scheme portrays a highly competitive trend in terms of response speed and settling time in addition to overshoot elimination ability. The new scheme has also provided a smooth transition to voltage growth from lower to higher level, a trend suitable for incorporation as a self-healing mechanism in the smart distribution grid. It can also be observed from the Figures that the constraints and safety margins have been significantly respected by the new MFPC.

6.2 Analysis of Results

6.2.1 Automatic FPD Vs. Manual FPD

Figures 6.1 and 6.2 were obtained after running the FT3PAK algorithm. The total time taken by the simulation was 12 seconds, starting from 14 : 21 : 10; ending at 14 : 21 : 22 as shown below:

tisim = 12-Apr-2012 14 : 21 : 10

tfsim = 12-Apr-2012 14 : 21 : 22

It is interesting to note the remarkable improvement provided by the automatic regime interms of rise-time and response time (bandwidth) when compared to the manual scheme. Referencing Figure 6.1 as interpreted in the results of Table 6.1, the automatic regime offers a speed of 1ms at 2ms rise-time to stabilise a 220 feeder voltage through switching angle input change of 0.0046 radians. Comparatively, the manual regime achieves the same level at a slower response (2ms), higher rise-time of 4ms, and with a strenuous control effort which is noted to overly react by initially reaching a maximum of 0.00562 radians for about 0.065 seconds before finally settling at 0.004619 radians, as shown in Figure 6.2. This is as a result of the transient dynamics in the manual scheme manifest in Figure 6.1, that occurred during the rise time. The consequence of a high switching angle is excessive system heating due to harmonics which releases more carbon into the atmosphere. However, the trend has been ameliorated through automation as a good stride for real-time control because the level of carbon foot-print so produced due to switching action in the converter is reasonably slashed harmoniously with the smart grid requirement of “green energy”.

6.2.2 MFPC Vs. Other Controllers

To further demonstrate the fitness of the new MFPC, Figure 6.3 compares the control efforts that produced the responses in Figure 6.6 from all four controllers. The PI, PD, and FPD schemes had to exert a control effort of 0.0046 radians to achieve the same response of 220 volts as compared to 0.0045 radians from the MFPC technique. This result is founded on a nonlinear model with capacitance, inductance and resistance values as initially specified. A sharper contrast could be achieved with changing model conditions with these parameters being robustly varied as was seen in subsection 4.5.2, where a much smaller effort could be attained to derive the same output value in the MFPC. Notice the discrete nature of the PD and FPD signals biting at precisely 0.0046

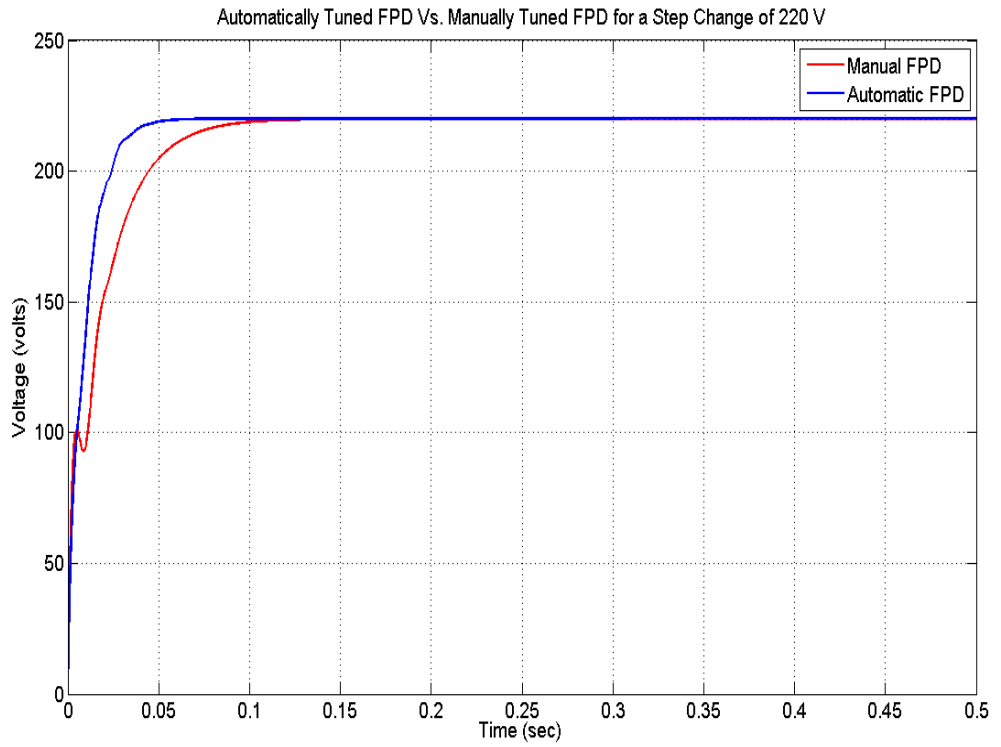


Figure 6.1: Automatic vs manual FPD tuning

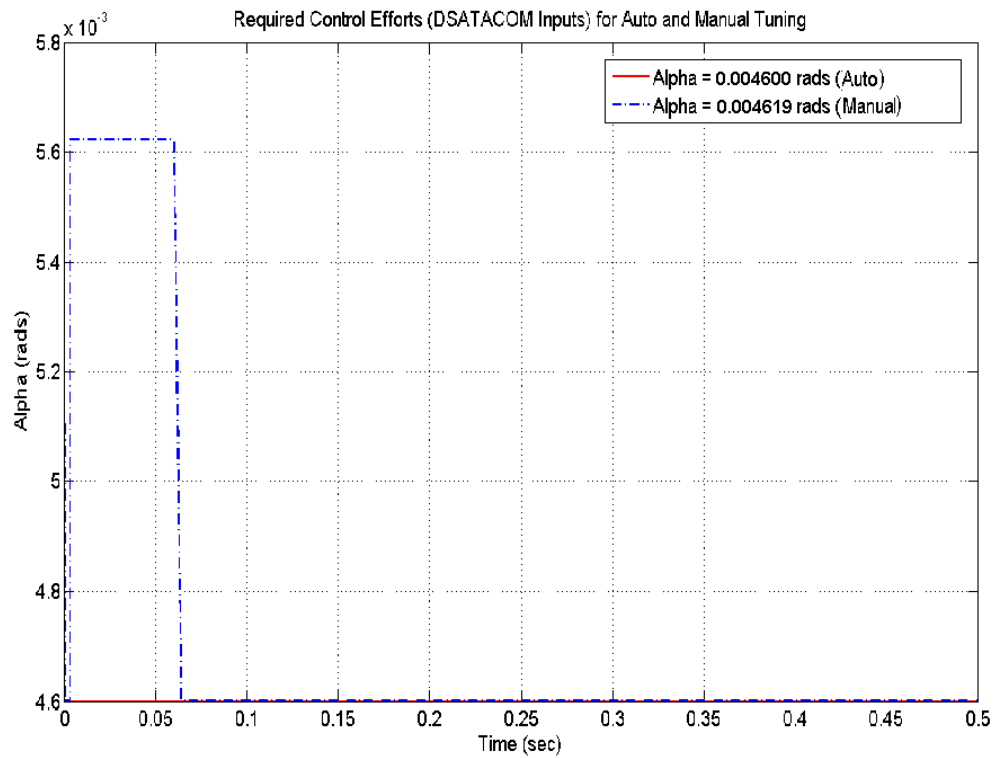


Figure 6.2: Required control inputs

radians and rose to 0.0058 and back again according to the transients of the response before reaching steady state at 0.0046 radians. However, the PI signal initially bit at 0.0058 radians and continued for 0.033 seconds before settling at 0.0046 radians. The dark blue line is an interpolation stance during fuzzy inference, a closer look would reveal the discrete signal properly. On the other hand, the MFPC signal started from 0.0145 radians at time $t = 0$ due its predictive nature while “looking ahead”, and discretely going through the transients, sampled at 0.002 before eventually settling at 0.0045 radians.

Table 6.1: Evolutionary MFPC Vs. Other DSTATCOM Control Techniques

Regime	T_r (s)	α (rads)	V (volts)	Q (MVA_r)
MFPC	0.001	0.004500	220	± 0.025
MPC	0.001	0.004528	220	± 0.025
Auto-FPD	0.002	0.004600	220	± 0.025
Manual-FPD	0.0022	0.004619	220	± 0.025
PI	0.0031	0.004600	220	± 0.025
PD	0.0022	0.004600	220	± 0.025
PureWave (PI)	0.005	0.005000	220	± 0.025
Hitachi (PI)	0.004	0.004812	220	± 0.025

It was found out that the speed offered by the new MFPC algorithm is way faster at 1 second as against the simulation speed of the CA_{tuo}D algorithm in subsection 6.2.1. The date and the timing are as recorded below. This is a clear confirmation of the superiority of this scheme which was already verified in Table 6.1 through dynamic system’s responses.

tisim = 18-May-2012 20 : 02 : 09

tfsim = 18-May-2012 20 : 02 : 10

To further verify the quality of the new MFPC, I compared its response to the conventional MPC using the same predictive and control horizons while keeping the filter coefficients to [0.5 0.05], respectively. The responses to step changes are shown in Figure 6.5 with constraints applied to each controller, where the conventional MPC showed a faster trend from the initial condition before it collapses during the 3rd cycle envisaging a voltage drop of about 155 volts before it rises up again. The new MFPC at that moment is noted to be steadily gaining momentum until settling after half cycle, while the MPC is still struggling with manifest ripples to settle after about one-and-a-half cycles. The trend has been better demonstrated in Figure 6.6 with a

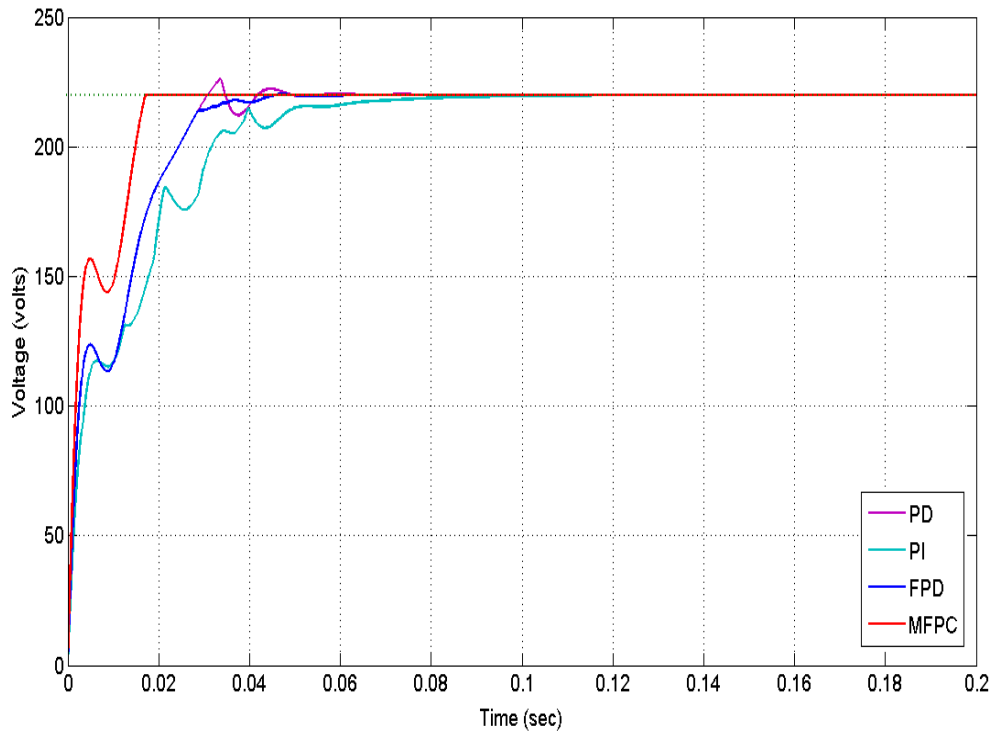


Figure 6.3: Nonlinear responses to step change

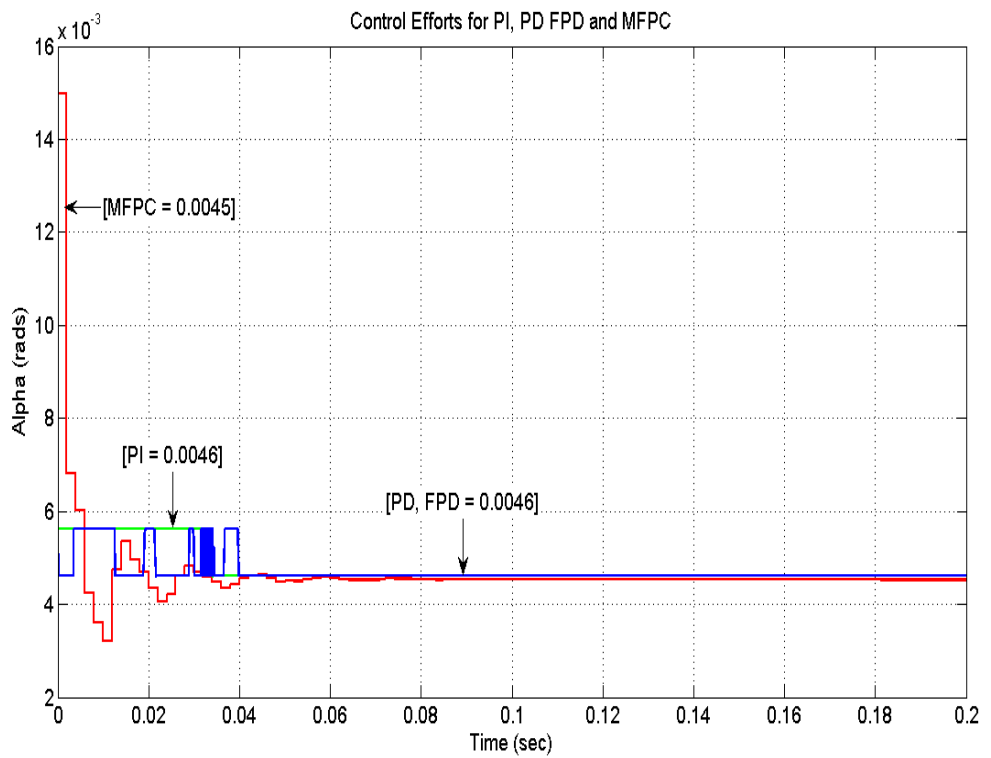


Figure 6.4: Step change in alpha

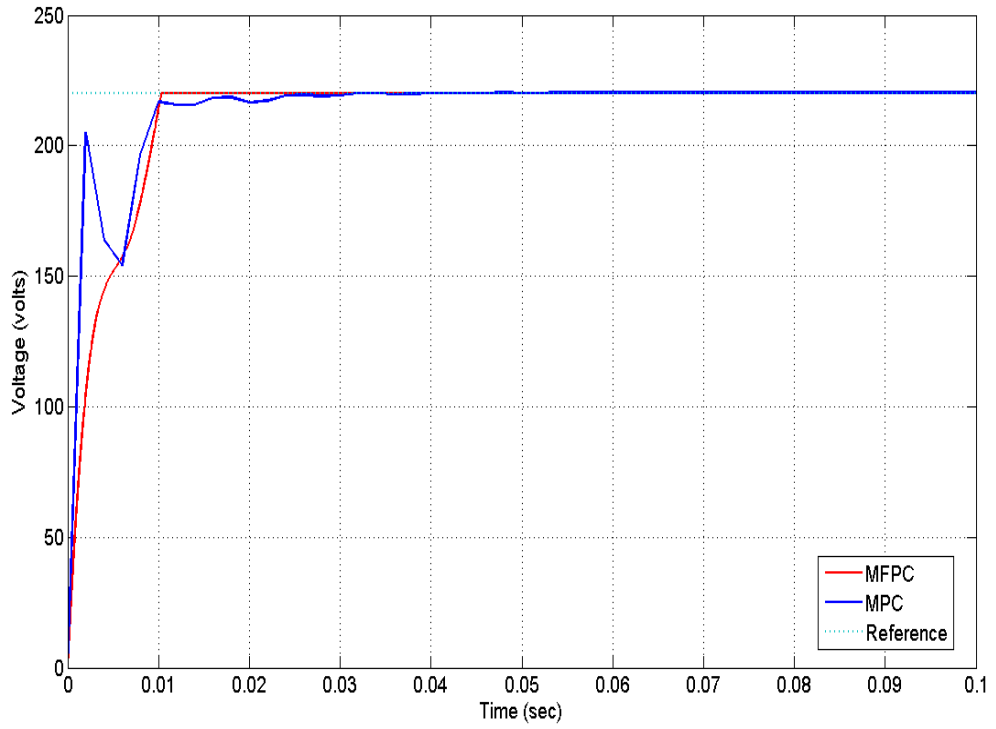


Figure 6.5: Responses to step change

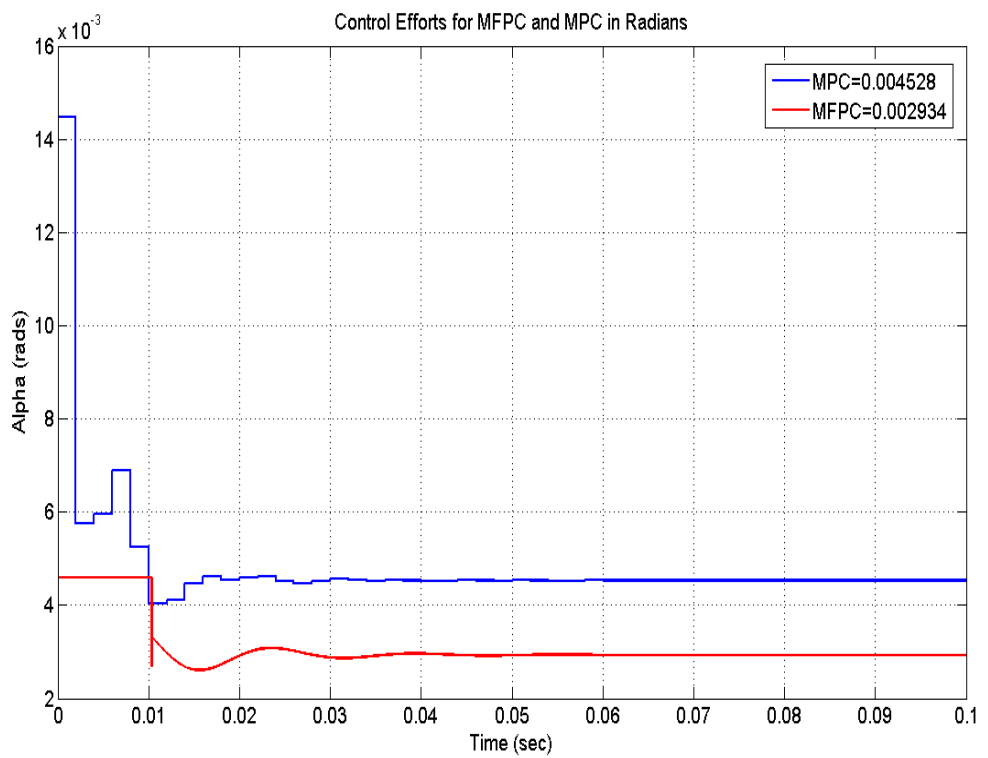


Figure 6.6: Step change in alpha

very much lesser control effort (0.002934) radians in the case of the MFPC against the (0.004528) radians taken by the MPC. It should be noted here that the MFPC can perform better than (0.004500) radians already recorded in Table 6.1, depending on the design strategy adopted, which is still way better than the MPC.

6.2.3 Self-Healing Property of MFPC Vs. MPC

One of the unique and most interesting feature of the MPC which has been inherited by the new MFPC is the look-ahead property. When the controller is operated respectively using prediction and control horizons of 20 and 2 in both unconstrained MFPC and MPC designs. The new MFPC automatically exhibits this mode and anticipates faults while they occur and provide predicted response to mitigate them. Figure 6.7 demonstrates this phenomenon during a step change due to a stalled voltage drop of 120 volts from initial condition, which is required to be raised to its nominal value of 220 volts. The drop condition persisted for about 2.5 cycles, until 5.2ms when prediction started and lasted for another 3 cycles (until 12ms) before restoration is achieved. Note the continuous nature of the transition swiftly incrementing the quantity against the discrete reference quantity. The exerted control effort also took about 2.5 cycles to implement this change from 0.0025 to 0.00456 radians as depicted in Figure 6.8. The same response from the MPC scheme is shown in Figure 6.9. The figure is seen to generate overshoot and ringing inhibited by delay characteristic which is evident in the prediction (look-ahead) loop. The prediction loop which in itself causes further sag to the magnitude is liable to cause considerable damage to the consumer equipment before mitigation. It took 3 cycles to occur and followed somewhat the same discrete change in the reference quantity to rise. The control effort responsible for this change shown in Figure 6.10 took several turns to arrive at its required value of 0.0046 radians for stabilisation. It can be said that the new MFPC is thus more suitable for self-healing smart distribution grid application in retrospect to providing lasting power quality solutions.

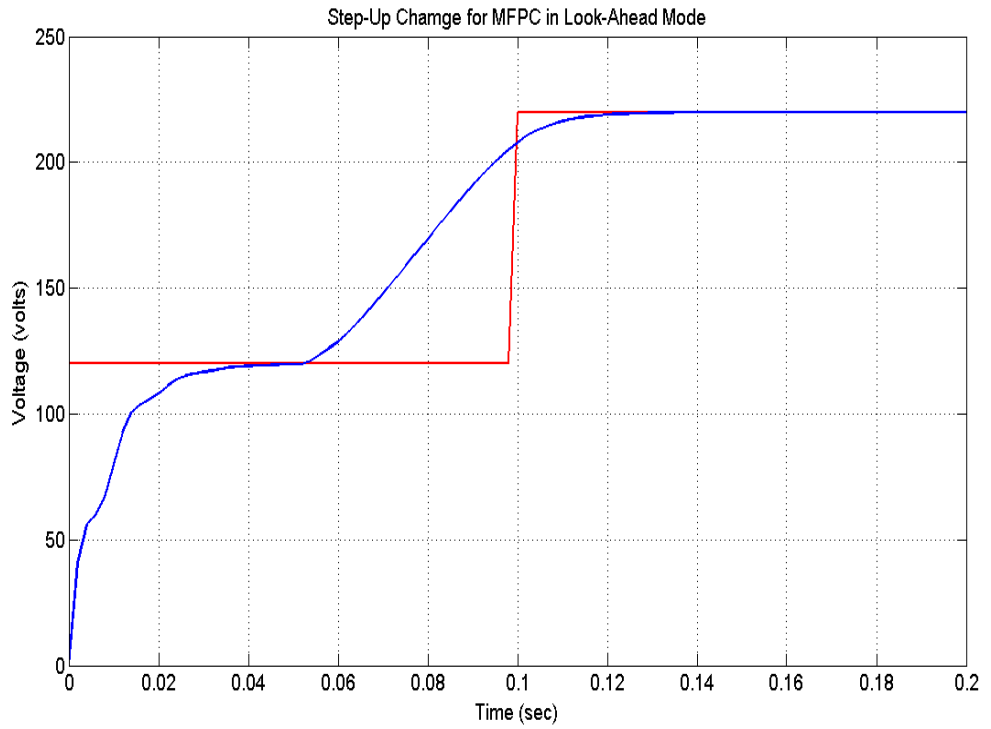


Figure 6.7: MFPC in look-ahead mode

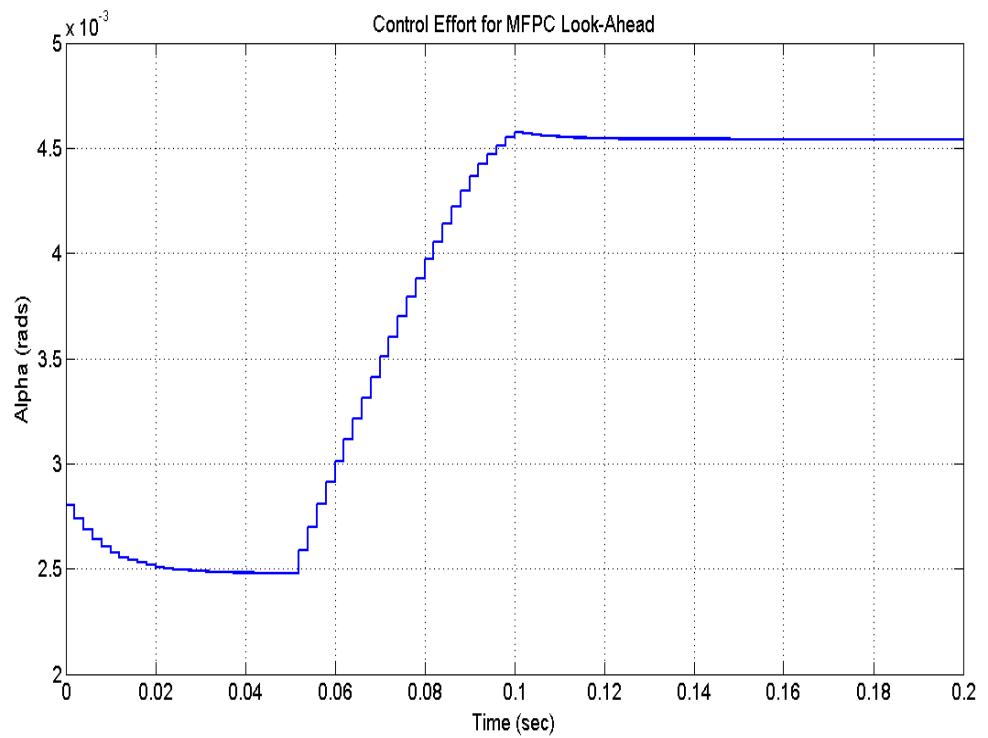


Figure 6.8: Control effort for MFPC look-ahead

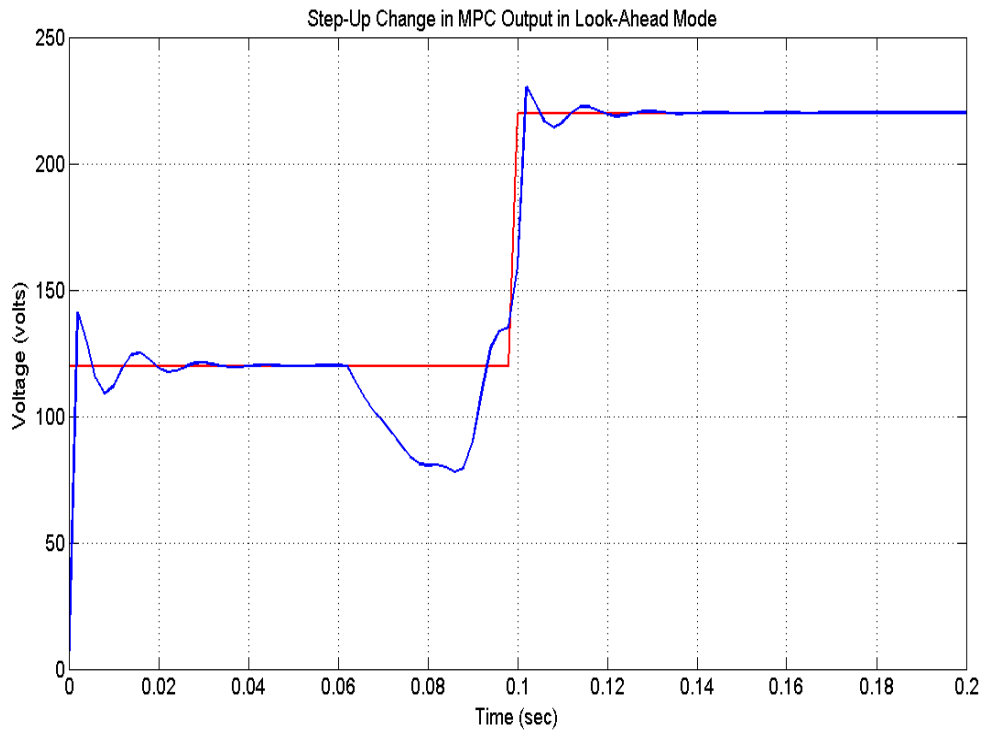


Figure 6.9: MPC in look-ahead mode

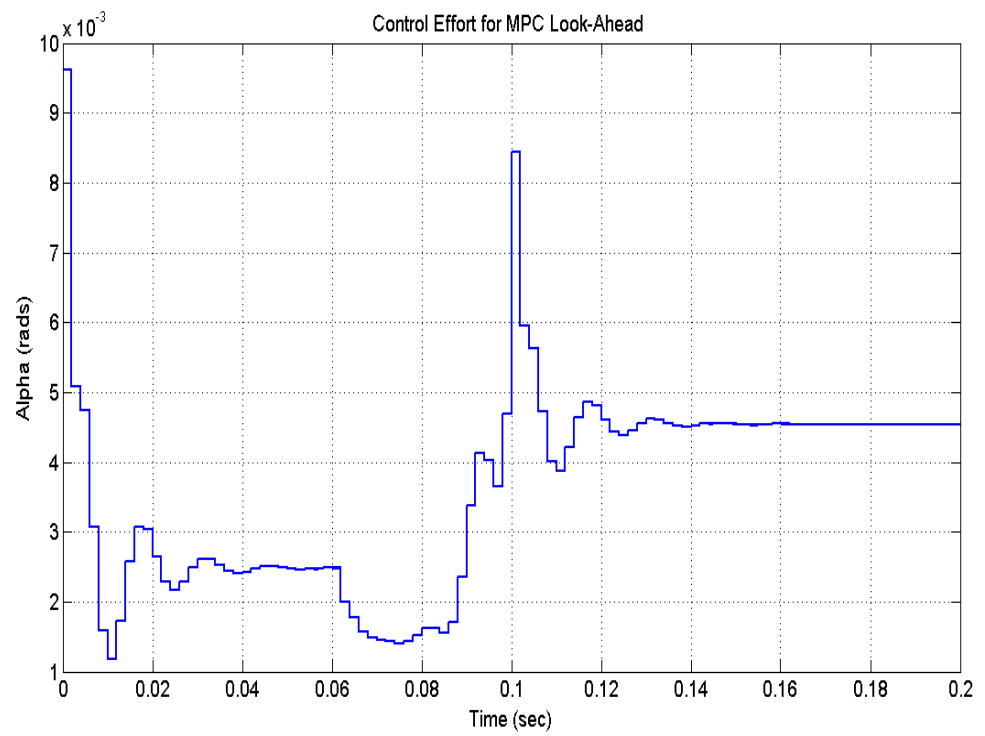


Figure 6.10: Control effort for MPC look-ahead

6.2.4 Gradient Vs. Non-Gradient Optimisers

A number of methods are available for solving optimisation problems (Bukata 2010). Table 6.2 presents the performances of the objective function subjected to different solvers as per Eq. 4.25. The correlation made here compares between the gradient methods and my novel non-gradient solver. In this context, the solution that gives the minimum value of the switching objective is the “best solution”. Recall that I upgraded the choice of my performance index for the CAutoD beyond the literature defined indices, and introduced a derivative error term in subsection 4.6.4 to ITSE, which I confirmed once again in Table 6.2 to be the best. The same index has been used to generate the results that follow in Figures 6.11 to 6.16 from which the Table is developed.

Table 6.2: Gradient Vs. Non-gradient Solvers

S/No	Search Method	f(x)	FeV
1	Pattern Search	-0.0046	136
2	Threshold Acceptance	10.9867	1019
3	Simulated Annealing	-0.0046	1325
4	Simplex	-0.0046	69
5	Simple GA	-0.0046	1620
6	EA	0	3031

The Table shows an interesting trend of the results obtained from the solvers. The value of the objective function “f(x)” i.e., the minimum solution ($\alpha = -0.0046$) during the first half negative cycle I expected was arrived at by most solvers, with fastest being the simplex algorithm having a function evaluation of 69 shown in Figure 6.11. Followed by pattern search (Figure 6.13), simulated annealing (Figure 6.14) and simple GA in Figure 6.15 all of which evaluated at 136, 1325 and 1620, respectively. It is interesting also to note that the simple GA has had higher cost as it was bound to stuck at local minima during the search as demonstrated in the Figure. Disparagingly, the worst solution was found by threshold acceptance algorithm which failed to converge despite its high cost of 1019 function evaluations as in Figure 6.16. However, the EA demonstrates its search power as indicated earlier by arriving at the global minimum 0 at 3031 function evaluations depicted in Figure 6.12. The high number of function evaluations explains its unsuitability in real-time application for having to take as long as 12 seconds to solve the problem. This research is of the opinion of adopting the simplex algorithm for locating the local minimum without any obvious snag at the highest possible speed and lowest cost.

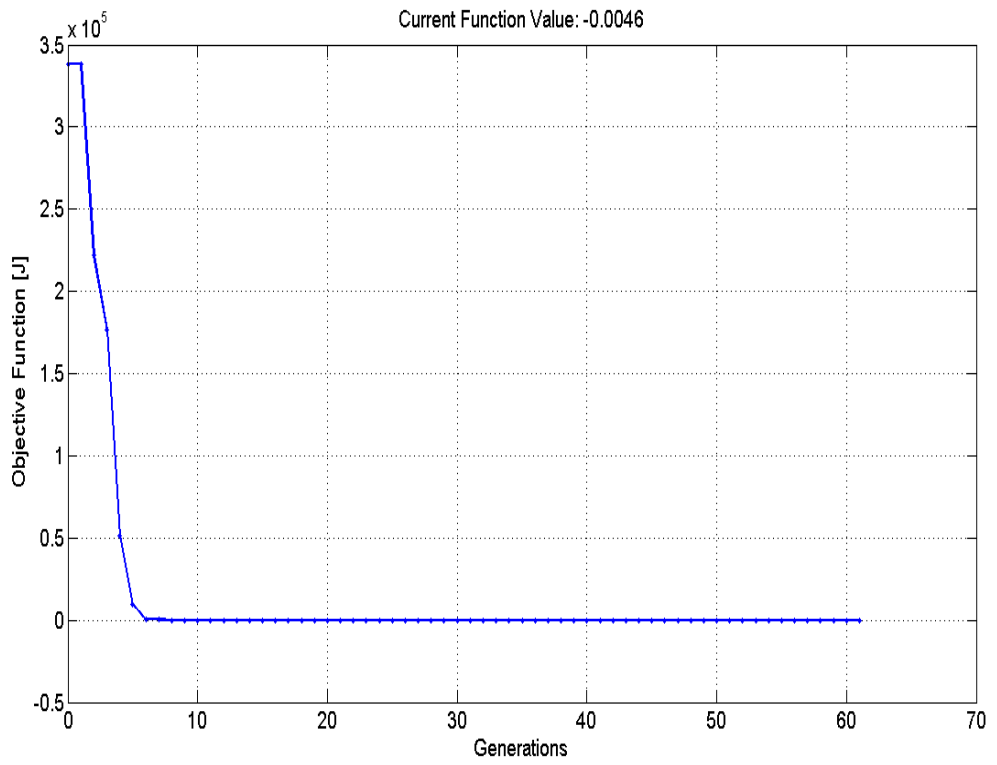


Figure 6.11: Simplex cost function

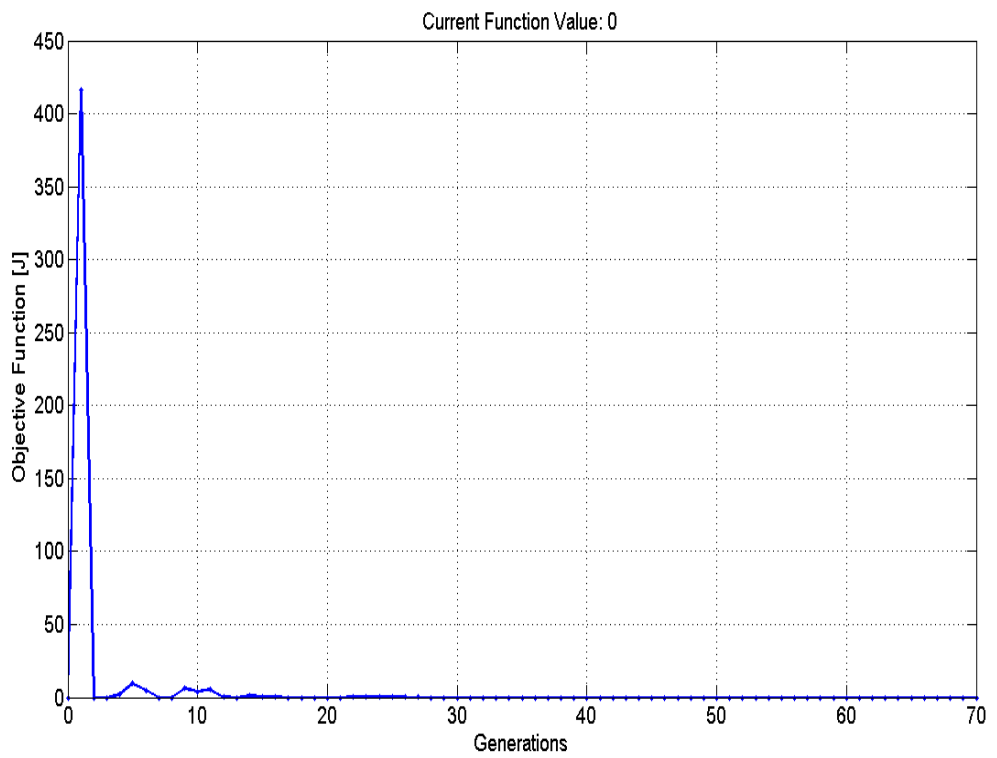


Figure 6.12: CAutoD cost function

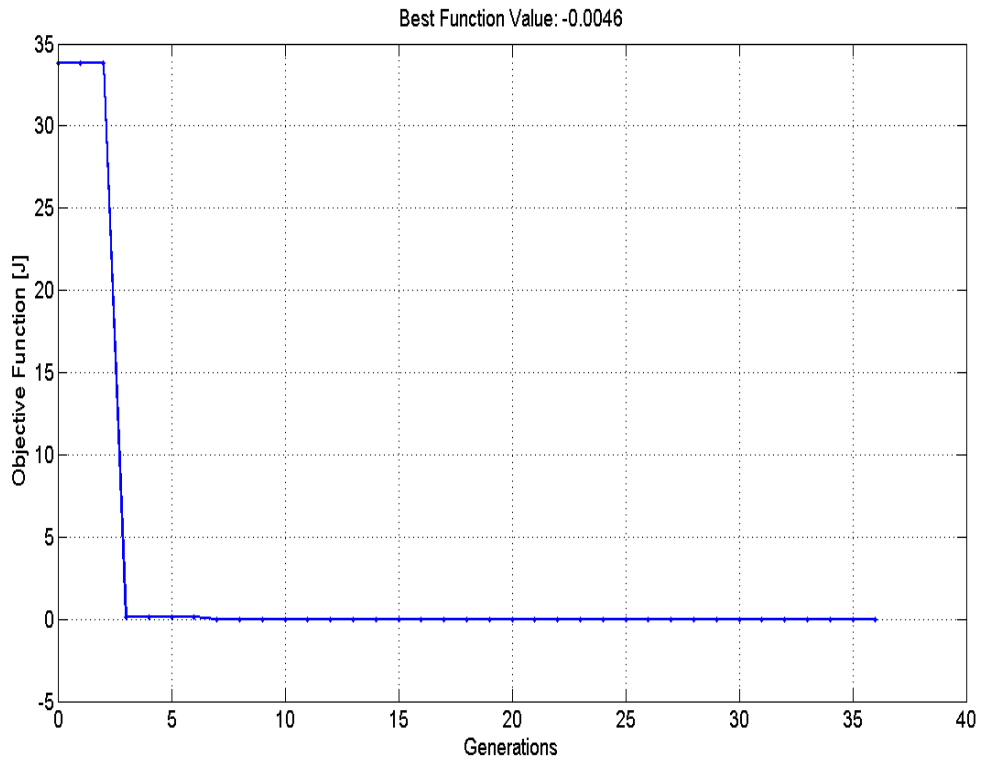


Figure 6.13: Pattern-search cost function

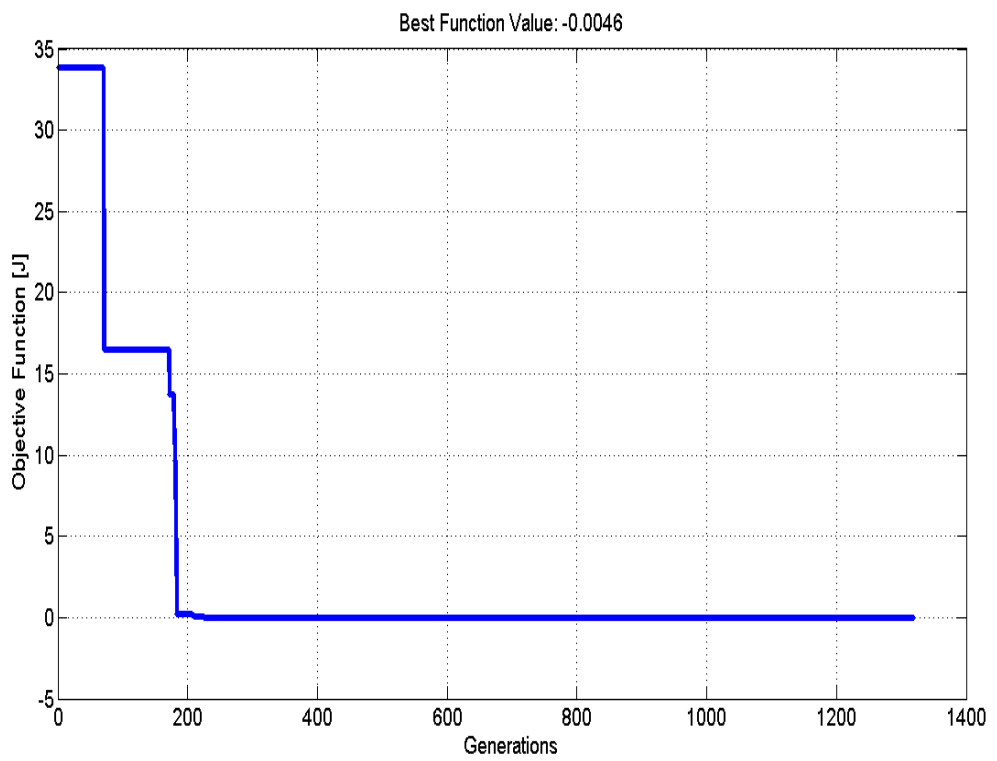


Figure 6.14: Simulated-annealing cost function

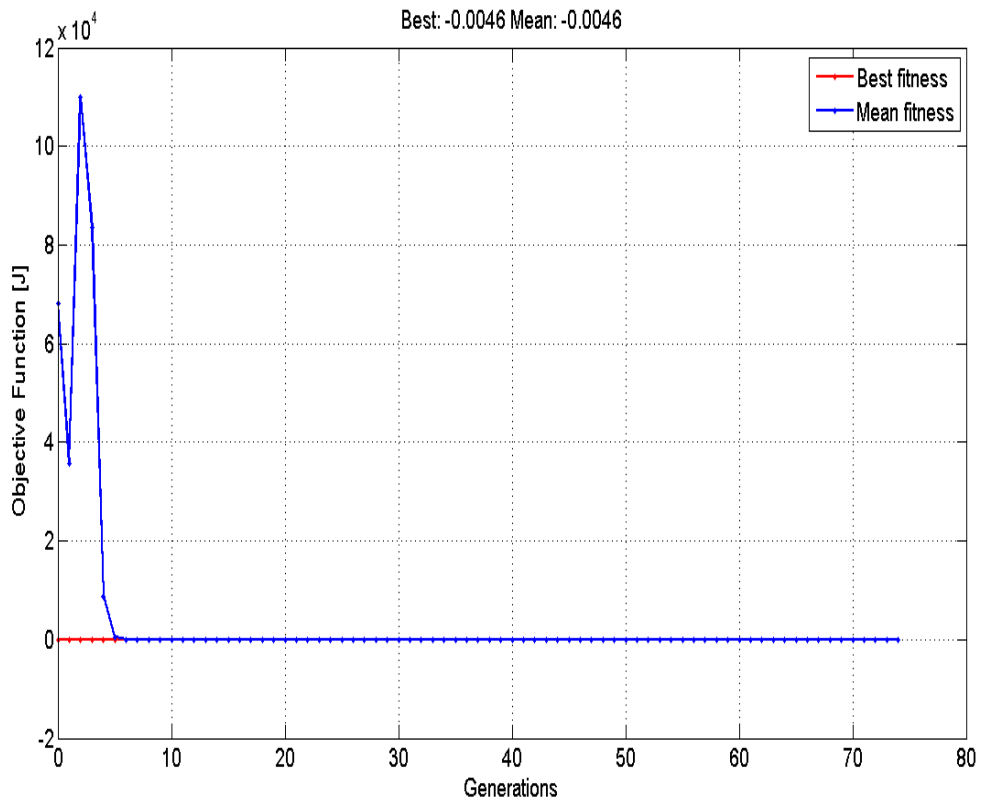


Figure 6.15: Simple GA cost function

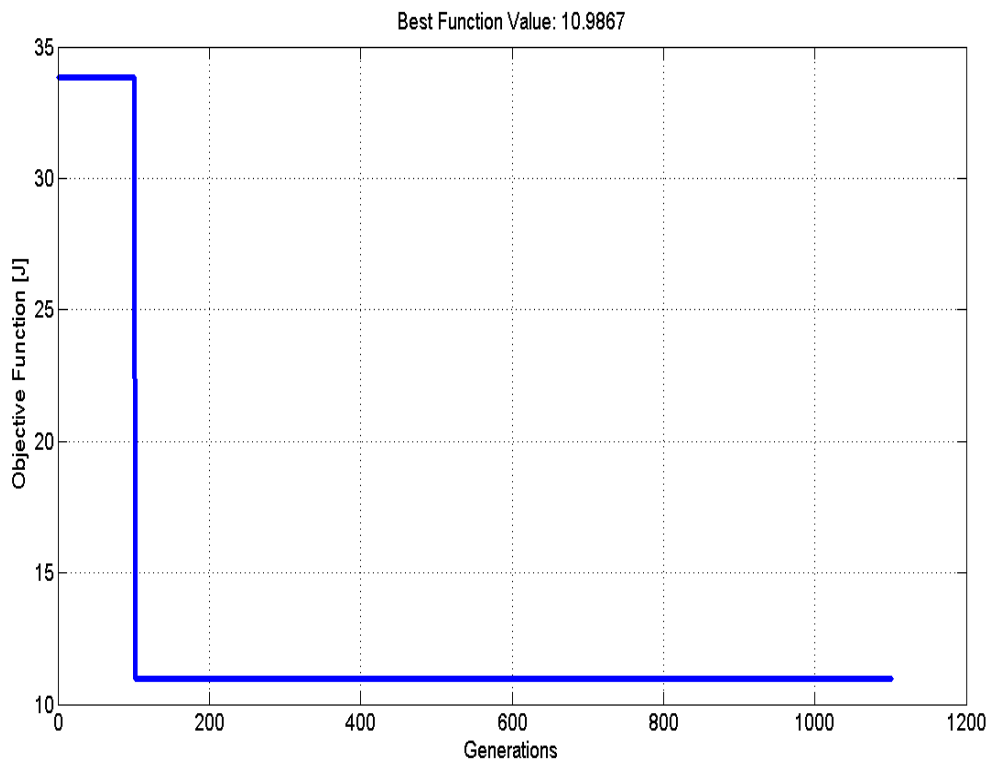


Figure 6.16: Threshold-acceptance cost function

6.2.5 Performance Decision Criteria

The 3-D plots shown in Figures 6.17 to 6.21 compared the various performance indices I investigated as a matter of decision criteria. I offered to choose a derivative enhanced ITSE in subsection 4.6.4 as a broad index for my design applications. This has been demonstrated in Figure 6.17, where the minimisation and maximisation criteria are both depicted as being complete when compared to the performances of ISE and ISTSE in Figures 6.18 and 6.19. The deficiencies from these indices are manifest following a vividly accomplished minimisation criteria, where the maximised function failed to reach its unit value, portraying irregular finishing as in an “erupted volcanic surface”. Conversely, Figures 6.20 and 6.21 showing respective representation of both IAE and ITAE indices comparing even woefully in both criteria, where the minimisation envelope could not be established, with failings in the maximisation function ending in a “comb structure” or “flattened” surface. These surfaces are a good representation of poor system stability, and hence unsuitable for stable control formulations. A summary of this comparison is given in Table 6.3.

Table 6.3: Summary of index performances

P/I	Sensitivity	Minimisation	Maximisation	Applicability
ITSE	$1.751e - 009$	Satisfactorily	Satisfactorily	Suitable
ISE	$-3.42e - 006$	Satisfactorily	Unsatisfactorily	Unsuitable
ISTSE	$-5.39e - 005$	Satisfactorily	Unsatisfactorily	Unsuitable
IAE	$2.251e - 007$	Unsatisfactorily	Unsatisfactorily	Unsuitable
ITAE	$3.002e - 008$	Unsatisfactorily	Unsatisfactorily	Unsuitable

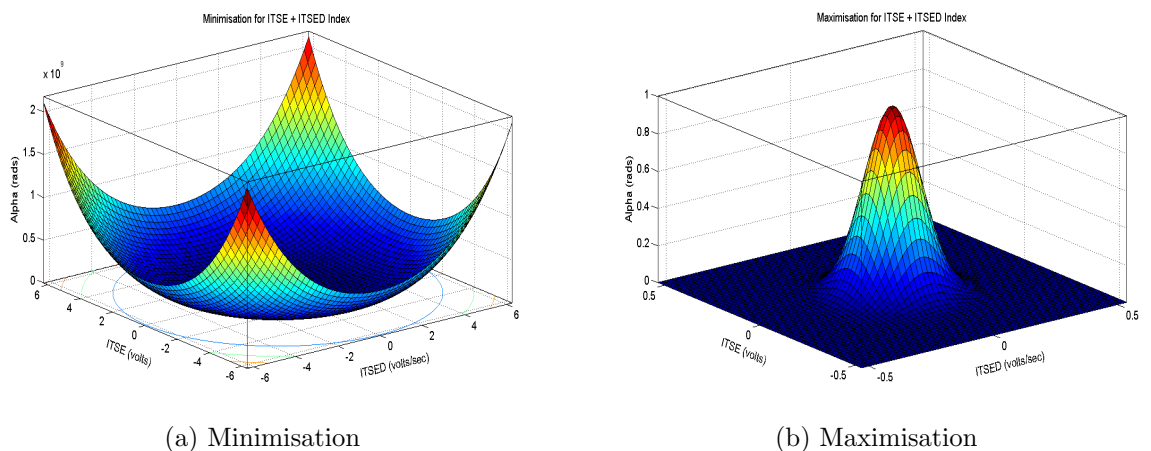
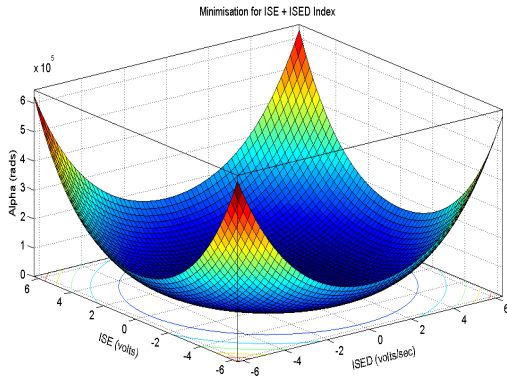
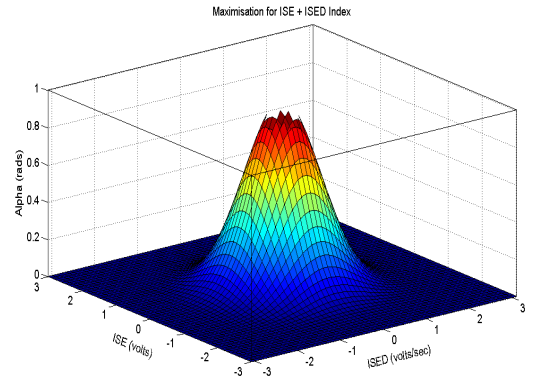


Figure 6.17: ITSE + ITSED performance

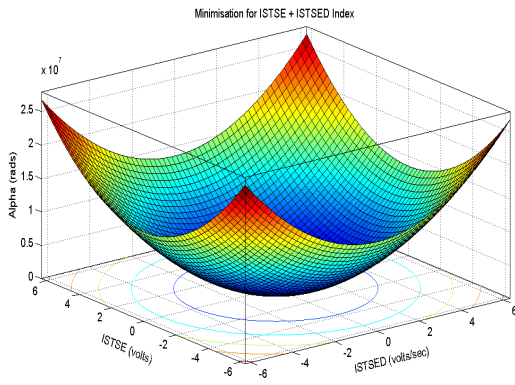


(a) Minimisation

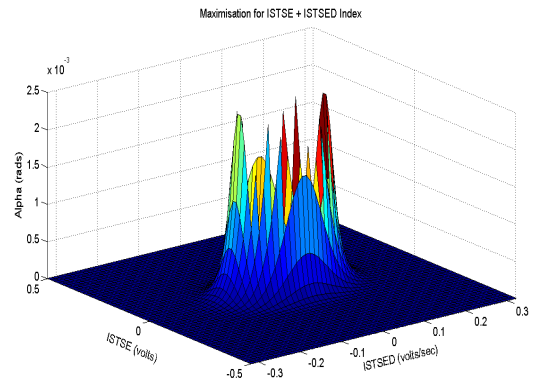


(b) Maximisation

Figure 6.18: ISE + ISED performance

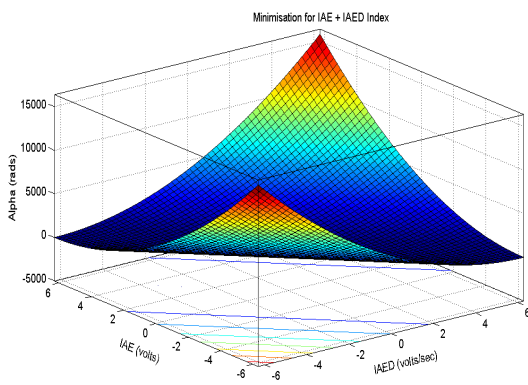


(a) Minimisation

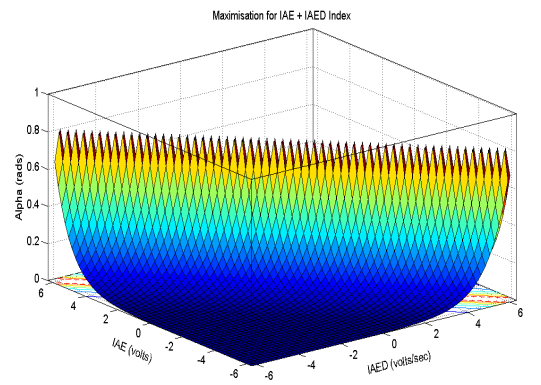


(b) Maximisation

Figure 6.19: ISTSE + ISTSED performance

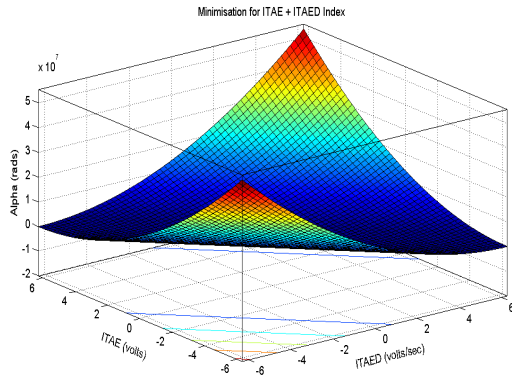


(a) Minimisation

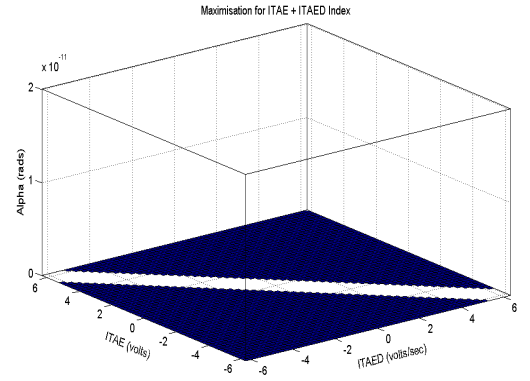


(b) Maximisation

Figure 6.20: IAE + IAED performance

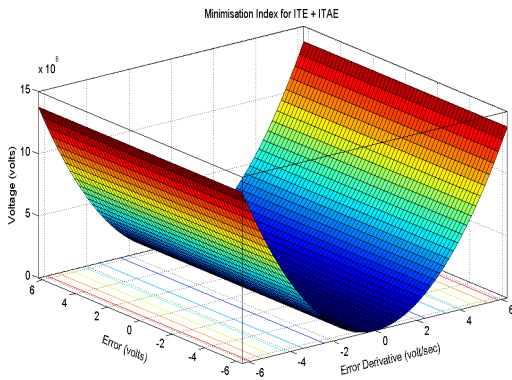


(a) Minimisation

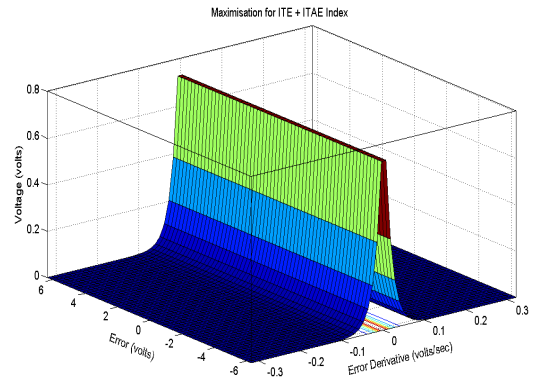


(b) Maximisation

Figure 6.21: ITAE + ITAED performance

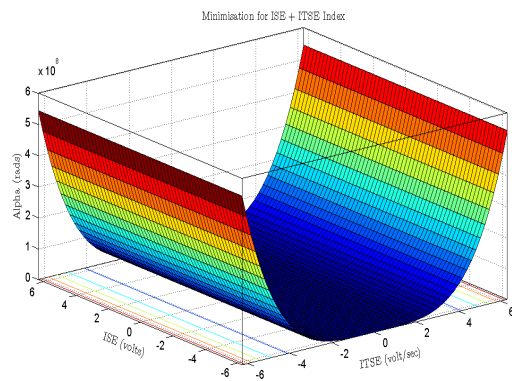


(a) Minimisation criteria

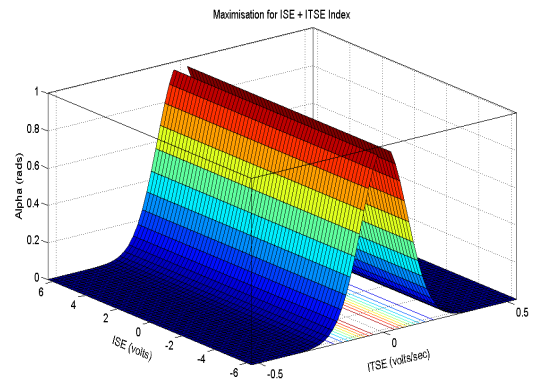


(b) Maximisation criteria

Figure 6.22: Time domain correlation of:
 e and \dot{e} with respect to α



(a) Minimisation criteria



(b) Maximisation criteria

Figure 6.23: Frequency domain correlation of:
 e and \dot{e} with respect to α

Similarly, I compared the viability of using either time or frequency domain methods for this design as shown in Figures 6.22 and 6.23. It is noticed from the Figures that both methods are feasible and I adopted the use of the combined ITSE index in this work for better results. In the frequency domain alone, the designer has the advantage of taking control over the system's bandwidth and certain measure of the system's response to unwanted noise and disturbances. While, adding the time domain builds-up the missing link between frequency response and a corresponding transient response needed to practically ease tuning through chosen design criteria.

6.2.6 Harmonics Reduction

The Figures 6.24 to 6.27 demonstrate the level of harmonic cancelation achieved by the various control strategies investigated here using the nonlinear DSTATCOM simulation model described above. It can be observed that the traditionally applied PI controller is the worst case with THD reduction of 4.66%. This follows a closed-loop analysis of a signal in the 3rd cycle when the system has fully attained its steady-state in all cases. The fundamental signal based on 50Hz with a dc component approaching zero is described in Figure 6.27. Using the same model, my novel MFPC scheme offers the best compensation as in Figure 6.24 with the THD reduction of 0.04%, almost replicating the fundamental. The second best showing a similar trend is produced by the EA-FPD scheme shown in Figure 6.25 yielding THD of 0.05%. On the hand, the improved conventional PD has also shown a much better prospect than the ubiquitous PI with a THD reduction of 1.63% as depicted in Figure and 6.26. Further comparison with an experimentally controlled PCC voltage using three-and-five level converters, which realised THD reduction of 1.6% and 0.5% from (Sensarma & Ramanarayanan 2000), still proves the efficiency of my novel solution via the evolutionary methods. Further comparison to an agent-based control for power quality enhancement in highly distributed generation networks from (Pachanapan et al. 2009), which yielded THD of 1.7 and 0.5 respectively is another support to my claim. The THD reduction of 0.04% and 0.05% from each evolutionary technique respectively achieved here has sufficiently satisfied the 5% standard requirement of the IEEE.

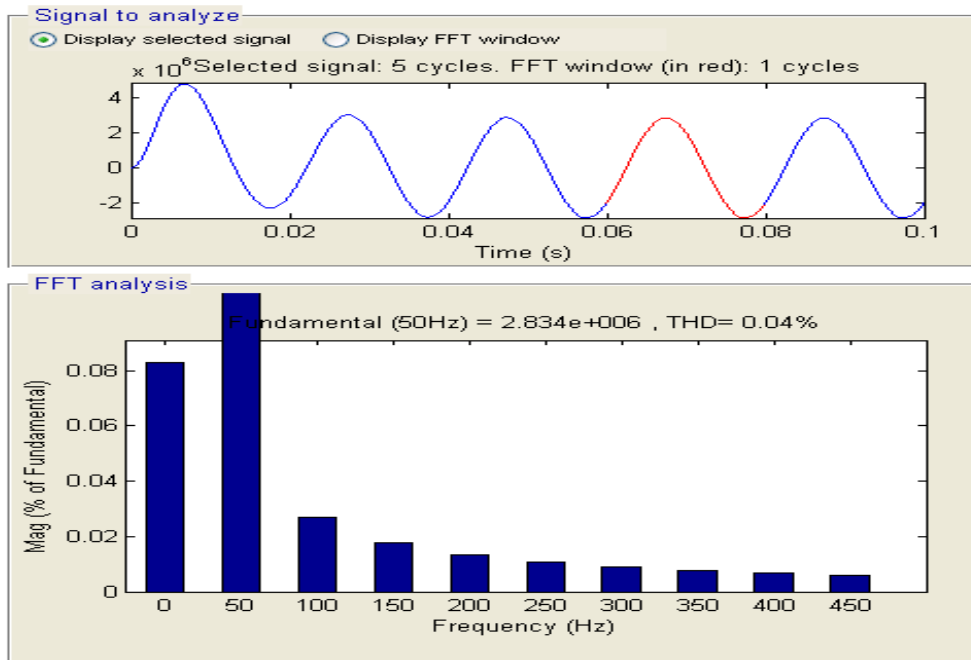


Figure 6.24: MFPC compensated
THD = 0.04%

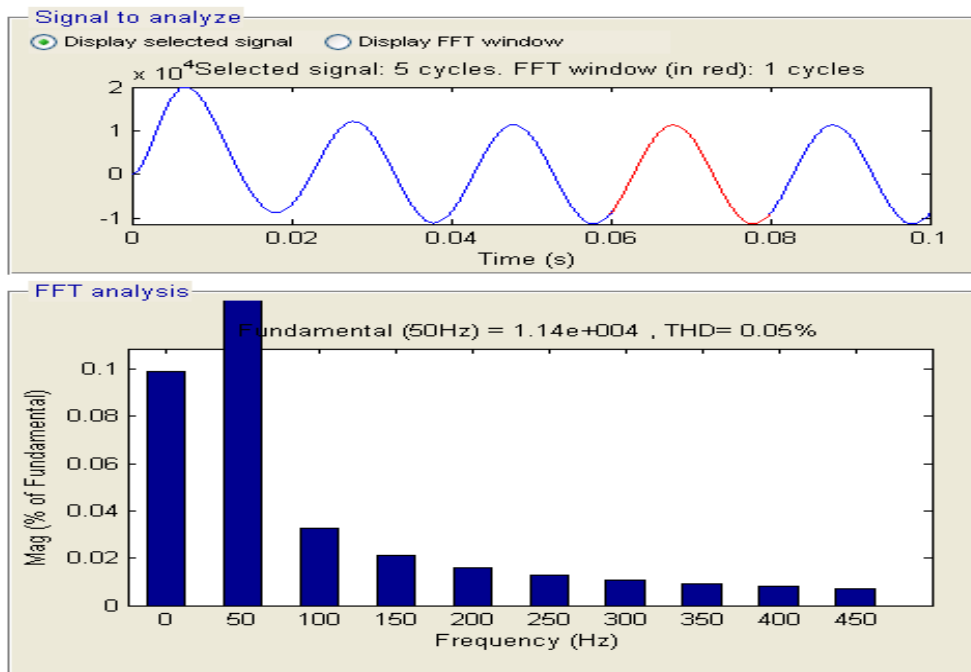


Figure 6.25: EA-FPD Compensated
THD = 0.05%

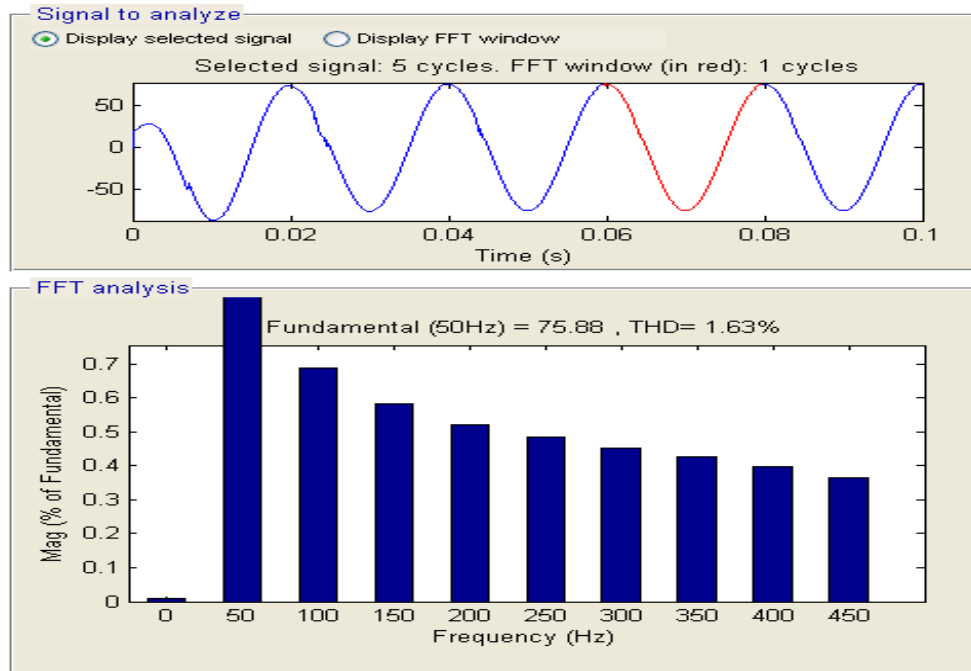


Figure 6.26: PD Compensated
THD = 1.63%

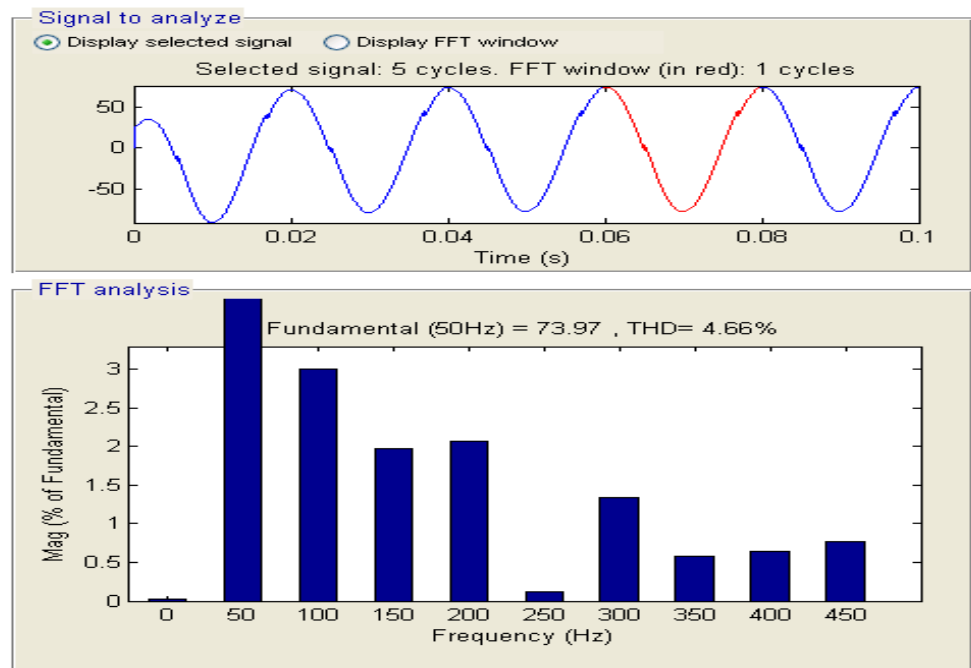


Figure 6.27: PI Compensated
THD = 4.66%

6.3 Summary

This chapter compares all the control methodologies advanced in the previous chapters in terms of their performances, such as setpoint following, rise time, and over-shoots. The automated evolutionary FPD scheme is particularly verified to perform better than its manual counterpart. The performance of the new MFPC routine against the MPC, FPD, PD and PI controllers in closed-loop, has proven to offer a faster and non-overshoot response which was produced with a lesser control effort. The self-healing effect of the new MFPC regime has also been compared with its MPC counterpart. This comparison has effectively been presented graphically as well as in tabular argument. The performance of the chosen index in relation to other measures of merit has also been established here, and graphically presented to support the reason for my choice. Correlations made between time and frequency domain functions of the error and the error-derivative inputs were also presented indicating the possibility of using either function for the system analysis. Later in the chapter, the superiority of the novel MFPC via the simulation (SimPowerSystems) model with respect to harmonics reduction has been compared to other control paradigms. By way of checking the effectiveness of the used simplex optimiser in the new MFPC, the optimisation criteria of the algorithm based on a chosen ITSE performance index was also compared with other optimisers such as pattern search, simulated annealing, simple GA, etc. And the new method arrived at the best solution (minima) at a remarkable speed with only 69 evaluated functions. Respective plots were generated to clearly show the extent to which overshoots and oscillations manifest in other controllers have been swiftly levelled by the new model-free method while respecting constraints and safety margins simultaneously.

Chapter 7

Conclusion and Future Work

7.1 Reconstruction of Enhanced DSTATCOM Controllers

This thesis has first synthesised a PI controller for DSTATCOMs using Draous model. A number of traditional tuning methods have been studied for the application, including Zeigler-Nichols and PIDeasy rules, for investigating the dynamic characteristics of the plant. To inform tuning, an initial open-loop first-order-plus-delay-time (FOPDT) model validation has been performed within a range of operating points. A closed-loop synthesis of a PD controller has then been performed towards understanding the effect of re-routing the filter coefficient in a feedforward path rather than in the customary feedback path. From this, a new value for the filter coefficient ($\rho = 11$) is established as compared to the value $\rho = 10$, previously discovered by (Ang 2005). Determining this coefficient is significant in eliminating amplification of noise from the output signal by the derivative term. As a result of the re-routing process, remarkable improvement in the systems dynamic response and stability are achieved. Since the output is independent of the plants feedback in this case, the system becomes free from oscillations subject to feedback.

For verifications, various tests have been conducted using different filter coefficients and control parameters in order to arrive at the linear PD controller that best suits the design needs. The effects of all three PID terms were individually checked as well as in groups (i.e., P, PI, and PD), so as to properly investigate their loop recovery efforts in the advent of system disturbances and also to generate PD control parameters for use with the design of a fuzzy logic controller.

7.2 Manual Computer-Aided Design for FPD Systems

In the process of designing an intelligent controller for DSTATCOM, the previously designed linear PD controller with its inherent parameters has been used to form a fuzzy PD structure. A simplified three rule-based structure is concatenated to develop a three-by-three input-output mapping based on the Macvicar-Whelan matrix. As a nonlinear controller, the FPD has been tested against a number of scenarios both in linear and nonlinear DSTATCOM models with uncertainties. The performance from each model has been shown to be promising. The effects of parametric tuning, including the scaling factor tuning, have also been studied to inform further designs.

7.3 CAutoD for PQ Control System Design

The manual FPD design technique has been extended to a CAutoD process based on evolutionary computation. Essentially, the FPD parameters are assessed by genetic tuning with the a-posteriori search mechanism of the EA. The best FPD parameter set is evolved in a manner akin to biological evolution. The resultant controller has the ability to enhance the systems robustness, too.

For practical control applications, the automation suite has been based upon a performance index comprising a number of figures of merit, including the ITSE and, its derivative ITSED. The automated scheme performs much better than the manual computer-aided-design process and yields controllers of an improved response speed and settling time. However, the design time of 12 seconds will make it deficient in real time for practical PQ solutions, if the controller needs to be adaptive in real time. Therefore, a faster solution to PQ problems has been proposed in Chapter 5.

7.4 Evolving MFPC for PQ Control System Design

To reduce the computational loading due to model presence in an online routine for solving PQ problems, a novel model-free predictive controller has been developed, using an a-priori simplex algorithm, as such a deterministic algorithm works faster while requiring no gradient information. In order to reduce the effect of nonlinearities from the model-free design, the DSTATCOM has been wired with an augmented saturation

describing function that locates the presence of limit circles and suppresses them. The same performance index (ITSE) as in Chapter 4. has been used. The steady state performance of the deterministic MFPC proves far superior to the nondeterministic evolutionary design if CAutoD is carried out online, with the control signal generation time down to fraction of a second. Further, the constraints and safety margin design issues which constitute a major MPC advantage, have notably been adhered to without violation.

A SimPowerSystems software simulation model has also been developed to check experimental validity of the designs. Where specific PQ problems such as harmonics distortion, voltage swells, voltage sags and flicker have been solved. Although these problems have been tackled using other conventional means in the past, the radical improvement offered by the model-free design achieved in this thesis is obvious. Noticeable respective record levels of THD reduction of 0.04% and 0.05% have also been achieved, almost reproducing the original fundamental input signal. It is therefore safe at this point to recommend to the industry the implementation of this model-free predictive control scheme at the distribution level. As the distribution system metamorphoses into decentralised smart grid featuring connectivity of virtual power plants mostly through power electronic converters, e.g., DSTATCOM, it stands to benefit from the full Volt-VAR automated controllability of the MFPCs low control rate.

Its practical implementation is possible via real-time workshop to automatically generate C or C++ codes from Simulink for executing continuous and discrete time models directly on a vast range of computer applications as briefly introduced in section 5.9. Its overall wired closed-loop structure with the DSTATCOM would offer advantages over its PID and SVC counterparts in terms of reduced hardware size, footprint (space occupation), almost maintenance free as it is model-free (and automated), where pickling the controller timers and model contingencies are unnecessary as would be with the PID or SVC controllers. Additionally, as a predictive entity it suppresses violation of the input and output limits and maintains accurate levels (no-overshoots) of the control (manipulated) and controlled variables with minimum human intervention throughout the operational period. More importantly, the scheme performs the aforementioned control functions robustly at a high speed in the range of $0.005 \rightarrow 0.01$ seconds, as time $t \Rightarrow \infty$. This is high enough to capture and deal with any ensuing PQ problem as it emanates due to changes in customers load and system disturbances from environmentally friendly, but less grid-friendly, renewable generators.

7.5 Future Perspectives

7.5.1 Single-Layered Neuro-Model-Free Predictive Control

Intelligence can be added to the MFPC through the power of a single-layered neuron network to counter the difficulty found in neural multi-layer backpropagation method. Influence of the gradient descent analysis on energy surfaces produced by weight spaces during training can readily be converted from its sluggish divergent criteria. This fact is supported by (Feng 2000), in which report carries it that neural control applications may outperform optimised linear and nonlinear controllers in plants with rate limits. As such may improve on the control effort of 0.003020 radians realised in one of my cases in chapter 5, which means faster response to capture PQ problems.

7.5.2 Fault Tolerant Fuzzy-Prediction in DSTATCOM

A fault tolerant scheme may be designed from the combination of the human type reasoning ability of fuzzy logic and the predictive ability of the model-free technique. This algorithm should be ideally applied to smart grid architecture where faults and fault locations could be spontaneously recognised and cleared before they result into a PQ problem. The scheme should be embedded in smart measuring devices and sensors for tracking and providing feedback about signal conditioning in real-time. Realising this would adorn the smart grid with all its features mentioned in Section 1.1.

References

- Acha, E. & Anaya-Lara, O. (2002), ‘Modeling and analysis of custom power systems by pscad/emtdc’, *IEEE Transactions on Power delivery* **17**(1), 266 – 272.
- AlRashidi, M. R. & El-Hawary, M. E. (2009), ‘A survey of particle swarm optimisation applications in electric power systems’, *IEEE Transactions on Evolutionary Computation*, Vol. 13, No. 4, August 2009, pp. 913-918. **13**, 913–918.
- Alvas da Silva, A. P. (2002), Applications of evolutionary computation in electric power system, in ‘Proceedings of the 2002 Congress on Evolutionary Computation, CEC02’, pp. 1057–1062.
- Amin, S. M. & Wollenberg, B. F. (2005), ‘Toward a smart grid: Power delivery for the 21st century’, *IEEE Power and Energy Magazine* **3**(5), 34–41.
- Ang, K. H. (2005), Evolutionary Learning & Global Search for Multi-Optimal PID Tuning Rules, PhD thesis, School of Engineering, University of Glasgow.
- Bajpai, R. S. & Gupta, R. (2008), Voltage and power flow control of grid connected wind generation system using dstatcom, in ‘Power and Energy Society General Meeting Conversion and Delivery of Electrical Energy in the 21st Century’, pp. 1–6.
- Bano, V., Ramirez, A. & Juan, M. (2010), ‘Dstatcom regulation by a fuzzy segmented pi controller’, *Electric Power Systems Research* **707-715**(6), 707–715.
- Bansal, R. C. (2003), ‘Bibliography on the fuzzy set theory applications in power systems (1994 - 2001)’, *IEEE Transactions on Power Systems* **18**(4), 1291 – 1299.
- Banzhaf, W. (2000), *Genetic Programming and Evolvable Machines*, Kluwer Academic Publishers.
- Barry, T. & Wang, L. (2004), A model-free predictive controller with laguerre polynomials, in ‘5th Asian Control Conference’, Vol. 1, pp. 177–184.
- Bhende, M., Mishra, M. K. & Suryawanshi, H. M. (2006), ‘A dstatcom modelling, analysis and performance for unbalanced and non-linear load’, *Journal of the Institution of Engineers (India): Electrical Engineering Division* **86**, 297–304.

- Brown, R. E. (2008), Impact of smart grid on distribution system design, *in* 'Conversion and Delivery of Electrical Energy in the 21st Century', pp. 1–4.
- Bukata, B. B. (2010), Evolving optimal fuzzy logic control for power distribution systems. 2nd Year Ph.D Report.
- Bukata, B. B. & Li, Y. (2009), A new smart dstatcom for enhancing reactive power exchange and voltage support at the distribution level, *in* '15th International Conference on Automation and Computing (ICAC09)', pp. 52–57.
- Bukata, B. B. & Li, Y. (2011), Reviewing dstatcom for smart distribution grid applications in solving power quality problems, *in* '17th International Conference on Automation and Computing (ICAC11)', Proceedings of the 17th International Conference on Automation & Computing (ICAC11).
- Canale, M., Milanese, M. & Novara, C. (2006), 'Semi-active suspension control using fast model-predictive techniques', *IEEE Transactions on Control System Technology* **14**, 10341046.
- Chapman, D. (2001a), 'Introduction to voltage dips'. Accessed: 03/11/2009.
URL: <http://www.leonardo-energy.org/apguige>
- Chapman, D. (2001b), 'Power quality and utilisation guide section 5 - introduction'. Accessed: 03/11/2009.
URL: <http://www.copperinfo.co.uk/powerquality/downloads/pqug/51-voltage-dips.pdf>
- Cheong, F. & Lai, R. (2000), 'Constraining the obtimisation of a fuzzy logic controller using an enhanced genetic algorithm', *IEEE Transactions on Systems, Man and Cybernetics* **30**, 31 – 46.
- Chowdhury, M. (1998), Evolutionary and Reinforcement Fuzzy Control, PhD thesis, School of Engineering, University of Glasgow.
- Cleveland, W. S. & Devlin, S. J. (1988), 'Locally weighted regression: An approach to regression analysis by local fitting', *Journal of the American Statistical Association* **Vol. 83**(403), 596–610.
- Clune, J. & Lipson, H. (2011), Evolving three-dimensional objects with a generative encoding inspired by developmental biology, *in* 'Proceedings of the European Conference on Artificial Life'.
- Coteli, R., Dandil, B. & Fikret, A. (2011), 'Fuzzy-pi current controlled d-statcom', *University Journal of Science* **24**(1), 91–99.
- Deniz, E., Tuncer, S., Coteli, R., Ata, F., Dandil, B. & Gencoglu, M. T. (2010), Neuro-fuzzy current controller for three-level cascade inverter based d-statcom, *in*

- ‘Proceedings of the Universities Power Engineering Conference, 45th International Universities’ Power Engineering Conference, UPEC’.
- DoyleIII, F., Ogunnaike, B. A. & Pearson, R. K. (1995), ‘Nonlinear model-based control using second-order volterra models’, *Automatica* **31**(5), 697.
- Dugan, R. C., McGranaghan, M. F., Santoso, S. & Beaty, H. W. (2003), *Electrical Power Systems Quality*, 2nd edn, McGraw-Hill, 2003.
- Elnady, A. & Salama, M. M. A. (2005), ‘An efficient control technique for dstatcom used for voltage flicker mitigation’, *Electric Power Components and Systems* **33**, 233–246.
- Engineering, P. (2011), ‘Hitachi-heads-smart-grid-technology-trial’. Accessed: 27/02/2012.
- Fan, S., Ruixiang, M. & F. Shen, C. T. (2009), ‘Frequency dividing coordinated control method for dstatcom based on the limit values judgment’, *Automation of Electric Power Systems*, **33**(4), 67–71+91.
- Feng, W. (2000), Evolutionary Design Automation for Control Systems with Practical Constraints. A PhD Thesis Submitted to the School of Engineering, University of Glasgow, July 2000, pp14-33., Phd, School of Engineering, University of Glasgow.
- George, V. & Mishra, M. K. (2009), ‘Design and analysis of user-defined constant switching frequency current-control-based four-leg dstatcom’, *IEEE Transactions on Power Electronics* **24**(9), 2148–2158.
- Giroux, P., Gilbert, S. & Hoang, L. H. (2001), Modeling and simulation of distribution statcom using simulinks power system blockset, in ‘IECON01: The 27th Annual Conference of the IEEE Industrial Electronics Society’.
- Goldberg, D. E. (1989), *Genetic Algorithms in Search, Optimization and Machine Learning*, Addison-Wesley, Reading, MA.
- Goyal, S. (2008), A hybrid discontinuous voltage controller for dstatcom applications, in ‘IEEE Power and Energy Society General Meeting: Conversion and Delivery of Electrical Energy in the 21st Century, PES’.
- Herrera, F., Lozano, M. & Verdegay, J. L. (1995), ‘Tuning fuzzy logic controllers by genetic algorithms’, *International Journal of Approximate Reasoning* **12**, 299–315.
- Hingorani, N. G. (1991), Facts - flexible ac transmission systems, in ‘International Conference on AC and DC Power Transmission’, pp. 1–7.
- Homaifar, A. & McCormick, E. (1992), Full design of fuzzy controllers using genetic algorithms, in ‘Proc. SPIE Conf. on Neural and Stochastic methods in Image and Signal Processing’, Vol. 1766, pp. 393–404.

- Hornby, G. S. (2003), Generative representations for computer-automated design systems, Technical report, NASA Ames Research Center, Mail Stop 269-3, Moffett Field, CA 94035-1000.
- Hoyle, W. J. (1996), Fuzzy logic, control, and optimisation, Master's thesis, University of Canterbury.
- Hsu, J. C. & Meyer, A. U. (1968), *Modern Control Principles and Applications*, McGraw Hill.
- IEEE (1993), 'Ieee recommended practices and requirements for harmonic control in electric power systems'.
- Johnson, M. A. & Moradi, M. H. (2005), *PID Control, New Identification and Design Methods*, Springer-Verlag London Limited.
- Jouanne, A. V. (2001), 'Assessment of voltage unbalance', *IEEE Trans. Power Del.*, **16**(4), 782790.
- Jung, S. Y., Kim, T. H., Lee, M. U., Moon, I. S. & Kwon, W. H. (2003), Modeling and control of dstatcom for voltage sag, in 'Proceedings of the IASTED International Conference on Modelling, Simulation and Optimisation', pp. 108–113.
- Kadalia, Ramesh, Huang, B. & Rossiter, A. (2003), 'A data driven subspace approach to predictive controller design', *Control Engineering Practice* **11**, 261278.
- Kamentsky, L. A. & Liu, C.-N. (1963), 'Computer-automated design of multiformat print recognition logic', *IBM Journal of Research and Development* **7**(1), p. 2.
- Kanjilal, P. P. (1995), *Adaptive Prediction and Predictive Control*, 52, Peter Pregrinus Ltd.
- Karami, M. S., Heidar, A., Tapeh, A. G. & Bandari, S. (2008), Learning techniques to train neural networks as a state selector in direct power control of dstatcom for voltage flicker mitigation, in 'Proceedings of the International Conference on Information Technology: New Generations (ITNG)', pp. 967–974.
- Kashiwagi, H. & Li, Y. (2004), 'Nonparametric nonlinear model predictive control', *Korean Journal of Chemical Engineering* **21**(2), 329–337.
- Lagarias, J. C., Reeds, J. A., Wright, M. H. & Wright, P. E. (1998), 'Convergence properties of the nelder-mead simplex method in low dimensions', *SIAM Journal of Optimisation, Society for Industrial and Applied Mathematics* **9**(1), 112–147.
- Larsson, M. (2000), Coordinated Voltage Control in Electric Power Systems, PhD thesis, Lund University.

- Lawrynczuk, M. (2007), 'A family of model predictive control algorithm with artificial neural networks', *Int. J. Appl. Math. Comput. Sci.* **17**(2), 217232.
- Levine, W. S. (2011), *Control System Advanced Methods*, CRC Press Taylor & Francis Group.
- Li, Y. (1995), Modern information technology for control systems design and implementation, in 'Proc. 2nd. Asia-Pacific Conf. Control Systems Design and Measurement', ChongQing, China.
- Li, Y., Ang, K. H. & Chong, G. C. Y. (2006), 'Pid control system analysis and design', *IEEE Control Systems Magazine* **26**(1), 32–41.
- Li, Y., Ang, K. H., Chong, G. C. Y., Feng, W., Tan, K. C. & Kashiwagi, H. (2004), 'Cautocsd-evolutionary search and optimization enabled computer automated control system design', *International Journal of Automation and Computing* **1**, 83–95.
- Li, Y. & Häule, A. (1996), 'Artificial evolution of neural networks and its application to feedback control', *Artificial Intelligence in Engineering* **10**(2), 143–152.
- Maciejowski, J. M. (2002), *Predictive Control with Constraints*, Prentice Hall.
- MathWorks, I. (2009a), 'Simpowersystems block sets, user's guide'. Accessed: 10/10/2009.
- Ndubuka, N. M. (2011), 'Power quality enhancement of nigerian distribution systems by use of distribution static compensator (d-statcom)', *International Journal of Electrical and Power Engineering* **5**(1), 8–12.
- Ng, K. C. (1995), *Switching Control Systems and Their Design Automation via Genetic Algorithms*, Degree of philosophy, University of Glasgow.
- Ng, K. C. & Li, Y. (1994), Design of sophisticated fuzzy logic controllers using genetic algorithms, in 'Proceedings of the third IEEE Conference on Fuzzy Systems, IEEE World Conference on Computational Intelligence', pp. 1708–1712.
- Nikolaou, M. (2001), 'Model predictive controllers: A critical synthesis of theory and industrial needs', *Advances in Chemical Engineering* **v 26**, 131–204.
- Pachanapan, P., Anaya-Lara, O. & Lo, K. L. (2009), Agent-based control for power quality enhancement in highly distributed generation networks, in 'Proceedings of the 44th International, Universities Power Engineering Conference (UPEC)', pp. 1 – 5.
- Pal, Y. & Swarup, A. (2008), A review of comprehensive type custom power devices for power quality improvement, in 'Joint International Conference on Power System Technology POWERCON and IEEE Power India Conference', POWERCON, pp. 356–364.

- Partners, U. P. (2009), ‘Smart grid technology’. Accessed: 16/02/2010.
- Passino, K. M. (1998), *Fuzzy Control*, ADDISON-WESLEY LONGMAN, INC.
- Perez, B. B. (2008), A-posteriori model predictive control with a grey-box model and step-response data, Master’s thesis, University of Glasgow.
- Rashid, M. H. (2001), *Power Electronics Handbook*, 2nd edn, Academic Press Series in Engineering.
- Åström, K. J. & Hägglund, T. (1985), ‘Method and an apparatus in tuning pid regulator’.
- Åström, K. J. & Hägglund, T. (2001), ‘The future of pid control’, *Control Engineering Practice* **9**, 1163–1175.
- Ruixiang, F., An, L., Min, S. & Zhikang, S. (2009), Harmonic prediction control for time delay canceling and its realization in distribution static synchronous compensator, *in* ‘Proceedings of the WRI Global Congress on Intelligent Systems (GCIS)’, Vol. 3, pp. 56–60.
- Sanchez, P. R., Acha, E., Calderon, J. E. O., Feliu, V. & Cerrada, A. G. (2009), ‘A versatile control scheme for a dynamic voltage restorer for power-quality improvement’, *IEEE Transactions on Power Delivery* **24**(1), 277–284.
- Sannino, A., Svensson, J. & Larson, T. (2003), Power electronic solutions to power quality problems, *in* ‘Science Direct’, number 66, pp. 71–82.
- Selvan, P. & Anita, R. (2011), ‘Transient enhancement of real time system using statcom’, *European Journal of Scientific Research*, **52**, 359–365.
- Sensarma, P. S. & Ramanarayanan, V. (2000), ‘Analysis and performance evaluation of a distribution statcom for compensating voltage fluctuations’, *IEEE Transactions on Industrial Applications* **16**(2), 259 – 264.
- Singh, B., Adya, A., Mittal, A. P. & Gupta, J. R. P. (2006), ‘Modeling of dstatcom for distribution system’, *Int. J. Energy Technology and Policy* **4**(), 2428 – 2434.
- Singh, B., Adya, A., Mittal, A. P. & Gupta, J. R. P. (2008), Modeling, design and analysis of different controllers for dstatcom, *in* ‘Joint International Conference on Power System Technology POWERCON and IEEE Power India Conference, POWERCON’.
- Singh, B., Solanki, J. & Verma, V. (2005), Neural network based control of dstatcom with rating reduction for three-phase four-wire system, *in* ‘Proceedings of the International Conference on Power Electronics and Drive Systems’, Vol. 2, pp. 920–925.

- Srivastava, S., K.S. Preet and, D. J. S. & Gupta, M. (2009), Online estimation and control of voltage flicker using neural network, *in* 'IEEE Region 10 Annual International Conference, Proceedings/TENCON'.
- Stenman, A. (1999), Model-free predictive control, *in* 'Proceedings of the 38th IEEE Conference on Decision and Control', pp. 3712–3717.
- Tan, K. C. (1997), Evolutionary Methods for Modelling and Control of Linear and Nonlinear Systems, PhD thesis, University of Glasgow.
- Tang, C. (2011), 'Nonlinear control method of dstatcom', *Electric Power Automation Equipment*, v 31, n 3, p 18-22+23, March 2011. **31**, 18–22+23.
- Tewari, A. (2002), *Modern Control Design*, JOHN WILEY & SONS, LTD.
- Thakare, S. G., Dalvi, H. S. & Joshi, K. D. (2009), Statcom based fuzzy controller for grid connected wind generator, *in* 'Second International Conference on Emerging Trends in Engineering and Technology', pp. 35–39.
- Trulsson, E. & Ljung, L. (1985), 'Adaptive control based on explicit criterion minimization', *Automatica* **21**(4), 385–399.
- Ushio, T. (2002), 'Expectations for hybrid systems', *Systems, Control and Information* **46**(3), 105–109.
- Visioli, A. (2006), *Practical PID Control*, Springer-Verlag London Limited.
- Wang, Y. & Boyd, S. (2008), Fast model predictive control using online optimization, *in* 'Proceedings of the 17th World Congress the International Federation of Automatic Control', Seoul, Korea, pp. 6974–6979.
- Wenjin, D. (2010), 'Dstatcom inverse system pi controller', *Key Engineering Materials, Advanced Measurement and TestX*. **439-440**, 372–377.
- Xing-ping, M., Hui, W., Liang, Z. & Hong, Z. (2009), Controlling study of d-statcom based on reinforcement learning adaptive pid, *in* 'IEEE International Conference on Automation and Logistics, ICAL', pp. 1208–1211.
- Xu, Y., Yang, L., Ma, C., Gong, Z., Pu, H. & Zhang, Z. (2010), Study on sliding mode control with rbf network for dstatcom, *in* 'International Conference on E-Product E-Service and E-Entertainment (ICEEE)'.
- Xue, D., Chen, Y. Q. & Atherton, D. P. (2007), *Linear Feedback Control Analysis and Design with MATLAB*, SIAM (Society for Industrial and Applied Mathematics).
- Yang, X. P., Yan-Ru, W. & Yan, K. (2007), A novel control method for dstatcom using artificial neural network, *in* 'Proceedings of the IPEMC: CES/IEEE 5th International Power Electronics and Motion Control Conference', Vol. 3, pp. 1724–1727.

Zanma, T. & Asano, N. (2010), *Off-Line Model Predictive Control of DC-DC Converter Model Predictive Control*, Model Predictive Control, Sciyo Janeza Trdine 9, 51000 Rijeka, Croatia, chapter 12, pp. 269–282. Accessed on 27/09/2010.
URL: *www.sciyo.com*

Zhang, P. (2008), *Industrial Control Technology*, William Andrew.

Zhu, Q. F., L. Huang, Z. B. H. & Tang, J. (2009), The fuzzy pi control for the dstatcom based on the balance of instantaneous power, *in* '5th Emerging Intelligent Computing Technology and Applications', Vol. 5754 LNCS, pp. 794–803.

Zhuang, M. & Atherton, D. P. (1993), Automatic tuning of optimum pid controllers, *in* 'IEE Proceedings -D', Vol. 140.

Appendix A

1.1 Model of DSTATCOM

The DSTATCOM model utilised for my control design is adopted from Draou et al., (Rashid, 2001). Figure A.1 is subdivided into sections and evaluated as follows.

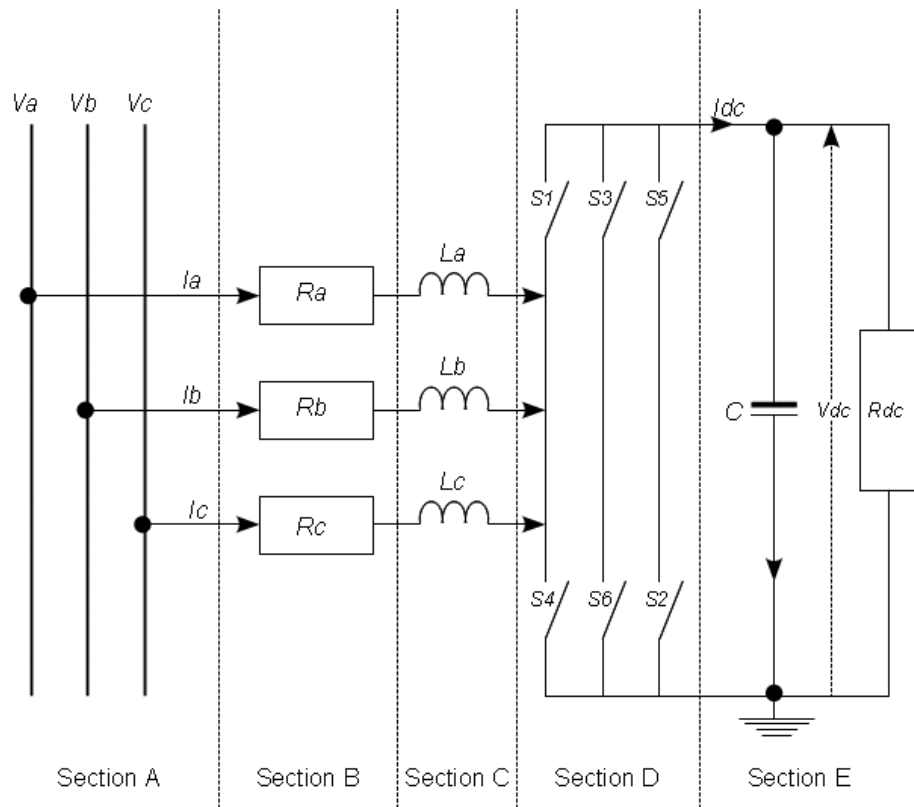


Figure A.1: Six-pulse DSTATCOM connected to distribution feeder

Section A: Three-Phase Voltage Transformations.

1) In (abc) stationary axis:

$$v_s = \begin{bmatrix} v_a \\ v_b \\ v_c \end{bmatrix} = \sqrt{\frac{2}{3}}V \begin{bmatrix} \sin(\omega t - \varphi) \\ \sin(\omega t - \frac{2\pi}{3} - \varphi) \\ \sin(\omega t + \frac{2\pi}{3} - \varphi) \end{bmatrix} \quad (\text{A.1})$$

where φ is the phase angle between source and inverter voltages.

2) In rotating (d-q) axis:

$$v_{s,qd0} = KV_{abc} = V \begin{bmatrix} -\sin\varphi \\ \cos\varphi \\ 0 \end{bmatrix} \quad (\text{A.2})$$

The Park's transform is defined as:

$$K = \sqrt{\frac{2}{3}} \begin{bmatrix} \cos(\omega t) & \cos(\omega t - \frac{2\pi}{3}) & \cos(\omega t + \frac{2\pi}{3}) \\ \sin(\omega t) & \sin(\omega t - \frac{2\pi}{3}) & \sin(\omega t + \frac{2\pi}{3}) \\ \frac{1}{\sqrt{2}} & \frac{1}{\sqrt{2}} & \frac{1}{\sqrt{2}} \end{bmatrix} \quad (\text{A.3})$$

Section B: Voltage/Current Equations for Resistor Section.

1) In (abc) stationary axis:

$$v_{s,abc} = Ri_{abc} + v_{abc} \quad (\text{A.4})$$

2) In rotating (d-q) axis:

$$v_{s,qd0} = Ri_{qd0} + v_{qd0} \quad (\text{A.5})$$

Section C: Voltage/Current Equations for Inductor Section.

1) In (abc) stationary axis:

$$L \frac{d}{dt}(i_{abc}) = v_{abc} - v_{0,abc} \quad (\text{A.6})$$

2) In rotating (d-q) axis:

$$L \frac{d}{dt}(i_{qd0}) = L \frac{d}{dt}(K)K_{-1}i_{qd0} + v_{qd0} - v_{0,qd0} \quad (\text{A.7})$$

$$L \frac{d}{dt}(i_q) = -\omega L i_d + v_q - v_0 q \quad (\text{A.8})$$

$$L \frac{d}{dt}(i_d) = \omega L i_q + v_d - v_0 d \quad (\text{A.9})$$

Collecting section B and C yields:

$$\frac{d}{dt} \begin{bmatrix} i_q \\ i_d \end{bmatrix} = \begin{bmatrix} -\frac{R}{L} & -\omega \\ \omega & -\frac{R}{L} \end{bmatrix} \begin{bmatrix} i_q \\ i_d \end{bmatrix} + \frac{1}{L} \begin{bmatrix} v_{sq} - v_0 q \\ v_{sd} - v_0 d \end{bmatrix} \quad (\text{A.10})$$

Sections D and E: Equations for Switching Functions (Neglecting Harmonics)

1) In (abc) stationary axis:

$$S = \begin{bmatrix} s_a \\ s_b \\ s_c \end{bmatrix} = \sqrt{\frac{2}{3}} m \begin{bmatrix} \sin(\omega t) \\ \sin(\omega t - \frac{2\pi}{3}) \\ \sin(\omega t + \frac{2\pi}{3}) \end{bmatrix} \quad (\text{A.11})$$

In a programmed PWM scheme, the modulation index (m) is normally kept constant, and be calculated from the following equation.

$$\frac{v_{0,peak}}{v_{dc}} = \sqrt{\frac{2}{3}} m \quad (\text{A.12})$$

The inverter output voltages are determined as:

1) In (abc) stationary axis:

$$v_{0,abc} = S v_{dc} \quad (\text{A.13})$$

2) In rotating (d-q) axis:

$$v_{0,qd0} = K S v_{dc} = m \begin{bmatrix} 0 \\ 1 \\ 0 \end{bmatrix} v_{dc} \quad (\text{A.14})$$

Thus, Eq. (A.10) can now be written as

$$\frac{d}{dt} \begin{bmatrix} i_q \\ i_d \end{bmatrix} = \begin{bmatrix} -\frac{R}{L} & -\omega \\ \omega & -\frac{R}{L} \end{bmatrix} \begin{bmatrix} i_q \\ i_d \end{bmatrix} + \frac{1}{L} \begin{bmatrix} -V \sin \alpha \\ V \cos \alpha - m v_{dc} \end{bmatrix} \quad (\text{A.15})$$

While, the dc side capacitor current is defined by

1) In (abc) stationary axis:

$$i_{dc} = S^T i_{abc} \quad (\text{A.16})$$

2) In rotating (d-q) axis:

$$i_{dc} = K^{-1} S^T i_{qd0} = m \begin{bmatrix} 0 & 1 & 0 \end{bmatrix} \begin{bmatrix} i_q \\ i_d \\ i_0 \end{bmatrix} \quad (\text{A.17})$$

Hence,

$$i_{dc} = m i_d \quad (\text{A.18})$$

The dc side voltage-current relation is found by

$$i_{dc} = C \frac{dv_{dc}}{dt} \quad (\text{A.19})$$

Substituting Eq. (A.18) in (A.19) produces the model of the dc section of the system as

$$\frac{dv_{dc}}{dt} = \frac{m}{C}i_d \quad (\text{A.20})$$

A complete mathematical model of the DSTATCOM system in d-q axis is achieved by collecting all the sections and adding Eq. (A.20) together as

$$\frac{d}{dt} \begin{bmatrix} i_q \\ i_d \\ v_{dc} \end{bmatrix} = \begin{bmatrix} -\frac{R}{L} & -\omega & 0 \\ \omega & -\frac{R}{L} & \frac{m}{L} \\ 0 & \frac{m}{C} & 0 \end{bmatrix} \begin{bmatrix} i_q \\ i_d \\ v_{dc} \end{bmatrix} + \frac{v_s}{L} \begin{bmatrix} -\sin\alpha \\ \cos\alpha \\ 0 \end{bmatrix} \quad (\text{A.21})$$

It follows from eq. (A.21) that transfer functions expressions for the system states (i_q , i_d , and V_{dc}) with active (P) and reactive (Q) power components can simply be deduced thus;

$$i_q(s) = \frac{-V \left[s^2 \frac{\sin\alpha}{L} + s \left(\frac{R}{L^2} \sin\alpha + \frac{\omega}{L} \cos\alpha \right) + \frac{m^2}{L^2 C} \sin\alpha \right]}{s^3 + 2s^2 \frac{R}{L} + s \left(\omega^2 + \frac{R^2}{L^2} + \frac{m^2}{LC} \right) + \frac{R}{L^2 C} m^2} \quad (\text{A.22})$$

$$i_d(s) = \frac{V \left[s^2 \frac{\cos\alpha}{L} + s \left(\frac{R}{L^2} \cos\alpha - \frac{\omega}{L} \sin\alpha \right) \right]}{s^3 + 2s^2 \frac{R}{L} + s \left(\omega^2 + \frac{R^2}{L^2} + \frac{m^2}{LC} \right) + \frac{R}{L^2 C} m^2} \quad (\text{A.23})$$

$$v_{dc}(s) = mV \frac{\left[s \frac{\cos\alpha}{LC} + \frac{R}{L^2 C} \cos\alpha - \frac{\omega}{LC} \sin\alpha \right]}{s^3 + 2s^2 \frac{R}{L} + s \left(\omega^2 + \frac{R^2}{L^2} + \frac{m^2}{LC} \right) + \frac{R}{L^2 C} m^2} \quad (\text{A.24})$$

$$P(s) = v_{sq}i_q + v_{sd}i_d = -V(i_q \sin\alpha - i_d \cos\alpha) \quad (\text{A.25})$$

$$Q(s) = v_{sq}i_q - v_{sd}i_d = -V(i_d \sin\alpha + i_q \cos\alpha) \quad (\text{A.26})$$

The linearised state space version of Eq. (A.21) used for linear control system design is given as

$$\begin{aligned} \mathbf{X} &= \mathbf{A}\mathbf{X} + \mathbf{B}\mathbf{U} \\ \mathbf{Y} &= \mathbf{C}\mathbf{X} \end{aligned} \quad (\text{A.27})$$

where

$$\mathbf{X} = \begin{bmatrix} i_q \\ i_d \\ v_{dc} \end{bmatrix}, \quad \mathbf{A} = \begin{bmatrix} -\frac{R}{L} & \omega & 0 \\ \omega & -\frac{R}{L} & \frac{m}{L} \\ 0 & \frac{m}{C} & 0 \end{bmatrix}, \quad \mathbf{B} = \begin{bmatrix} -\frac{V}{L} \\ 0 \\ 0 \end{bmatrix}, \quad \mathbf{U} = \alpha,$$

and

$$\mathbf{C} = \begin{bmatrix} -V & 0 & 0 \end{bmatrix}$$

Then the input/output linear transfer function for the DSTATCOM is calculated from

$$G(s) = \frac{v(s)}{\alpha(s)} = C [sI - A]^{-1} \quad (\text{A.28})$$

Hence,

$$G(s) = \frac{V^2 \left[\frac{s^2}{L} + \frac{R}{L}s + \frac{m^2}{L^2 C} \right]}{s^3 + 2s^2 + s \left(\omega^2 + \frac{R^2}{L^2} + \frac{m^2}{LC} \right) + \frac{R}{L^2 C} m^2} \quad (\text{A.29})$$

Appendix B

4.1 System Design

Table B.1: Linear and Nonlinear Plant Parameters

Parameter	Value
Frequency (f)	50Hz
Resistance (R)	1 Ω
Capacitance(C)	550 μF
Inductance(L)	3mH
Total reactance($jX = X_c + X_l$)	5.13 Ω
Feeder ac-voltage(V)	415/220 volts
Modulation-index(m)	1
Angular-frequency(ω)	377 rads/sec
Switching-angle(α)	$\pm 30^\circ (\pm 0.5326)$ rads
Reactive-current(i_q)	38 amps
Direct-current(i_d)	0.2 amps
Capacitor-link dc-voltage(V_{dc})	380 volts

Table B.2: Ziegler-Nichols Emperical Tuning

Controller	Tuning Rules			Initial Parameters		
	K_p	T_i	T_d	K_p	T_i	T_d
P	$1/a$	-	-	0.0014	-	-
PI	$0.9/a$	$3L$	-	0.0012	0.501	-
PID	$1.2/a$	$2L$	$L/2$	0.0016	0.334	$0.0835L$

Table B.3: AMIGO Tuning Rules

Controller	Tuning Rules			Initial Parameters		
	K_p	T_i	T_d	K_p	T_i	T_d
P	$\frac{1}{a} \left(1 + \frac{0.35\tau}{1-\tau}\right)$	-	-	0.0015	-	-
PI	$\frac{0.9}{a} \left(1 + \frac{0.92\tau}{1-\tau}\right)$	$\frac{3.3-3\tau}{1+1.2\tau} L$	-	0.0015	0.41	-
PD	$\frac{1.24}{a} \left(1 + \frac{0.13\tau}{1-\tau}\right)$	-	$\frac{0.27-0.36\tau}{1-0.87\tau} L$	0.0018	-	0.042
PID	$\frac{1.35}{a} \left(1 + \frac{0.18\tau}{1-\tau}\right)$	$\frac{2.5-2\tau}{1-0.39\tau} L$	$\frac{0.37-0.37\tau}{1-0.81\tau} L$	0.002	0.39	0.06

Table B.4: CHR Tuning for Setpoint Following

Controller	with 0% overshoot			with 20% overshoot		
	K_p	T_i	T_d	K_p	T_i	T_d
P	$0.3/a$	-	-	$0.7/a$	-	-
PI	$0.35/a$	$1.2T$	-	$0.6/a$	T	-
PID	$0.6/a$	T	$0.5L$	$0.95/a$	$1.4T$	$0.47L$

Table B.5: CHR Parameters for Setpoint Following

Controller	with 0% overshoot			with 20% overshoot		
	K_p	T_i	T_d	K_p	T_i	T_d
P	0.0042	-	-	0.0098	-	-
PI	0.0049	1.2	-	0.0084	1	-
PID	0.0084	1	0.0835	0.0013	1.4	0.0785

Table B.6: CHR Tuning for Disturbance Rejection

Controller	with 0% overshoot			with 20% overshoot		
	K_p	T_i	T_d	K_p	T_i	T_d
P	$0.3/a$	-	-	$0.7/a$	-	-
PI	$0.6/a$	$4L$	-	$0.7/a$	$2.3L$	-
PID	$0.95/a$	$2.4L$	$0.42L$	$1.2/a$	$2L$	$0.42L$

Table B.7: CHR Parameters for Disturbance Rejection

Controller	with 0% overshoot			with 20% overshoot		
	K_p	T_i	T_d	K_p	T_i	T_d
P	0.0042	-	-	0.0098	-	-
PI	0.0084	0.668	-	0.0098	0.3841	-
PID	0.0013	0.4008	0.0701	0.0017	0.3340	0.0701

Table B.8: Derivative in the Feedforward loop vs. Feedback Path

ρ	Normal PID [P=0.1; I=0.15; D=0.3]			Re-routed PID [P=0.1; I=0.15; D=0.3]		
	Overshoot	63%-Rise Time	Error	Overshoot	63%-Rise Time	Error
1	Unstable	0	Unstable	stable	1.48	$e \Rightarrow 0$
2	Unstable	0	Unstable	stable	1.28	$e \Rightarrow 0$
3	1.29	Transients	> 1 : 0/25s	1.34	0.962	> 1 : 0/25s
4	1.29	Transients	> 1 : 0/27s	1.34	0.940	> 1 : 0/25s
5	1.29	Transients	> 0.75 : 0/24s	1.34	0.924	0.75 : 0/25s
6	1.29	1.14	> 0.79 : 0/28s	1.34	0.915	0.75 : 0/25s
7	1.29	1.16	Do	1.34	0.909	Do
8	1.29	1.18	Do	1.34	0.905	Do
9	1.29	1.19	Do	1.34	0.900	Do
10	1.29	1.20	Do	1.34	0.898	Do
**11	1.29	1.20	Do	1.34	0.896	Do
12	1.29	1.35	Do	1.34	1.01	Do
30	1.29	1.25	0.81 : 0/28s	1.34	0.883	0.81 : 0/28s

Appendix C

5.1 I/O Mappings and Robustness Tables

Table C.1: Input - Output Mapping

Rules	e	\dot{e}	S_1	S_2	S_o	α
1	-0.589(<i>Neg</i>)	-0.323(<i>Slow</i>)	1.0011	1.0011	0.9998	0.5(<i>Med</i>)
2	-0.404(<i>Neg</i>)	0.0045(<i>Norm</i>)	1.0011	1.0011	0.9998	0.5(<i>Med</i>)
3	-1(<i>Neg</i>)	0.159(<i>Fast</i>)	1.0011	1.0011	0.9998	0(<i>Low</i>)
4	0(<i>Zero</i>)	-0.168(<i>Slow</i>)	1.0011	1.0011	0.9998	0.5(<i>Med</i>)
5	0(<i>Zero</i>)	0.0045(<i>Norm</i>)	1.0011	1.0011	0.9998	0.5(<i>Med</i>)
6	0(<i>Zero</i>)	0.314(<i>Fast</i>)	1.0011	1.0011	0.9998	0.5(<i>Med</i>)
7	0.404(<i>Pos</i>)	-0.405(<i>Slow</i>)	1.0011	1.0011	0.9998	1(<i>High</i>)
8	0.183(<i>Pos</i>)	0.0045(<i>Norm</i>)	1.0011	1.0011	0.9998	0.5(<i>Med</i>)
9	0.44(<i>Pos</i>)	0.314(<i>Fast</i>)	1.0011	1.0011	0.9998	0.5(<i>Med</i>)

Table C.2: Performance indicators to uncertain phase-angle model

Parameter	PI_L	PD_L	FPD_L	PI_{NL}	PD_{NL}	FPD_{NL}
P	1.163	10	1	1.163	10	1
I	0.5	0	0	0.5	0	0
D	0.01	0.001	0.01	0.01	0.001	0.01
e	-0.00793	-0.00794	-ve	4.008e - 005	4.00e - 005	+ve
\dot{e}	-1.619	-1.619	Fast	-0.00067	-0.00067	Fast
α	0.005	0.00499	0.005	0.0173	0.0173	0.0173
S_1	1.0011	1.0011	1.0011	0.0011	0.0011	0.001
S_2	0.0011	0.0011	0.0011	0.0011	0.0011	0.0011
S_o	1.00004	0.9998	1	4.233	4.233	4.233
Overshoot (%)	0	3.96	0.17	38.9	43.0	41.9
Rise Time (sec)	0.011	0.008	0.008	0.0018	0.0015	0.0015
Settling Time (sec)	0.078	0.065	0.03	0.065	0.07	0.035
Target Output (volts)	220	220	220	220	220	220

Table C.3: Model Performance due to uncertain inductance change

Parameter	Nonlinear Model Inductance Change			Linear Model Inductance Change		
	PI_{NL}	PD_{NL}	FPD_{NL}	PI_L	PD_L	FPD_L
S_1	0.0011	0.0011	0.0011	1.0011	1.0011	1.0011
S_2	0.0011	0.0011	0.0011	0.0011	0.0011	0.0011
S_o	2.7600	2.7600	2.7600	2.7338	2.7338	2.7338
α	0.01129	0.01129	0.01129	0.01367	0.01367	0.01367
e	0.04387	0.04387	4.83e - 5	0.1422	0.1422	0.1422
\dot{e}	-0.000131	0 - 0.000131	-0.000131	-0.0046	-0.0046	-0.0046
V	180.2	180.2	220	220.5	219.5	220

Table C.4: Model Performance due to uncertain resistance change

Parameter	Nonlinear Model Resistance Change			Linear Model Resistance Change		
	PI_{NL}	PD_{NL}	FPD_{NL}	PI_L	PD_L	FPD_L
S_1	0.0011	0.0011	0.0011	1.0011	1.0011	1.0011
S_2	0.0011	0.0011	0.0011	0.0011	0.0011	0.0011
S_o	2.7600	2.7600	2.7600	2.7278	2.7278	2.7278
α	0.01129	0.01129	0.01129	0.01364	0.01364	0.01364
e	$2.71e-5$	$2.71e-5$	$2.71e-5$	0	20.0	20.0
\dot{e}	0	0	0	0	4.462	4.462
V	180	180	220	220	200	200

Table C.5: Model Performance due to uncertain capacitance change

Parameter	Nonlinear Model Capacitance Change			Linear Model Capacitance Change		
	PI_{NL}	PD_{NL}	FPD_{NL}	PI_L	PD_L	FPD_L
S_1	0.0011	0.0011	0.0011	1.0011	1.0011	1.0011
S_2	0.0011	0.0011	0.0011	0.0011	0.0011	0.0011
S_o	1.1245	1.1245	0.9200	1.0226	0	0
α	0.004601	0.004601	0.0046	0.004184	0.004092	0.004092
e	0.02464	0.02464	$2.71e - 005$	-0.04485	-0.04485	-0.0448
\dot{e}	0	0	$-1.075e - 010$	0	0	-1.649
V	220	220	220	220	220	220

Table C.6: Linear (L) vs. Nonlinear (NL) Model Performance Indicators

Parameter	PI_L	PD_L	FPD_L	PI_{NL}	PD_{NL}	FPD_{NL}
P	1.163	10	1	1.163	10	1
I	0.5	0	0	0.5	0	0
D	0.01	0.001	0.01	0.01	0.001	0.01
e	-0.00793	-0.00794	-ve	$3.664e - 005$	$3.664e - 005$	+ve
\dot{e}	-1.619	-1.619	Slow	-0.00067	-0.00067	Slow
α	0.004091	0.004091	0.004091	0.0046	0.0046	0.0046
S_1	1.0011	1.0011	1.0011	0.0011	0.0011	0.001
S_2	0.0011	0.0011	0.0011	0.0011	0.0011	0.0011
S_o	0.9998	0.9998	0.9998	1.1241	1.1241	0.9200
<i>Overshoot%</i>	0	3.96	0.17	12.55	7.34	0.74
<i>RiseTime(sec)</i>	0.011	0.008	0.008	0.0078	0.0074	0.0074
<i>SettlingTime(sec)</i>	0.078	0.065	0.03	0.080	0.086	0.05
<i>TargetOutput(volts)</i>	220	220	220	220	220	220

Table C.7: JBest Controllers from Parameter Evolution

Parameters	KP_1	KP_2	KP_3	KP_4	KP_5
Min	0.00026	0.0039	0.00010	0.00015	0.00016
Max	0.0023)	0.0068	0.0020	0.0042	0.0013
Range	0.0020	0.0064	0.0019	0.0041	0.0011
Parameters	KD_1	KD_2	KD_3	KD_4	KD_5
Min	0.0413	0.0222	0.0930	0.0130	0.0428
Max	0.2689	0.1336	0.0992	0.2840	0.1153
Range	0.2276	0.1114	0.0062	0.2710	0.0725
Parameters	α_1	α_2	α_3	α_4	α_5
Min	0	0	0	0	0
Max	0.9648	1.3247	2.0692	0.3185	0.9862
Range	0.9648	1.3247	2.0692	0.3185	0.9862
$J_{FPDbest}$	J_1	J_2	J_3	J_4	J_5
Min	352.87	414.65	361.75	451.45	333.14
Max	679.53	584.64	1063.1	679.89	935.62
Range	326.67	169.99	701.33	228.44	602.48

Appendix D

6.1 Control Strategy

For practical purposes, the control strategy used in the simulation model in Figure 5.37 consists of the following functional blocks which have been explained in turn (MathWorks, 2009a):

1. Two measurement circuit blocks (V_m) and (I_m)
2. One inner current control loop
3. One outer voltage control loop
4. One DC voltage regulator
5. One phased locked loop (PLL)

The measurement blocks compute the $d - q$ axes components of the voltages and currents through $abc - dq$ transformation obtained from $\sin(\omega t)$ and $\cos(\omega t)$ provided by the PLL in the synchronous reference plane. Normally, the inner current control loop would consist of two PI controllers for compensating the d and q axes currents. The output of these controllers are the v_d and v_q voltages normally generated by the PWM inverter. These voltages are then converted to v_a , v_b , and v_c phase voltages which are used to synthesise the PWM voltages. The i_q and i_d reference quantities each comes from the outer voltage control loop and the DC-link voltage controller, respectively. The outer voltage control loop has one PI controller to maintain the primary voltage output against the reference value. Finally, a DC voltage regulator to maintain the DC side voltage constant.

Compatible with a simple direct ac voltage outer loop control strategy based on instantaneous power balance theory, the DSTATCOM can thus be controlled to provide the

p-q axes components required for ac voltage regulation and dc link capacitor charging, i.e., (Bukata, 2010).

According to the power balance theory, the DSTATCOM output $P_o + jQ_o$ must equal system's input power $P_i + jQ_i$ plus the power taken by the filter and the equivalent resistance and inductance of the coupling transformer $P_F + jQ_F$ such that:

$$P_o = P_i + P_F \quad (\text{D.1})$$

$$Q_o = Q_i + Q_F \quad (\text{D.2})$$

Figure D.1 demonstrates a current to voltage conversion scheme, which can be achieved by assuming a 3ϕ symmetrical grid voltage in the $dq0$ axis through the following equations:

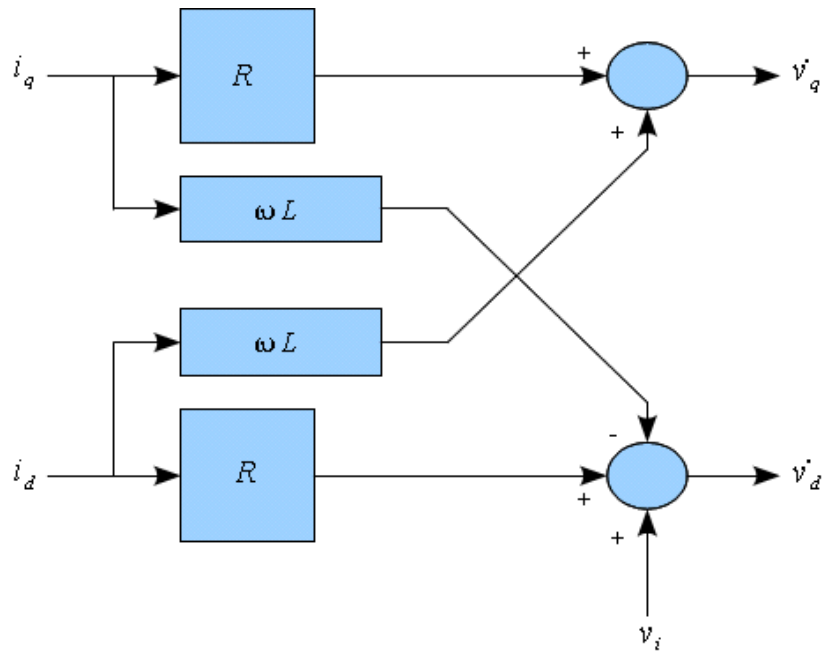


Figure D.1: Outer loop voltage control

$$P_o = \frac{3}{2} (v_d i_d + v_q i_q) \quad (\text{D.3})$$

$$Q_o = \frac{3}{2} (v_q i_d + v_d i_q) \quad (\text{D.4})$$

Equating $v_d = v_i$ and $v_q = 0$ so that

$$P_o = \frac{3}{2}v_d i_d = v_i i_d \quad (\text{D.5})$$

$$Q_o = \frac{3}{2}v_d i_q = +v_i i_q \quad (\text{D.6})$$

The power consumed at the filter and transformer is given as

$$P_F = \frac{3}{2}i^2 R = \frac{3}{2}(i_d^2 + i_q^2) R \quad (\text{D.7})$$

$$Q_F = \frac{3}{2}i^2 \omega L = \frac{3}{2}(i_d^2 + i_q^2) \omega L \quad (\text{D.8})$$

By properly substituting Eqs. C.7 and C.8 into Eqs. A.25 and A.26, we get

$$v_d = R i_d - \omega L i_q + v_i \quad (\text{D.9})$$

$$v_q = R i_q + \omega L i_d \quad (\text{D.10})$$

It is noted at this point that realisation of the direct voltage strategy is much easily done from power balance theory as it does not require inductor and current detection circuits normally found in the inner current control loop technique. But, as can be seen, the outer voltage scheme also suffers from over reliance on equivalent parameters of the filter and the coupling transformer which causes performance deterioration, and this is why I considered re-designing my PD controller with a cascaded first-order linear low-pass filter in chapter 3.